TWR-17591

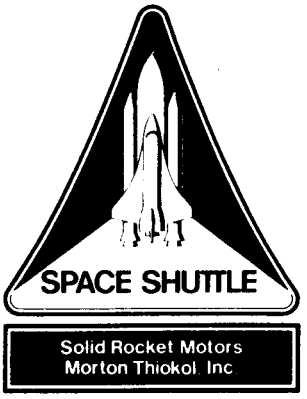

Qualification Motor No. 8 (QM-8) Final Test Report

Volume 1

March 1989

Prepared for

National Aeronautics and Space Administration
George C. Marshall Space Flight Center
Marshall Space Flight Center, Alabama 35812

Contract No. NAS8-30490
DR No. 5-3
WBS No. HQ302-10-10
ECS No. SS1004

MORTON THIOKOL, INC.
Aerospace Group
Space Operations
P.O. Box 707, Brigham City, Utah 84302-0707 (801) 863-3511

Publications No. 89605

Qualification Motor No. 8
(QM-8)
Final Test Report

Prepared by:

D. M. Garecht
Test Planning and Reporting
Systems Engineer

Approved by:

Neal Black
Test Planning and Reporting
Supervisor

Space Systems Engineering
Manager

Michael Wilkins
Systems Test and Support
Manager

for D. M. Ketner
Space Engineering Design
Manager

T. Swaton
Project Engineer

S. G. Harris
Program Manager

Charles W. Johnson
Flight Certification

Keith L. Ebbert
Systems Safety

Fred Dwinnell Jr.
Reliability

P. C. Tydeck 3-21-89
Data Management
ECS #SS1004

ABSTRACT

All inspection and instrumentation data indicate that the QM-8 static test firing conducted 20 January 1989 was successful. Ambient temperature at T-0 was 28°F. With two flights successfully accomplished, this final test in the RSRM program certified that the design meets motor performance requirements under extreme cold conditions. This test was a prerequisite to third fllight. The entire test article was cold conditioned at 20° to 25°F for approximately 31 days to assure a maximum PMBT of 40°F, making it the lowest PMBT in the history of the program. Calculated PMBT at time of firing was 39°F. It is highly unlikely that conditions at the launch site would be sufficiently severe for this to occur, even under the most extreme winter situation. The lowest PMBT attained prior to QM-8 was 52°F on STS-20 (Mission 51-C, 24 January 1985).

This extreme condition also presented the opportunity to certify critical components at low temperatures. Certification of field joint and igniter heaters, adhesive bondline integrity, flex bearing performance, flight instrumentation performance, RSRM seal performance, and LSC and nozzle plug performance, to name a few, was accomplished.

Prior to motor ignition, the field joints were maintained between 75° to 130°F, the igniter-to-case joint was maintained between 75° and 123°F, and the case-to-nozzle joint was maintained between 75° and 120°F. Thermal conditioning in the aft end, field joint heaters, and igniter strip heater were all controlled at the lower end of their respective limits.

QM-8 was tested with induced side loads to simulate the strut loads experienced during ignition and maximum aerodynamic loading conditions.

The ability of the safe and arm device to change position from safe-to-arm and arm-to-safe was certified.

Ballistics performance was certified at the lower limits. Values were within specification requirements. Nozzle performance was nominal with typical erosion. The use of Fiberite® carbon-cloth phenolic was certified. The water deluge system, CO_2 quench, and other test equipment performed as planned during all required test operations.

CONTENTS

CONTENTS (Cont)

FIGURES

FIGURES (Cont)

TABLES

ACRONYMS

ac	alternating current
AP	amonium perchlorate
ATVC	ascent thrust vector control
AVPP	adjustable vent port plug
BCU	bus control unit
CCP	carbon-cloth phenolic
CF	capture feature
COR	Contractor Operations Review
CP	circular perforated
CTPB	carboxyl-terminated polybutadiene
DAS	Data Acquisition System
DFI	development flight insturmentation
ETA	external tank attach
FEP	fluoroethylene polymer
FJPS	field joint protection system
FT	Fourier Transform
GCP	glass-cloth phenolic
GEI	ground environmental instrumentation
GFI	ground fault interrupter
HPM	high performance motor
HPU	hydraulic power units
ID	inner diameter
JPS	joint protection system
LVDT	linear variable displacement/xducer
MAP	manual/automatic panel
Max Q	maximum aerodynamic
MEM	Maximum Entropy Method
NBR	acrylonitrile butadiene rubber
OBR	outer boot ring
OD	outer diameter
OFI	operational flight instrumentation
OPT	operational pressure transducer
PBAN	polybutadiene acrylic acid acrylonitrile terpolymer binder
PMBT	propellant mean bulk temperature
PSD	power spectrum density
RSRM	redesigned solid rocket motor
RTD	resistance temperature device
S&A	safety and arming device
SAPMD	stand-alone pressure measuring device
SCP	silica-cloth phenolic
SRB	solid rocket booster
SRM	solid rocket motor
TVC	thrust vector control
USBI	United States Boosters, Inc.
Vac	volts alternating current

1

INTRODUCTION

The solid rocket motor (SRM), used in pairs, is the primary Space Shuttle propulsive element, providing impulse and thrust vector control (TVC) from SRM ignition to solid rocket booster (SRB) separation. The Qualification Motor No. 8 (QM-8) test was a full-scale full-duration test of a redesigned solid rocket motor (RSRM). This test report includes a presentation and discussion of QM-8 performance and of test result concurrence with the objectives outlined in CTP-0060, Rev D. A major focus of this report is placed on the test objectives, anomalies and motor performance.

QM-8 was successfully fired on 20 January 1989 at Morton Thiokol Utah-based Operations, Test Bay T-97. The test was conducted in accordance with the requirements of CTP-0060, Rev D, "Space Shuttle Qualification Motor No. 8 (QM-8) Static Fire Test Plan." Postfire inspection procedures followed TWR-16473, Vol 1 through Vol IX, and are documented in TWR-17591, Vol 1 through Vol XI.

1.1 TEST ARRANGEMENT AND FACILITIES

The QM-8 static test arrangement was in accordance with Drawing 7U75880 and is shown in Figure 1.1-1. T-97 is equipped with a water deluge system, a CO_2 quench, side load system, and an in-bay conditioning system.

1.2 TEST ITEM DESCRIPTION

The QM-8 static test article was configured to approximate the RSRM flight motors. The RSRM static test motor consisted of a lined, insulated, segmented rocket motor case loaded with solid propellant; ignition system complete with electro-mechanical safety and arming device (S&A), initiators, and loaded igniter; movable nozzle with flexible bearing and exit cone. A 360-deg external tank attach (ETA) ring (primary structure only) and an SRB aft skirt were attached with TVC systems and actuators, electrical and instrumentation items, and a thermal curtain assembly. Side load actuators were attached to the ETA ring to introduce simulated flight loads. An overall view of the test article is shown in Figure 1.2-1. The QM-8 configuration is detailed in Section 10 of this report.

N108280-5

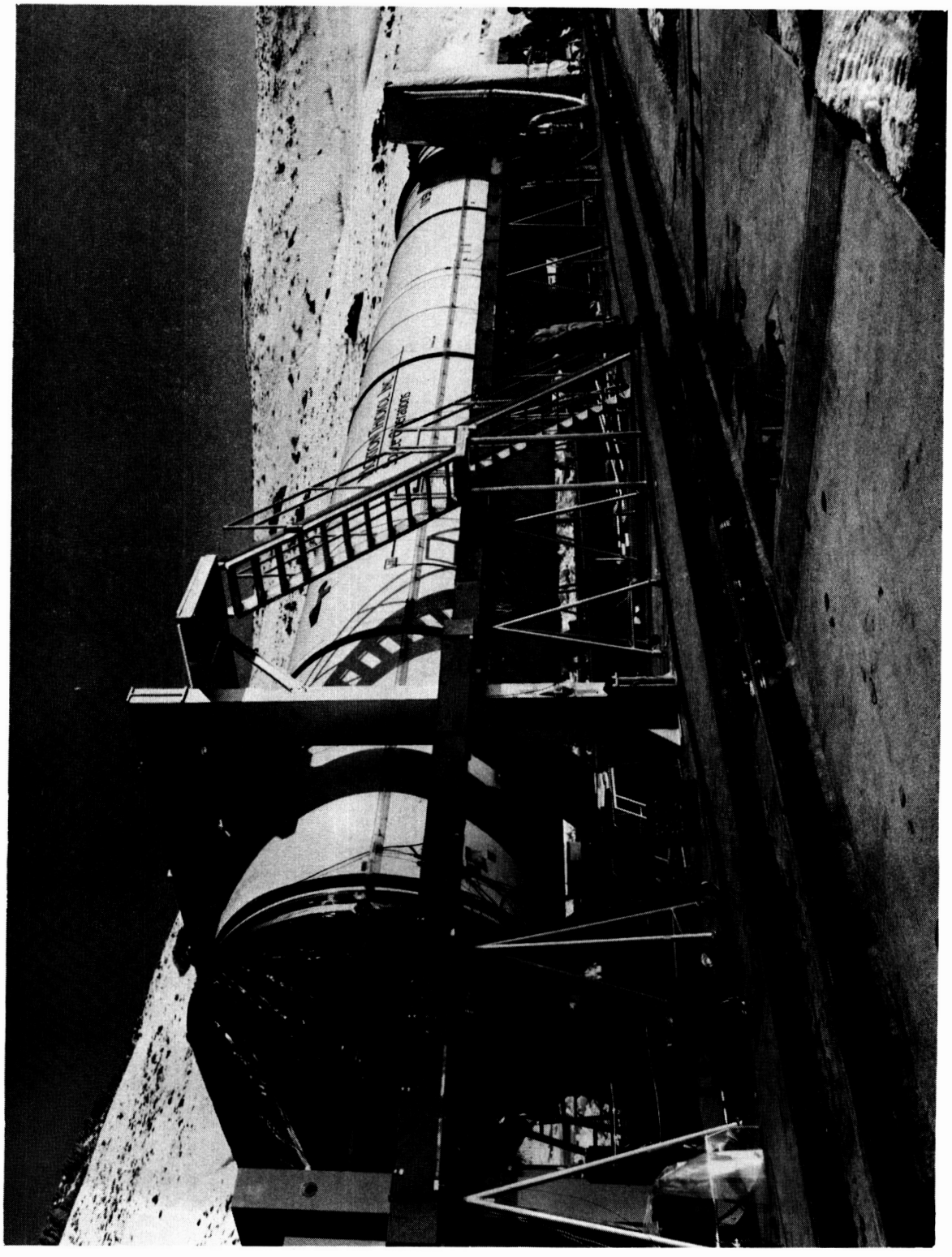

Figure 1.1-1 QM-8 Static Test Motor During Assembly at T-97 Test Bay

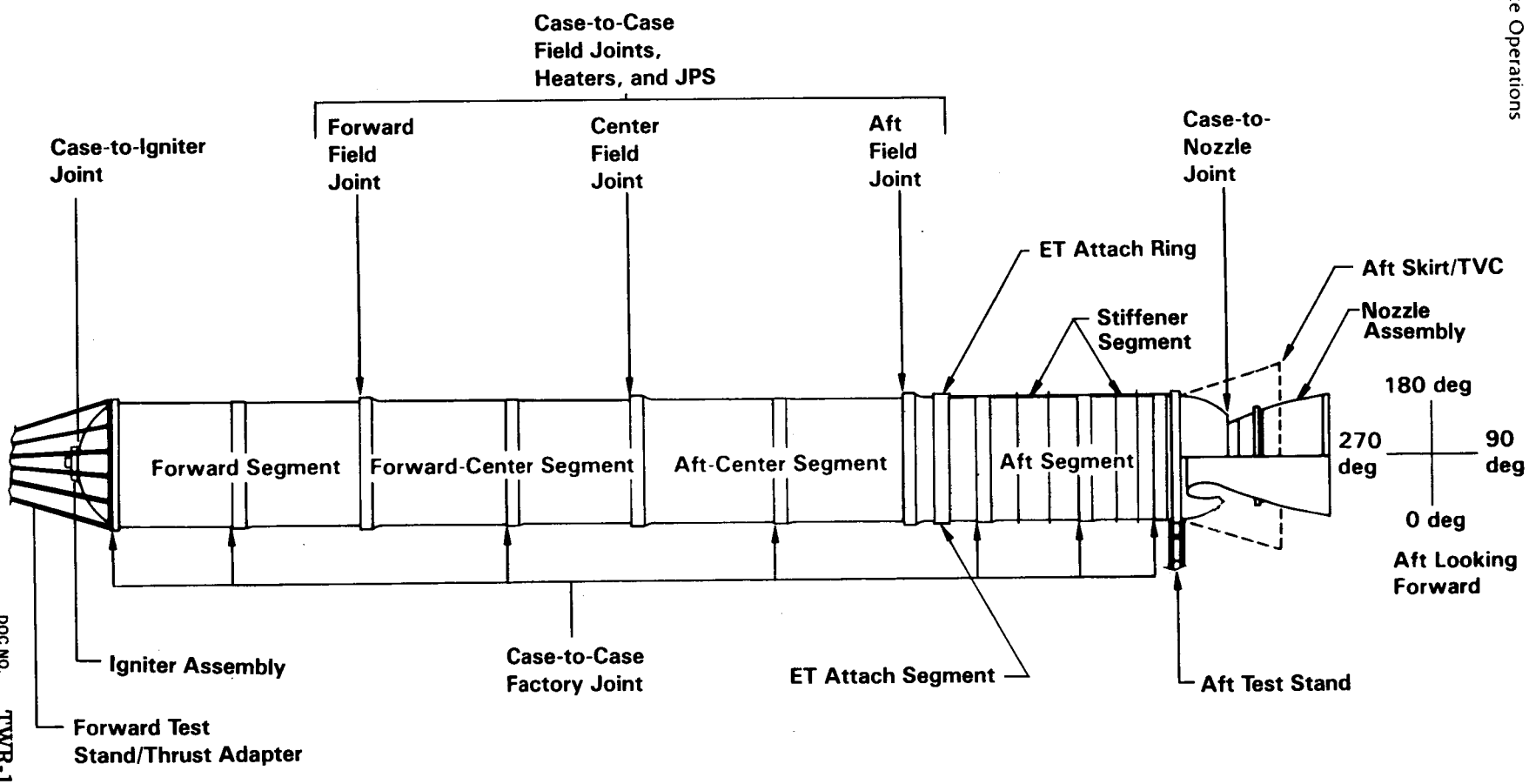

Figure 1.2-1. Overall View of QM-8 Test Article and Comparison Matrix

A011309 R8

2

TEST OBJECTIVES

The QM-8 test objectives, derived from objectives in TWR-15723 to satisfy the requirements of Specification CPW1-3600 Addendum D, dated 3 August 1987, are listed below. The specific paragraphs from CEI are listed with the objectives.

Qualification Objectives (CEI Paragraph)

A. Certify the motor performance at 40°F PMBT (3.2.1)

B. Certify the ignition interval (3.2.1.1.1.1)

C. Certify the maximum pressure rise rate (3.2.1.1.1.2)

D. Certify the lower allowable rate of maximum pressure buildup (3.2.1.1.1.2, Morton Thiokol Imposed)

E. Determine the thrust-time curve for QM-8 and apply the data to the nominal thrust-time curve for certification of the RSRM design (3.2.1.1.2.1)

F. Certify the performance tolerances and limits (determined from chamber pressure data) (3.2.1.1.2.2)

G. Determine the impulse attained by QM-8 and apply the data to the nominal thrust-time curve for certification of the RSRM design (determined from chamber pressure data) (3.2.1.1.2.4)

H. Certify that all RSRM seals, including adjustable vent port plug seals in the field joints, experience no erosion or blow-by throughout the static test (3.2.1.2)

I. Certify the verifiability of the RSRM seals (except for the case-to-nozzle joint primary seal, the factory joint primary seal, the fixed housing-to-aft end ring primary seal, the igniter dual seal plugs (5 places) and the operational pressure transducer (OPT) primary and secondary seals) (3.2.1.2)

J. Certify that the case field joint and case-to-nozzle joint seals, if pressurized, accommodate static test motor and side load induced structural deflections (3.2.1.2.1.a)

K. Certify that the case field joint and case-to-nozzle joint seals, if pressurized, operate when PMBT is at 40°F (3.2.1.2.1.b)

L. Certify that the case field joint and case-to-nozzle joint seal verification does not degrade the performance or integrity of the sealing system. (3.2.1.2.1.c)

M. Certify that the bore seals for the field joint are verifiable in the proper direction (3.2.1.2.1.d)

N. Certify that the case-to-nozzle joint O-ring temperature is maintained prior to static firing (3.2.1.2.1.f)

O. Certify that the factory joint insulation as a seal accommodates static test motor structural deflections and erosion. (3.2.1.2.2.a)

P. Certify that the factory joint insulation as a seal operates when PMBT is at 40°F. (3.2.1.2.2.b)

Q. Certify that the insulation performs the seal function for the factory joint. (3.2.1.2.2.d)

R. Certify that the factory joint insulation is adequate to preclude leaks. (3.2.1.2.2.e)

S. Certify that the flex bearing sealing accommodates static test motor structural deflections. (3.2.1.2.3.a)

T. Certify that the flex bearing operates as a seal at 40°F PMBT. (3.2.1.2.3.b)

U. Certify that the flex bearing seal verification does not degrade the performance or integrity of the sealing system. (3.2.1.2.3.c)

V. Certify that the flex bearing maintains a positive gas seal between its internal components. (3.2.1.2.3.d)

W. Certify that the ignition system seals, if pressurized, accommodate static test motor structural deflections. (3.2.1.2.4.a)

X. Certify that the ignition system seals, if pressurized, operate when PMBT is at 40°F. (3.2.1.2.4.b)

Y. Certify that the ignition system seal verification does not degrade the performance or integrity of the sealing system. (3.2.1.2.4.c)

Z. Certify that the nozzle internal seals and the aft exit cone field joint seals, if pressurized, can accommodate static test motor structural deflections. (3.2.1.2.5.a)

AA. Certify that the nozzle internal seals and the aft exit cone field joint seals, if pressurized, operate when PMBT is at 40°F. (3.2.1.2.5.b)

AB. Certify that the nozzle internal seals and the aft exit cone field joint seals verification does not degrade the performance or integrity of the sealing system. (3.2.1.2.5.c)

AC. Certify that the bore seals for the nozzle are verifiable in the proper direction. (3.2.1.2.5.e)

AD. Certify that the case is capable of containing the static test internal pressure. (3.2.1.3.a)

AE. Certify that the case ET attach risers do not degrade the integrity of the case. (3.2.1.3.c)

AF. Certify by demonstrating horizontal assembly that the case segment mating joints incorporate provisions to insure proper segment orientation and alignment. (3.2.1.3.f)

AG. Certify the function of the pin retainer band. (3.2.1.3.g)

AH. Certify that the RSRM is designed using motor internal pressure drop from head end to aft end. (3.2.1.3.k)

AI. Certify that the nozzle assembly and exit cone design are compatible with the system performance requirements. (3.2.1.4, Morton Thiokol Imposed)

AJ. Certify that the nozzle assembly is capable of vectoring through the planned duty cycle. (3.2.1.4.1)

AK. Certify the minimum gimbal rate. (3.2.1.4.1)

AL. Certify the geometric nozzle alignment. (3.2.1.4.2)

AM. Certify the misalignment of the dynamic thrust vector with respect to the nozzle centerline. (3.2.1.4.3 and 3.2.1.4.3.a)

AN. Certify the radial offset between the dynamic thrust vector and the nozzle centerline. (3.2.1.4.3 and 3.2.1.4.3.b)

AO. Certify the null offset angle at 0 psi nozzle stagnation pressure. (3.2.1.4.4.a)

AP. Certify the null offset angle at 615 psi nozzle stagnation pressure. (3.2.1.4.4.b)

AQ. Certify the null offset angle at 915 psi nozzle stagnation pressure. (3.2.1.4.4.c)

AR. Certify that the nozzle snubbing device will not adversely affect the nozzle assembly vectoring capability. (3.2.1.4.6)

AS. Certify the nozzle assembly TVC actuator attach points. (3.2.1.4.8)

AT. Certify the nozzle flame front liner design and fabrication. (3.2.1.4.13)

AU. Certify that the ignition system precludes hot gas leakage during and subsequent to motor ignition. (3.2.1.5.a)

AV. Certify that the igniter and the S&A are separable from each other. (3.2.1.5.b)

AW. Certify the enable function of the S&A device. (3.2.1.5.1.a)

AX. Certify the S&A change of position from safe-to-arm and arm-to-safe. (3.2.1.5.1.d)

AY. Certify that the S&A device will provide simplex remote position indication. (3.2.1.5.1.e)

AZ. Certify the igniter design. (3.2.1.5.2)

BA. Certify the igniter heater maintains the igniter gasket rubber seals at the required temperature. (3.2.1.5.3)

BB. Certify the operation and installation of the motor chamber operational pressure transducer. (3.2.1.6.2.1)

BC. Certify the ability of the case joints internal insulation to protect the case metal structural and sealing integrity from thermal degradation. (3.2.1.8.1.1.a)

BD. Certify the field joint, case-to-nozzle joint and igniter to case joint leak test compatibility. (3.2.1.8.1.1.b)

BE. Certify that the internal insulation provides thermal protection to ensure that system performance and structural integrity are maintained during assembly and operation. (3.2.1.8.1.1.c)

BF. Certify that the field joint, case-to-nozzle joint and igniter to case joint internal insulation provide seal protection. (3.2.1.8.1.1.d)

BG. Certify the ability of the field joint, case-to-nozzle joint and igniter to case joint internal insulation to meet performance requirements during a 40°F PMBT full duration motor burn. (3.2.1.8.1.1.e)

BH. Certify that the field joint, case-to-nozzle joint and igniter to case joint insulation do not shed fibrous or particulate matter during assembly which could prevent sealing. (3.2.1.8.1.1.f)

BI. Certify that the field joint, case-to-nozzle joint and igniter to case joint insulation will withstand slag accumulation during motor operation. (3.2.1.8.1.1.g)

BJ. Certify that the ballistic performance is not affected by the field joint, case-to-nozzle joint and igniter to case joint insulation. (3.2.1.8.1.1.i)

BK. Certify that the igniter insulation provides adequate thermal protection for the main igniter chamber and adapter metal parts. (3.2.1.8.3)

BL. Certify the ability of the field joint heater assembly to maintain the temperature of the field joints. (3.2.1.11.a)

BM. Certify the inert weight. (3.2.2.2.1)

BN. Certify the nozzle forward section weight. (3.2.2.2.1, Morton Thiokol Imposed (3))

BO. Certify the exit cone weight. (3.2.2.2.1, Morton Thiokol Imposed (5))

BP. Certify the propellant weight. (3.2.2.2.2)

BQ. Certify the loaded RSRM center of gravity for the longitudinal (X) axis. (3.2.2.2.3)

BR. Certify the reliability of the RSRM design. (3.2.3)

BS. Certify that the primary structure, thermal protection and pressure vessels meet design safety factors. (3.2.3.1)

BT. Certify that the RSRM segments are capable of horizontal assembly/disassembly. (3.2.5.1)

BU. Certify that the shedding of external debris is precluded. (3.2.6.5)

BV. Certify the performance at lower temperature limit. (3.2.7.1.a2)

BW. Certify that structural and electrical bonding meet the requirements in all areas except the area of lightning protection. (3.3.5.2)

BX. Certify that static electricity and lightning protection meets the requirements. (3.3.5.5)

BY. Gather data to validate the analytical model which certifies the general structural safety factors for the nozzle. (3.3.6.1.1.1)

BZ. Certify structural minimum safety factor for the adhesive bond for DFI/OFI/GEI. (3.3.6.1.1.2.b)

CA. Certify the thermal erosion minimum safety factor for case internal insulation. (3.3.6.1.2.2)

CB. Certify the thermal erosion minimum safety factor for the case internal insulation adjacent to metal part field joints and extending over factory joints. (3.3.6.1.2.3)

CC. Certify the thermal erosion minimum safety factor for the case internal insulation sandwich construction regions (aft dome and center segment aft end). (3.3.6.1.2.4)

CD. Certify the insulation performance. (3.3.6.1.2.6)

CE. Certify the thermal minimum safety factors for the nozzle. (3.3.6.1.2.7)

CF. Certify the nozzle performance margin of safety. (3.3.6.1.2.8)

CG. Certify that the RSRM design minimizes the need for new on-plant logistics facilities, and that existing facilities and facility equipment are used for the storage of spares and maintenance functions to the maximum possible extent. (3.4.3)

Process Qualification Objectives

CH. Qualify the installation of the systems tunnel floor plate by paint stripper surface preparation.

CI. Qualify higher pre-load and torque values for case-to-nozzle axial and radial bolts.

Vendor Qualification Objective

CJ. Qualify Fiberite carbon phenolic material in the three nose inlet rings and in the throat ring.

Development Objectives

CK. Acquire engineering data for model validation.

CL. Measure joint gap opening in nozzle internal joints.

CM. Evaluate Nozzle Joint No. 2 bonding process change.

CN. Assess capability of the RSRM to structurally withstand the side loads provided by MSFC and defined in the test plan.

CO. Obtain data on chamber pressure oscillations and compare to the RSRM and HPM data base.

Other Test Objectives

CP. Demonstrate that the Outer Boot Ring (OBR) shows:

1. No evidence of hot gas erosion inside the flex boot cavity except that produced by the vent holes.

2. OBR hoop continuity through the beginning of motor pressure tail off.

Qualification of Adjustable Vent Port Plug Installation Fixture

The adjustable vent port plug installation tool test objectives, derived from objectives in TWR-15723, Rev C, to satisfy the requirements of Specification, CDW2-3679, dated 26 May 1988, are listed below. The specific paragraphs from the CEI are listed with the objectives.

CQ. Certify the performance of the Adjustable Vent Port Plug Installation Tool as a means of installing, rotating, and torquing the bottom section of the adjustable vent port plug. (3.2.1.1)

CR. Certify that the installation fixture is efficient and does not require special and additional tooling. (3.2.1.1)

Qualification of Adjustable Vent Port Plug Installation Fixture (Cont)

CS. Certify that the use of the vent port plug installation tool does not affect the safe and reliable use and reusability of the RSRM. (3.2.1.1)

CT. Certify that the tool allows for a threaded installation to the bottom section of the adjustable vent port plug. (3.2.1.2.1)

CU. Certify that interlocking allows for rotation and torquing of the bottom section of the adjustable vent port plug. (3.2.1.2.2)

CV. Certify the capability of interlocking the installed installation tool with the bottom section of the adjustable vent port plug, and the utilization of the notch in the bottom section of the adjustable vent port plug. (3.2.1.2.2)

CW. Certify that the tool is capable of applying a minimum torquing force of 70 inch pounds to the bottom section of the adjustable vent port plug. (3.2.1.2.4)

CX. Demonstrate that the tool is capable of being transported to the work site. (3.2.8)

3

EXECUTIVE SUMMARY

3.1 SUMMARY

All of the objectives that can be addressed to date have been met. All inspection and instrumentation data indicate that the QM-8 static test firing was successful. Data was gathered at instrumented locations during pretest, test, and post-test operations. Dimensional measurements were taken before and after static testing to document insulation performance. The information assembled from the test procedures has supplied valuable knowledge and understanding about the cold environment performance of the RSRM design components utilized in QM-8. This test validates the lower end of the launch commit criteria (LCC) for flight motors (Tables 3.1-1 and 3.1-2).

PRE-TEST INSPECTIONS AND EVENTS

QM-8 Full-Bore Inspection

The full-bore inspection was performed when the bore temperature was very close to 40°F and the building temperature was 30°F. This was the coldest motor ever inspected in the history of the program.

No propellant cracks or tears were observed in the aft, center, or forward segments. The slight variations of the smooth bore surfaces due to core skinning and Teflon touchup were evident. If any propellant cracks had developed due to the combined thermal cooldown and horizontal slump loading, they would have been highly visible.

Between segment slot width measurements were taken at the bore and compared to analysis. Results indicate that the effective propellant properties need to be investigated further.

The J-joint slot was also inspected for gaps; there was no indication of noncontact of the J-leg against the clevis insulation.

Pressurization gaps in the vertically stacked position were evaluated for the center segments at 90°, 75°, and 40°F propellant mean bulk temperature (PMBT). These analysis can be used to predict the change in gap size due to temperature change. Over a 32°F PMBT range, the predicted change in pressurization gap is 0.070 inch. The measured change averaged over all degree locations for the joints is 0.086 inch. There is a difference of 18.6 percent between measured and predicted values, indicating that the CTLE is low.

Table 3.1-1. QM-8 Static Test Commit Criteria Summary

Criterion	Time Period	Minimum	Maximum	QM-8 Minimum/Maximum
S&A Device Safed	T - 6 hr to T - 5 min	Safe on	Arm off	Safe on until T - 45 sec
S&A Device Armed	T - 5 min to ignition CMD	Safe off	Arm on	Arm S&A at T - 45 sec
Chamber Pressure	T - 1.5 hr to T - 31 sec	5 psia	37 psia	Verified at final day run
Igniter Joint Temperature	T - 6 hr to T - 9 min*	66°F	123°F	74°/75.5°F
Field Joint Temperature	T - 6 hr to T - 5 min**	85°F	122°F	85°/106°F
Case-to-Nozzle Joint Temperature	T - 6 hr to T - 5 min**	75°F	115°F	78°/84°F
Nozzle Bondline Temperature	T - 6 hr to T - 9 min**	NA	115°F	75°F maximum
Case Temperature	T - 6 hr to T - 9 min	35°F	NA	29°/65°F
Flex Bearing Temperature (OMRSD)	85 hr to T - 6 hr***	60°F	115°F	73°/80°F

Note: Per Launch Commit Document (NSTS 16007 Rev D)

*Igniter heater turned off at T - 4 hr per RCN 8756 approved 23 Feb 1989
**Expires prior to S&A device armed
***Initial flex bearing mean bulk temperature is calculated from the previous two week GEI temperature data. Case-to-nozzle joint temperature requirements ensure the flex bearing will remain within its specified temperature range from T - 6 hr to T - 5 min

Table 3.1-2. QM-8 Static Fire Temperature Constraints

Component	Temperature Requirement At Component (°F)	Temperature Requirement At Sensor (setpoint) (°F)	Instrumentation	Actual Temperature (°F) Minimum	Actual Temperature (°F) Maximum
Ignition System Gask-O-Seals	64 to 130	75 to 123 (78 ±1)	T875 - T878	74	75.5
Field Joint Seals	75 to 130	85 to 122 (86 ±1)	T1001 - T1012	85 85 87	101 106 106
Case-to-Nozzle Joint Seals	75 to 130	75 to 115*	T807 - T809	78	84
Flex Bearing	60 minimum		T816 - T818	73	80
Case Skin Acreage	20 minimum	20 minimum**	58 gages total	29***	65
Tunnel Bondline	20 minimum	20 minimum**	T160 - T161	31	35
PMBT	40	40**	Calculated	40.2	

*Controlled by aft end heating. Recirculated hot air at 110° to 115°F until TVC on-motor duty cycle, then drop to 80° to 85°F until T - 0

**Controlled by test bay cold conditioning at 20° to 25°F. Ambient temperature at T - 0 was 28°F

***Based on data available before QM-8 test, a minimum case skin temperature of 20°F was acceptable

S&A Checks

A prefire dry run of the S&A arming procedure demonstrated the capability of the unit to cycle in the safe and arm directions. For the full-motor firing the unit cannot be cycled back to the safe position after the motor has fired. Pretest results of voltage and cycling times will be presented in TWR-17591, Vol VI.

Aft Segment Changeout

The aft segment originally designated for QM-8 (nozzle excluded) was used to replace the Flight-4B aft segment, which was found to have excessive insulation unbonds in the aft dome region. Because of the changeout, no girth gages were installed on the factory joint. All other instrumentation was unchanged.

Nozzle Overextension. During pretest setup, the QM-8 nozzle was inadvertently vectored in the wrong direction and too far. A propellant bore inspection was performed to determine if the propellant had been hit by the OBR and if the boot ring had been damaged.

A visual inspection using a high-intensity Jet-light revealed some circumferentially-oriented scuffing marks left by propellant cleanup. There were no propellant marks longitudinally oriented due to nozzle vectoring. The inspection also revealed no damage to the OBR (DR 16874).

Joint Heater Pretest. A test of the joint heater was performed according to CTP-0060, Rev D. Actual test data can be seen in Figure 3.1-1 with the corresponding predicted heater response. The predicted sensor response time of 2.33 hr matched closely the actual sensor response where a 91°F temperature was reached in 2.42 hr. Actual and predicted cooldown rates also compared closely during the first 0.5 hr following heater shutoff, indicating that a heat transfer coefficient of 2.0 can be used in an enclosed building where there is some air circulation. The cooldown results also imply that the 5-minute and 1-minute cooldown values, as found in the Launch Commit Criteria Redline Justification, are accurate with the assumption that the NASA Large Cylinder Heat Transfer Coefficient Equation is also accurate.

Igniter Heater. Igniter heater checks were in progress on QM-8. The primary element checked out satisfactorily so the power was switched to the redundant element. Shortly thereafter, sparks were observed coming from the power leads. Power was shut off immediately. A heater short was later identified.

In the future, the igniter heater will have additional vendor acceptance tests and the heater circuits will have a fuse and GFI (ground fault interrupter) installed.

Calibration of P8, P9, and P10 Load Cells. The Contractor Operations Review (COR) audit revealed that the load cells used on the side load fixture for the QM-8 static test had exceeded the normal recalibration date of one year.

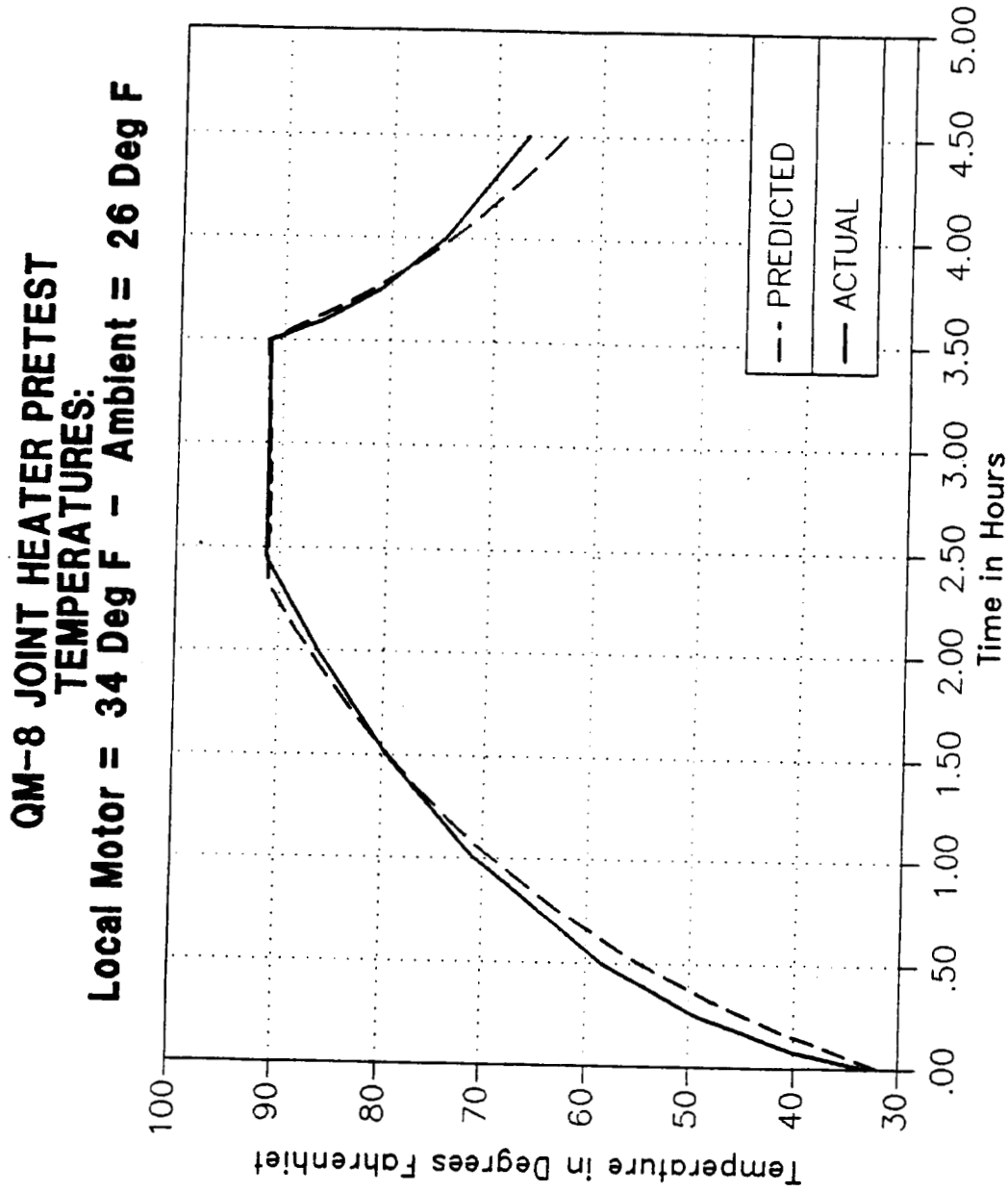

Figure 3.1-1. QM-8 Joint Heater

Due to the electrical and mechanical complexity of the side load system, Project and Test Engineering had not intended to recalibrate between QM-7 and QM-8 as long as the system was repeatable. Proper authorization should have been obtained before the QM-8 test, but was not.

QM-7 pretest data was compared to RM-1 to verify the integrity and repeatability prior to the QM-7 test. QM-8 pretest data before and during cold conditioning was compared to QM-7 to verify the data. The data has been very repeatable, indicating that not only the load cells, but the complete system has been functioning properly.

In the future, the calibration verification system will be changed to ensure that all transducers have a valid calibration prior to static test.

T - 0 Reference Anomaly

The current pulse meant to trigger the T - 0 detection circuit was not long enough, resulting in the loss of the T - 0 signal. This caused data reduction delays and data timing problems. Ignition time was estimated by correlation to the side load actuators. The backup system is being modified to retrieve T - 0.

POST-TEST INSPECTION RESULTS

3.1.1 Case Performance

No anomalies associated with case or joint hardware occurred in the QM-8 static test. Assembly procedures proved adequate, and valuable motor structural response data was gathered during the test. Chamber pressure was contained, and joint gap openings were restrained well under the maximum allowable values. No local yielding was measured. TWR-17591, Vol II, will contain a complete discussion of case performance including a discussion on the data from the instrumented bolts used at the stiffener rings.

3.1.1.1 Field Joints. All results were as expected. The radial growth compared very closely to that on other static tests. The greatest value occurred on the forward field joint, and had a value of 0.175 in. (Table 3.1.1.1-1). No fretting was observed at the field joints during inspection. Interference fit as calculated is shown in Table 3.1.1.1-2.

Forward Field Joint. The overall condition of the joint was excellent. No corrosion was found on either the tang or clevis. The V_2 volume filler was in a nominal condition. Typical metal pinhole slivers were found in the following pinholes in the bottom of the inner clevis leg: 52, 54, 58, 60, 62, 232, 282, 286, 288, 290, and 292. No other metal damage was found in the joint.

Small thin lines of a white material, suspected to be Teflon tape, were found on the CF metal-to-J-leg interface (aft of the CF groove on the tang J-leg) at 153, 178, 180, 227, 228, and from 230 to 233 deg. On the clevis, the white material was found on the top of the J-leg (near the inner clevis leg metal) at 138, 150, 152, 178, 180, and from 162 to 165, 167 to 170, 230 to 234,

Table 3.1.1.1-1. Forward Field Joint and Center Field Joint Radial Growth Comparisons to QM-8

Forward Field Girths													Joint Pressure (psig) = 847
		Strain		STS-27		STS-26		Radial Growth (in.)					
Loc	Gage	QM-8 (μin./in.)	QM-8 (in.)	Right	Left	Right	Left	PV-1	QM-7	QM-6	DM-9	DM-8	Pred
1	R303	ND	ND	ND	ND	ND	ND	ND	0.186	0.155	0.156	0.162	0.158
2	S677	ND	ND	ND	0.150	ND	0.191	ND	0.143	0.135	0.150	0.145	0.145
3*	S965	2150	0.157	ND	0.166	ND	0.168	ND	0.161	0.158	ND	0.159	0.148
4	S621	2400	0.175	0.180	0.178	ND	0.184	ND	0.178	0.178	0.170	0.181	0.183
Center Field Girths													Joint Pressure (psig) = 823
1	R304	2100	0.154	ND	ND	ND	ND	ND	ND	ND	0.156	0.162	0.153
2	S682	1850	0.136	0.137	0.142	ND	0.143	ND	0.142	0.134	0.152	0.143	0.141
3*	S966	2050	0.151	ND	0.159	0.161	ND	0.157	0.158	0.152	0.137	0.158	0.143
4	S635	2300	0.168	0.167	0.169	ND	ND	0.176	0.174	0.170	0.168	0.179	0.178

Notes: All test radial growths are ratios of STS-27 test pressure
ND = No data
DM-8 is 0.33 in. more forward than the other motors

Table 3.1.1.1-2. QM-8 Joint Summary

Joint	Gap (in.)*	Shim Size	Interference (radial) Pi-Tape	Interference (radial) PMD
Forward Field	0.023	-13	0.014	0.004
Center Field	0.023	-12	0.008	0.005
Aft Field	0.030	-14	0.014	0.015

Note: All leak check ports were inspected by eddy current technique
Aft dome threaded holes inspected for cracks by eddy current

*All joint calculations based on STW7-3480, Rev A

and from 252 to 254 deg. The Teflon tape is used to mask the J-leg during grease application and O-ring installation.

Center Field Joint. No corrosion was found on either the tang or clevis, with the exception of what appeared to be a very light thin line of corrosion which crossed the landing between the O-ring grooves at 134 deg. The V_2 filler was nominal. There was no joint metal damage observed. A metal pinhole sliver was found in the 268 deg pinhole, which is a common occurrence.

Aft Field Joint. No corrosion was found on either the tang or clevis. The pinhole at 136 deg contained a small metal sliver which fell on the aft face of the secondary O-ring during joint disassembly operations. Otherwise, no apparent metal damage was found during the inspection.

3.1.1.2 Case-to-Nozzle Joint. No corrosion or metal damage was found. Case-to-nozzle joint radial growth comparisons are shown in Table 3.1.1.2-1.

3.1.1.2.1 Qualification of Case-to-Nozzle Joint Bolt Preloads.

Introduction

A major objective of the QM-8 test was to qualify the case-to-nozzle joint radial and axial bolts at the originally designed preload levels. This situation arose from incorrect ultrasonic calibration factors being used in previous static motor assemblies, resulting in the actual bolt preloads being lower than measured. Accordingly, new calibration factors were determined, verified, and implemented into the ultrasonic bolt loading procedure; the higher and desirable preloads designed and analyzed. The lower preloads, which came from the erroneous ultrasonic calibration factors, and the original design (higher) preloads are listed in Table 3.1.1.2.1-1.

Since all static RSRM tests previous to QM-8 had been fired with the low preloads, a decision was made to continue preloading flight motors to these low levels until the higher levels could be qualified. QM-8 was designated as the motor to do that.

With the higher preloads and the difficulty of determining an exact relationship between the required torque and desired preload, high torques particularly in the axial bolts, can occur. In order to safeguard against high assembly stresses resulting from a combination of torque and preload, a torque limitation was imposed on the radial and axial bolts. This limitation is stated such that the bolts are loaded to either the preload range or the torque limit, whichever is reached first. The torque limits, determined to protect against high (more than yield strength) stresses, are listed in Table 3.1.1.2.1-2.

Conclusions/Recommendations

The QM-8 case-to-nozzle joint radial and axial bolts performed as expected. No assembly problems were encountered. Only 4 percent of the axial bolts failed to meet the low end of the preload

Table 3.1.1.2-1. Case-to-Nozzle Joint Radial Growth Comparisons to QM-8

Forward Field Girths

Joint Pressure (psig) = 807

		Strain		STS-27		STS-26		Radial Growth (in.)					
Loc	Gage	QM-8 (μin./in.)	QM-8 (in.)	Right	Left	Right	Left	PV-1	QM-7	QM-6	DM-9	DM-8	Pred
1	S880	1180	0.059	0.060	0.061	ND	0.052	0.088	0.068	0.082	0.073	ND	0.076
2	S874	1600	0.088	0.066	0.064	0.074	0.071	0.085	0.087	0.087	0.087	0.091	0.078

Notes: All test radial growths are ratios of STS-27 test pressure
ND = No data

Table 3.1.1.2.1-1. Low Preloads and Higher (design) Preloads

	Low Preloads (kips)	High Preloads (kips)
Axial Bolts	95.5 ±10	140 ±14
Radial Bolts	39.8 ±3.8	45 ±4.5
Radial Bolt (-01)	31.1 ±3.0	35 ±3.5

Table 3.1.1.2.1-2. Maximum Torque Allowed

Axial Bolts	3,000 ft-lb
Radial Bolts	750 ft-lb

range as a result of first reaching the torque limitation. Of these, the lowest preload was 110 kips. All of the radial bolts easily achieved preload without first reaching the torque limit. Test data correlated well with analysis. It is recommended that the current case-to-nozzle preloads being used for flight be revised to reflect the higher preloads which were qualified on QM-8. This recommendation, however, is contingent upon the ultrasonics being capable of consistently producing repeatable measurements.

Ultrasonic Bolt Results

Axial Bolts. Ninety-two axial bolts were ultrasonically loaded to the higher preloads. Of these 92 bolts, only 4 failed to reach the lower end of the preload range as a result of first reaching the maximum torque. The loads in these bolts at 3,000 ft-lb of torque were 110.9, 116.6, 122.2, and 122.2 kips. These bolts were single occurrences (i.e., adjacent bolts were within the preload range). An analysis is currently being run to investigate the effects of a single, low axial bolt preload. The results will most likely show a much less severe effect on gap opening than did an analysis performed which simulated all bolts at the low preload.

The average torque and standard deviation to achieve preload was 2,478 ft-lb and 307 ft-lb, respectively. Assuming a normal distribution, statistics tells us that approximately 95 percent of the bolts will reach preload between a torque of 1,864 and 3,092 ft-lb. This range reflects a two sigma and was selected because of the torque limit. With the torque limitation of 3,000 ft-lb imposed, the percentage decreases slightly. Ninety-two percent of the axial ultrasonic bolts reached preload within the above limits; but more importantly, 96 percent of the bolts reached preload prior to meeting the torque limitation requirement. Of the 4 percent which did not meet the minimum preload requirement, the lowest preload was still greater than the current maximum flight preload requirement.

With the higher preload requirement, a 2.0 tracking factor at 75°F can be met based on WOW dimensions. Even with a small number of bolts not reaching the minimum preload, a lower than current possibility of hardware selection restraints exists. Currently, and even with the higher preloads, when bolts fail to meet the minimum preload level, actual hardware dimensions must be used to ensure that the required squeeze is met. These measurements are frequently not available for analysis until after the assembly has been made. By going to the higher preloads, the possibility of not meeting the minimum required squeeze is reduced, if not eliminated.

Post-test ultrasonic loads were measured for comparison to original preloads. Previous applications have shown several disconcerting load differences between pre and post-test measurements. The range between QM-8 pretest and post-test ultrasonic measurements was -25.6 to 22.2 kips with an average of -2.6 kips (negative indicates load loss) and a standard deviation of 6.8 kips. The post-test measurements were questionable; however, due to a cal-bar being used

rather than the cal-bolt. As a result, a calculated load had to be subtracted from the measured load to arrive at the correct load.

Breakaway torques were also measured for comparison to assembly torques. These showed very close comparison. The percentage of breakaway torque to assembly torque was representative of that seen in the NJES-H3 burst cycle, which was also preloaded to the higher levels. The assembly torque ranged from 1,800 to 3,000 ft-lb, with an average of 2,478 ft-lb. The breakaway torque ranged from 1,169 to 3,197 ft-lb, with an average of 2,437 ft-lb.

Radial Bolts. Ninety-two radial bolts were ultrasonically preloaded to the higher preloads. All bolts met the preload requirement prior to the torque limit.

Post-test ultrasonic loads and breakaway torques were measured. As was the case with the axial bolts, a small load had to be subtracted from the measured load to compensate for the difference between using the cal-bolt and cal-bar. This makes the post-test measurements somewhat suspect. The pre and post-test ultrasonic readings differed in the range of -10.4 to 1.8 kips, with an average of -2.8 kips. These results indicate very little, if any, load is lost as a result of pressurization.

Assembly and breakaway torques correlated closely. The torque required to achieve preload ranged from 350 to 575 ft-lb, with an average of 438 ft-lb. The breakaway torques ranged from 320 to 580 ft-lb, and averaged 436 ft-lb. These results indicate insignificant load loss due to pressurization. Again, with the higher preloads, the 2X tracking factor at 75°F requirement can be met with WOW dimensions, whereas with the lower preloads this is not the case.

Strainsert Bolt Results

Axial Strainserts. Eight axial strainsert bolts were monitored during the test. Seven of these bolts made the preload requirement prior to the torque limit. These bolts are loaded using a minidas computer which reads cards with eight channels per card. Each strainsert requires one channel. The bolt which did not meet preload requirement was on the eighth channel. It was later hypothesized by test personnel that the eighth channel on the card was erroneous since when the bolts were connected to the Data Acquisition System (DAS) in the test bay, which was believed to be reading the correct load, the preload was within limits (103 kips versus 139 kips). Of the other 7 strainserts, an average relaxation of -7.8 kips occurred between assembly and T-0. This data agreed closely with previous static motor strainserts.

The average change in load at maximum headend pressure was -8.9 kips, as compared to a predicted change of -9.1 kips (Table 3.1.1.2.1-3). This shows that at the higher preload levels, the bolt loads are less than during preload only. Also observed from the data plots, was that the loads return to or very near the preload after firing.

Table 3.1.1.2.1-3. Fixed Housing, Aft Dome (strainsert, radial and axial readings)

Loc	Gage	Angular Loc	Preload Stress (ksi)	Preload Load (kip)	0 to 1 sec Meas Stress (ksi)	0 to 1 sec Meas Load (kip)	12 to 22 sec Meas Stress (kip)	12 to 22 sec Meas Load (kip)	120 to 130 sec Meas Stress (kip)	120 to 130 sec Meas Load (kip)	Anal Preload (kip)	at 920 psig Anal Load (kip)
Radial	R150	358.2	78.6	40.0	75.2	38.3	75.6	38.5	77.0	39.2	46	44
Radial	R151	45.0	85.4	43.5	80.9	41.2	80.7	41.1	84.4	42.9	46	44
Radial	R152	88.2	81.2	41.3	75.3	38.4	75.9	38.6	80.3	40.9	46	44
Radial	R153	135.0	81.9	41.7	76.9	39.1	76.2	38.8	80.0	40.7	46	44
Radial	R154	178.2	80.9	41.2	72.8	37.0	75.2	38.3	82.0	41.7	46	44
Radial	R155	225.0	80.4	40.9	73.6	37.5	75.2	38.3	80.0	40.7	46	44
Radial	R156	268.2	81.0	41.2	72.7	37.0	73.6	37.4	80.8	41.1	46	44
Radial	R157	315.0	107.7	54.9	98.7	50.2	98.1	49.9	107.8	54.9	46	44
Axial	S397	0.0	98.7	129.7	90.7	119.2	91.1	119.8	100.1	131.7	140.0	130.9
Axial	S401	46.8	96.6	127.0	89.6	117.8	89.0	117.0	96.1	126.4	140.0	130.9
Axial	S398	90.0	94.6	124.4	88.2	115.9	87.4	114.9	94.1	123.8	140.0	130.9
Axial	S399	180.0	94.2	123.9	87.2	114.6	87.1	114.6	94.5	124.3	140.0	130.9
Axial	S400	270.0	94.6	124.4	87.5	115.1	87.1	114.6	94.4	124.1	140.0	130.9
Axial	S402	136.8	93.2	122.6	86.3	113.6	86.5	113.7	94.2	123.9	140.0	130.9
Axial	S403	226.8	98.1	129.1	91.7	120.6	91.5	120.3	97.2	127.8	140.0	130.9
Axial	S404	316.8	105.8	139.2	99.6	131.0	99.0	130.2	104.9	138.0	140.0	130.9

Description: Radial--Sta 1874.3, Axial--Sta 1875.2
Time range: 0.0 to 120.0 sec

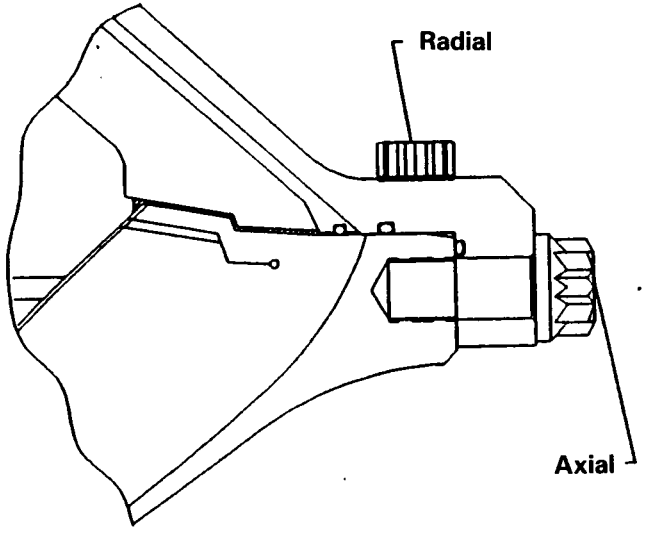

89605-8.12

Radial Strainserts. Eight radial strainsert bolts were monitored during the test. Again, the eighth channel on the minidas card was reading low. R157, was the strainsert using this channel, took 600 ft-lb to reach 40.5 kips, while the remaining seven required from 400 to 500 ft-lb to achieve preload. Upon hookup to the test bay DAS, this bolt was found to have a preload of 55 kips. Of the remaining seven, an average relaxation occurred between assembly and T-0 of -0.4 kips. This relaxation agreed with data from previous motor strainserts.

The average change in load at maximum headend pressure was -2.8 kips as compared to a predicted change of -1.8 kips (Table 3.1.1.2.1-3). Also, upon completion of the test, the loads returned to or very near the preloads.

3.1.1.3 Internal Nozzle Joints

Aft Exit Cone-to-Forward Exit Cone (Joint 1). No anomalous conditions were encountered. The grease application was per design with no areas of corrosion found.

Forward End Ring-to-Nose Inlet Housing (Joint 2). The sealing surfaces suffered no assembly/disassembly damage.

Nose Inlet Housing-to-Throat Support Housing (Joint 3). The sealing surfaces showed no assembly/disassembly damage. The joint showed no signs of heat effect (heat-effected grease or soot).

Forward Exit Cone-to-Throat Support Housing (Joint 4). The sealing surfaces showed no assembly/disassembly damage.

Fixed Housing-to-Aft End Ring (Joint 5). The joint showed no signs of heat effect (heat-effected grease or soot). The sealing surfaces showed no damage.

3.1.1.4 Igniter Adapter-to-Forward Dome Joint. No erosion or joint contamination was found upon inspection of the sealing surfaces.

3.1.2 Case Internal Insulation Performance

TWR-17591, Vol III, will contain a detailed description of the insulation test results.

3.1.2.1 Case-to-Case Field Joints. The insulation performance in all three of the redesigned case field joints was excellent. The joint bondline for all three case field joints appeared to have made contact for the full circumference as evidenced by the postfire indication of pressure-sensitive adhesive contact. There was a region of questionable contact on the forward field joint tang tip shown by glossy pressure-sensitive adhesive; however, this was liquefied adhesive due to post-test heat soak and was not considered a problem. There was no evidence of circumferential flow or hot gas penetration (i.e. sooting and charring) into the field joints beyond the nominal expected char and erosion. The field joint capture feature (CF) O-rings, primary O-rings, and secondary

O-rings showed no evidence of heat effect or erosion. Crazing was observed in all field joints. TWR-17591, Vol III, will include details.

3.1.2.2 Case-to-Case Factory Joints. An internal walk-through was performed at the demate of the aft field joint. No abnormal erosion, blistering, or other anomalous condition was observed on the factory joints or the internal acreage insulation. The slag pool was similar to that seen on previous static fire motors and was found to be 2,201 lbf.

3.1.2.3 Case-to-Nozzle Joint. The case-to-nozzle joint performance was excellent. No significant voids in the polysulfide adhesive were observed. No blowholes, soot, or gas paths were noted in the joint bondline. The case-to-nozzle joint wiper O-ring, primary O-ring, and secondary O-ring showed no evidence of heat effect or erosion.

3.1.2.4 External Insulation. There were no hotspots on the external case. The external water deluge system operated correctly on QM-8, as did the CO_2 forward and aft end quench systems. The external insulation over the factory joints was in place and performed as expected with no anomalous conditions.

3.1.3 Seals Component/Leak Check Performance

TWR-17591, Vol IV, will contain a complete description of seals component/leak check performance.

3.1.3.1 Field Joints

Forward Field Joint. No hot gas or soot was observed past the J-leg. There was no evidence of damage to the O-rings while in the grooves.

A 0.400 in. long thin line of white material, suspected to be adhesive from Teflon tape, was found on the aft edge of the CF O-ring at 169 deg. More thin lines of the same material were found intermittently on the aft edge from 164 to 167 deg. The Teflon tape is used to mask the J-leg during grease application and O-ring installation.

Center Field Joint. The overall condition of the joint was excellent. No hot gas or soot was observed past the J-leg. There was no evidence of damage to the O-rings while in the grooves.

Aft Field Joint. The condition of the joint was nominal. No hot gas or soot was observed past the J-leg. There was no evidence of damage to the O-rings while in the grooves.

A small amount of foreign material had fallen onto the joint during or after disassembly.

3.1.3.2 Case-to-Nozzle Joint. The overall condition of the joint was excellent. No pressure was seen between the primary and secondary O-rings, as shown by the pressure transducer (P000024) installed in the joint. No hot gas or soot was observed past the polysulfide. No O-ring damage was found during the in-groove inspection. A heavy rub mark was found on the primary O-ring at 354.6 deg. This occurred on disassembly because the radial bolt hole plug at 354.6 deg was in the

bottom of the bolthole. A heavy impact mark was found on the top of the plug. The plug appeared to be in this condition before disassembly.

Polysulfide got past the wiper O-ring through the vent slots 360 deg around the joint.

Flow lines were observed in the Stat-O-Seal which was installed under the radial bolts in the case-to-nozzle joint.

3.1.3.3 Igniter Adapter-to-Forward Dome Joint. The outer gasket was visually inspected at the time of disassembly. No soot was found on either side of the gasket retainer, but heavy soot deposits were found on the inside edge of the gasket, covering the entire circumference. A blowhole occurred through the igniter exterior putty at 15 deg. No soot was found to or past the primary seal.

3.1.3.4 Internal Nozzle Joints

Aft Exit Cone-to-Forward Exit Cone (Joint 1). There were no voids in the RTV which would allow pressure to reach the primary O-ring. There was no evidence of damage to the O-rings while in the grooves.

Forward End Ring-to-Nose Inlet Housing (Joint 2). The primary O-ring experienced pressure, but no apparent damage to the O-ring was found. One very small pressure path through the RTV of the joint interface was found. The pressure path started at 355 deg and flowed circumferentially to 350 deg before penetrating into the metal interface of the joint. The RTV backfill of this joint was much better than the current (buttering) application of RTV to this joint. No soot or evidence of blowby was present past the primary O-ring. No apparent damage to the primary or secondary O-rings was found during preliminary inspection.

Nose Inlet Housing-to-Throat Support Housing (Joint 3). There was no joint pressurization, and the O-rings had no apparent damage. The joint showed no signs of pressure past the RTV. The sealing surfaces showed no assembly/disassembly damage.

Forward Exit Cone-to-Throat Support Housing (Joint 4). The primary O-ring experienced pressure, but no damage to the O-ring was found. One pressure path through the RTV backfill was found at 205 deg. No damage to the primary or secondary O-rings was found during the in-groove inspection.

Fixed Housing-to-Aft End Ring (Joint 5). There was no joint pressurization as shown by the pressure transducer (P000030) installed in the joint. Detailed inspection of the O-rings revealed no damage. There were no signs of pressure past the RTV.

3.1.3.5 Factory Joints

Aft Segment Factory Joints. The condition of all three aft segment factory joints was nominal. The three joints had small areas of light to medium corrosion on the outer clevis leg. Scratches

were observed on the land between the O-ring grooves in each joint. The leak check port plugs had been removed in the post-fire inspection log so there were no break away torque values recorded or in-groove inspections of the leak check port plugs. The in groove inspection of the O-rings in each joint showed a nominal conditions.

All factory joint disassembly and evaluation is not complete. TWR-17591, Vol IV, will contain a complete discussion of factory joint seal performance.

3.1.3.6 Leak Test. Based on the satisfaction of all QM-8 objectives, it is concluded that all leak tests currently performed on the RSRM joints are certified for use on flight motors. These certification objectives were also satisfied during DM-9, QM-6, QM-7, and PV-1, except for the igniter inner gasket leak test, which was also certified on QM-7 and PV-1. No further conclusions or recommendations are reached. TWR-17591, Vol IV, will contain a description of leak check procedure test results.

3.1.3.7 O-ring Squeeze. TWR-18811 will document O-ring squeeze calculation and temperature requirement.

3.1.4 Nozzle Assembly Performance

Erosion of the QM-8 forward nozzle assembly and aft exit cone carbon-cloth phenolic (CCP) ablative liner was smooth and uniform. Preliminary inspection of the QM-8 forward nose ring, aft inlet ring, nose cap, and throat ring shows performance characteristics were as good or better than on previous RSRM nozzles. No unusual or abnormal erosion patterns were observed. While actual char and erosion measurements need to be taken, visual analysis supports qualification of Fiberite carbon-cloth phenolic for these rings (Test Objective CJ).

TWR-17591, Vol V, will contain a complete discussion of nozzle assembly performance, including data and hardware inspection from the nozzle boot cavity instrumentation.

3.1.4.1 Aft Exit Cone Assembly. The QM-8 aft exit cone was severed by an linear-shaped charge (LSC) aft of the compliance ring. The severed ends appeared cleanly cut, with no unusual tearing or breaking.

The aft exit cone liner erosion was nominal, showing no major washing, pocketing, or surface ply lifting. Postburn popped-up and wedged-out charred CCP material was observed on the forward 0.75 in. intermittently around the circumference.

The polysulfide on the forward end of the aft exit cone showed void areas along the inner diameter (ID) and outside diameter (OD) interfaces intermittently around the circumference. These are typical observations which occur on static test nozzles due to cooldown liner shrinkage. The polysulfide groove radial width measured a maximum of 0.30 in. (0.10 in. greater than pretest nominal). The polysulfide also shrank axially aft approximately 0.15 in., which is typically seen on all poststatic test and postflight aft exit cones.

Separations within the glass-cloth phenolic (GCP) were observed on the forward end of the aft exit cone from 19 to 33 deg (0.05 in. maximum radial separation), and 205 to 229 deg (0.10 in. maximum radial separation). No other bondline separations were observed on the forward end of the aft exit cone.

3.1.4.2 Forward Exit Cone Assembly. The QM-8 forward exit cone liner erosion was nominal showing no major washing or pocketing.

Visual inspection of the forward exit cone showed a dimpled erosion pattern located around the circumference and along the aft half of the cone. The erosion pattern measured a maximum of 0.15 in. deep radially. This is a typical observation which has occurred on all post-test and postflight forward exit cones. The forward half of the liner showed smooth erosion.

Bondline separations between the metal and EA946 adhesive were observed on the aft end of the forward exit cone circumferentially, except from 75 to 79, 198 to 205, and at 253 deg. These were typically 0.06 in. wide radially and extended more than 6 in. axially. The remainder of the circumference showed adhesive-to-GCP separations which measured between 0.03 to 0.06 in. wide radially.

The forward end of the forward exit cone showed metal-to-EA946 adhesive bondline separations around most of the circumference. These separations ranged from 0.02 to 0.04 in. wide radially and 0.25 to >6.0 in. deep axially. Separations were also observed within the EA946 adhesive intermittently around the circumference. These ranged from 0.03 to 0.06 in. wide radially and 0.25 to 2.0 in. deep axially.

3.1.4.3 Throat Assembly. Erosion of the throat and throat inlet rings was smooth and uniform. The flow surface bondline gap between the throat ring and throat inlet ring was 0.10 in., which is typical of past static test and flight nozzles. The throat postfired mean diameter was 55.88 in. (erosion rate of 8.1 mil/sec based on an action time of 125.0 sec). Nozzle postburn throat diameters have ranged from 55.787 to 56.38 inch.

The aft end of the throat ring showed no bondline separations.

The throat inlet ring forward end showed one bondline separation between the steel housing and EA913 NA adhesive at 285 deg (0.002 in. radial width).

3.1.4.4 Nose Inlet Assembly. The QM-8 nose inlet assembly liner eroded smoothly, with no visible pockets or wash areas. The aft inlet (-504) ring and forward nose (-503) ring showed no popped-up or wedged-out CCP. Postburn charred CCP plies popped up on the aft 2 in. of the nose cap intermittently around the nozzle circumference, but no material was missing. The flow surface bondline gap between the -504 ring and the -503 ring was 0.18 inches. The flow surface bondline gap between the -503 ring and the nose cap was 0.03 inches.

The -504 aft inlet ring aft end showed no bondline separations.

The nose cap flow surface showed smooth erosion, with no wedgeouts observed on the forward or aft ends. Typical popped-up charred CCP material was noted on the aft 2 in., from 21 to 39, 130 to 160, 203 to 223, 260 to 265, and 284 to 317 deg. No material was missing.

The nose cap aft end showed bondline separations between the metal and EA946 adhesive (typically 0.002 in. wide radially) and between the adhesive and GCP (0.001 to 0.003 in. wide radially).

3.1.4.5 Cowl Ring. The QM-8 cowl ring was completely intact. Typical ridged erosion was observed around the circumference. The forward end eroded approximately 0.2 in. more than the aft end. All cowl vent holes appeared plugged with slag on the OD of the ring. The flow surface bondline gap between the cowl ring and the nose cap was 0.10 in., which is typical of past static test and flight nozzles.

The forward end of the cowl showed bondline separations between the EA913 NA adhesive and silica-cloth phenolic (SCP) (0.001 to 0.003 in. wide radially) and separations within the adhesive (0.001 to 0.010 in. wide radially).

3.1.4.6 Outer Boot Ring. The structural backup OBR was intact. Typical wide delaminations were observed 360 deg circumferentially on the OBR aft end. The charred CCP aft tip adjacent to the flex boot appeared intact. The flow surface bondline gap between the OBR and cowl was 0.20 in., and is typical of past static test and flight nozzles.

3.1.4.7 Fixed Housing Insulation. Erosion was smooth and uniform, and appeared typical of previous motors. Light slag deposits evenly coated the aft 6 in. of the insulation. Typical delaminations of charred CCP were observed on the forward end intermittently around the circumference. There were no bondline separations observed at the inner boot ring-to-fixed housing interface or at the aft end of the fixed housing insulation.

3.1.4.8 Flex Boot. The cavity side of the flex boot showed no evidence of flow or erosion. It was uniformly sooted and charred, and appeared typical of previous flight and static test motors.

3.1.4.9 Bearing Protector. The QM-8 bearing protector was sooted along the entire length and circumference. Heavier soot and erosion were observed in line with the cowl ring vent holes at the thickened portion of the bearing protector. Three soft spots 0.3 in. in diameter were noted at 70, 72, and 75 deg, approximately 4 to 5 in. aft of the thick portion of the bearing protector. An apparent gouge (which was also soft) measuring 1.1 in. axial by 0.1 in. circumferential by 0.05 in. deep radially was observed in the rubber at 115 deg. The four areas were determined to be voids that had been repaired with RTV silicone rubber. The soft areas were localized to the OD surface, approximately 0.020 in. deep radially. The remainder of the RTV, below the surface, was not heat

effected. It appears that the RTV softens prior to ablation, versus the char layer formed on the parent silicone rubber material. There was no evidence of heat effect on the ID surface.

3.1.4.10 Nozzle Plug. A modified nozzle plug was installed on QM-8 to allow access for a bore inspection. The nozzle plug performed nominally after being subjected to the cold environment, bursting into multiple pieces at ignition. The largest chunk located following the test was approximately 6 by 8 by 12 in., and weighed 0.84 lb.

3.1.4.11 Nozzle Internal Joints. Post-test subassembly flow surface gaps are shown in Figure 3.1.4.11-1. All gaps were typical of previous static test and flight nozzles.

3.1.4.11.1 Aft Exit Cone-to-Forward Exit Cone Field Joint (Joint 1). The backfilled RTV extended below the joint char line 360 deg circumferentially, and reached the primary O-ring everywhere except from 0 to 60 deg. RTV also extended down the high-pressure side of the primary O-ring groove from 262 to 285, and 300 to 0 deg, but did not extend past the primary O-ring. There were no voids or blowpaths in the RTV, and the joint was free of soot. The primary O-ring did not see pressure, and showed no signs of assembly damage. Grease coverage was not excessive and did not inhibit the RTV backfill.

No metal damage was observed.

3.1.4.11.2 Throat Inlet-to-Forward Exit Cone Joint (Joint 4). The backfilled RTV extended below the joint char line circumferentially except at 205 deg. The RTV extended onto the radial OD portion of the joint from 56 to 109, 111 to 204, 206 to 261, 293 to 294, 296 to 299, and 301 to 304 deg. RTV reached up to the primary O-ring at 86 to 102, 120, 125, 132, 157.5 to 160, and 177 deg. Excessive grease was noted on the radial OD surfaces, inhibiting the RTV backfill.

One blowpath was observed at 205 deg, and measured 1.0 in. long circumferentially at the entrance. The blowpath extended from the flow surface, through the RTV, to an unfilled void area caused by excessive grease. No soot was observed at this location. There was no heat effect to the phenolic surfaces or the grease. The primary O-ring saw pressure, but showed no signs of blowby, erosion, or heat effect.

No metal damage was observed.

3.1.4.11.3 Nose Inlet-to-Throat Joint (Joint 3). The backfilled RTV extended below the joint char line 360 deg circumferentially. RTV extended to the axial portion of the bondline over approximately 30 percent of the circumference. There were no voids or blowpaths observed in the RTV, and the joint was free of soot. The primary O-ring did not see pressure, and showed no signs of assembly damage.

No metal damage was observed.

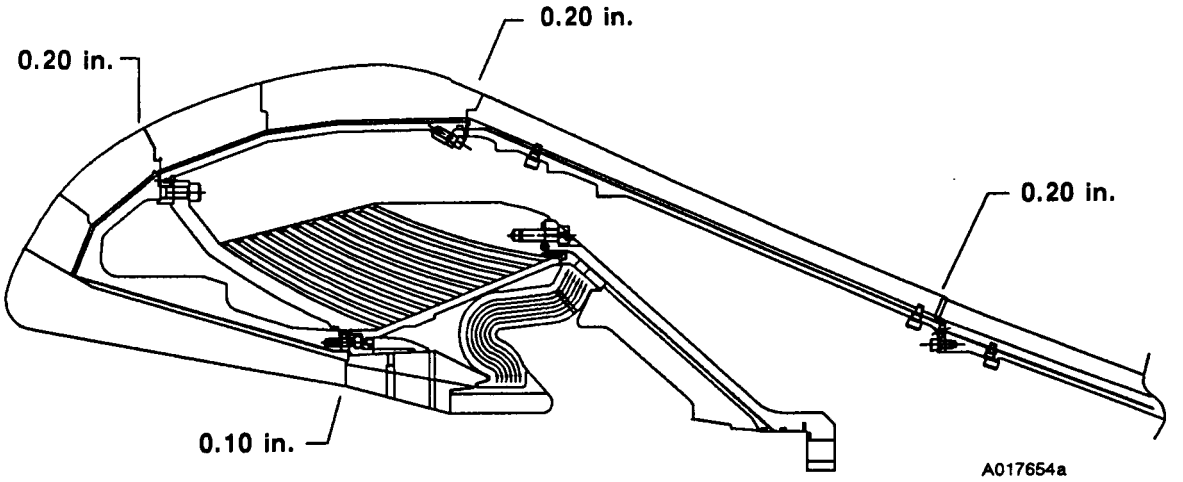

Figure 3.1.4.11-1. QM-8 Joint Flow Surface Gap Openings

3.1.4.11.4 Nose Cap-to-Forward End Ring-to-Cowl (Joint 2). The RTV backfill extended below the joint char line 360 deg circumferentially, and reached the axial portion of the joint circumferentially, except from 88 to 90 and at 99 deg, and extended onto the nose inlet housing from 342 to 54 deg and at 147 deg. Two blowpaths which extended cohesively through the RTV were observed. The first was at 226 deg, and measured 0.20 in. circumferentially by 0.80 in. radially. This blowpath terminated within the RTV. There was no erosion or heat effect to the phenolics. The primary O-ring did not see pressure at this location. The second blowpath occurred at 355 deg. Soot was observed on the RTV surfaces on both sides of the joint, and extended up to the boltholes on the nose inlet housing (aft face) and forward end ring (forward face) surfaces. There was no erosion or heat effect to the phenolics or metal surfaces. The primary O-ring saw pressure, but there were no signs of blowby, erosion, or heat effect. A discussion of the nozzle Joint 2 process change, as compared to PV-1, will be included in TWR-17591, Vol V.

3.1.4.11.5 Fixed Housing-to-Bearing Aft End Ring Joint (Joint 5). RTV filled the radial portion of the fixed housing-to-bearing aft end ring joint 360 deg circumferentially. The RTV extended to the high-pressure side of the primary O-ring groove at 35, 48, 140 to 150, 173 to 175, 240, 255, 270 to 275, and 290 deg. Small voids were observed isolated within the radial portion of the bondline at 135, 203 and 347 deg. The maximum void dimension was 0.70 in. circumferentially by 0.25 in. radially. There were no blowpaths or soot observed within the joint. The primary O-ring did not see pressure, and showed no signs of assembly damage.

No metal damage was observed.

3.1.4.12 Boot Cavity Pressure. The boot cavity was instrumented with two real-time pressure transducers, two thermocouples, and two JSC stand-alone pressure measuring devices (SAPMDs). The data from the real-time transducers indicated that one failed at approximately 5.6 to 5.8 sec, providing no data from thereon; the other showed a significant drop in pressure shortly after the first gage failed. The remaining gages indicated that cavity pressure was following nozzle stagnation pressure.

The SAPMDs were removed from the cavity, returned to JSC for interrogation, and the raw data provided to Morton Thiokol. When the data was plotted against nozzle stagnation, it indicated that there was a positive pressure in the cavity from about 126 sec to 144 to 148 sec.

3.1.4.13 Flex Bearing Performance. The QM-8 flex bearing appeared in good condition with no heat effect or other anomalies observed.

3.1.4.14 Nozzle Thrust Vector Control Performance. The TVC system appears to have performed as planned and followed the specified duty cycle well. (Figure 3.1.4.14-1)

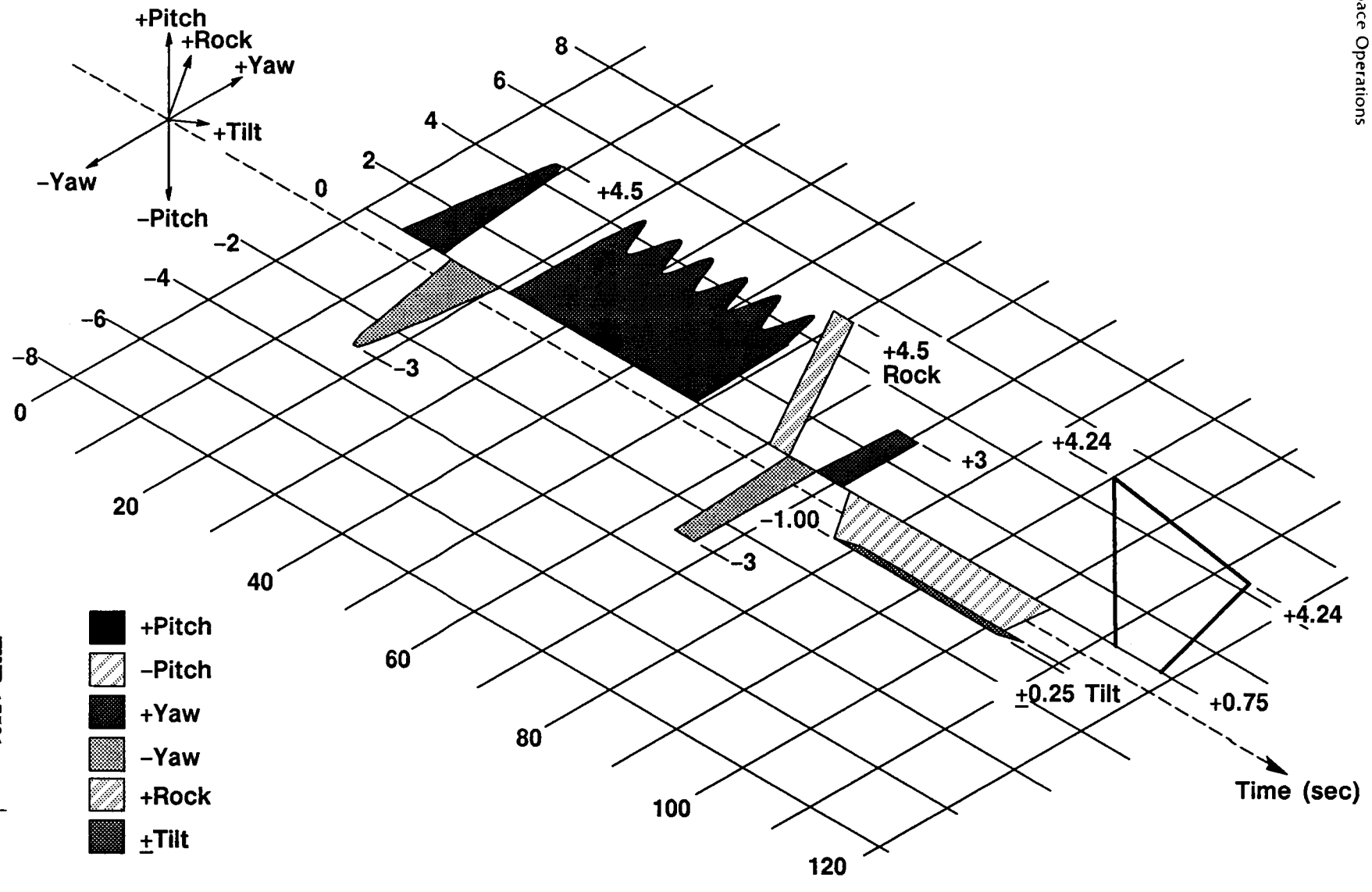

Figure 3.1.4.14-1. Nozzle Thrust Vector Control Performance

A015191a-1R1

3.1.4.15 Nozzle Composite Structures Performance. Evaluation is not complete and will be included in TWR-17591, Vol V, of this report.

3.1.4.16 Linear-Shaped Charge. The LSC performed nominally, even after being subjected to the cold environment.

3.1.5 Igniter Performance

Postfire inspection revealed no anomalies. Igniter performance was within specification limits (Figure 3.1.5-1). Thermocouples placed on the igniter grain (T000953 and T000954) showed that igniter PMBT tracked the main motor PMBT. Postfire inspection of the S&A device showed that the system performed as predicted with no anomalies. A detailed description of QM-8 igniter performance will be in
TWR-17591, Vol VI.

3.1.5.1 S&A Device. The S&A enabled the motor ignition sequence, as evidence by the successful firing. The S&A was separated from the QM-8 igniter during disassembly at T-97, demonstrating separability.

During the motor firing, the S&A provided simplex position indication to the control center, allowing continuation of the motor countdown.

3.1.5.2 Igniter Heater. Heater performance was nominal. The igniter heater, cork insulation, T-bolt latch band clamp, and heater power cables were intact and properly secured on the igniter adapter and forward dome with no anomalies noted. No discoloration, charring, buckling or warping of the heater was noted. There was a 0.30 in. air gap approximately 0.50 in. long between the heater and case at the location of the clamp buckle; however, no buckling or warping of the heater was noted. The heater will undergo additional vendor acceptance tests due to a short identified during pretest igniter heater checks.

3.1.6 Joint Protection System (JPS)/Factory Joint Weather Seal Performance

3.1.6.1 Heater Performance. The JPS system performed its intended function as designed and predicted without failure. All components of the JPS system remained bonded in place during the test, generating no debris.

A complete discussion of JPS performance will be included in TWR-17591, Vol VII.

Field Joint Temperatures. Field joint heaters maintained the temperature at the controlling resistance temperature devices (RTDs) at 86°F and maintained this temperature with a maximum deviation of +0.6° to -0.5°F. Figure 3.1.6.1-1 is a plot of the temperature of the controlling RTD of the three field joints. The drop in temperature at 0600 and 1000 hours was due to heater power shut-off. Figure 3.1.6.1-2 is a plot of the maximum differential temperature of the three joints. Pretest temperatures at the igniter-to-case joint sensors were a minimum of 77°F.

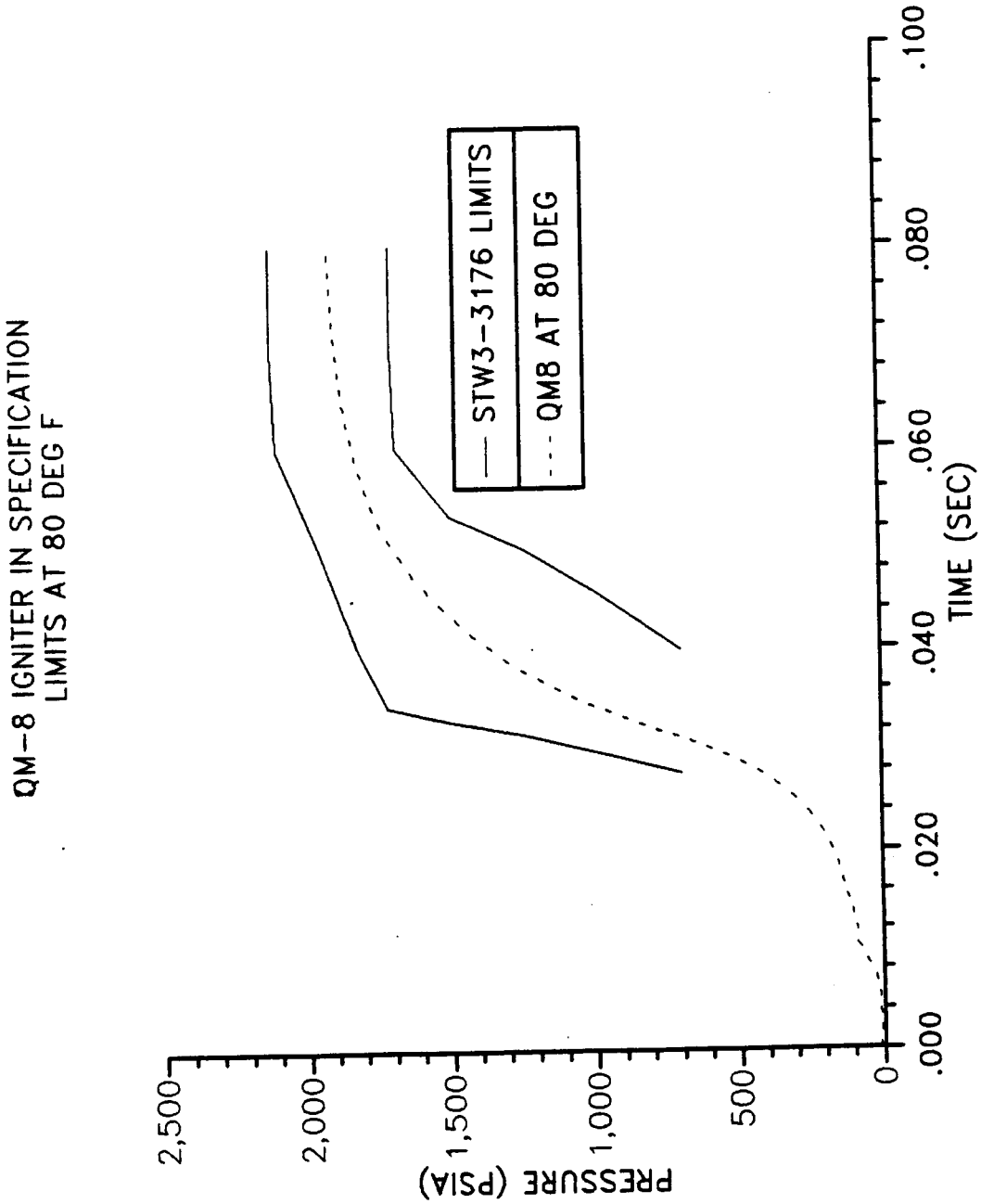

Figure 3.1.5-1. QM-8 Igniter

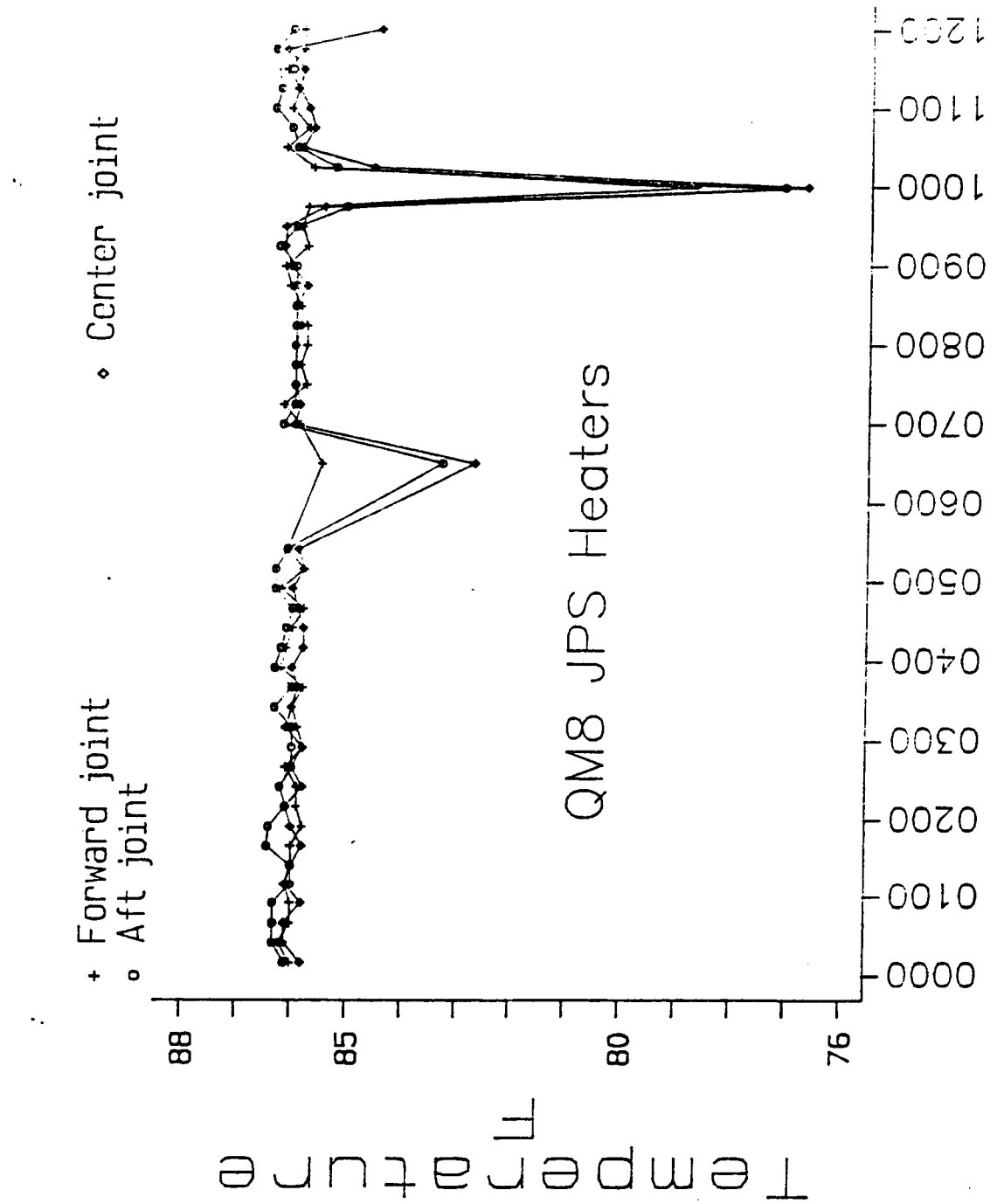

Figure 3.1.6.1-1. Temperature of Controlling RTD of the Field Joints

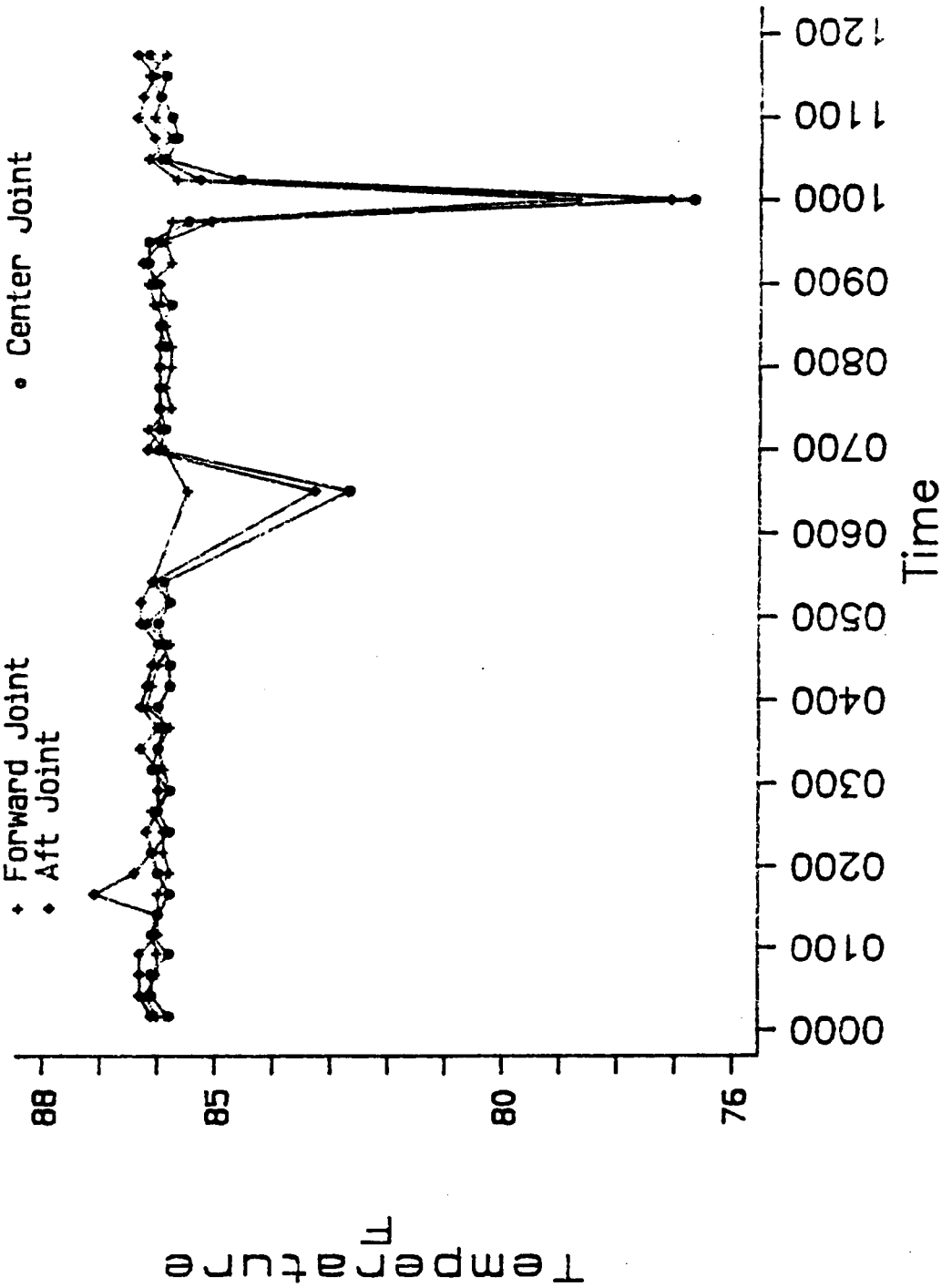

Figure 3.1.6.1-2. Maximum Differential Temperature of the Field Joints

3.1.6.2 Field Joint Protection System (FJPS)/Factory Joint Weather Seal. Post-test inspection revealed no anomalies related to the factory joint weather seal. The FJPS and factory joint weather seals performed as predicted. Inspection data was positive, and there was no evidence of seal integrity being compromised as a result of static test. All the cork appeared to be intact and bonded to the case. After the cork was stripped from the case on the joints, the bondlines were inspected for voids.

The case-to-cork bondline was free of any cracks, but areas of debond or voids were found under the cork external insulation on all three field joints. These had resulted from improper positioning of the cork during installation, and from insufficient adhesive. The improper positioning of the cork occurred with one piece of cork on the center joint. This cork was installed 0.5 in. forward of its intended position on the moisture seal, resulting in a long narrow void between the leading edge of the moisture seal and the cork. Some of the voids resulting from insufficient adhesive extended to the leading edge of the cork.

EDPM Moisture Seal-to-Cork Bondline. The cork was peeled off the moisture seal with considerable force. The peeled surfaced showed that the EA 934NA remained on the cork with small black EPDM particles embedded in the adhesive surface, indicating that EPDM-to-EA 934NA interface is the weaker of the bond surfaces.

Kevlar Strap-to-Cork Bondline. This bondline was difficult to peel back. In some areas, the EA 934NA was embedded in both the inside and outside straps, especially where the pin retainer band bolts lift the Kevlar strap and allow adhesive to flow underneath the band.

Moisture Seal Condition. The moisture seals showed no evidence of rips or tears in the areas where the pin retainer bolts contact the moisture seal. However, because of the excellent bond between the EA934 and the moisture seal, an occasional piece of the moisture seal was ripped up during disassembly.

Kevlar Strap Condition. The straps were fully intact. No evidence of fiber damage or adhesive cracking at the buckle interfaces was observed. The areas where the pin retainer bolts raise the strap showed no fiber distortion or breakage, and had adhesive underneath forming a smooth surface for the Kevlar strap to ride on.

Heater. The heaters showed no evidence of delamination, cracking, or overheating.

Sensor. The sensor assemblies could not be observed until after the cork insulation was removed. There were no anomalies, such as cracking, except those caused by the removal of the cork insulation.

Factory Joint Weather Seal. Post-test inspection was conducted before removal, and no evidence of damage was observed.

A moisture seal integrity test was not conducted, but the deluge system was run for 10 minutes without moisture penetrating the seals.

3.1.7 Systems Tunnel

Aluminum floor plate systems tunnel segments were installed on the forward three segments of QM-8. The forward and forward center segments were prepared by grit blasting. The aft center segment was prepared by use of a chemical paint stripper. Postfire inspection of the bondlines on each floor plate assembly showed no anomalies. Visual inspections, as well as a bondline probing, were performed. All bondlines were of good quality post-test. The installation of aluminum floor plate systems tunnel segments using the chemical paint-stripper process was successfully qualified.

A complete discussion of the systems tunnel will be included in TWR-17591, Vol VIII.

3.1.8 Instrumentation

All instrumentation-related test objectives were met. Instrumentation performed well with only a few exceptions. A detailed discussion is included in Section 5 of this report, and in TWR-17591, Vol IX.

3.1.9 Ballistics/Performance and Mass Properties

The QM-8 ballistic performance was typical of the RSRM design and within expected limits. This motor experience the lowest PMBT at 39°F of any SRM. The longer than normal ignition interval and lower rise rate indicates that the ignition of the motor is sensitive to the temperature of the propellant. Previous correlation studies between PMBT and ignition had shown only a weak correlation. The current Morton Thiokol-imposed lower limit on maximum pressure rise rate of 70.9 psi/10ms was not exceeded; however, it needs to be reassessed with the new data. Despite the unusual ignition values, the ignition interval and the maximum pressure rise rate met the CEI specification limits. The igniter performed successfully and as predicted.

The QM-8 ballistic performance compared closely with PV-1, QM-7, QM-6, DM-9 and DM-8 performance and HPM historical data. Thrust data was not measured for QM-8 because the broken load cells at the test bay (T-97) have not been replaced. All thrust and impulse data were reconstructed using past pressure to thrust conversion factors. Table 3.1.9-1 lists the predicted and reconstructed values for the performance of QM-8 against the CPW1-3600 Specification Table 2 values. All the values were within the limits. The QM-8 data was added to the appropriate population and applied to the thrust-time envelope and impulse gates and the CEI requirements were met. Figures 3.1.9-1 and 3.1.9-2 show the predicted values versus the measured headend pressure and reconstructed vacuum thrust values, respectively.

QM-8 slag weight has been measured, and the weight was found to be 2,201 lbf. The low PMBT may have increased the slag accumulation because of the lower operating pressure and longer burn time.

Table 3.1.9-1. QM-8 Performance Summary With CPW1-3600 CEI Specification Limits

	Vacuum Spec Limits (60°F)	QM-8 Predicted (60°F)	QM-8 Delivered (60°F)
Web Time (sec)	106.1 - 117.2	112.2	110.9
Action Time (sec)	115.4 - 131.4	124.0	122.3
MOP Head-End (psia)	858.7 - 978.1	908.5	904.1
Maximum Sea Level Thrust (Mlbf)	2.87 - 3.25	3.03	3.07
Web Time Average Head-End Pressure (psia)	625.8 - 695.8	656.4	666.2
Web Time Average Vacuum Thrust (Mlbf)	2.45 - 2.72	2.57	2.605
Web Time Total Impulse (Mlbf-sec)	286.1 - 291.8	288.5	288.9
Action Time Impulse (Mlbf-sec)	293.3 - 299.2	296.2	296.3
Average Delivered (lbf-sec/lbm)	265.3 - 269.0	268.2	268.2
I_{sp} Ignition Interval (sec), Time 563.5 psia	0.202 - 0.262	0.232	0.252
Maximum Pressure Rise Rate (psi/10-ms)	X < 115.9	91.8*	72.3

Loaded Propellant Weight of 1,105,399 lb

*Based on an average of 24 motor firings.

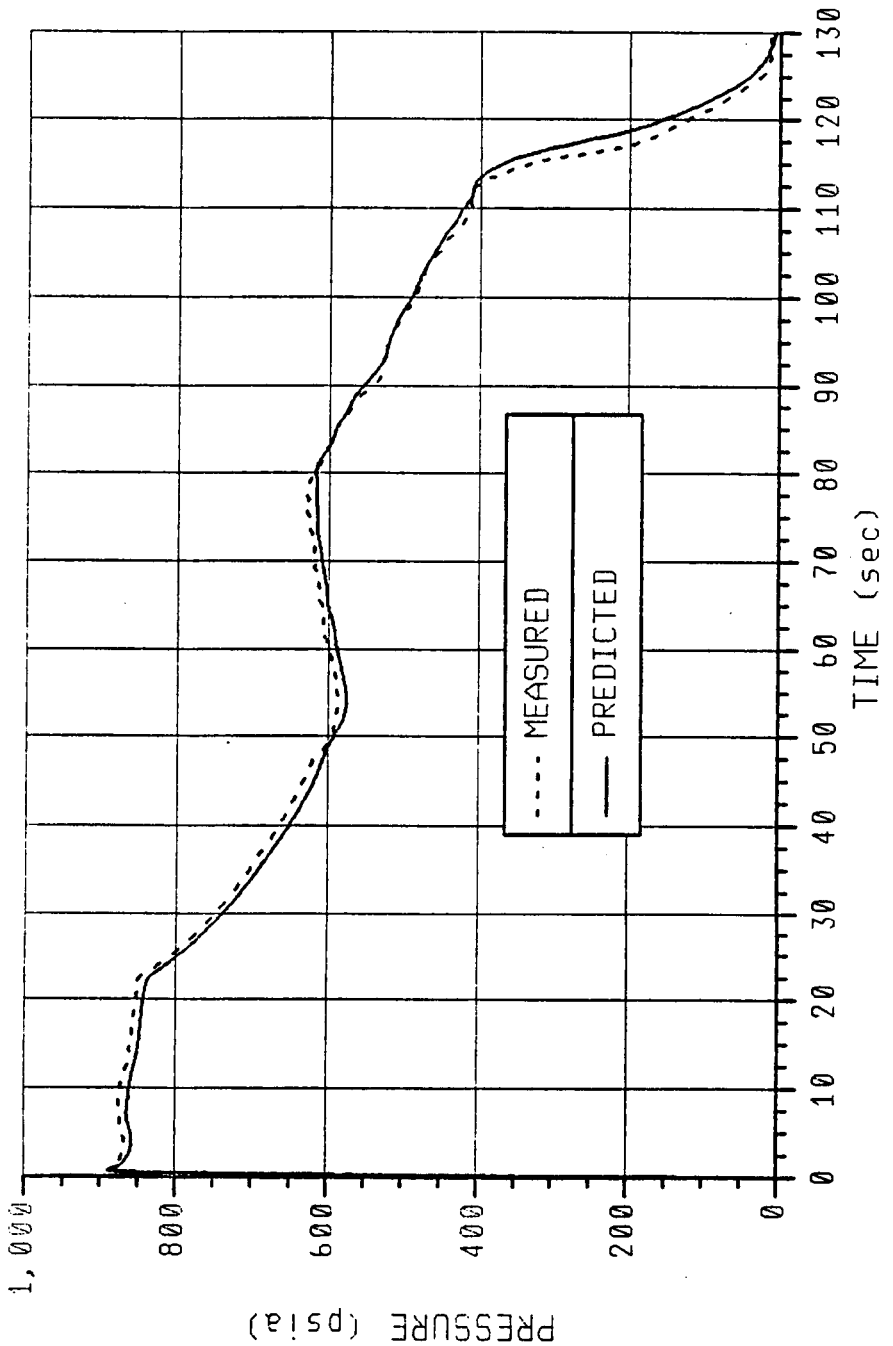

Figure 3.1.9-1. QM-8 Predicted and Measured Pressure Data at 39°F

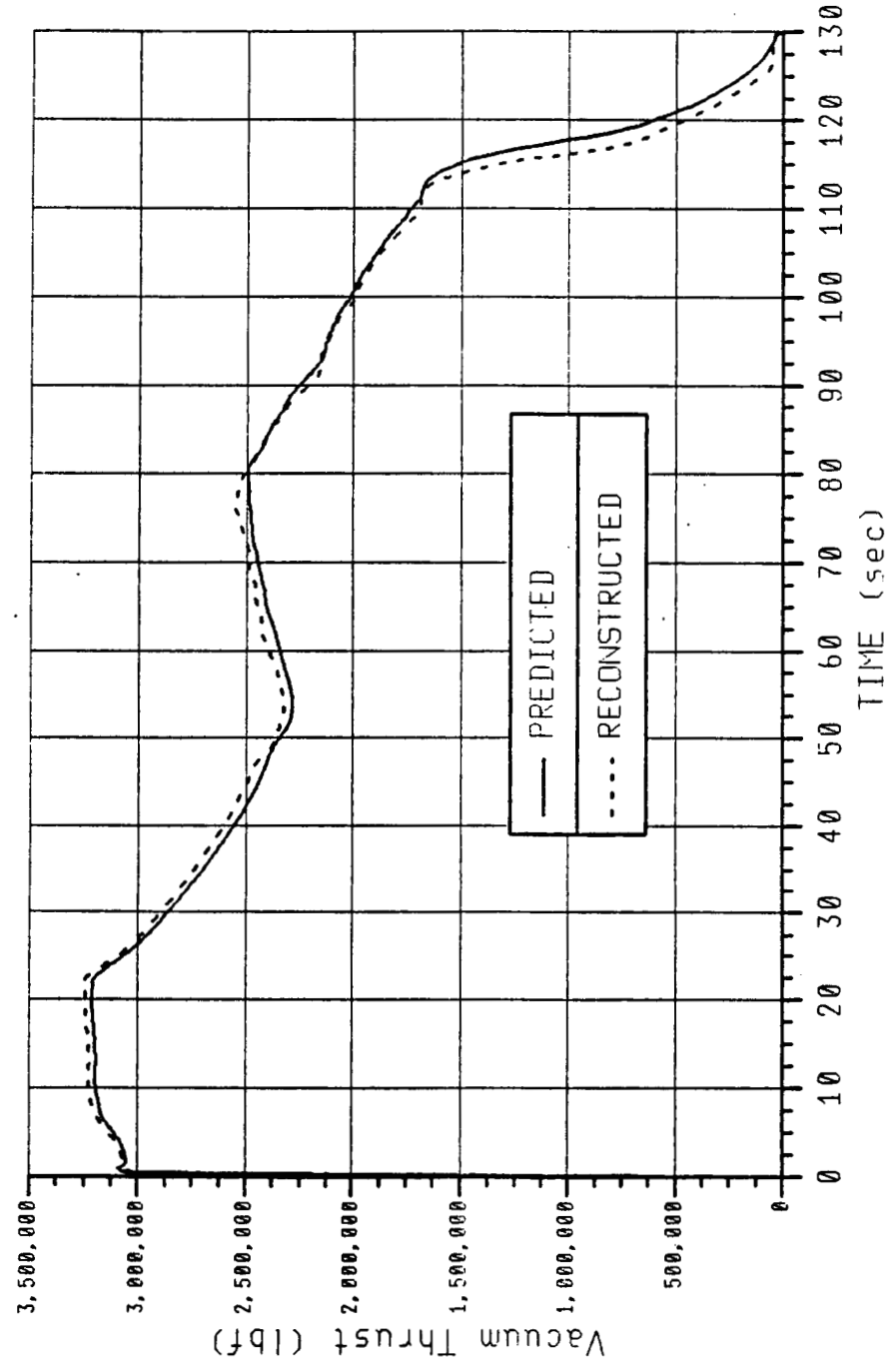

Figure 3.1.9-2. QM-8 Predicted and Reconstructed Thrust Data at 39°F

The QM-8 motor exhibited chamber pressure oscillation similar to previously tested Space Shuttle RSRMs. A possible cause for the increased oscillations from HPM to RSRM is the change in the joint insulation. The clevis side base thickness of the insulation has decreased, and late in burn time the NBR inhibitor is supported by this insulation. This would allow more flexibility in the inhibitor, and cause increased pressure oscillation. Investigation into this theory is being conducted. The two pairs of flight RSRMs fired to date did not experience the same increase that the static motors have. Reasons for the difference between flight and static test motors are currently unknown.

3.1.9.1 PMBT Calculation. The calculated PMBT for QM-8 at the time of firing (20 January 1989, 2:30 pm MST) was 39°F. The calculated PMBT for the 32 days of cold motor conditioning, as well as the ambient and average skin case temperature, is shown in Figure 3.1.9.1-1.

CALCULATION PROCEDURE

Model Development. The QM-8 PMBT models consist of the propellant, insulation, and steel case. The boundary conditions of the 3-D Supertab SINDA model used the impressed ground environmental instrumentation (GEI) surface temperature data from the external steel case and in-bore propellant grain surfaces. The PMBT and thermal gradients calculated are based upon these driving temperatures and the thermal properties of the propellant, insulation and steel case. The accuracy of the calculated PMBT and thermal gradients is dependent upon the accuracy of the thermocouple measurements. The SINDA program has been verified with exact analytical solutions with similar geometry and boundary conditions.

Modeling Summary. Three Supertab SINDA models were developed to be used to calculate the PMBT for QM-8. Each model differs in the type of data it uses as input. The first model is a two dimensional axisymmetric Supertab SINDA model created for each segment using the ambient temperature data recorded by portable hygrothermographs. A single portable hygrothermograph was located adjacent to each motor segment during transit from the casting pits, through final assembly and until received by the test area. The second model is a two dimensional axisymmetric Supertab SINDA model created for the entire motor. When all of the segments arrived at T-97, two hygrothermographs recorded the ambient temperature in T-97 which was input into the model. When motor cold conditioning began, GEI data from the motor case and propellant grain surfaces became available and were input into a third model, a three dimensional (3-D) Supertab SINDA model.

SINDA Modeling. One continuous recording portable hygrothermograph was located adjacent to each segment as each segment was processed from the casting pits to the test area. From the continuous hygrothermograph recordings, a daily average was determined for each segment until all of the segments arrived at T-97 (11 November 1988) and used as input to the two-dimensional (2-D) axisymmetric Supertab SINDA model created for each segment. A constant

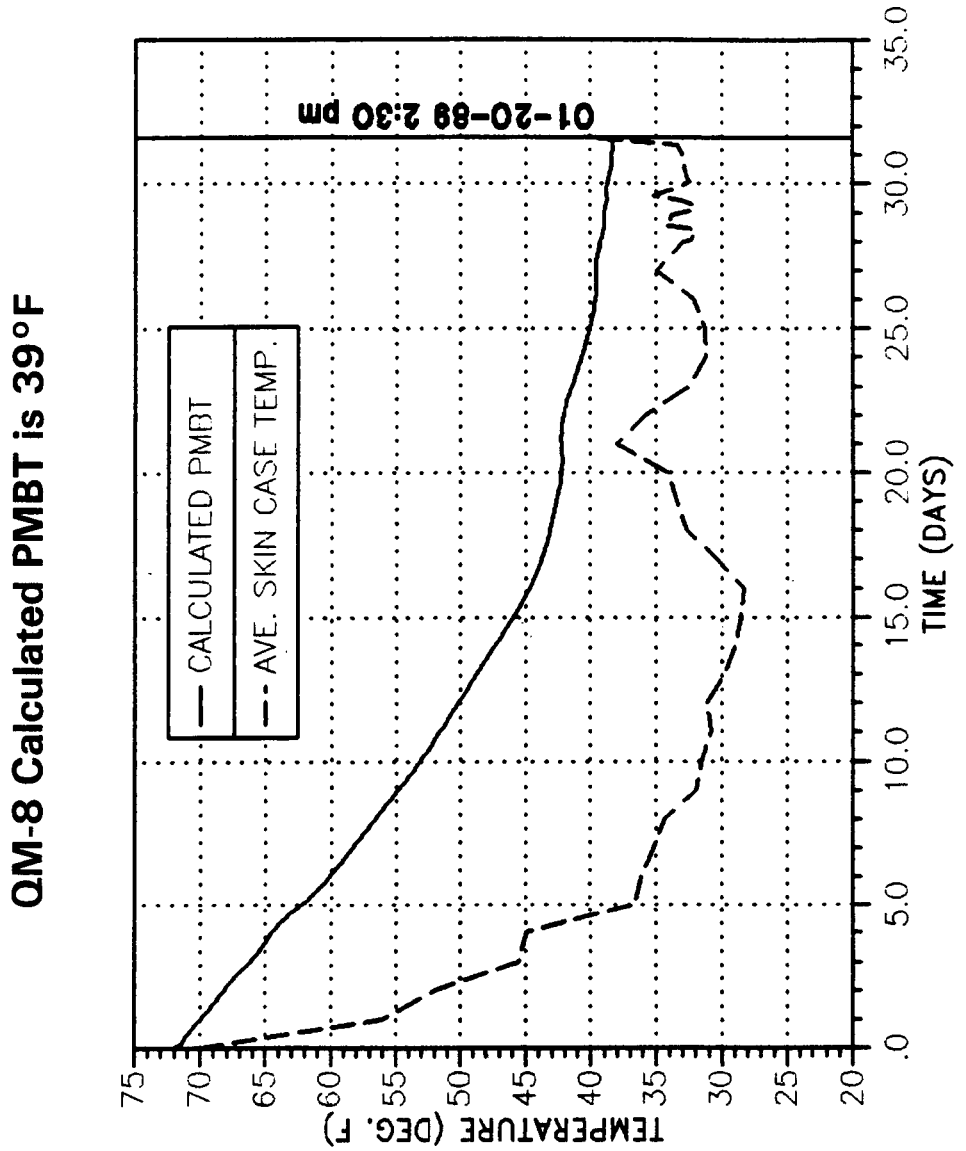

Figure 3.1.9.1-1. QM-8 Calculated PMBT and Average Skin Case Temperature

forced convective heat transfer coefficient was used for each segment from the casting pits to the test area. However, no hygrothermograph data was available for the aft segment due to the switch that took place between Flight Set 4 and QM-8 aft segments.

From the individual PMBTs calculated for each segment, an overall initial PMBT was determined for the 2-D axisymmetric Supertab SINDA model used to determine the PMBT from the time when all the segments arrived at T-97 to the start time of motor conditioning. The highest, or warmest, value for PMBT from the individual segments was used as the initial PMBT for the entire motor for this phase of the calculation. This was done in order to be conservative in the final calculation of PMBT. By using the warmest value, the PMBT calculated at the end of this phase would be insured of being at or below the actual PMBT. From two continuous hygrothermograph recordings, a daily average temperature was determined. An average temperature for each day was determined for both the upper and lower positions, which were then averaged together to come up with the final daily average. A constant forced convective heat transfer coefficient based upon past experience was used.

For calculations during the cold conditioning process, a 3-D model was created with the option of using thermocouple data from the steel case and propellant grain surface or using ambient temperature data with an assumed heat transfer coefficient (the method used in previous PMBT calculations). By using the real-time thermocouple data, no assumed value for the heat transfer coefficient was necessary, since the thermocouple temperatures were directly impressed on the surfaces in the model. Skin case temperatures were recorded by the T800 series thermocouples on each segment at 45, 135, 225, and 315 deg. A linear interpolation scheme was used to calculate skin case temperatures for the remainder of the motor case. Propellant grain temperatures were recorded by 10 thermocouples at various locations in the motor. Only the thermocouples located at the approximate middle of the segment of the propellant surface of each segment were used. This resulted in only 6 thermocouples being used; one thermocouple for each segment, along with readings from the forward and aft domes. The resulting thermocouple readings were used as the value for the entire propellant surface over the corresponding motor section. Thermocouple data was received daily from the test area starting on 5 January 1989 through the day prior to firing. On the day of firing, data was received at T-6 hr, at T-3 hr, and immediately after firing. Once the data was received, it was reduced into a SINDA input format and the model was run.

TWR-17591, Vol X, will contain a complete summary and discussion of the performance results from QM-8.

3.1.10 Dynamics

The QM-8 static test was the second static firing in the T-97 test facility, which is equipped with side load actuators for the purpose of simulating the external side loads to a 360 deg ETA ring

during motor burn. The control of the side load actuation system is briefly discussed in this section. Transducers mounted on QM-8 to monitor the RSRM dynamic behavior included accelerometers, acoustic gages, pressure transducers, and displacement gages. The accelerometer data are also briefly discussed. Detailed discussions will be in TWR-17591, Vol XI.

All of the accelerometer data show that the vibration level is high (above 10 G) right after ignition as compared to previous motors. Seconds after ignition, the vibration level returns to normal.

Test data from command channels and force channels, as shown in Figures 3.1.10-1 through 3.1.10-12, show that the control system performed as predicted and tracked the specified load command duty cycle. The peak forces were generally lower than the command, which was as expected since there was a lag in the response of the control system.

Only data from accelerometer Channel A428 is discussed. All the remaining accelerometers and acoustic channels will be discussed in Vol XI. Channel A428 was located at aft dome area (Station 1829.5) and measured in the radial direction. Figure 3.1.10-13 shows the time-history plot. The power spectrum density (PSD) for three different time frames (ignition, mid-burn, and end of burn) are shown and compared to NASA criteria (SE-019-049-2H) in Figure 3.1.10-14. Generally, those PSDs were well enveloped by NASA criteria.

The waterfall plots for Channel A428 are shown in Figures 3.1.10-15 and 3.1.10-16. Two methods were used to compute the waterfall spectrum. The first method used is the direct Fourier Transform (FT). The second method used is the Maximum Entropy Method (MEM). The direct FT method has been widely used to compute the waterfall spectrum. The disadvantage of using direct FT is the poor estimation of the frequency spectrum, which is due to the quick change of motor characteristics, especially the modal frequencies. MEM is used to overcome this disadvantage. Figure 3.1.10-15 shows the waterfall using direct FT, and Figure 3.1.10-16 shows the waterfall using MEM. As can be seen from these figures, both waterfall plots show a strong frequency increasing trend. This trend starts at about 12 Hz after ignition, and ends at about 22 Hz, at the end of burn. This mode, as compared with recent modal survey, is believed to be the third vertical bending mode. Another extreme peak shown in the waterfall plots occurred at 70 sec after ignition, at 16 Hz. This is believed to be caused by nozzle command. Another important observation from Figures 3.1.10-15 and 3.1.10-16 is that the internal acoustic mode (1-L, 15 Hz) can be clearly identified at the end of burn.

Regarding the side load system, both the analytical predictions and test results have demonstrated that the control system can be operated adequately with acceptable stability margin at ignition and mid-burn. However, no analysis was performed at end of burn. Due to the frequency change with loss of mass at mid-burn, the stability margin would be slightly decreased.

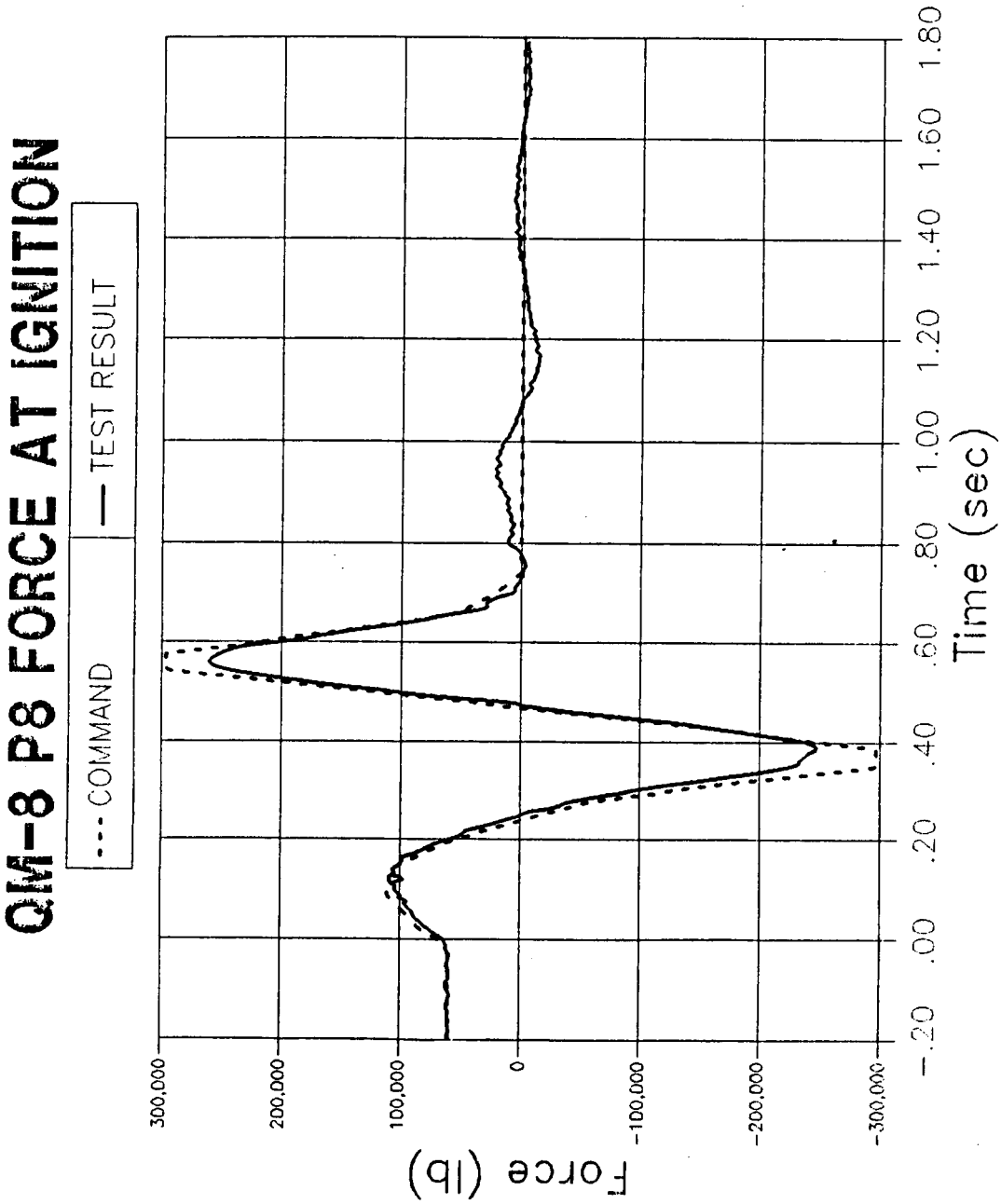

Figure 3.1.10-1. QM-8 P8 Force at Ignition

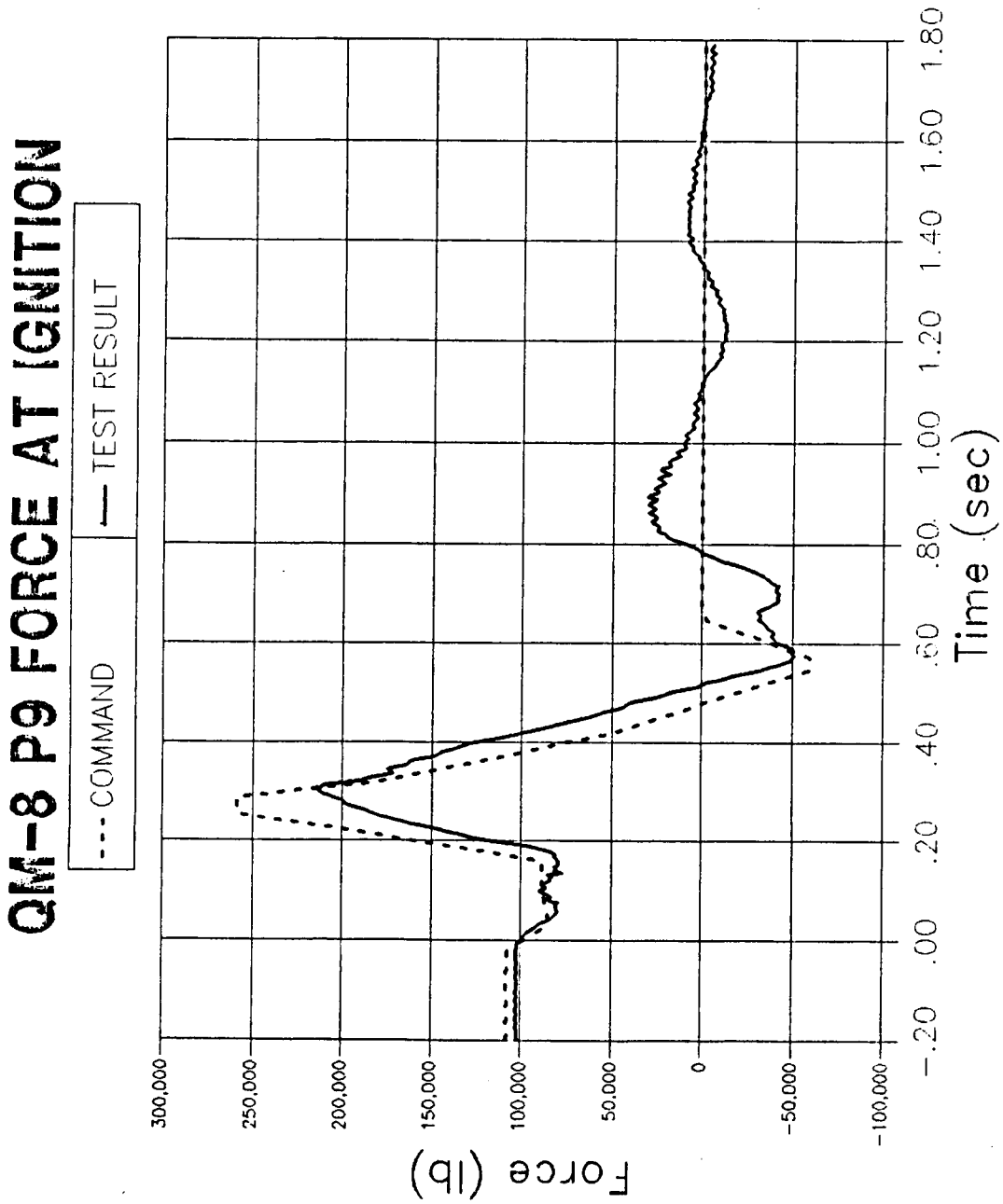

Figure 3.1.10-2. QM-8 P9 Force at Ignition

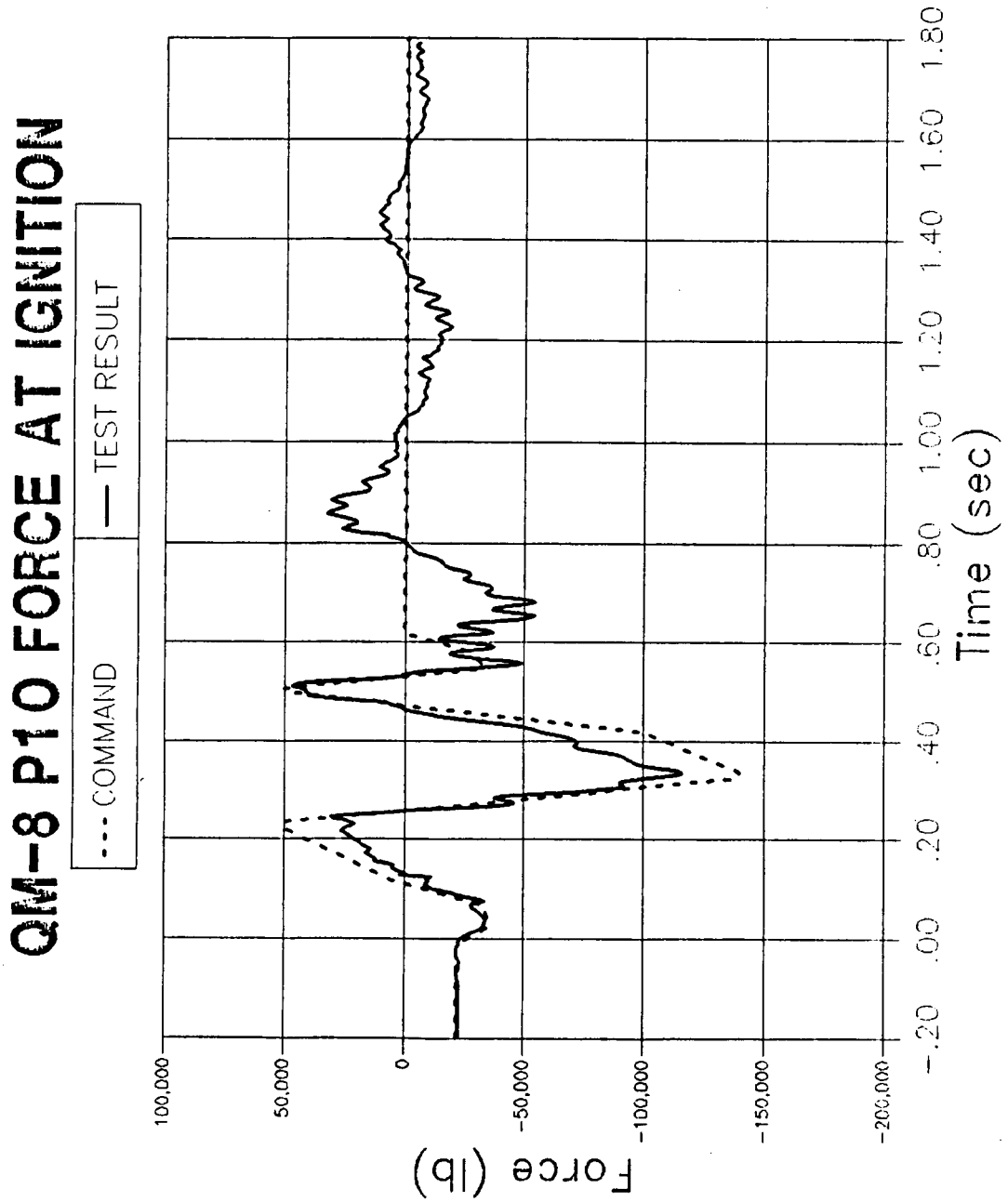

Figure 3.1.10-3. QM-8 P10 Force at Ignition

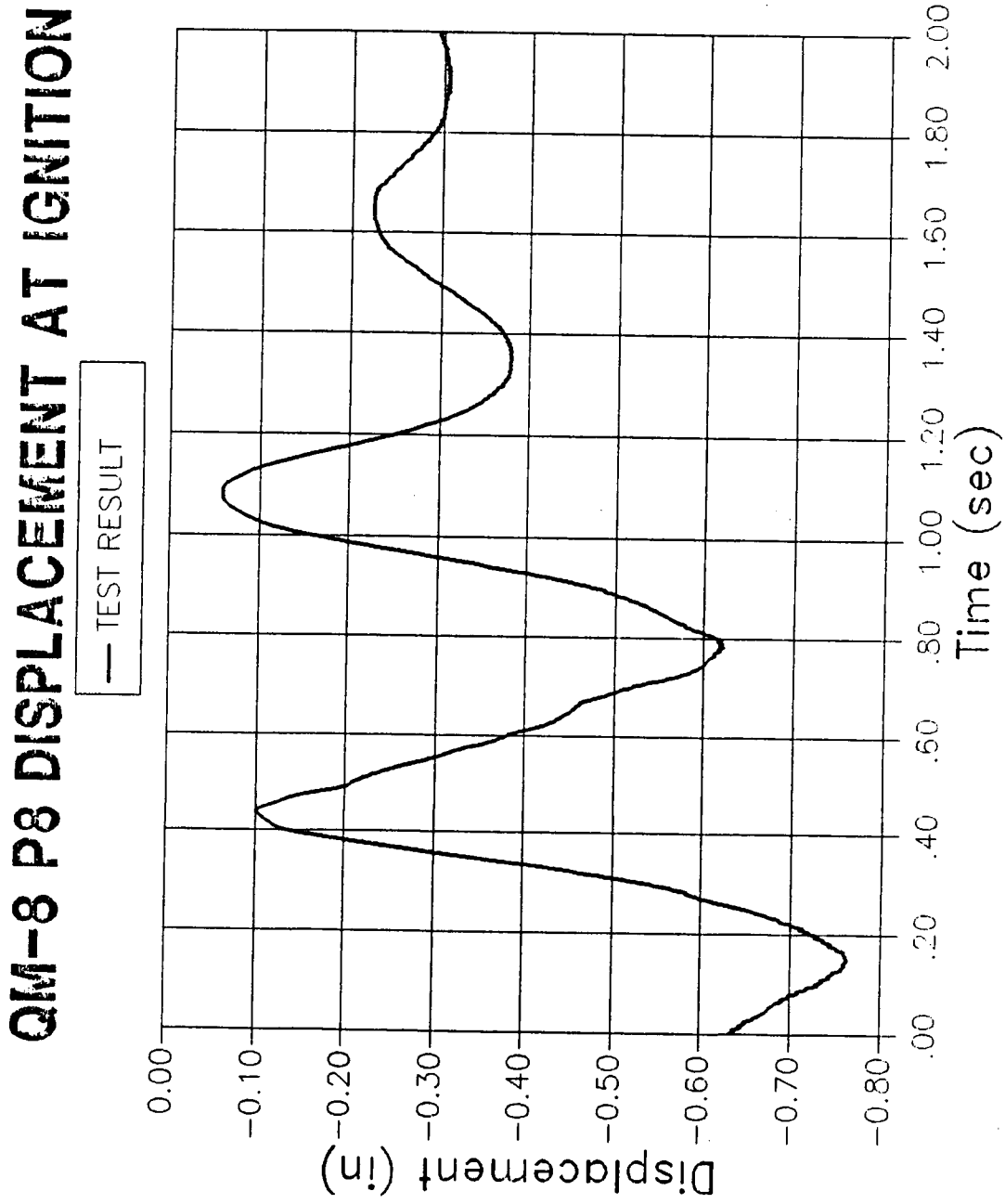

Figure 3.1.10-4. QM-8 P8 Displacement at Ignition

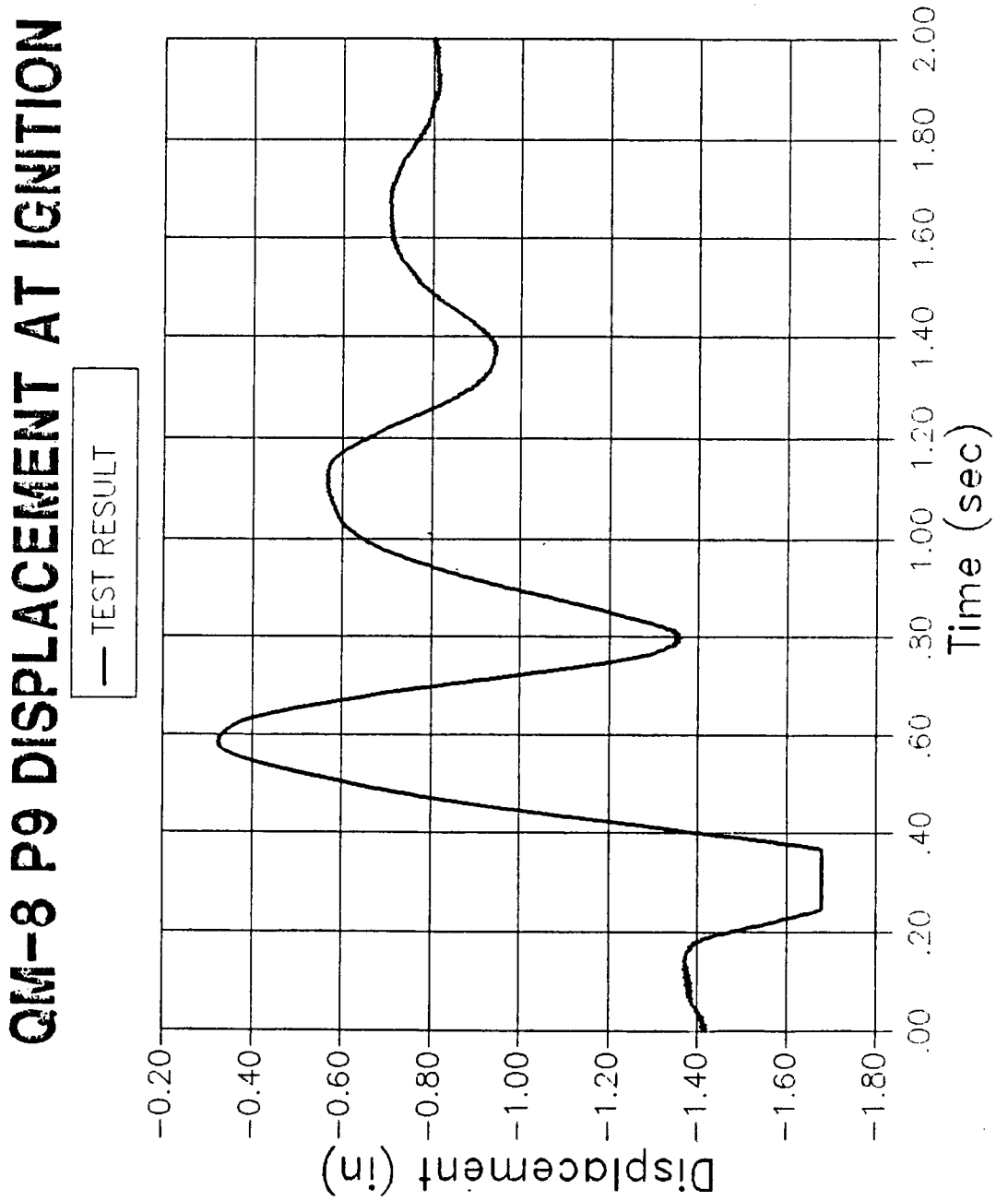

Figure 3.1.10-5. QM-8 P9 Displacement at Ignition

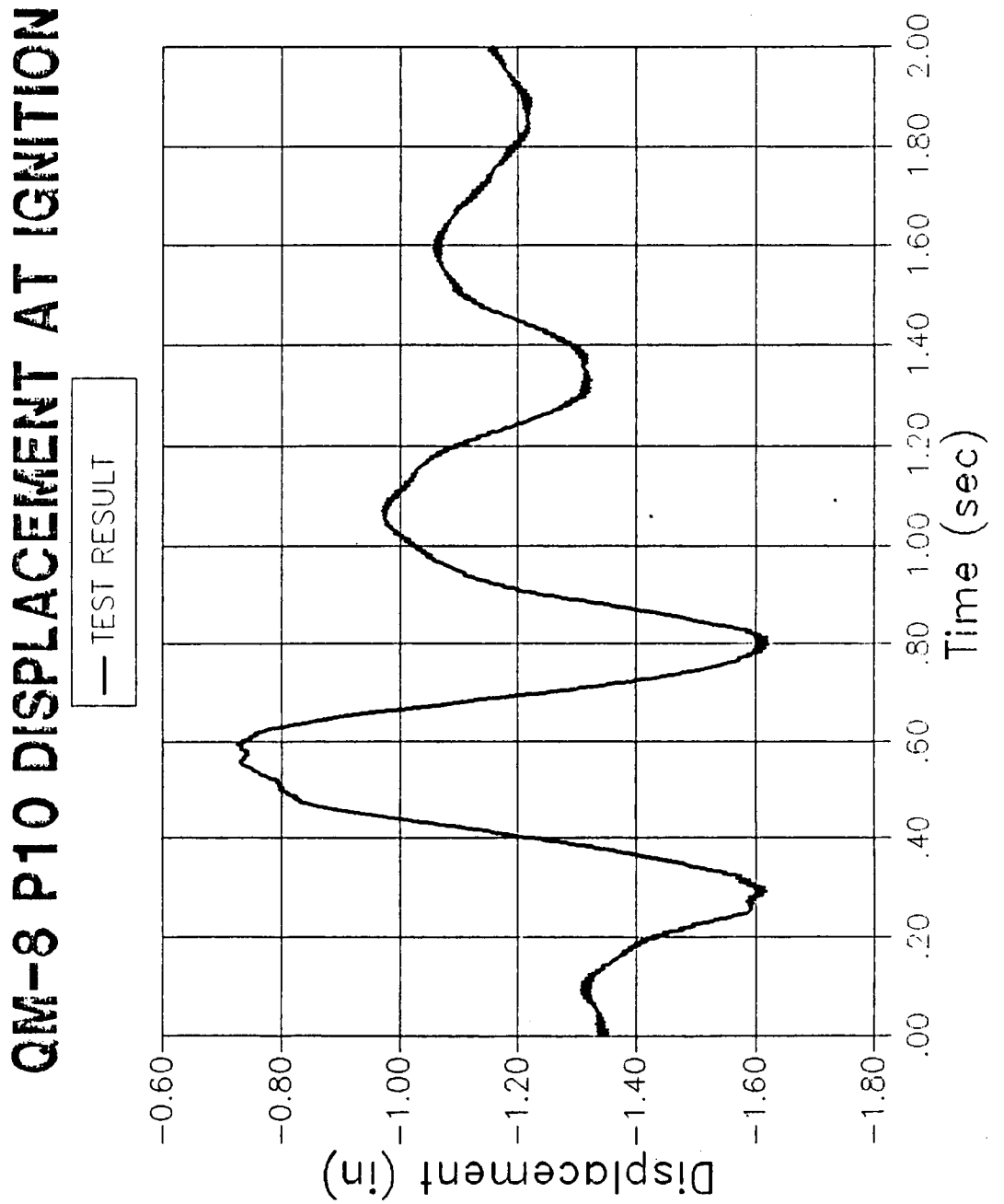

Figure 3.1.10-6. QM-8 P10 Displacement at Ignition

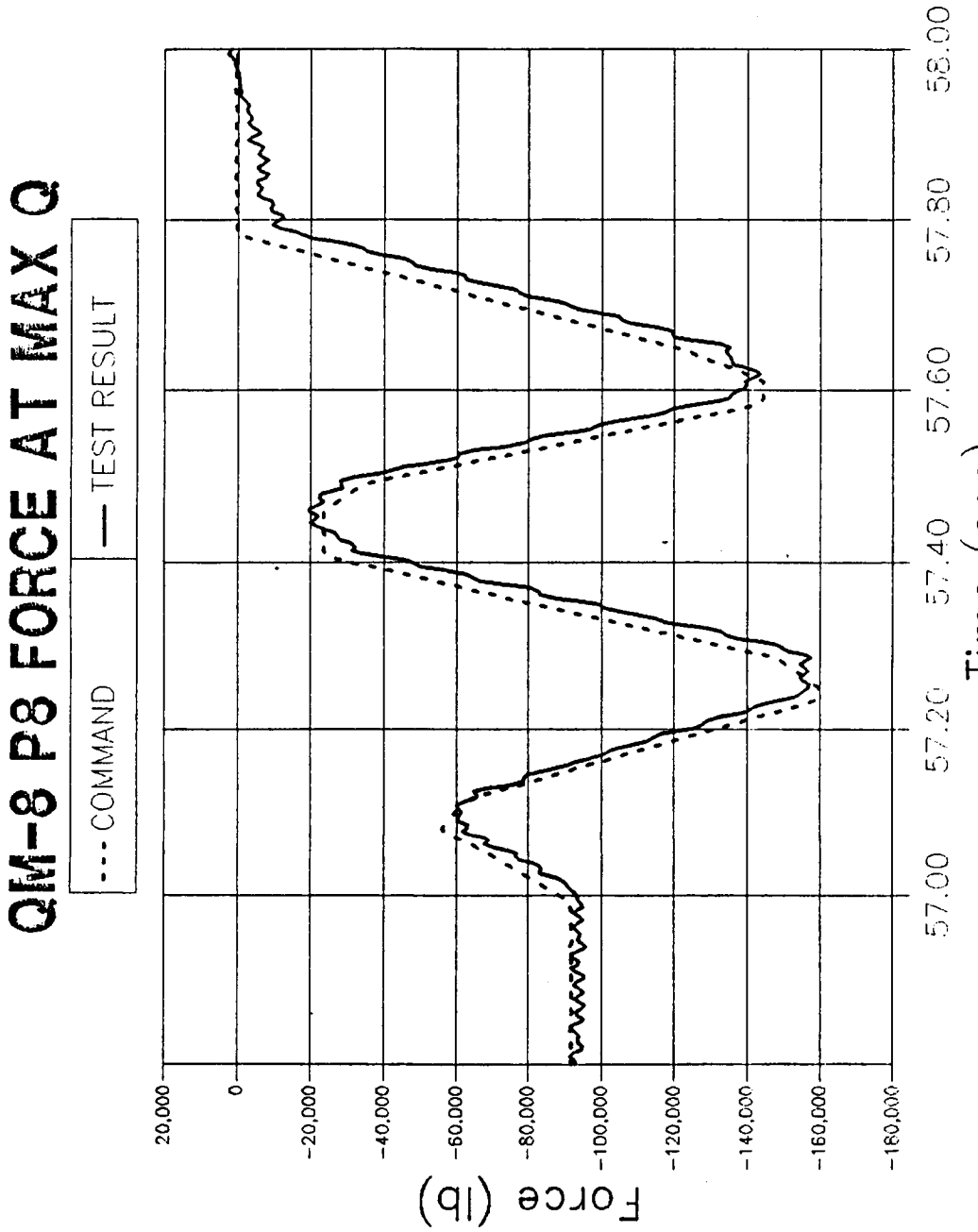

Figure 3.1.10-7. QM-8 P8 Force at Max Q

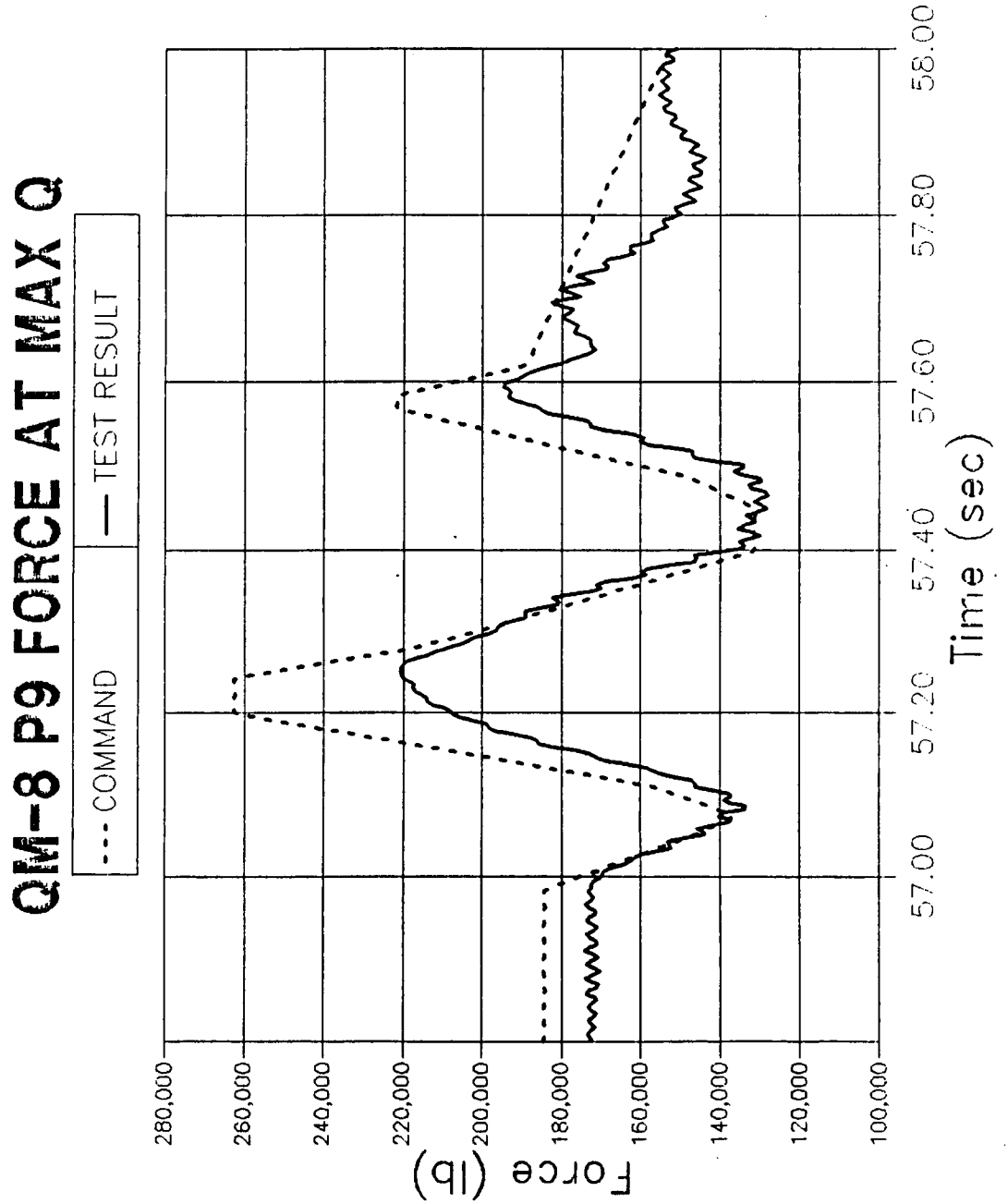

Figure 3.1.10-8. QM-8 P9 Force at Max Q

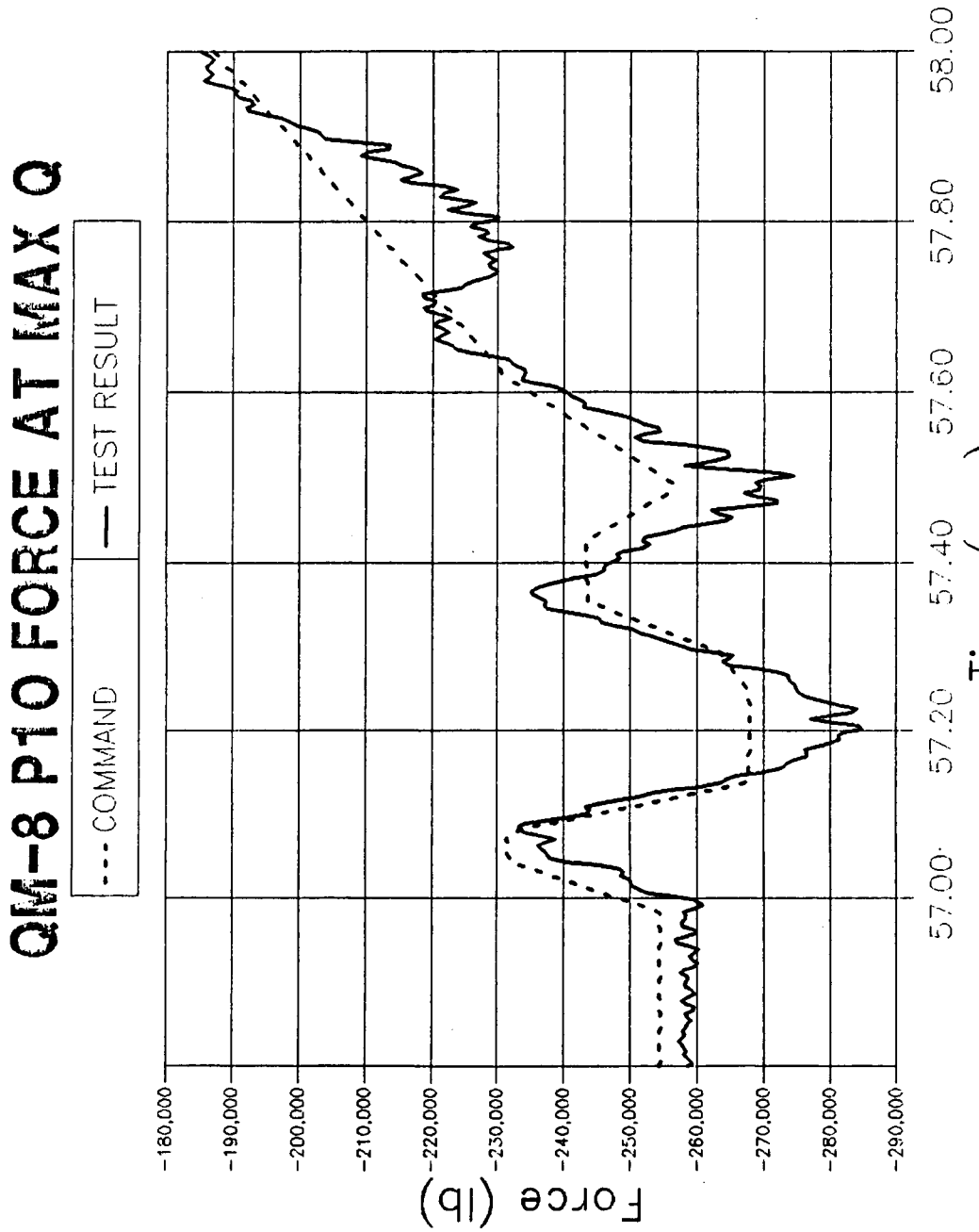

Figure 3.1.10-9. QM-8 P10 Force at Max Q

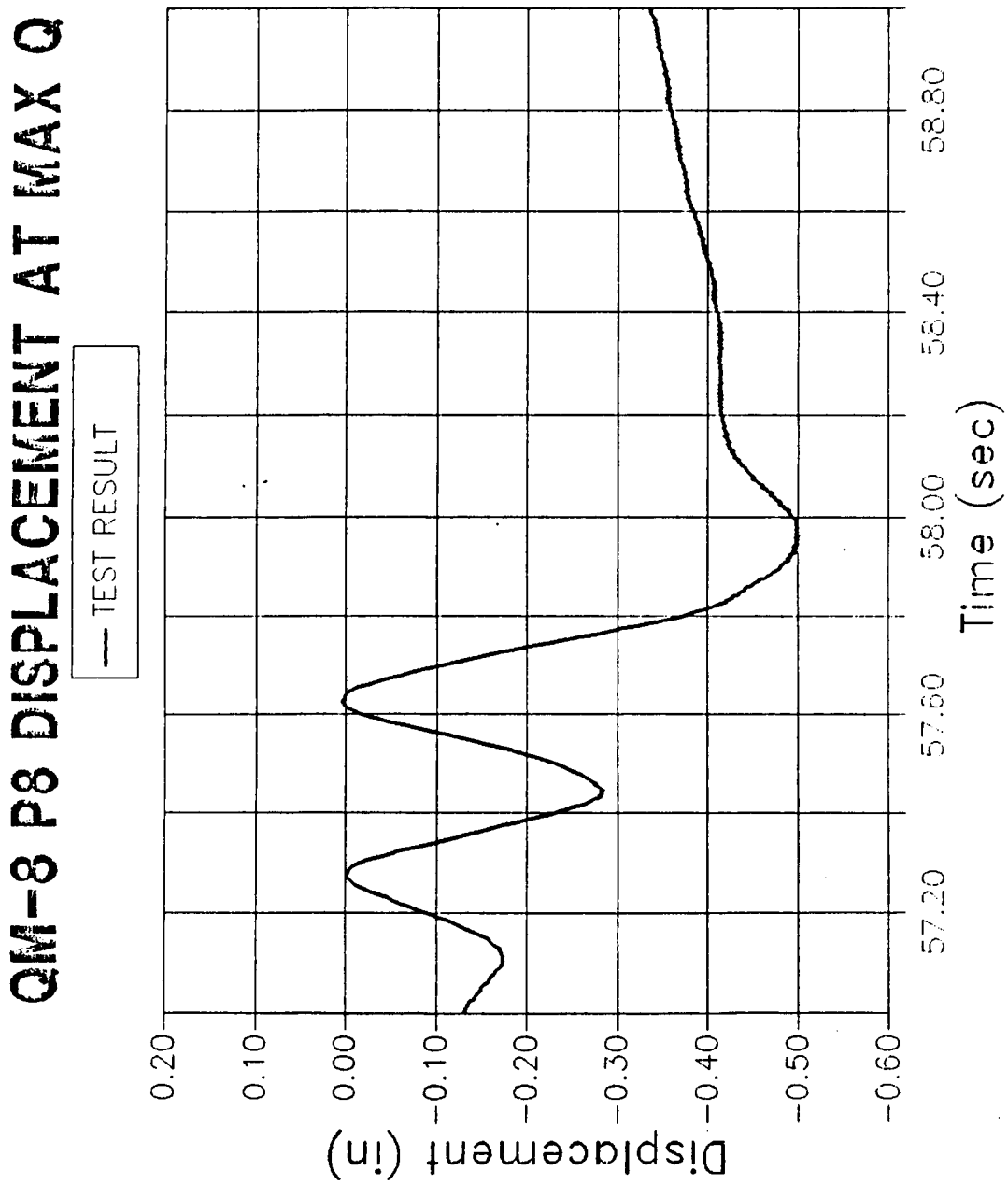

Figure 3.1.10-10. QM-8 P8 Displacement at Max Q

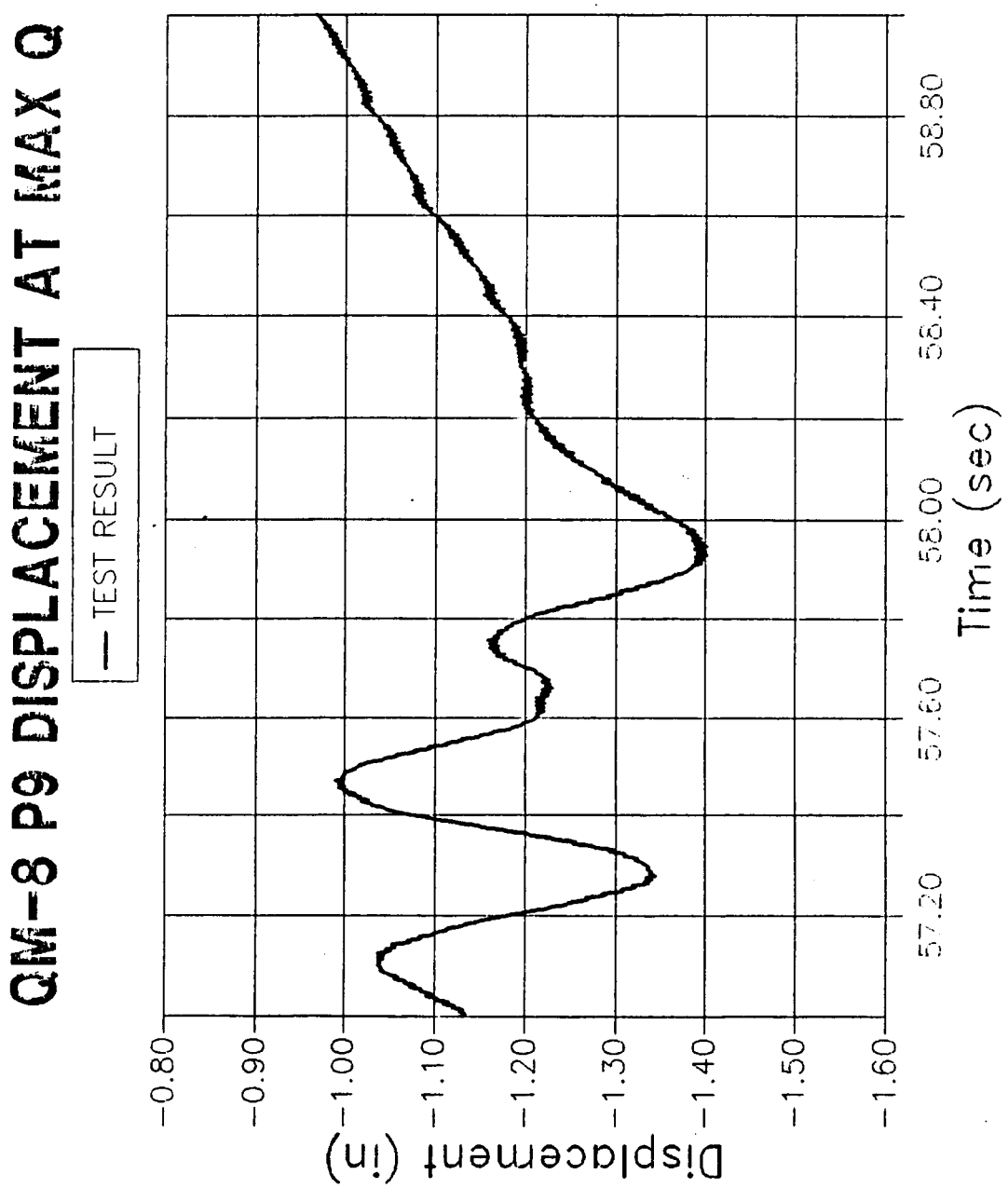

Figure 3.1.10-11. QM-8 P9 Displacement at Max Q

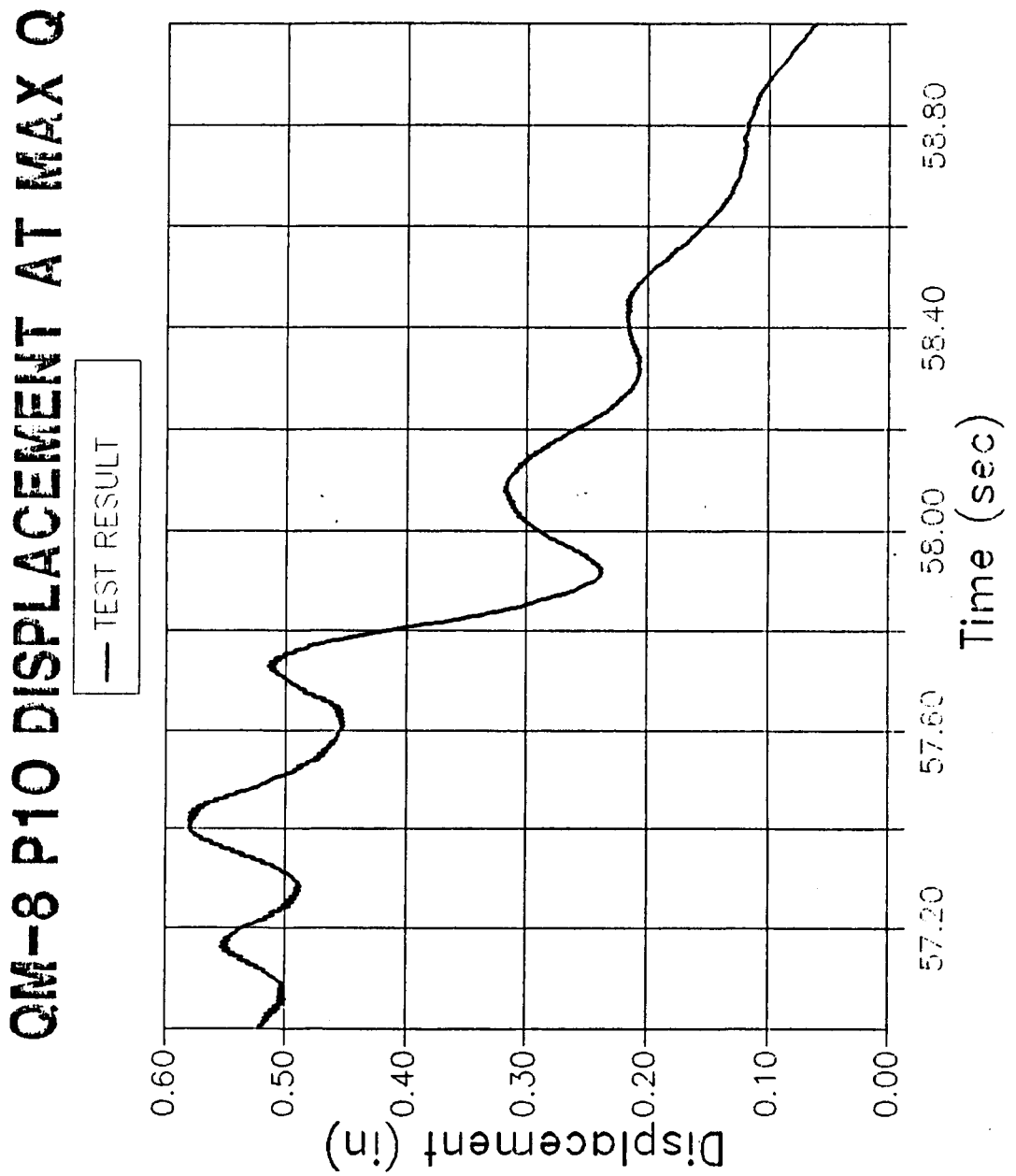

Figure 3.1.10-12. QM-8 P10 Displacement at Max Q

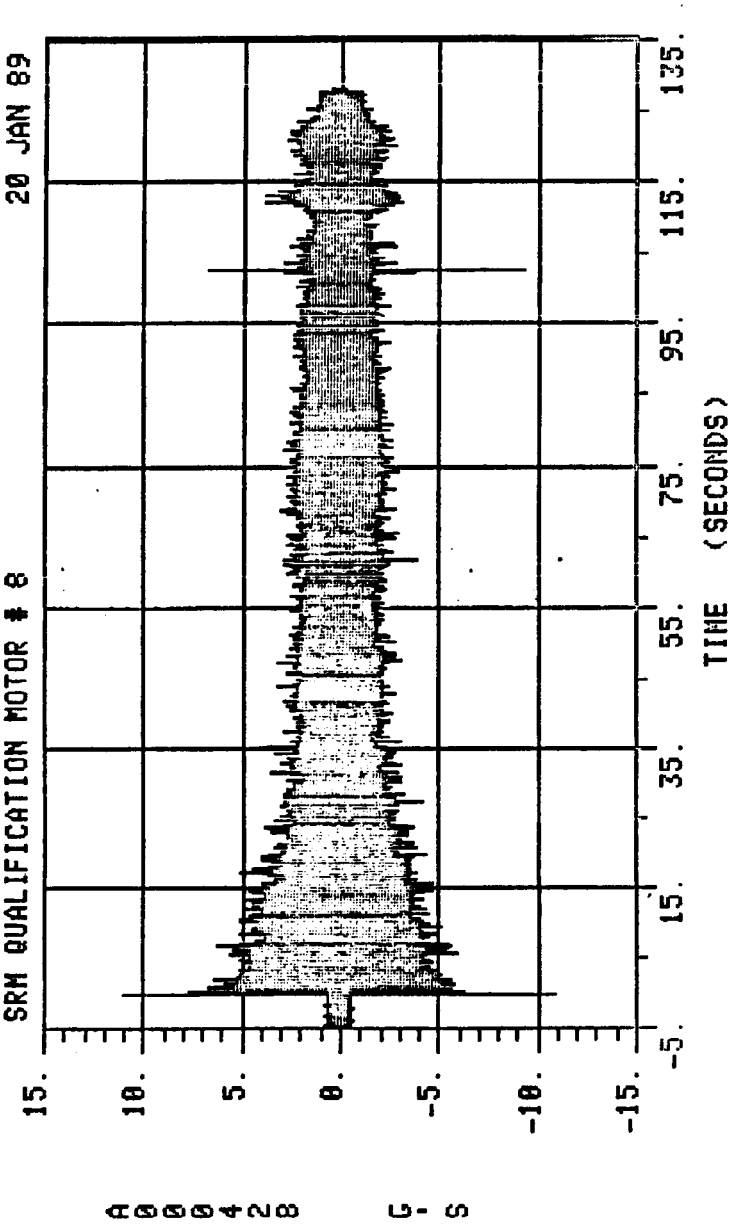

Figure 3.1.10-13. Aft Dome Accelerometer Time-History

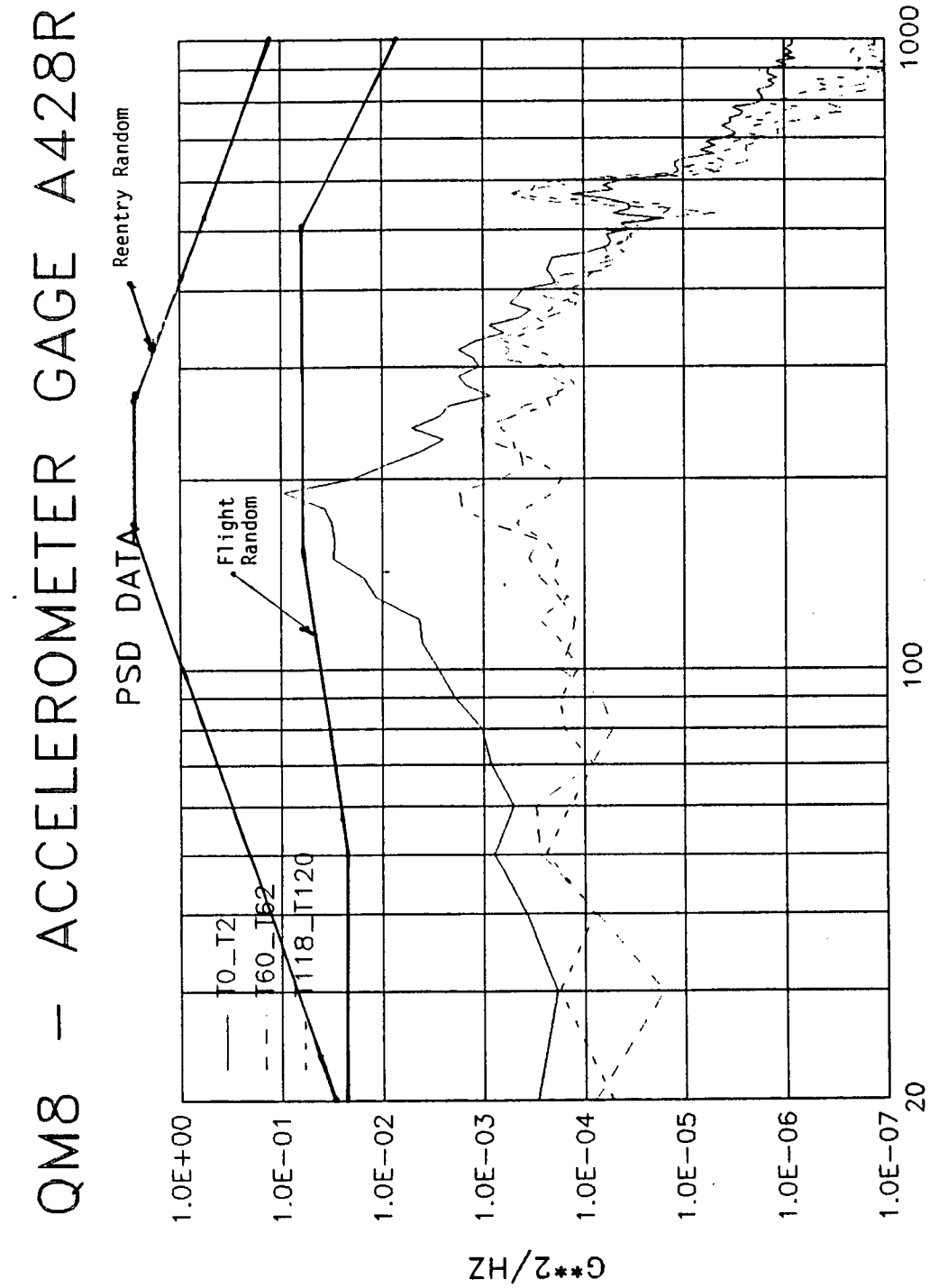

Figure 3.1.10-14. QM-8 Accelerometer Gage A428R

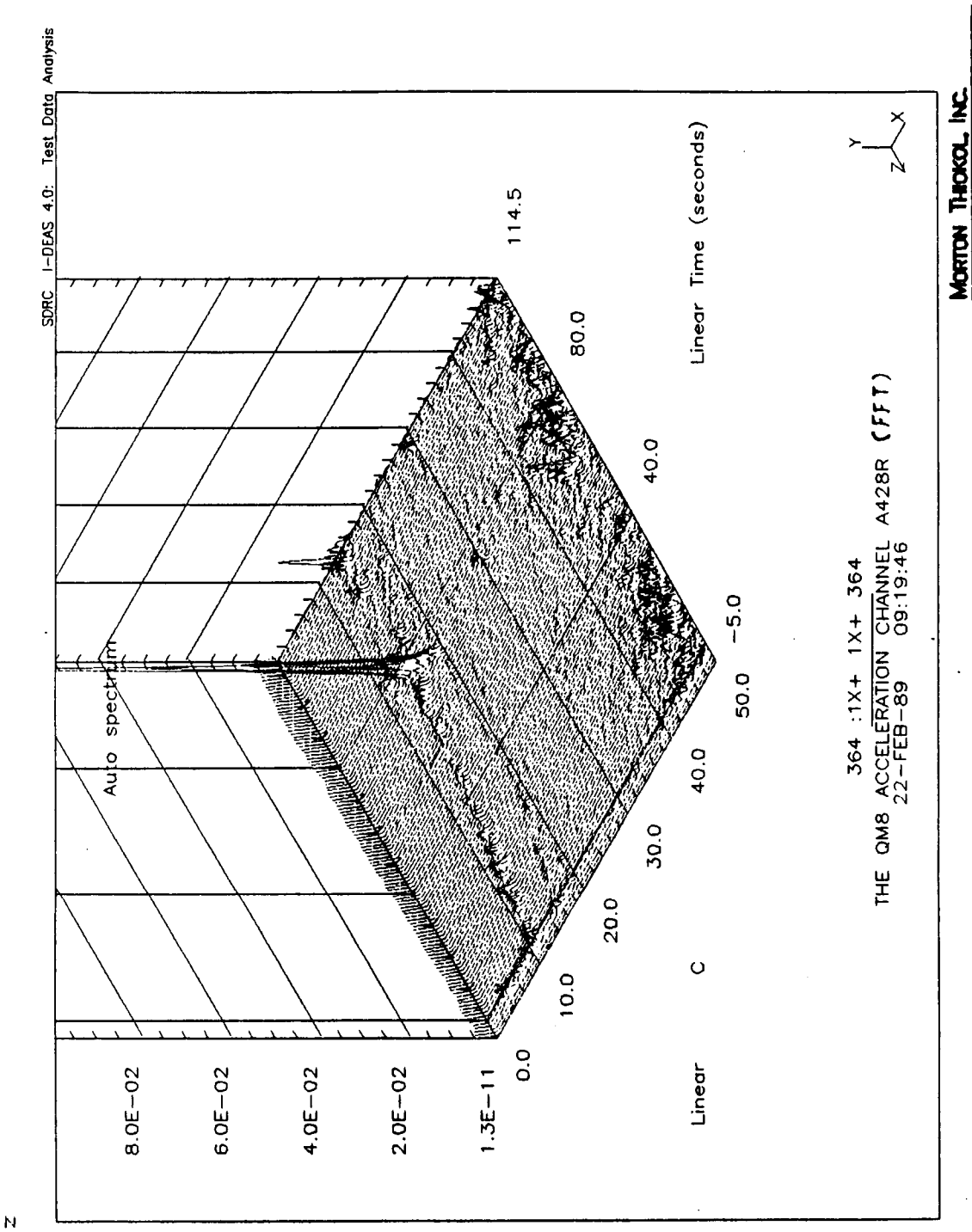

Figure 3.1.10-15. QM-8 Acceleration Channel A428R (FFT)

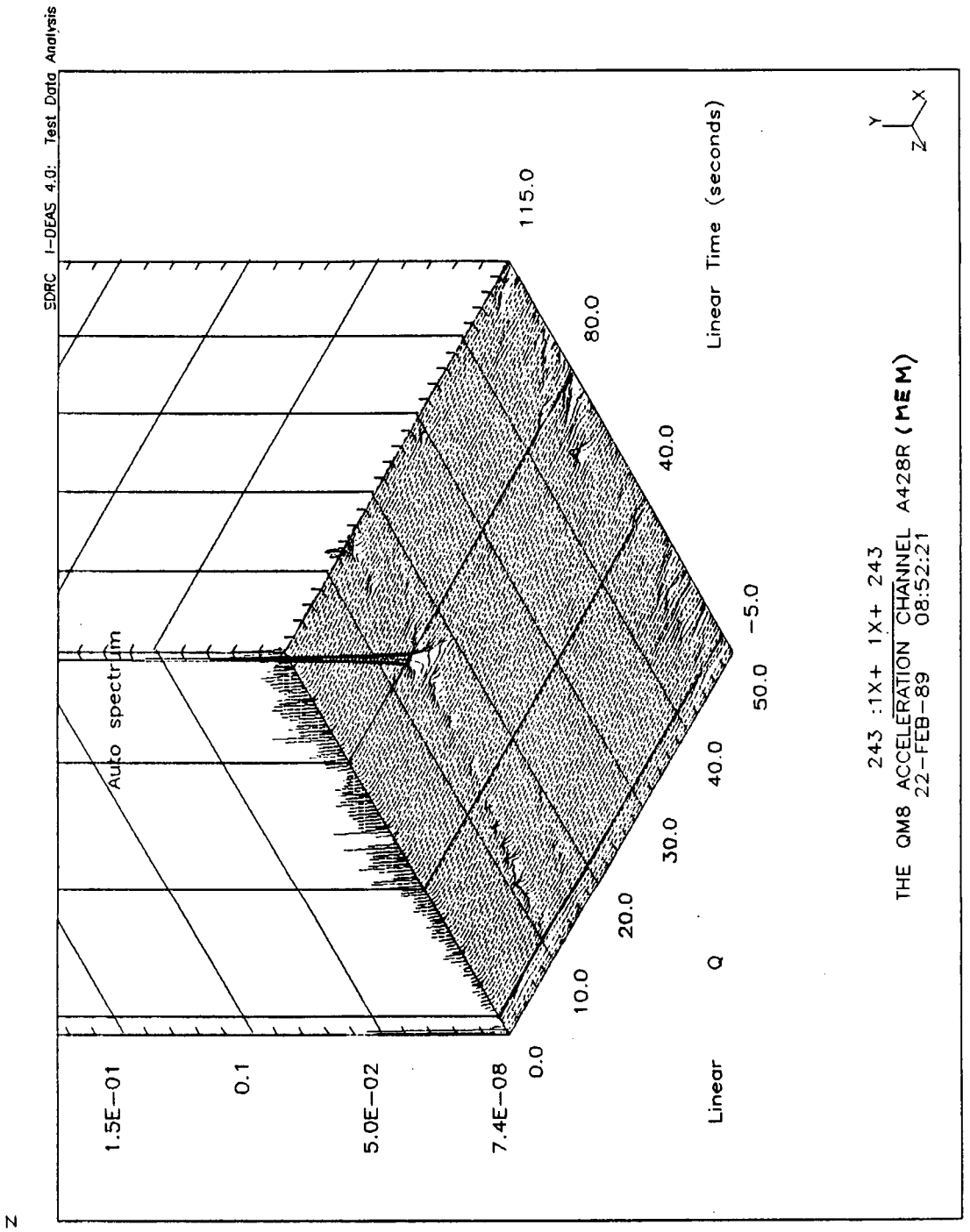

Figure 3.1.10-16. QM-8 Acceleration Channel A428R (IMEM)

In general, a 3 dB gain margin for the overall burn time was more reliable. Additional stability analysis between ignition and mid-burn is recommended.

Test data from QM-8 have shown that the motion of the RSRM due to ignition, nozzle vectoring, and propellant depletion does not introduce large force transients. The P8 and P9 displacements tend to follow the nozzle motion from 5 to 50 sec. The P10 displacement also ramps up to a certain position at the end of burn. This was due to the motor rising up as the propellant burned. Predictions of displacements through nozzle vectoring should be made. Further stability analysis is recommended to investigate the pressure effects during motor operation.

3.1.11 Aero/Thermal

Considering the thermal objectives, the test was a success. Qualitatively, the test shows the motor can perform at low temperatures. A more detailed discussion is contained in Section 9 of this report.

3.1.11.1 Temperature Data. Temperature data were nominal. Ambient temperature at the time of ignition was 28°F and calculated PMBT was 39°F.

3.1.11.2 Deluge System. The deluge system operated as planned for the QM-8 static test. There were no problems caused by the cold conditions. A maximum case temperature of 177°F was reached at Station 1598 at the 0.0 deg location. This is consistent with all other static motors with the current deluge system (Figure 3.1.11.2-1). Plotting the difference between the case temperature at motor ignition and the peak case temperature versus slag weight shows that QM-8 is consistent with all other static test motors (Figure 3.1.11.2-2). The temperature rise rates are all normal.

3.1.11.3 Aft End Heating. The overall results indicated that the recycle aft end heating system was very efficient for an average building temperature of 29°F. All critical components such as case-to-nozzle joint, internal nozzle joint seals, flex bearing, and hydrazine fluid met their temperature criteria (Table 3.1.11.3-1).

3.1.12 Loads and Environments

The QM-8 static test was completed successfully with the strut loads reacting in a similar manner as the input load cases for lift-off and High Q. The input load cases were extracted from TWR-16674, and they were time shifted slightly in order to match the time and strut loads activated during the test. The lift-off load case, L02044, was shifted -25 ms and the High Q was shifted +2 sec. The lift-off time shift was negligible, but while the High Q shift may seem large, it is well within the High Q region which extends from 26 to 76 sec. A more detailed discussion is contained in Section 8 of this report.

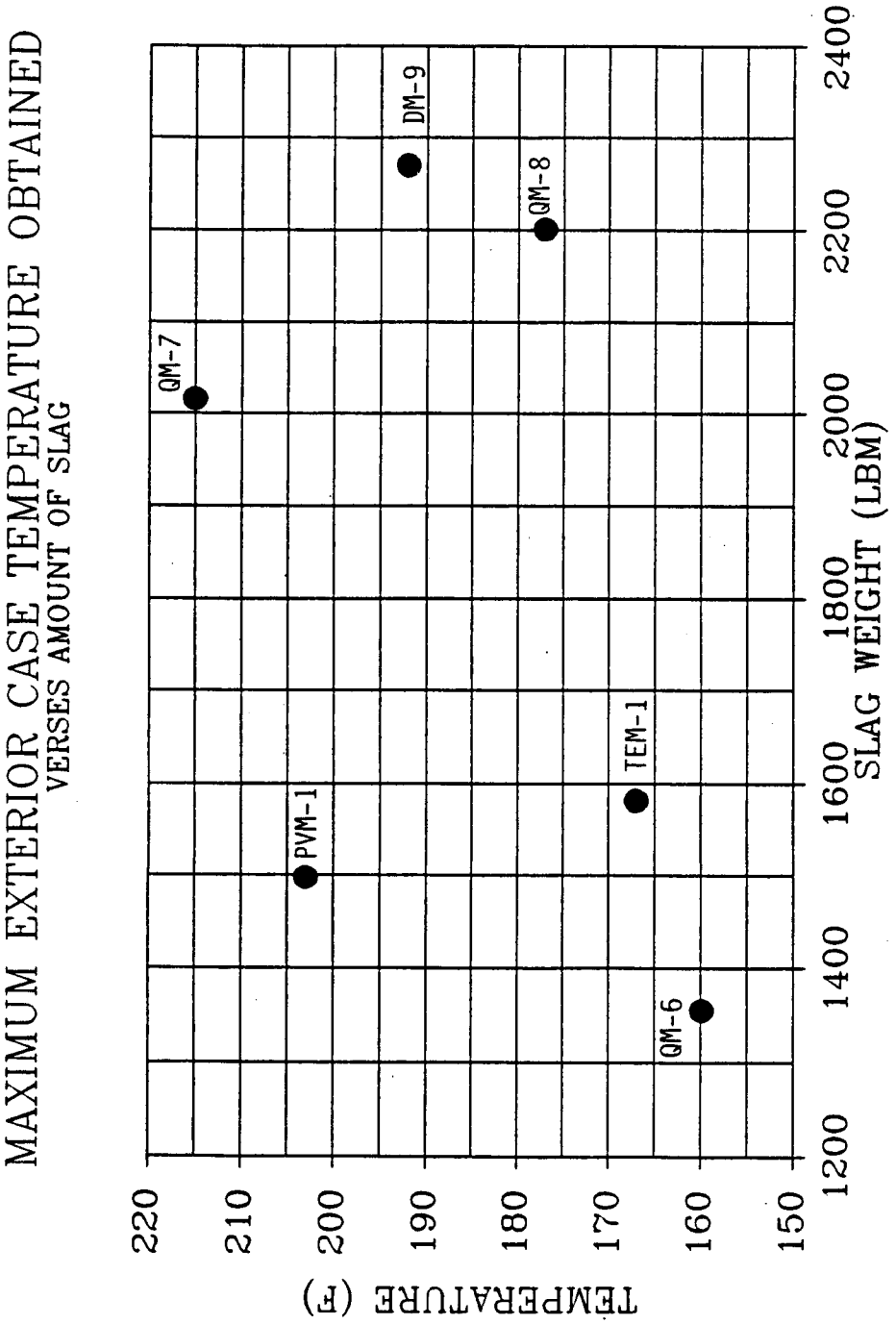

Figure 3.1.11.2-1. Maximum Exterior Case Temperature Obtained

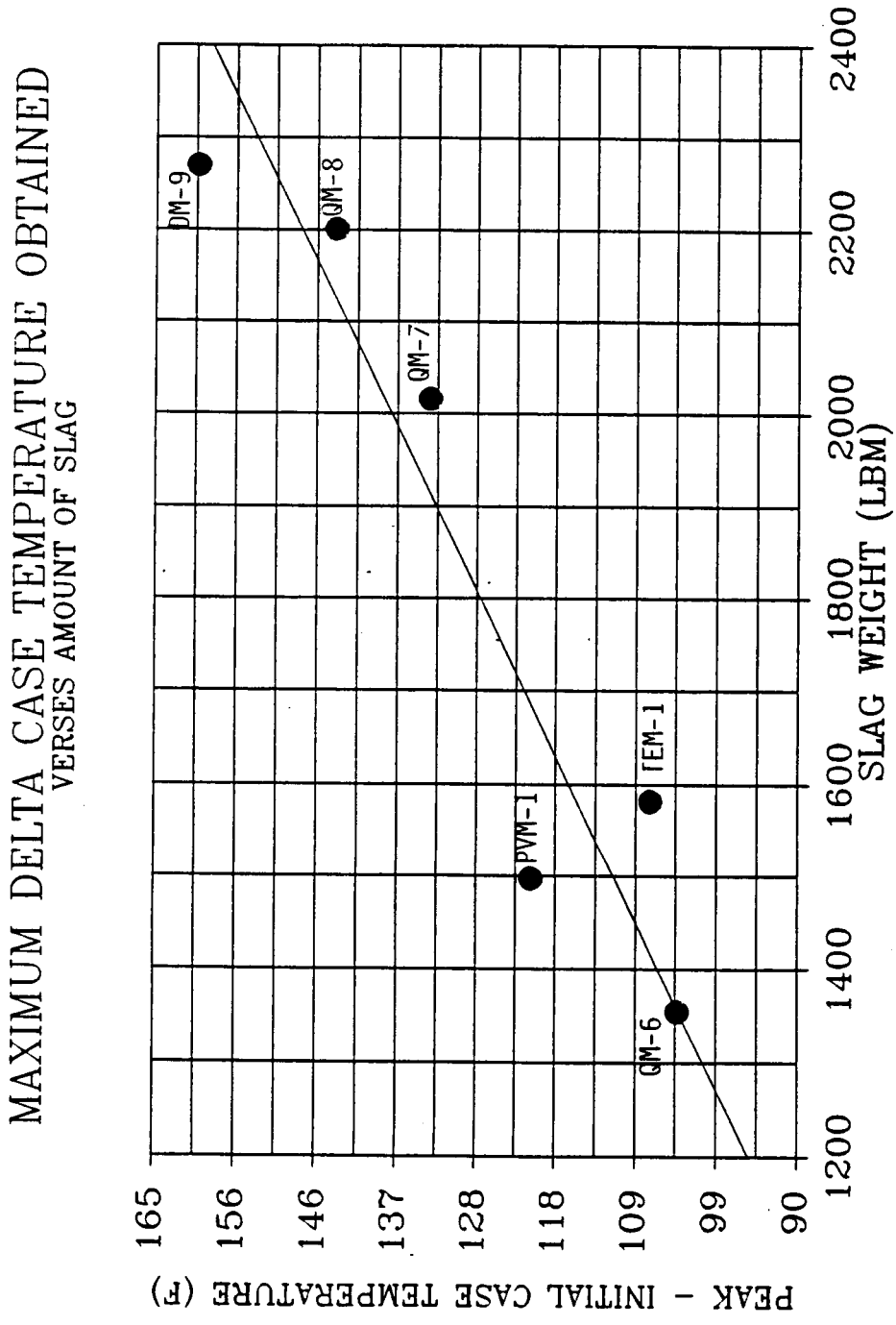

Figure 3.1.11.2-2. Maximum Delta Case Temperature Obtained

Table 3.1.11.3-1. QM-8 Component Sensor Temperatures at Firing (°F)

Location	Minimum Temperature Requirement	0	120	180	240
Flex Bearing Aft End Ring	60	76	73	NA	80
Case-to-Nozzle Joint	75	82	78	NA	84
Throat Housing		70	66	NA	74
Free Air (adjacent to case-to-nozzle joint)		63	NA	NA	77
Flexible Boot		64	NA	NA	NA
Forward Inlet Housing		59	NA	64	NA
Inlet (270 deg)		62			
Outlet (164 deg)		74			
Hydrazine Fluid					
Tilt		63			
Rock		71			

Internal Nozzle Joint Seals

Location	42	52	62	82
Joint 1	75	74	72	71
Joint 2	-Flexible boot sensor temperature			
Joint 3	-Forward inlet housing sensor temperature			
Joint 4	-Nozzle throat housing sensor temperature			
Joint 5	-Aft end ring sensor temperature			

3.1.13 Ground Support Equipment (Adjustable Vent Port Plugs)

Four adjustable vent port plugs (AVPPs) were successfully installed in the case field joints and the case-to-nozzle joint vent ports at 135 deg. Post-test inspection results indicate that all AVPPs were nominal. No motor pressure reached the AVPPs so no assessment of blowby or erosion can be made on the seals. A more detailed discussion can be found in Section 7 of this report.

3.2 RECOMMENDATIONS

3.2.1 Igniter Heater

The igniter heater will undergo additional vendor acceptance tests and the heater circuits will have fuse and GFI installed.

3.2.2 Performance and Mass Properties

Ignition interval was the longest and maximum pressure rise rate was the lowest ever experienced by an SRM, indicating that the ignition of the motor is sensitive to the temperature of the propellant. Previous correlation studies between PMBT and ignition had shown only a weak correlation. The current Morton Thiokol-imposed lower limit on maximum pressure rise rate of 70.9 psi/10ms needs to be reassessed with the new data.

3.2.3 Aft End Conditioning

For future conditioning, it is recommended that the thermal curtains be taped with aluminum foil to limit the amount of air entering or exiting the compartment. The inlet and outlet ducts should be inserted with valves at the thermal curtain entrance to reduce the internal air heat exchange with the environment.

Measurement taken during heating showed an air temperature drop of about 20°F in the 10 ft long inlet duct (located between the heating unit and the thermal curtain) during system operation at a building temperature of 30°F or below. It is recommended that more insulation be added to that part of the ducting system.

3.2.4 Shop Traveler Data

To save time and reduce typing errors in reproducing data from the hard copies on the computer terminals, it is suggested that the data be recorded directly from the terminal onto a hard disk instead of onto paper. In addition, the data stored in this form can be accessed easily and quickly.

3.2.5 Propellant

Results indicate that the effective propellant physical properties at low temperatures need to be investigated further.

3.2.6 Adjustable Vent Port Plug Tool

Training needs to be implemented to teach the correct use of the tool to prevent further problems with raised metal on the bottom plug. Presentation TWR-18838 documents a procedure on how to correctly use the AVPP installation tool.

3.2.7 Dynamics

Additional stability analysis between ignition and mid-burn is recommended.

Predictions of displacements through nozzle vectoring should be made. Further stability analysis is recommended to investigate the pressure effects during motor operation.

3.2.8 Chamber Pressure Oscillation

The magnitude of chamber pressure oscillations should continue to be observed on future motors.

3.2.9 Nozzle Instrumentation

Continued instrumentation of nozzle components is important to adequately monitor nozzle response. Development of methods to more directly monitor the thermostructural response of the phenolic parts should be pursued.

3.2.10 Qualification of Case-to-Nozzle Joint Bolt Preloads

It is recommended that the current case-to-nozzle preloads being used for flight be revised to reflect the higher preloads which were qualified on QM-8. This recommendation, however, is contingent upon the ultrasonic being capable of consistently producing repeatable measurements.

CEI SPECIFICATIONS

This section shows QM-8 static test compliance with Specification CPW1-3600, Addendum D, dated 3 Aug 1987. The following comments are drawn from the test with a one-to-one correlation to the test objectives listed in Section 2.

Qualification Objectives (CEI paragraph number)		Pass/Fail Criteria	Results (Reference Section)
A	Certify the motor performance at 40°F PMBT (3.2.1).	Motor must meet the performance requirements of the CEI specification when PMBT is calculated and performance extrapolated to a 60°F thermal environment.	Motor performance was extrapolated to +60°F and all performance requirements were met. (Table 3.1.9-1)
B	Certify the ignition interval (3.2.1.1.1.1).	Ignition interval (time to reach head-end pressure of 563.3 psia) must be between 202 and 262 ms after ignition command to the SRM ignition initiators.	The ignition interval was 252 ms.(Table 3.1.9-1)
C	Certify the maximum pressure rise rate (3.2.1.1.1.2).	Maximum pressure rise rate must not exceed 115.9 psi for any 10-ms time period.	Maximum pressure rise rate was 72.3 psia/10 ms. (Table 3.1.9-1)
D	Certify the lower allowable rate of maximum pressure buildup (3.2.1.1.1.2, Morton Thiokol imposed).	Lowest allowable rate of maximum pressure buildup must be 70.9 psi for any 10-ms time period.	Maximum pressure rise rate was 72.3 psia/10 ms. (Table 3.1.9-1)
E	Determine the thrust-time curve for QM-8 and apply the data to the nominal thrust-time curve for certification of the RSRM design (3.2.1.1.2.1).	Nominal (arithmetic average) vacuum thrust-versus-time curve (corrected to 60°F PMBT) for all appropriate RSRM motors will fall between the upper and lower bounds of Table I in the RSRM CEI Specification.	The nominal vacuum thrust-time curve lies within the values of Table I of the CEI Specification. (3.1.9)
F	Certify the performance tolerances and limits (determined from chamber pressure data) (3.2.1.1.2.2).	Individual motor performance parameters will fall within the limits specified in Table II of the RSRM CEI Specification.	Individual motor performance values are listed in Table 3.1.9-1.

G	Determine the impulse attained by QM-8 and apply the data to the nominal thrust-time curve for certification of the RSRM design (determined from chamber pressure data) (3.2.1.1.2.4).	Nominal thrust-versus-time curve must comply with the impulse requirements in the RSRM CEI specification.	Impulse requirements in the redesign CEI specification were met. (3.1.9)
H	Certify that all RSRM seals, including adjustable vent port plug seals, experience no erosion or blowby throughout the static test (3.2.1.2).	There must be no erosion or blowby for the specified seals (acceptable erosion is allowed on factory joint insulation acting as the primary seal).	No evidence of erosion or blowby past the RSRM seals. (3.1.3, 7.3)
I	Certify the verifiability of RSRM seals (except for the case-to-nozzle joint primary seal, the factory joint primary seal, the fixed housing-to-aft end ring primary seal, the igniter dual seal plugs (5 places) and the OPT primary and secondary seals (3.2.1.2).	The leak check on RSRM seals must be successfully completed.	The leak check on RSRM seals was successfully completed. (3.1.3.5)
J	Certify that the case field joint and case-to-nozzle joint seals, if pressurized, accommodate static test motor and side load induced structural deflections (3.2.1.2.1.a).	There must be no erosion or gas leakage past the field joint or case-to-nozzle joint seals due to structural deflections.	No evidence of blowby detected due to structural deflections. (3.1.3)
K	Certify that the case field joint and case-to-nozzle joint seals, if pressurized operated when PMBT is at 40°F (3.2.1.2.1.b).	There must be no erosion or gas leakage past the field joint or case-to-nozzle joint seal.	No evidence of gas leakage past the case field joint and nozzle to case joint seals.(3.1.3)

L	Certify that the case field joint and case-to-nozzle joint seal verification does not degrade the integrity of the sealing system (3.2.1.2.1.c).	There must be no damage to insulation, adhesives or seals due to leak check procedures.	No evidence of leak check related damage to insulation, adhesives or seals. (3.1.3.5)
M	Certify that the bore seals for the field joints are verifiable in the proper direction (3.2.1.2.1.d).	The leak check must be successfully completed.	Field joint leak check performance was acceptable. (3.1.3.5, Table 7.4-1)
N	Certify that the case-to-nozzle joint O-ring temperature is maintained prior to static firing (3.2.1.2.1.f).	Pretest data must show that the case-to-nozzle joint temperature was 75°F to 120°F until time of motor ignition.	Aft skirt conditioning kept the case-to-nozzle joint temperature between 78°F and 84°F until motor ignition.(Table 3.1.11.3-1)
O	Certify that the factory joint insulation as a seal accommodates static test motor structural deflections and erosion (3.2.1.2.2.a).	There must be no hot gas leakage to the primary or secondary O-rings due to structural deflections.	Disassembly of factory joints is incomplete. Initial inspection indicates no anomalous conditions.
P	Certify that the factory joint insulation as a seal operates when PMBT is at 40°F (3.2.1.2.2.b).	There must be no hot gas leakage to the primary or secondary O-rings.	Disassembly of factory joints is incomplete. Initial inspection indicates no anomalous conditions.
Q	Certify that the insulation performs the seal function for the factory joint (3.2.1.2.2.d).	At least one virgin ply of insulation will remain over the factory joint with no evidence of hot gas leakage to the primary or secondary O-rings.	Disassembly of factory joints is incomplete. Initial inspection indicates no anomalous conditions.
R	Certify that the factory joint insulation is adequate to preclude leaks (3.2.1.2.2.e).	There must be no hot gas leakage to the primary or secondary O-rings.	Disassembly of factory joints is incomplete. Initial inspection indicates no anomalous conditions.
S	Certify that the flex bearing accommodates static test motor structural deflections (3.2.1.2.3.a).	There must be no erosion or gas leakage between the flex bearing internal components due to structural deflections.	The flex bearing will be fully inspected and tested during completion of post-test acceptance testing. Visual inspection indicated no obvious problems.

T	Certify that the flex bearing operates as a seal at 40°F PMBT (3.2.1.2.3.b).	There must be no erosion or gas leakage between the flex bearing internal components.	The flex bearing will be fully inspected and tested during completion of post-test acceptance testing. Visual inspection indicated no obvious problems.
U	Certify that the flex bearing seal verification does not degrade the performance or integrity of the sealing system (3.2.1.2.3.c).	There must be no damage to the flex bearing due to leak check procedures.	The flex bearing will be fully inspected and tested during completion of post-test acceptance testing. Visual inspection indicated no obvious problems.
V	Certify that the flex bearing maintains a positive gas seal between its internal components (3.2.1.2.3.d).	There must be no gas leakage between the flex bearing internal components.	The flex bearing will be fully inspected and tested during completion of post-test acceptance testing. Visual inspection indicated no obvious problems.
W	Certify that the ignition system seals, if pressurized, accommodate static test motor structural deflections (3.2.1.2.4.a)	There must be no erosion or gas leakage past the ignition system seals due to structural deflections.	Disassembly is incomplete. Details will be included in TWR-17591, Vol VI.
X	Certify that the ignition system seals, if pressurized, operate when PMBT is at 40°F (3.2.1.2.4.b).	There must be no erosion or gas leakage past the ignition system seals.	Disassembly is incomplete. Details will be included in TWR-17591, Vol VI.
Y	Certify that the ignition system seal verification does not degrade the performance or integrity of the sealing system (3.2.1.2.4.c).	There must be no damage to the ignition system seals due to leak check procedures.	Disassembly is incomplete. Details will be included in TWR-17591, Vol VI.
Z	Certify that the nozzle internal seals and the aft exit cone field joint seals, if pressurized, can accommodate static test motor structural deflections (3.2.1.2.5.a).	There must be no erosion or gas leakage past the nozzle internal seals or the aft exit cone joint seals due to structural deflections.	No evidence of damage, blowby or erosion on the nozzle internal seals or the aft exit cone joint seals. (3.1.4.1, 3.1.4.11)

AA	Certify that the nozzle internal seals and the aft exit cone field joint seals, if pressurized, operate when PMBT is at 40°F (3.2.1.2.5.b).	There must be no erosion or gas leakage past the nozzle internal seals or the aft exit cone joint seals.	No evidence of erosion or gas leakage past the nozzle internal seals or the aft exit cone joint seals. (3.1.4.1, 3.1.4.11)
AB	Certify that the nozzle internal seals and the aft exit cone field joint seals verification does not degrade the performance or integrity of the sealing system (3.2.1.2.5.c).	There must be no damage to the nozzle internal seals or the aft exit cone field joint seals due to leak check procedures.	No evidence of leak check-related damage to the nozzle internal seals or the aft exit cone field joint seals. (3.1.3.5)
AC	Certify that the bore seals for the nozzle are verifiable in the proper direction (3.2.1.2.5.e).	Leak check must be successfully completed.	Nozzle leak check performance was acceptable. (3.1.3.5)
AD	Certify that the case is capable of containing the static test internal pressure (3.2.1.3.a).	There must be no damage to the case due to internal pressure.	No evidence that the case allowed leakage of internal pressures or local yielding. (3.1.1)
AE	Certify that the case ETA risers do not degrade the integrity of the case (3.2.1.3.c).	Case must show no damage due to the ETA risers.	No evidence of damage or local yielding of the case at the ETA risers. (3.1.1)
AF	Certify by demonstrating horizontal assembly that the case segment mating joint incorporate provisions to insure proper segment orientation and alignment (3.2.1.3.f).	Horizontal assembly with proper assembly must be demonstrated.	Horizontal assembly with proper alignment was demonstrated. (3.1.1)
AG	Certify by inspection the function of the pin retainer band (3.2.1.3.g).	There must be no anomalies in the pin retainer band.	There were no anomalies in the pin retainer band. (3.1.1)
AH	Certify that the RSRM is designed using motor internal pressure drop from head end to aft end (3.2.1.3.k).	Test data must correlate to the analysis predictions.	Test data correlated to the analysis predictions. (3.1.3)

AI	Certify that the nozzle assembly and exit cone design are compatible with the system performance requirements (3.2.1.4, Morton Thiokol imposed).	Nozzle assembly and exit cone design must be compatible with the specified Morton Thiokol-imposed system performance requirements.	Morton Thiokol-imposed system performance requirements were met. (3.1.4)
AJ	Certify that the nozzle assembly is capable of vectoring through the planned duty cycle (3.2.1.4.1).	Nozzle assembly must follow the planned duty cycle within the expected range as determined by engineering from the historical performance data base.	The nozzle assembly followed the planned duty cycle within the expected range. (3.1.4)
AK	Certify the minimum gimbal rate (3.2.1.4.1).	Minimum nozzle gimbal rate must be at 5 deg/sec.	Evaluation is imcomplete and will be included in TWR-17591, Vol V.
AL	Certify the geometric nozzle alignment (3.2.1.4.2).	With nozzle and motor centerlines within 0.5 deg of each other, the radial offset of the nozzle centerline at the nozzle throat plane must not exceed 0.25 in. from the motor centerline.	With nozzle and motor centerlines within 0.5 deg of each other, the radial offset of the nozzle centerline at the nozzle throat plane was a maximum of 0.078 in. from the motor centerline. (3.1.4.13)
AM	Certify the misalignment of the dynamic thrust vector with respect to the nozzle centerline (3.2.1.4.3 and 3.2.1.4.3.a).	Misalignment of the dynamic thrust vector with respect to the nozzle centerline will not deviate more than 1 deg during nozzle vectoring between null and 8 deg.	Thrust data not collected. No thrust instrumentation in test bay.
AN	Certify the radial offset between the dynamic thrust vector and the nozzle centerline (3.2.1.4.3 and 3.2.1.4.3.b).	Radial offset between the dynamic thrust vector and the nozzle centerline at the nozzle throat plane will not exceed 1.13 in. during nozzle vectoring between null and 8 deg.	Thrust data not collected. No thrust instrumentation in test bay.
AO	Certify the null offset angle at 0 psi nozzle stagnation pressure (3.2.1.4.4.a).	Nozzle null offset angle with respect to zero actuator command will not exceed +0.96 deg at 0 psi nozzle stagnation pressure.	The nozzle null offset angle with respect to zero actuator command was a maximum of 0.636 deg at 0 psi nozzle stagnation pressure. (3.1.4.13)

AP	Certify the null offset angle at 615 psi nozzle stagnation pressure (3.2.1.4.4.b).	Nozzle null offset angle with respect to zero actuator command will not exceed ±0.30 deg at 615 psi nozzle stagnation pressure.	The nozzle null offset angle with respect to zero actuator command was a maximum of -0.28 deg at 615 psi nozzle stagnation pressure. (3.1.4.13)
AQ	Certify the null offset angle at 915 psi nozzle stagnation pressure (3.2.1.4.4.c)	Nozzle null offset angle with respect to zero actuator command will not exceed -0.50 deg at 915 psi nozzle stagnation pressure.	The nozzle null offset angle with respect to zero actuator command was a maximum of -0.402 deg at 915 psi nozzle stagnation pressure. (3.1.4.13)
AR	Certify by post-test inspection that the nozzle snubbing device will not adversely affect the nozzle assembly vectoring capability (3.2.1.4.6).	There must be no adverse effects on the nozzle vectoring capability due to the snubbing device.	Nozzle vectoring was not adversely effected by the snubbing device. (3.1.4.13)
AS	Certify by demonstration the nozzle assembly TVC actuator attach points (3.2.1.4.8).	Nozzle assembly TVC actuator points must be compatible with the TVC actuators.	The nozzle assembly TVC actuator attach points were compatible with the TVC actuators. (3.1.4.13)
AT	Certify the nozzle flame front liner design and fabrication (3.2.1.4.13).	There must be no pockets greater than 0.250 in. deep, no wedgeouts greater than 0.250 in. deep and no prefire anomalies except as allowed by TWR-16340.	The nozzle flame front liner met the requirements of TWR-16340 and there were no pockets or wedgeouts occurring during motor operation observed as a result of design or fabrication. (3.1.4)
AU	Certify that the ignition system precludes hot gas leakage during and subsequent to motor ignition (3.2.1.5.a).	There must be not hot gas leakage.	Disassembly is incomplete. Details will be included in TWR-17591, Vol VI.
AV	Certify that the igniter and the S&A are separable from each other (3.2.1.5.b).	Separation of the igniter and S&A will be demonstrated.	The igniter and S&A were separated during teardown, demonstrating that the S&A can be removed from the igniter during routine disassembly. (3.1.5.1)
AW	Certify the enable function of the S&A device (3.2.1.5.1.a).	S&A device barrier-booster assembly must provide the energy flow required to achieve igniter initiation upon command.	The S&A device both enabled and inhibited ignition upon command. (3.1.5.1)

AX	Certify the S&A change of position from safe to arm and arm to safe (3.2.1.5.1.d).	S&A will change position from safe to arm and arm to safe.	The S&A changed position from safe to arm and arm to safe upon command. (3.0)
AY	Certify that the S&A device will provide simplex remoter position indication (3.2.1.5.1.e).	Safed and armed device must provide remote indication of position in both the safed and armed positions.	The S&A provided remote indication of position. (3.1.5.1)
AZ	Certify the igniter design (3.2.1.5.2).	There must be no debris formed that can damage any other component which is attributable to the igniter, and the igniter must be installed in only one predetermined rotational position into the igniter port from the outside of the forward segment.	Disassembly is incomplete. Details will be included in TWR-17591, Vol VI.
BA	Certify the igniter heater maintains the igniter gasket rubber seals at the required temperature (3.2.1.5.3).	Igniter gasket rubber seals must be maintained between 64° and 130°F just prior to motor ignition.	Igniter gasket rubber seals were maintained within the temperature requirements prior to motor ignition. (3.1.6.1)
BB	Certify the operation of the motor chamber pressure transducer (3.2.1.6.2.1).	Motor chamber pressure transducers must be installed and must function correctly.	The motor chamber pressure transducer remained positively locked and accurately monitored the motor chamber pressure. (Sec 5)
BC	Certify the field joint, case-to-nozzle joint and igniter-to-case joint insulation temperature control(3.2.1.8.1.1.a).	There must be no damage to the field joint, case-to-nozzle joint or igniter-to-case joint metal structural integrity or sealing integrity due to temperature effects.	No evidence of damage to the field joint, case-to-nozzle joint or igniter-to-case joint metal structural integrity or sealing integrity. (3.1)
BD	Certify by demonstration the field joint, case-to-nozzle joint and igniter-to-case joint leak test compatibility (3.2.1.8.1. 1.b).	There must be no damage to the field joint, case-to-nozzle joint or igniter-to-case joint metal structural integrity or sealing integrity due to leak check procedures.	No leak check related damage found at field joints, case-to-nozzle joint or igniter-to-case joint. (3.1.3.5)

BE	Certify by demonstration that the insulation ensures that system performance and structural integrity are maintained during assembly and operation (3.2.1.8. 1.1.c).	Insulation structural integrity must be maintained during assembly and disassembly of the segments.	Insulation structural integrity was maintained during assembly and disassembly of the segments. (3.1.2)
BF	Certify that the field joint, case-to-nozzle joint and igniter-to-case joint insulation provide seal protection (3.2.1.8. 1.1.d).	There must be no erosion or hot gas jetting on the field joint, case-to-nozzle joint or igniter-to-case joint primary and secondary seals.	No evidence of erosion or hot gas jetting on the field joint or case-to-nozzle joint primary and secondary seals. (3.1.2) Igniter-to-case joint information will be included in TWR-17591, Vol II.
BG	Certify the ability of the insulation to protect case joints from thermal degradation during a 40°F PMBT full duration motor burn (3.2.1.8. 1.1.e).	There must be no thermal degradation to the field joint, case-to-nozzle joint and igniter-to-case joint.	No evidence of thermal degradation to the field joint or case-to-nozzle joint. (3.1.2) Igniter-to-case joint information will be included in TWR-17591, Vol II.
BH	Certify by inspection that the field joint, case-to-nozzle joint and igniter-to-case joint insulation do not shed fibrous or particulate matter during assembly which could prevent sealing (3.2.1.8. 1.1.f).	There must be no fibrous or particulate matter attributable to the insulation materials during assembly or disassembly inspections.	No evidence of fibrous or particulate matter attributable to the insulation materials during assembly or disassembly inspections. (3.1.2) Igniter-to-case information will be included in TWR-17591, Vol II and III.
BI	Certify by inspection that the field joint, case-to-nozzle joint and igniter-too-case joint insulation will withstand slag accumulation during motor operation (3.2.1.8.1.1.g).	Slag accumulation in joints must not degrade the case or the sealing capability of the joints.	No evidence of measurable slag damage to joint insulation or case occurring during motor burn. (3.1.1, 3.1.2, Sec 9.4)

BJ	Certify that the ballistic performance is not affected by the field joint, case-to-nozzle joint and igniter-to-case joint insulation (3.2.1.8. 1.1.i).	There must be no anomaly in the ballistics trace attributable to the field joint, case-to-nozzle joint and igniter-to-case joint insulation design.	Changes in insulation design did not measurably alter ballistic performance (Table 3.1.9-1).
BK	Certify that the igniter insulation provides adequate thermal protection for the main igniter chamber and adapter metal parts (3.2.1.8.3).	There must be no damage to the main igniter chamber or adapter metal parts due to temperature effects.	Evaluation is incomplete, will be included in TWR-17591, Vol VI.
BL	Certify the ability of the field joint heater assembly to maintain the temperature of the field joints (3.2.1.11.a).	Field joint temperatures must be maintained between 75° and 130°F prior to motor ignition.	Field joint temperatures were maintained between 75° and 130°F prior to motor ignition.(3.1.6)
BM	Certify the inert weight by inspection (3.2.2.2.1).	Inert weight must not exceed 150,847 lb.	The inert weight was 148,919 lb. (TWR-17331)
BN	Certify the nozzle forward section weight by inspection (3.2.2.2.1, Morton Thiokol imposed (3)).	Nozzle forward section weight must not exceed 17,512 lb.	Nozzle forward section weight was 17,211 lb. (TWR-17331)
BO	Certify the exit cone weight by inspection (3.2.2.2.1, Morton Thiokol imposed (5)).	Exit cone weight must not exceed 6,643 lb.	Exit cone weight was 6,384 lb. (TWR-17331)
BP	Certify the propellant weight by inspection (3.2.2.2.2).	Propellant weight will be at least 1,104,714 lb.	Propellant weight was 1,105,399 lb. (TWR-17331)
BQ	Certify the loaded RSRM center of gravity for the longitudinal (X) axis (3.2.2.2.3).	Loaded condition longitudinal center of gravity must be between 1,179 and 1,165.	Loaded condition longitudinal center of gravity was 1,171 lb. (TWR-17331)
BR	Certify the reliability of the RSRM design (3.2.3).	Postfire engineering evaluation limits (TWR-17198) must be met.	Certification and reliability data were collected for evaluation.(3.1.6, Sec 8 and Sec 9)

BS	Certify that the primary structure, thermal protection and pressure vessels meet design safety factors (3.2.3.1).	Primary structure, thermal protection and pressure vessel subsystems must preclude motor failure.	Evaluation is incomplete and will be included in TWR-17591, Vol II.
BT	Certify by demonstration that the RSRM segments are capable of horizontal assembly/ disassembly (3.2.5.1).	Successful horizontal assembly and disassembly must be demonstrated.	Horizontal assembly and disassembly was demonstrated. (3.1.1)
BU	Certify that the shedding of external debris is precluded (3.2.6.5).	There must be no shedding of debris.	There was no shedding of external debris.(3.1.6)
BV	Certify the performance at lower temperature limit (3.2.7.1.a2).	Motor performance requirements must be met at 40°F PMBT.	Motor performance requirements were met at 40°F PMBT (see Table 3.1.9-1).
BW	Certify that structural and electrical bonding meets the requirements of MIL-B-5087 in all areas except the area of lightning protection (3.3.5.2).	Electrical bonding requirements must not exceed 0.1Ω.	Bonding requirements did not exceed 0.1Ω. (Sec 5)
BX	Certify that static electricity and lightning protection meet the requirements (3.3.5.5).	Electrical bonding resistance measurements must not exceed 2.5mΩ.	Electrical bonding resistance measurements did not exceed 2.5mΩ. (Sec 5)
BY	Gather data to validate the analytical model which certifies the general structural safety factors for the nozzle (3.3.6.1.1.1).	Design safety factors must be used to calculate performance margins of safety.	Evaluation is incomplete, but will be included in TWR-17591, Vol. V.
BZ	Certify minimum structural safety factor for the adhesive bond for DFI/OFI/GEI (3.3.6.1.1.2.b).	No debond allowed during firing.	Evaluation is incomplete, but will be included in TWR-17591, Vol. III.

CA	Certify the thermal erosion minimum safety factor for case internal insulation (3.3.6.1.2.2).	There must be a minimum case insulation thermal safety factor of 1.5 (excluding joints).	Evaluation is incomplete, but will be included in TWR-17591, Vol. III.
CB	Certify the thermal erosion minimum safety factor for case internal insulation adjacent to metal part field joints and extending over factory joints (3.3.6.1.2.3).	There must be a minimum case insulation thermal safety factor of 2.0 for the specified joints.	Evaluation is incomplete, but will be included in TWR-17591, Vol. III.
CC	Certify the thermal erosion minimum safety factor for the case internal insulation sandwich construction regions (aft dome and center segment of aft end) (3.3.6.1.2.4).	There must be a minimum safety factor of 1.5.	Evaluation is incomplete, but will be included in TWR-17591, Vol. III.
CD	Certify the insulation performance (3.3.6.1.2.6).	The insulation erosion must not exceed design safety when corrected using minimum design thickness.	Evaluation is incomplete, but will be included in TWR-17591, Vol. III.
CE	Certify the nozzle design safety factors (3.3.6.1.2.7).	Nozzle ablative components must meet or exceed the design safety factors.	Evaluation is incomplete, but will be included in TWR-17591, Vol. V.
CF	Certify the nozzle performance margin of safety (3.3.6.1.2.8).	Nozzle ablative components must meet or exceed the design safety factors.	Evaluation is incomplete, but will be included in TWR-17591, Vol V.
CG	Certify that the RSRM design minimizes the need for new on-plant facilities, and that existing facilities and facility equipment are used for the storage of spares and maintenance functions to the maximum possible extent (3.4.3).	Motor must be manufactured and tested using a minimum of new on-plant logistics facilities.	A minimum of new on-plant logistics facilities were used to test and manufacture QM-8.
CH	Qualify the installation of the systems tunnel floor plate by paint stripper surface preparation.		The installation of aluminum floor plate systems tunnel segments using the chemical paint stripper process was successfully qualified. (3.1.7)

CI	Qualify higher preload and torque values for case-to-nozzle axial and radial bolts.	Higher preload and torque values for case-to-nozzle axial and radial bolts were qualified. (3.1.1.2.1)
CJ	Qualify the use of Fiberite carbon phenolic material in the three nozzle inlet rings and in the throat ring.	The use of Fiberite carbon phenolic material in the three nose inlet rings was qualified. (3.1.4)

Development Objectives:

CK Acquire engineering data for model validation.

CL Measure joint gap opening in nozzle internal joints.

CM Evaluate nozzle joint No. 2 bonding process change

CN Assess capability of the RSRM to structurally withstand the side load provided by MSFC and defined in the test plan (CTP-0060, Rev D).

CO Obtain data on chamber pressure oscillations and compare to the RSRM and HPM data base.

Other Qualification Test Objectives:

CP Success criteria for the OBR

1. No evidence of hot gas erosion inside the flex boot cavity except that produced by the vent holes.

2. OBR hoop continuity exists through the beginning of motor pressure tailoff.
   - o Delamination and wedgeout of 35 deg wrap acceptable
   - o Need not comply with CEI specification 3.2.1.4.13.b dealing with general wedgeouts

Qualification of the adjustable vent port plug installation fixture:

Qualification Objectives CEI CDW2-3679 (paragraph number)	Pass/Fail Criteria	Results (Reference Section)
CQ Certify the performance of the vent port plug installation tool as a means of installing, rotating, and torquing the bottom section of the adjustable vent port plug (3.2.1.1).	Vent port plug installation tool must provide necessary torque to install and rotate the bottom section of adjustable vent port plug.	Vent port plug installation tool performed satisfactorily as a means of installing, rotating and torquing the bottom section of the adjustable vent port plug. (Sec 7)

CR	Certify that the installation fixture is efficient and does not require special and additional tooling (3.2.1.1).	Additional tools must not be required for installation procedures.	No additional tools were required for installation procedures. (Sec 7)
CS	Certify that the use of the vent port plug installation tool does not affect the safe and reliable use and reusability of the RSRM (3.2.1.1).	No damage can result to the adjustable vent port plug during installation.	No damage occurred to the adjustable vent port plug during installation. (Sec 7)
CT	Certify that the tool allows for a threaded installation to the bottom section of the adjustable vent port plug (3.2.1.2.1).	Threaded installation to bottom section of the adjustable vent port plug must be obtained.	Threaded installation to the bottom section of the adjustable vent port plug was obtained. (Sec 7)
CU	Certify that interlocking allows for rotation and torquing of the bottom section of the adjustable vent prot plug (3.2.1.2.2).	Tool must interlock with the adjustable vent port plug without slippage.	The tool successfully interlocked with the adjustable vent port plug without slippage. (Sec 7)
CV	Certify the capability of interlocking the installed installation tool with the bottom section of the adjustable vent port plug, and the utilization of the notch in bottom of the adjustable vent port plug (3.2.1.2.2).	Tool must interlock with the bottom notch of the adjustable vent port plug during installation operation.	Tool interlocked with the bottom notch of the adjustable vent port plug during installation operation. (Sec 7)
CW	Certify that the tool is capable of applying a minimum torquing force of 70 in.-lb to the bottom section of the adjustable vent port plug (3.2.1.2.4).	Minimum of 70 in.-lb must be applied to the adjustable vent port plug by installation tool.	Tool was capable of applying minimum torquing force to the bottom section of the adjustable vent port plug. (Sec 7)
CX	Demonstrate that tool is capable of being transported to work site (3.2.8).	Tool must be easily transportable by hand.	Tool was easily transportable by hand. (Sec 7)

5

INSTRUMENTATION

5.1 INTRODUCTION

The QM-8 Test Article included instrumentation similar to that used on previous static motors and subscale test articles. Instrumentation was installed on the test article per Drawing 7U75880. Figures 5.1-1 through 5.1-7 show instrument locations. Table 5.1-1 summarizes the instrumentation on QM-8. See Appendix B for instrumentation list, and Appendix C for data plots. A complete discussion of instrumentation performance will be included in TWR-17591, Vol IX.

5.2 OBJECTIVES

QM-8 was instrumented to collect the engineering and motor performance data necessary to evaluate the following objectives taken from Section 2.

Qualification Objectives

BB Certify the operation and installation of the motor chamber operational pressure transducer.

BW Certify that structural and electrical bonding meet the requirements in all areas except the area of lightning protection.

BX Certify that static electricity and lightning protection meets the requirements.

BZ Certify structural minimum safety factor for the adhesive bond for DFI/OFI/GEI.

5.3 CONCLUSIONS/RECOMMENDATIONS

Overall, the instrumentation performed well with the exceptions noted in Table 5.3-1. Instrumentation installation was successfully completed and performed as expected.

The instrumentation test objectives were met. The operational transducer was installed and performed properly. The structural and electrical bonding met the requirements. The lightning protection system was included in the low-pressure transducer installation, but the function of the system cannot be tested on full-scale test motors. The requirement to pull test the accelerometer fairings was deleted because of interference with the rounding rings used for motor disassembly. The low-pressure transducer fairing and low-pressure pick-up fairing will be pulled to failure when the forward segment is shipped to H-7.

Twelve gages were declared anomalous after the static test. Table 5.3-1 shows the anomaly list.

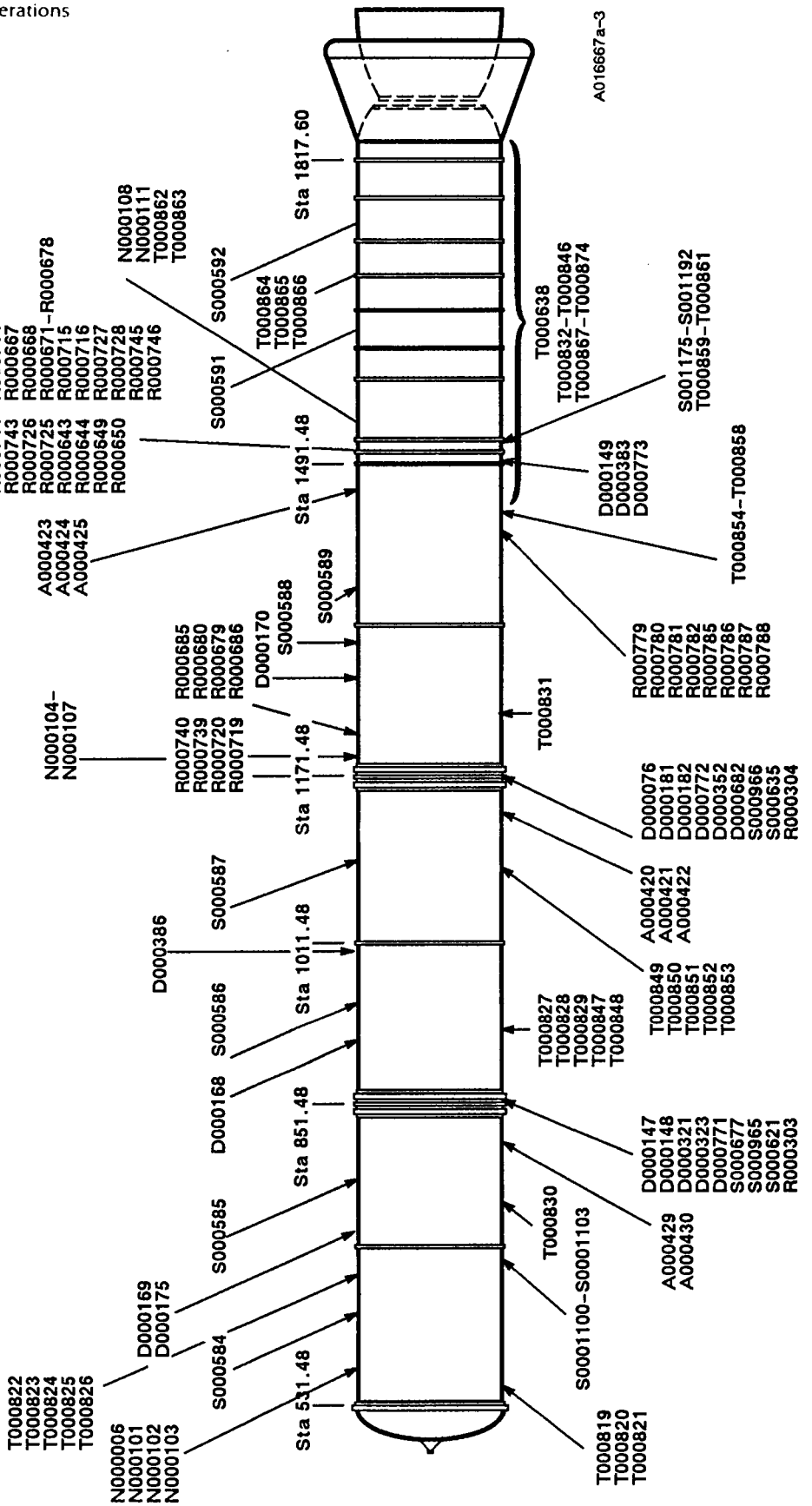

Figure 5.1-1. QM-8 Case Instrumentation

A016669aR2

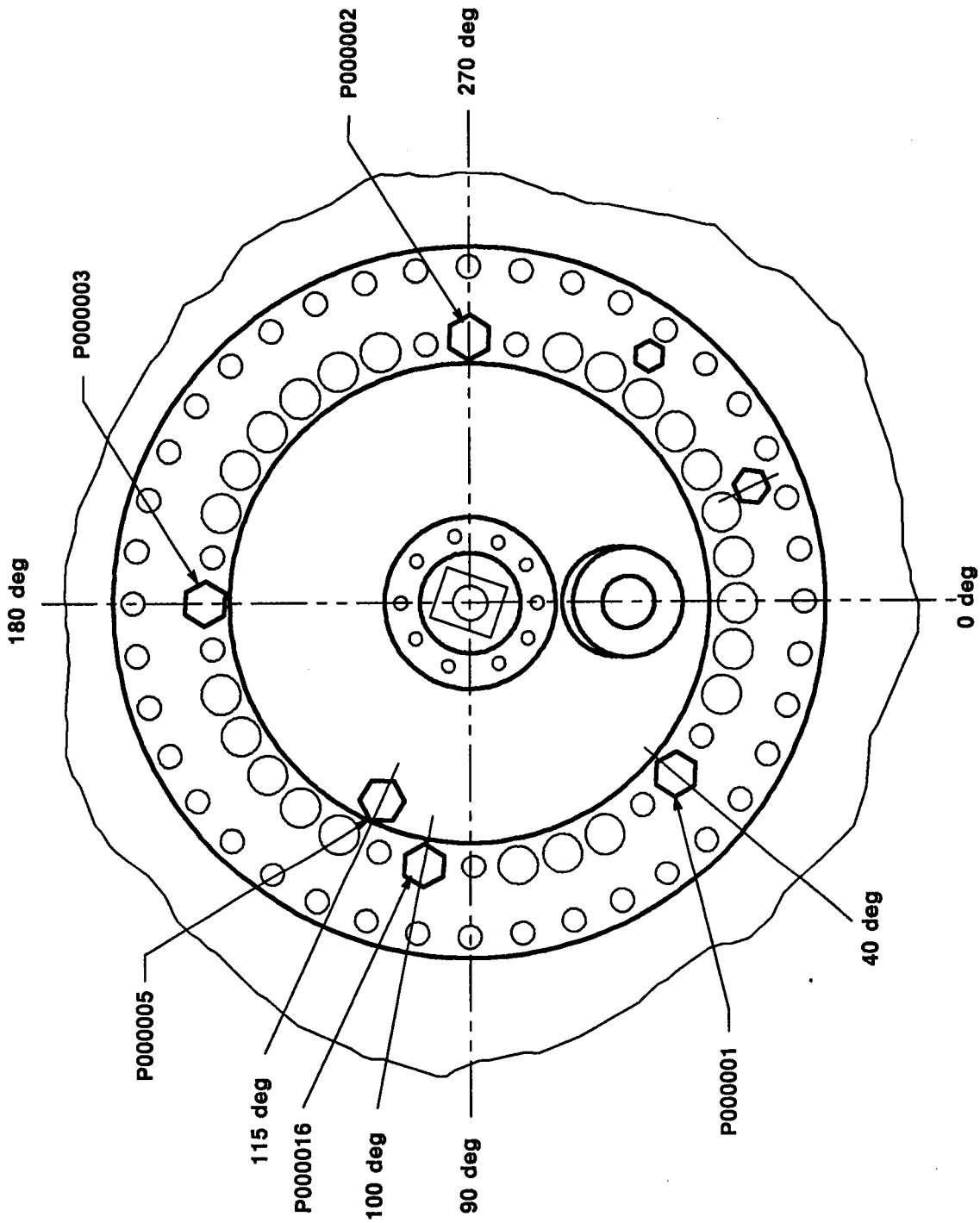

Figure 5.1-2. QM-8 Head End Pressure Transducer Locations

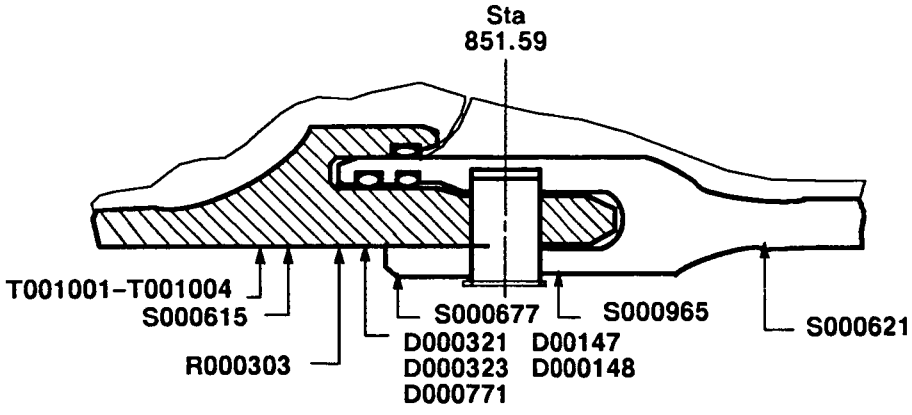

Forward Field Joint

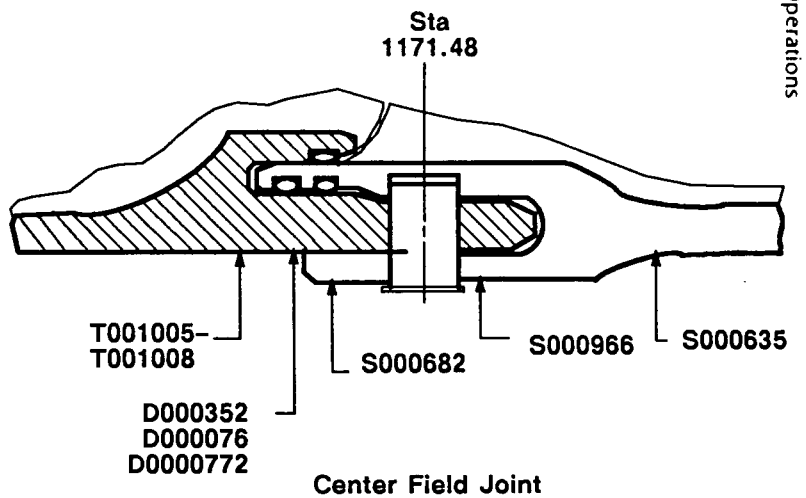

Center Field Joint

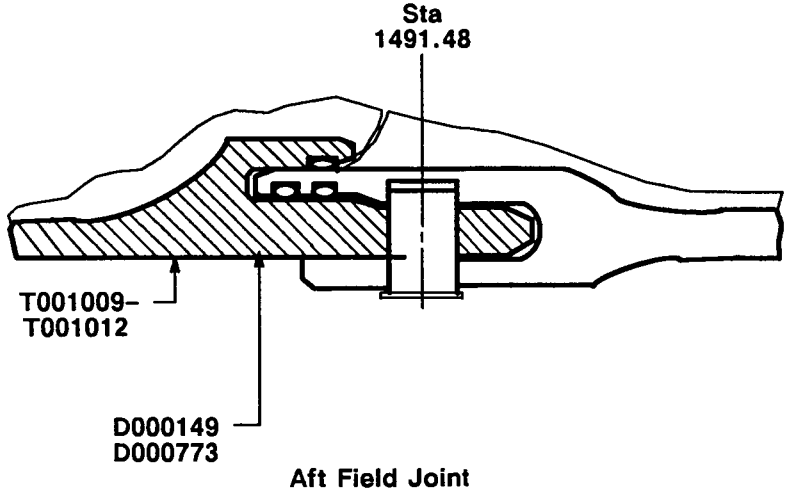

Aft Field Joint

Figure 5.1-3. QM-8 Joint Growth

A017664a1

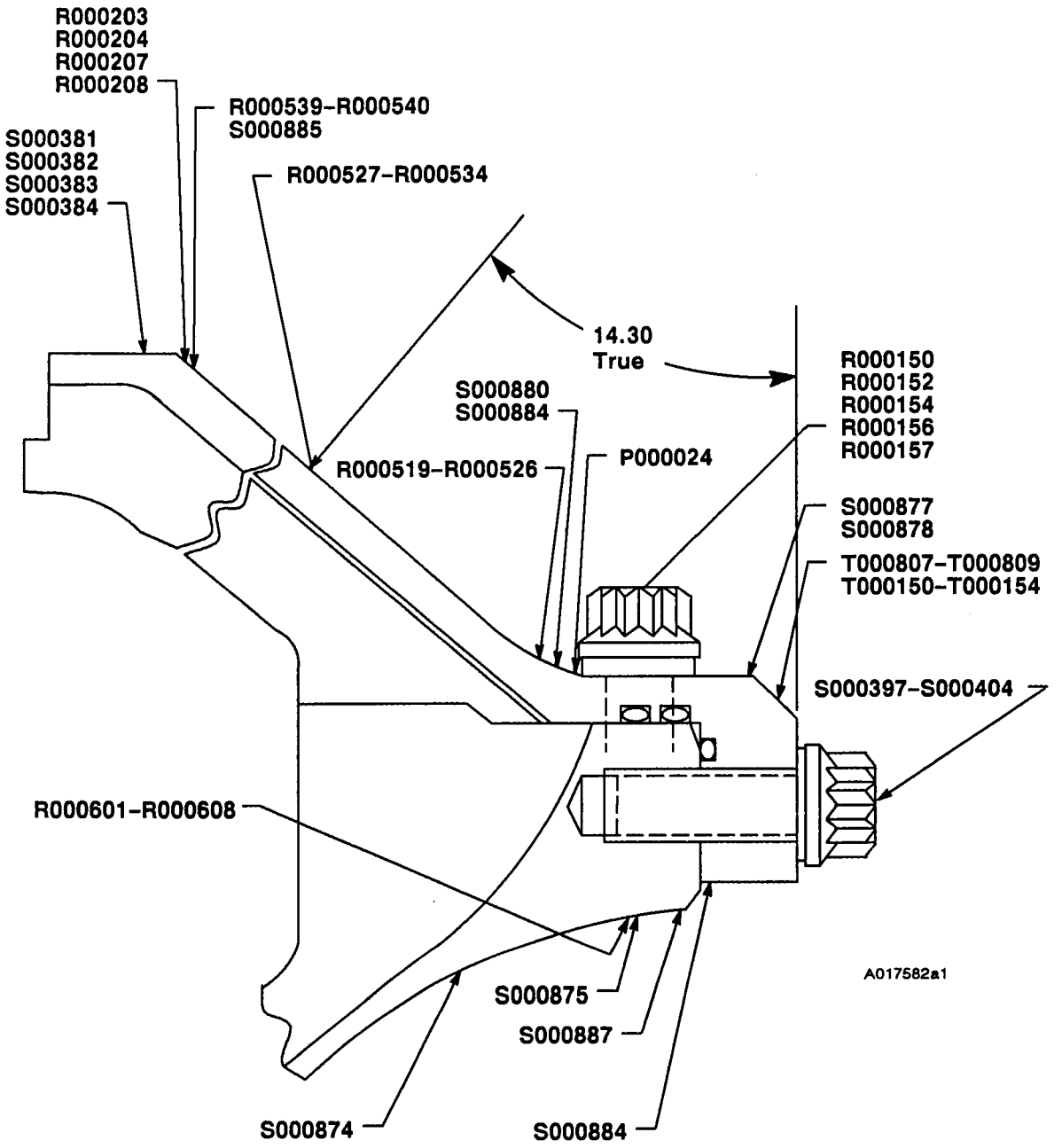

Figure 5.1-4. QM-8 Case-to-Nozzle Joint Instrumentation

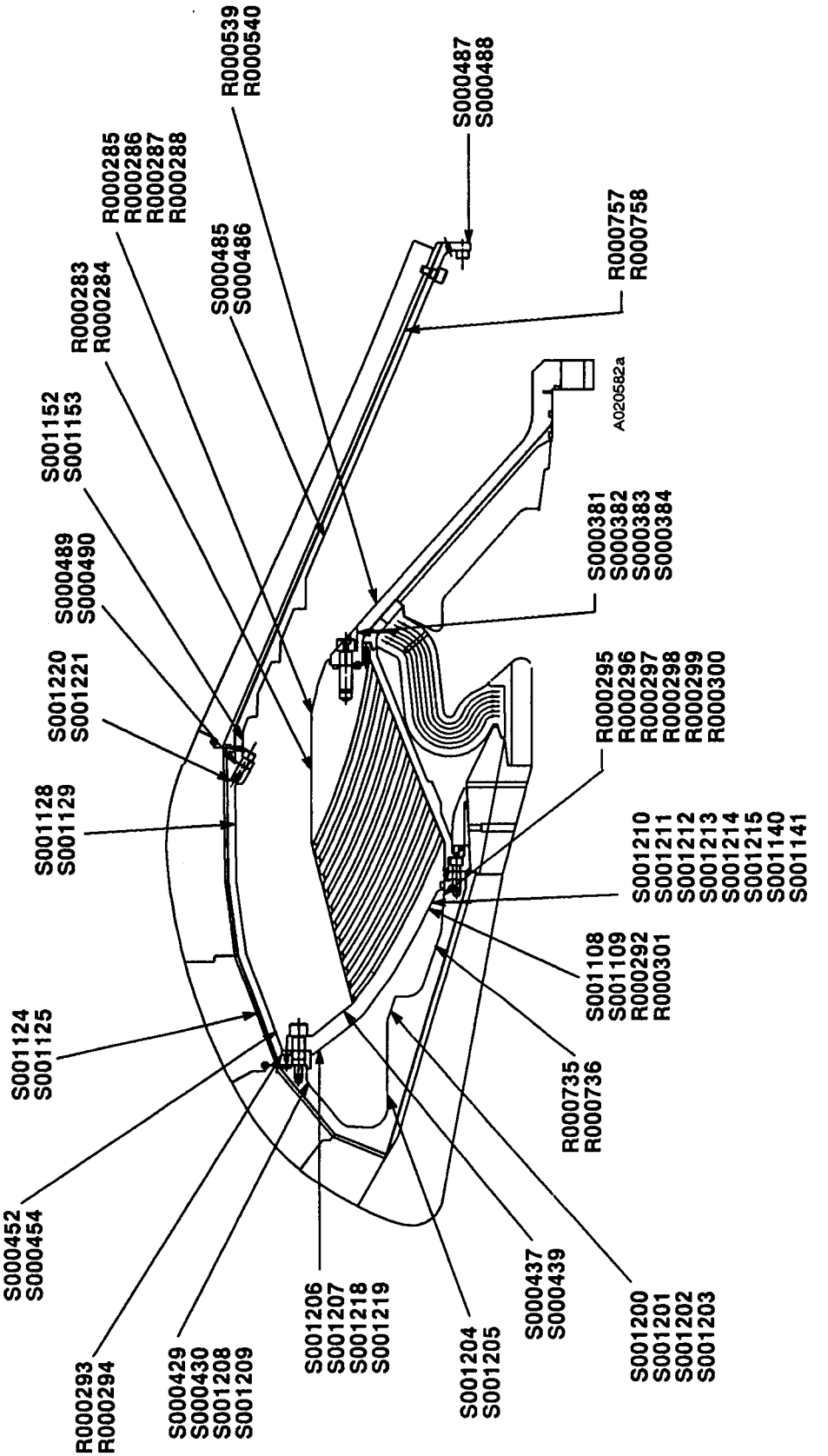

Figure 5.1-5. QM-8 Strain Gage Nozzle Instrumentation

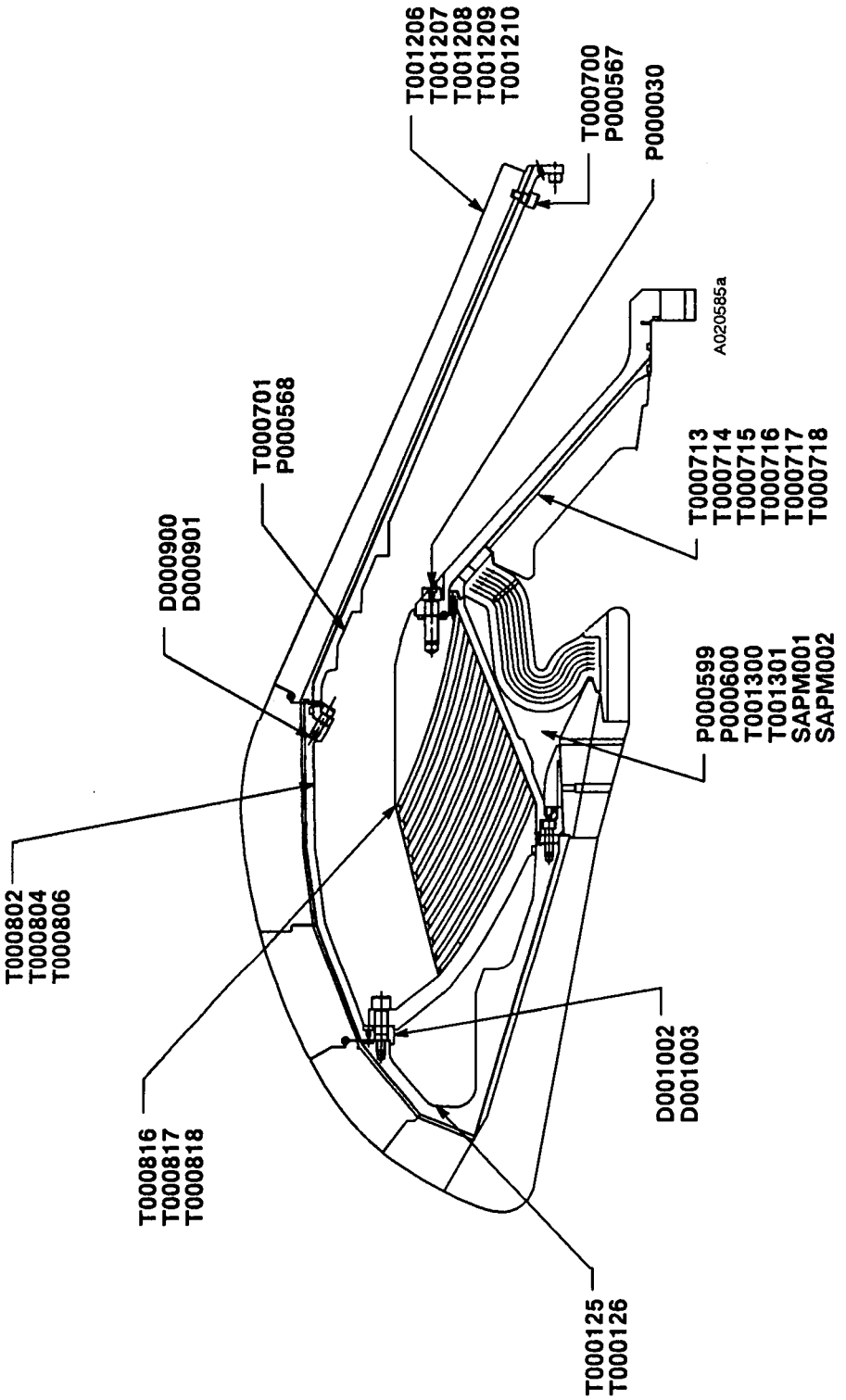

Figure 5.1-6. QM-8 Nozzle Instrumentation Displacement, Temperature, and Pressure

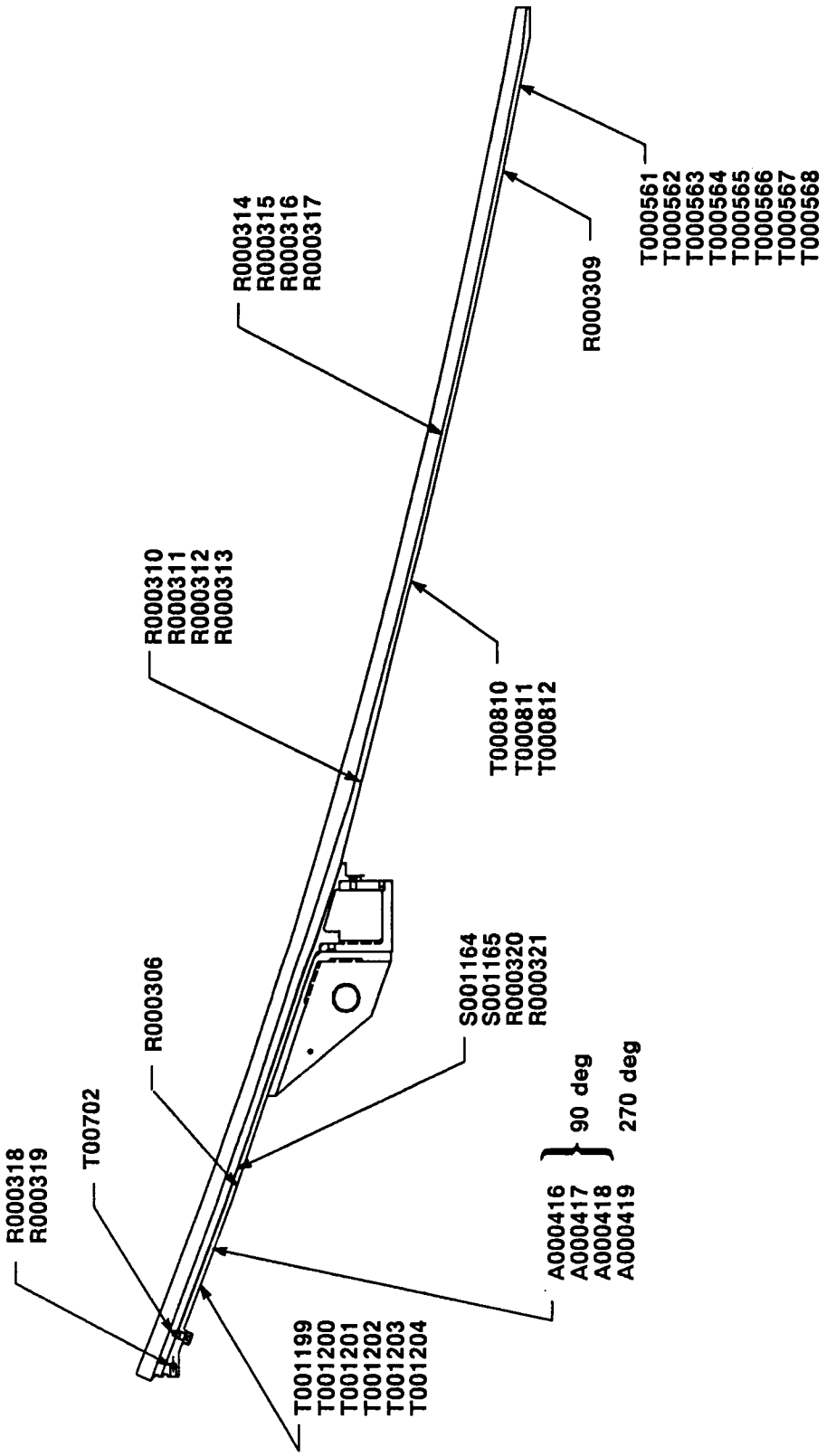

A020820a

Figure 5.1-7. QM-8 Aft Exit Cone Instrumentation

Table 5.1-1. Instrumentation Summary

Type of Instrumentation	Area of Investigation	Number of Channels
Accelerometer (A)	Nozzle and case vibration TVC vibration and shock	39
Extensometers (D)	Unreinforced membrane Motor sag nozzle position axial growth	29
Proximity (D)	Exit cone bondline separation	3
LVDT (D)	Field joint movement	3
Dog Bone (D)	Nozzle joint movement	6
Voltage (E)	TVC and side load	15
Force (F)	Side load	3
Current (I)	TVC system	11
TVC Interlock (K)	TVC system	6
Microphones (N)	Forward segment Center segments Aft segment	12
Pressure (P)	Chamber pressure Igniter pressure Chamber oscillation Case-to-nozzle joint Nozzle internal joint No. 4 Boot cavity TVC system Side load Water deluge	36
Strain Gage (S&R)	Case line loads ETA ring effects Nozzle component Aft dome/fixed housing Pressure drop-in bond Joint radial growth Aft exit cone growth Case-to-nozzle expansion Case-to-nozzle joint skip/rotation	218

Table 5.1-1. Instrumentation Summary (Cont)

Type of Instrumentation	Area of Investigation	Number of Channels
Strainserts* (R-radial) (S-axial)	Case-to-nozzle joint bolt loads	16
Temperature (T)	External joint	186
	TVC system	
	Slag	
	Exit cone temperature	
	Case-to-nozzle joint	
	Igniter joint	
	Igniter grain	
	Propellant grain	
	Field joint heaters	
	Boot cavity	
	Nozzle components	
	Bondline	
	Case skin	
	S&A joint	
	Free air	
	Bay temperature	
Event	Primary ignition	14
	TVC system	
	Total	597

Table 5.3-1. QM-8 Anomaly List

Parameter No.	Symptom	Remark
A000427	No data	Broken cable
D000323	No data	Bad bus control unit (BCU)
D000772	Bad data	Sticky probe
D000773	No data	Bad ac LVDT
D000568	No data	Broken lead wire
D000900	No data	Gage damaged during snubber installation
R000303	No data	Shorted to case
S000489	No data	Open gage
S000878	No data	Open gage
X000001	No data	Unknown
T000152	No data	Unknown
P000599	No data after 6 sec	Shorted cable

5.4 INSTRUMENTATION DISCUSSION

There were 599 channels of instrumentation installed on the motor, including pressure, force, acceleration, displacement, strain, and temperature gages. All instrumentation that penetrated the pressure vessel remained tight and showed no evidence of blowby.

An LVDT was located in each of the field joints at 45 deg (Figure 5.4-1). The LVDT in the aft field joint, D000773, went bad during the test. The LVDT in the center field joint, D000772, had a sticky probe and did not follow joint movement properly. The LVDT in the forward field joint, D000771, performed properly.

Pressure transducers were located in the head end of the motor, case-to-nozzle joint leak check port (Figure 5.4-2), internal nozzle Joint 5, and in the boot cavity. All pressure transducers performed well with the exception of P000599, which was located in the boot cavity. Output from P00599 was lost at T+6 sec due to a shorted cable. Three other pressure transducers were located in the boot cavity. P000600, which was the same type as P000599, performed for the full-test duration. SAPM001 and SAPM002 were the stand alone pressure measuring devices furnished by Johnson Space Center. The stand-alone gages appeared to be in good condition after removal from the boot cavity. They must be sent to Johnson Space Center to have the data recovered from them. Gages that were deleted before the QM-8 static fire are listed in Table 5.4-1.

A016670a1

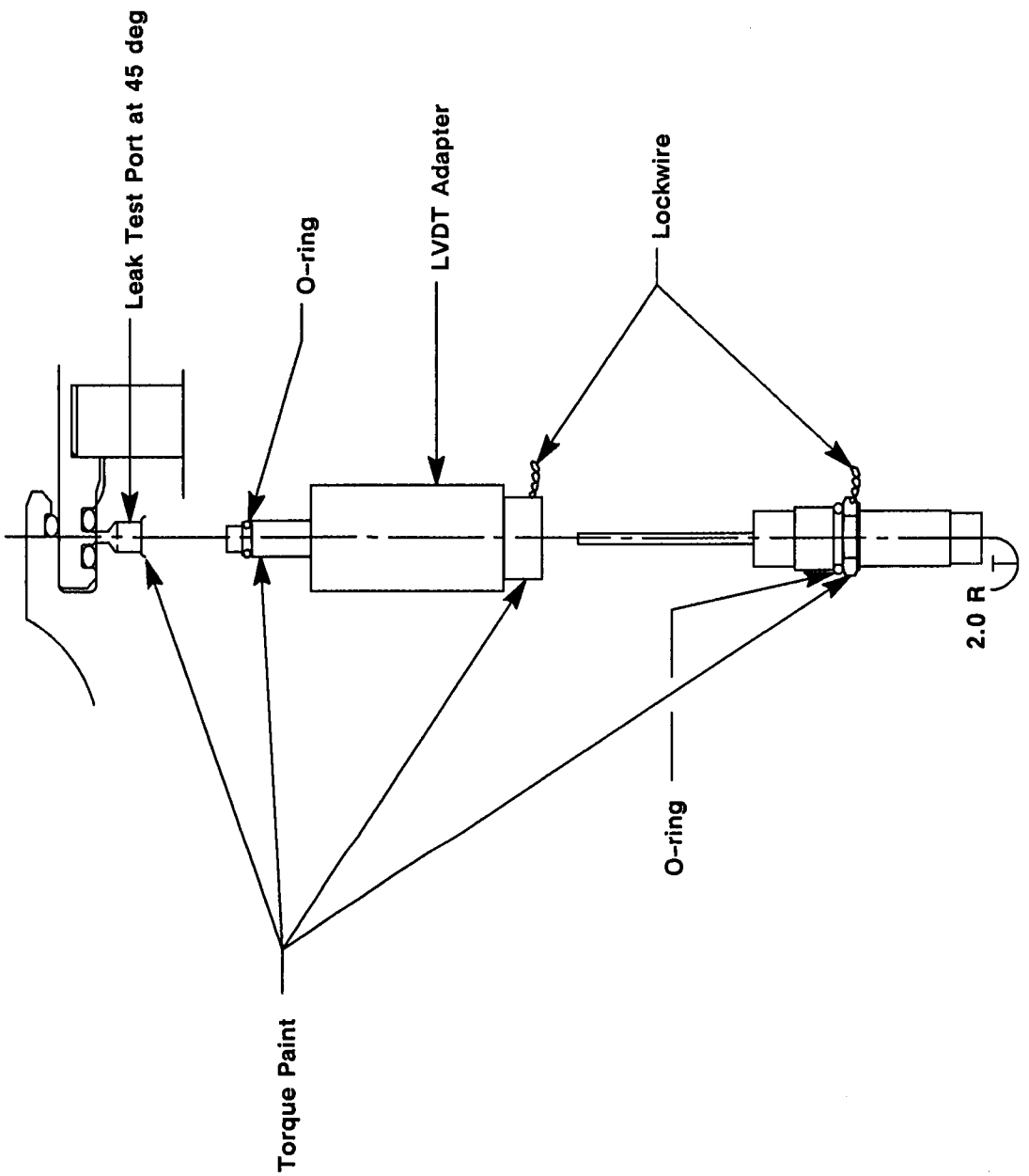

Figure 5.4-1. LVDT Assembly at Forward, Center, and Aft Field Joints

A016671a1

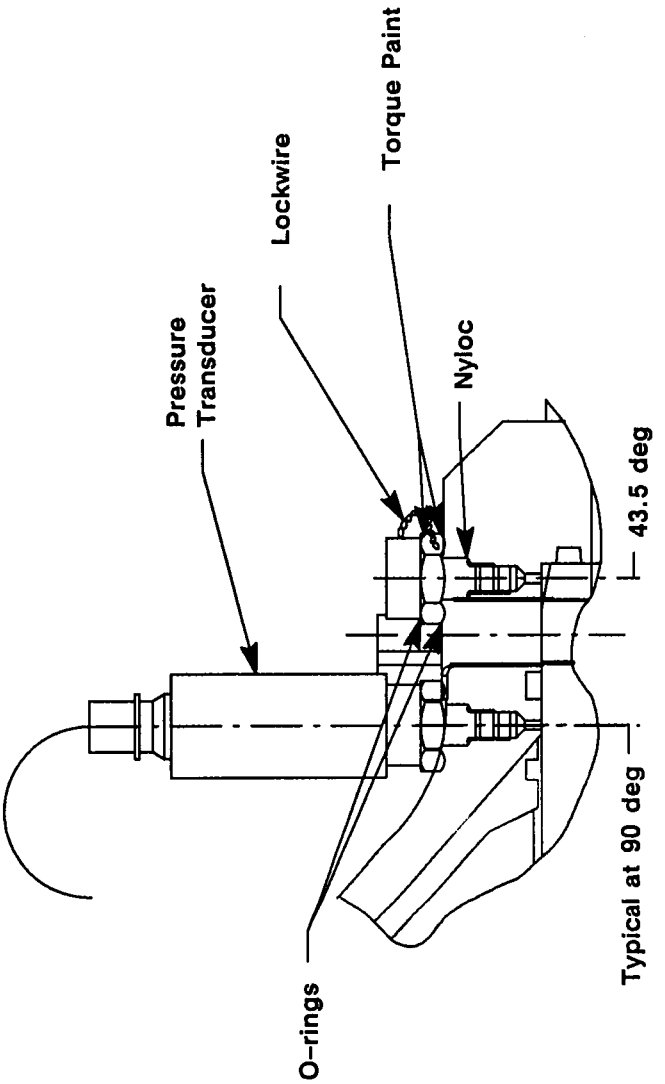

Figure 5.4-2. Case-to-Nozzle Joint Pressure Transducer

Table 5.4-1. QM-8 Deleted Gages

Parameter No.	Location	Type
D000150	Case-to-ground	Displacement
R000305	Aft field joint	Strain
R000307	Aft exit cone	Strain
R000308	Aft exit cone	Strain
R000352	Stiffener/aft dome factory joint	Strain
R000353	Stiffener/aft dome factory joint	Strain
S000686	Aft field joint	Strain
S000689	Aft field joint	Strain
S000968	Aft field joint	Strain
S001104	Stiffener/aft dome factory joint	Strain
S001105	Stiffener/aft dome factory joint	Strain
S009034	Stiffener ring splice plate bolt	Strain
S009035	Stiffener ring splice plate bolt	Strain
S009036	Stiffener ring splice plate bolt	Strain
S009037	Stiffener ring splice plate bolt	Strain
T000813	Tunnel bondline	Temperature
T000814	Tunnel bondline	Temperature

6

PHOTOGRAPHY

Photographic coverage was required to document the test, test configuration, instrumentation, and any anomalous conditions which may have occurred. The QM-8 photographs and video tapes are available from the Morton Thiokol Photo Lab.

6.1 STILL PHOTOGRAPHY

Still color photographs of the test configuration were taken before, during, and after the test. Photographs were taken of joints each 45 deg minimum, and of anomalous conditions. A large number of photographs were taken during disassembly.

6.2 MOTION PICTURES

Color motion pictures of the test were taken with 3 video, 10 documentary, and 17 high-speed cameras. Coverage included the nozzle severance test. Documentary motion pictures were recorded on Roll 7805 and high-speed motion pictures on Roll 7804. Cameras are listed in Tables 6.2-1 and 6.2-2. Camera setup is shown in Figures 6.2-1 through 6.2-3.

Table 6.2-1. Static Test Motor Photography and Video Coverage

Camera	Station	Location	Type*	Coverage
1	1	No fwd barricade	Doc	Motor and plume
1A	1	No fwd barricade	Doc	Motor case and plume
2	1	No fwd barricade	HS	Fwd dome, center fwd joints
3	1	No fwd barricade	HS	Overall case joints
4	2	No aft barricade	Doc	Motor and plume
4A	2	No aft barricade	Doc	Aft case and plume
5	2	No aft barricade	HS	Aft case nozzle and plume
5A	2	No aft barricade	HS	Nozzle and 200 ft plume
5B	2	No aft barricade	HS	CU of thermal curtain
5C	2	No aft barricade	EHS	Nozzle plug expulsion
6	2	No aft barricade	EHS	Nozzle severance
7	3	So aft barricade	HS	Overall case joints
7A	3	So aft barricade	HS	Aft case nozzle and plume
8	3	So aft barricade	EHS	Nozzle severance
9	3	So aft barricade	Doc	Overall motor and plume
9A	3	So aft barricade	Vid	Overall motor and plume
10	4	So ctr barricade	HS	Center, center aft joints
10A	4	So ctr barricade	HS	Nozzle, 200 ft plume
11	4	So ctr barricade	Doc	Overall motor, nozzle, and plume
11A	4	So ctr barricade	Doc	Aft case nozzle and plume
12	4	So ctr barricade	EHS	Nozzle plug expulsion
12A	4	So ctr barricade	Vid	Overall motor and plume
13	5	So fwd barricade	HS	Fwd dome, ctr fwd joint
13A	5	So fwd barricade	SQ	Overall motor and plume
14	5	So fwd barricade	Doc	Overall motor and plume
15	5	So fwd barricade	Doc	Forward deluge
15A	5	So fwd barricade	Doc	Aft deluge
16	6	Side load	HS	Fwd side load attach point
16A	6	Side load	HS	Aft side load attach point
18	6	Side load	Doc	Motor and plume
19	7	Thrust block	Doc	Overall case and plume
19A	7	Thrust block	Vid	Overall case and plume
20	7	Thrust block	HS	Overall case and plume
20A	7	Thrust block	SQ	Overall case and plume

*EHS --High speed at 1,000 pps
HS --High speed at 300 pps
Doc --Documentary at 24 pps
SQ --Sequence at 1 pps
Vid --Video at real-time
No --North
So --South

Table 6.2-2. Static Test Motor Camera Control and Priority Requirements

Camera	Station	Start Time	Stop Time	Priority
1	1	T-15 sec	T+180 sec	R
1A	1	T-15 sec	T+180 sec	R
2	1	T-5 sec	T+150 sec	M
3	1	T-5 sec	T+150 sec	M
4	2	T-15 sec	T+180 sec	R
4A	2	T-15 sec	T+180 sec	R
5	2	T-5 sec	T+150 sec	M
5A	2	T-5 sec	T+150 sec	M
5B	2	T-5 sec	T+150 sec	M
5C	2	T-5 sec	T+150 sec	M
6	2	T-535 sec	T+560 sec	R
7	3	T-5 sec	T+150 sec	M
7A	3	T-5 sec	T+150 sec	M
8	3	T-535 sec	T+560 sec	R
9	3	T-15 sec	T+180 sec	R
9A	3	T-15 sec	T+180 sec	R
10	4	T-5 sec	T+150 sec	M
10A	4	T-5 sec	T+150 sec	M
11	4	T-15 sec	T+180 sec	R
11A	4	T-15 sec	T+180 sec	R
12	4	T-5 sec	T+150 sec	M
12A	4	T-15 sec	T+180 sec	R
13	5	T-5 sec	T+150 sec	M
13A	5	T-5 sec	T+180 sec	R
14	5	T-15 sec	T+180 sec	R
15	5	T-2 sec	T+33 min	R
15A	5	T-2 sec	T+33 min	R
16	6	T-5 sec	T+150 sec	M
16A	6	T-5 sec	T+150 sec	M
18	6	T-15 sec	T+180 sec	R
19	7	T-15 sec	T+180 sec	R
19A	7	T-15 sec	T+180 sec	R
20	7	T-5 sec	T+150 sec	M
20A	7	T-5 sec	T+150 sec	M

Station	Location
1	North forward barricade
2	North aft barricade
3	South aft barricade
4	South center barricade
5	South forward barricade
6	Side load
7	Thrust block

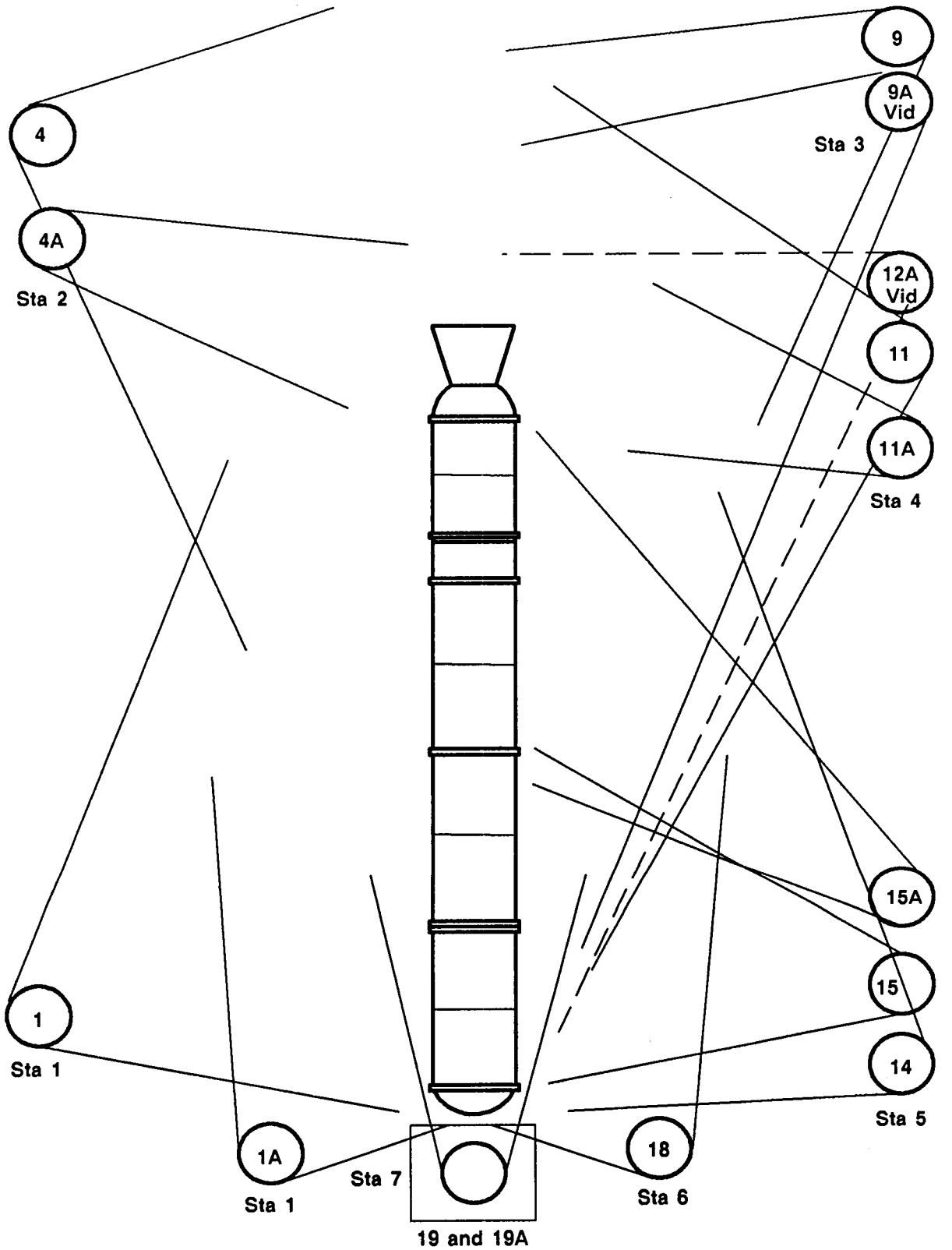

-Figure 6.2-1. Documentary (real-time) and Video Coverage

A013164a

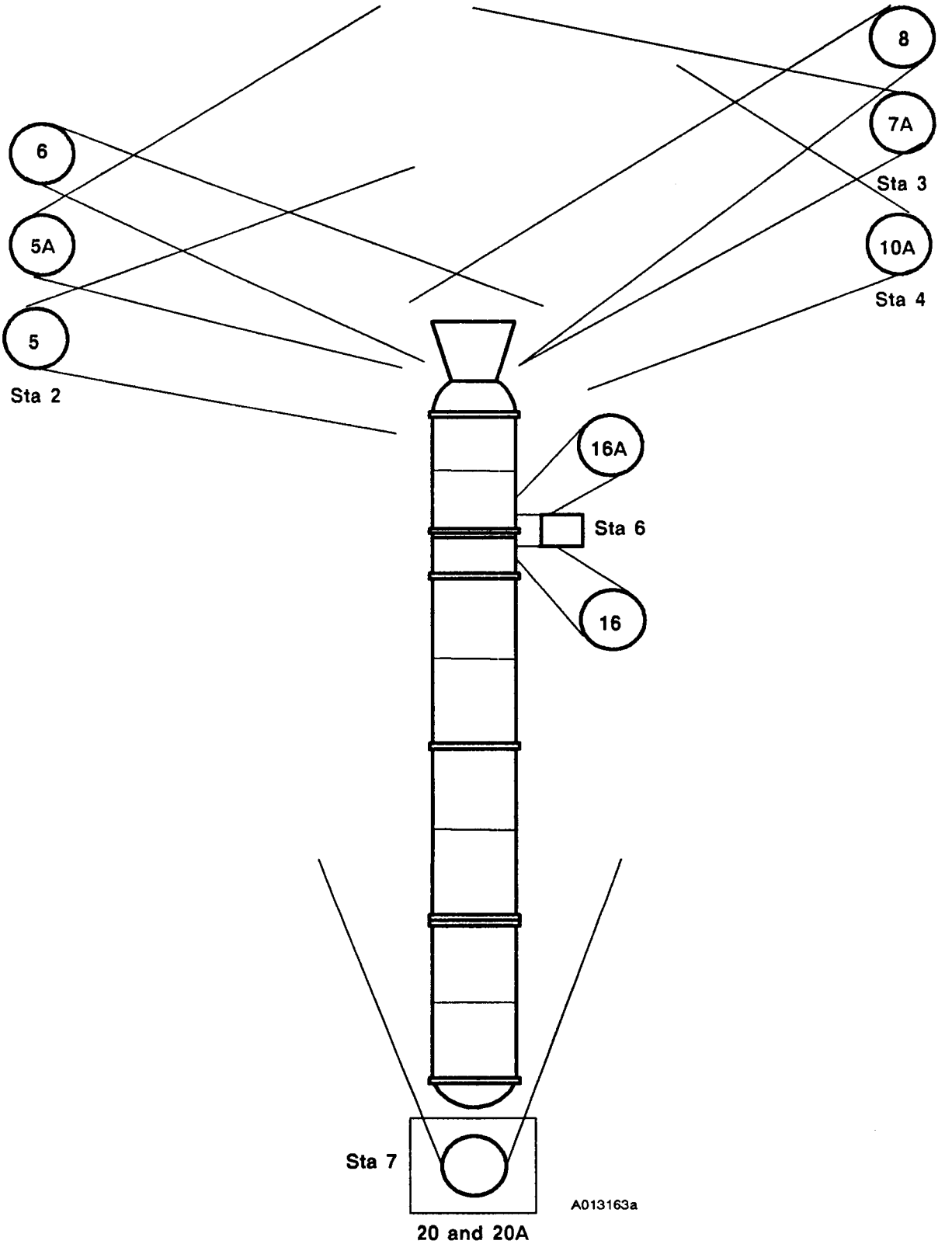

Figure 6.2-2. High-Speed Coverage, Plum and Side Load Coverage

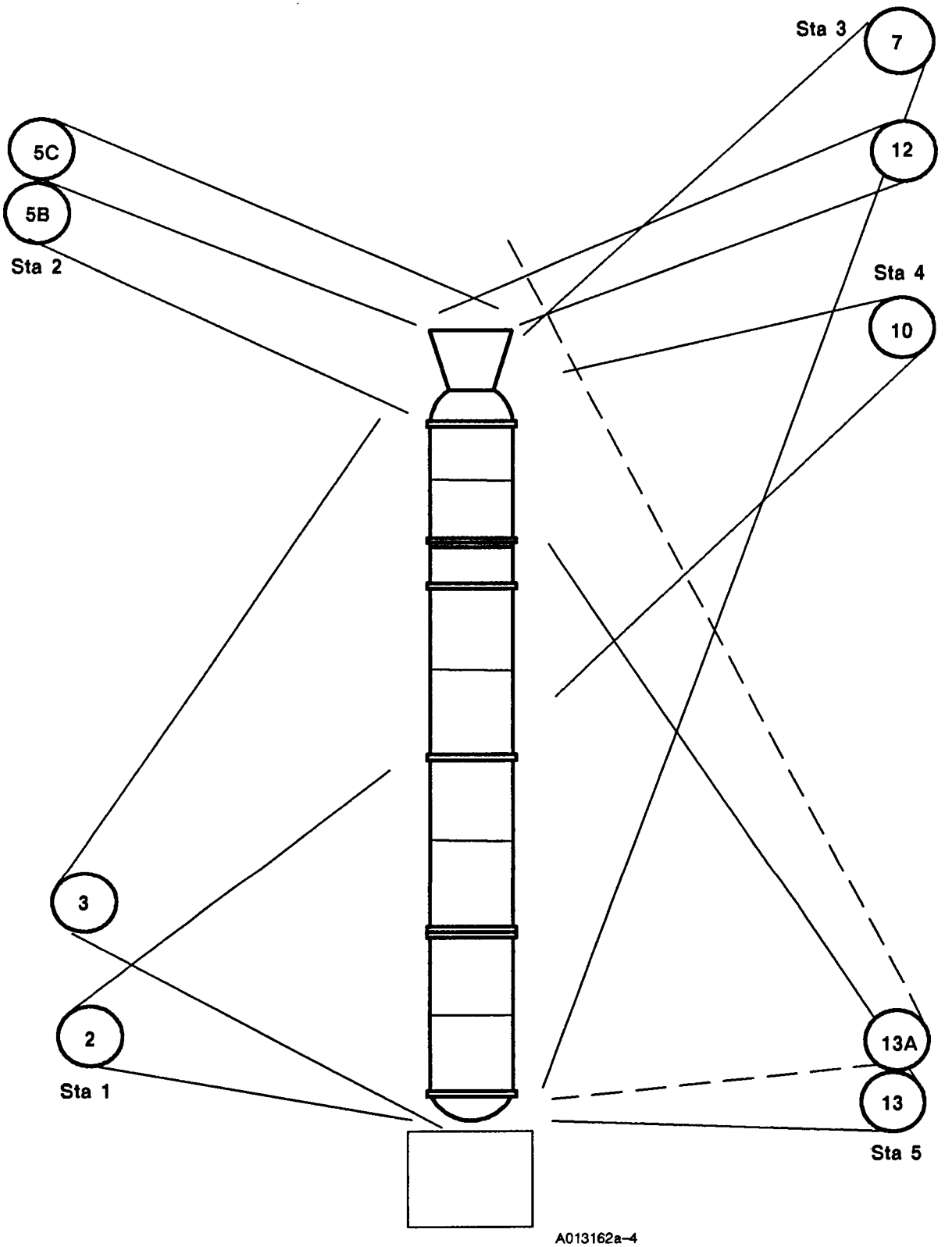

Figure 6.2-3. High-Speed Coverage (case, joints, and nozzle plug expulsion)

7

GROUND SUPPORT EQUIPMENT

7.1 INTRODUCTION

Four AVPPs were successfully installed in the case field joints and the case-to-nozzle joint vent ports at 135 deg. A 2U132133 (8U76549) installation tool was used to install the bottom portion of the AVPPs in the vent ports.

7.2 OBJECTIVES

The adjustable vent port plug installation tool test objectives, derived from objectives in TWR-15723, Rev C, to satisfy the requirements of Specification CDW2-3679, dated 26 May 1988, are listed below. The specific paragraphs from the CEI are listed with the objectives.

CQ. Certify the performance of the Adjustable Vent Port Plug Installation Tool as a means of installing, rotating, and torquing the bottom section of the adjustable vent port plug (3.2.1.1)

CR. Certify that the installation fixture is efficient and does not require special and additional tooling (3.2.1.1)

CS. Certify that the use of the vent port plug installation tool does not affect the safe and reliable use and reusability of the RSRM (3.2.1.1)

CT. Certify that the tool allows for a threaded installation to the bottom section of the adjustable vent port plug (3.2.1.2.1)

CU. Certify that interlocking allows for rotation and torquing of the bottom section of the adjustable vent port plug (3.2.1.2.2)

CV. Certify the capability of interlocking the installed installation tool with the bottom section of the adjustable vent port plug, and the utilization of the notch in the bottom section of the adjustable vent port plug (3.2.1.2.2)

CW. Certify that the tool is capable of applying a minimum torquing force of 70 inch pounds to the bottom section of the adjustable vent port plug (3.2.1.2.4)

CX. Demonstrate that the tool is capable of being transported to the work site (3.2.8)

7.3 CONCLUSIONS/RECOMMENDATIONS

All test objectives were met. No major problems occurred during installation, but three bottom portions had to be replaced when the AVVP tool slipped causing raised metal on the bottom plug.

This anomaly was caused from the incorrect use of the installation tool. Technicians were trained in the use of the tool and no further problems occurred. The installation tool performed as designed to install the bottom portion of the AVPP into the port to the 70 in-lb maximum torque. The removal of the tool did not affect the installed plug and the installation process did not cause any damage to the tool. Two bottom portions had to be replaced per the installation specification because the installation torques exceeded the requirements (too much locking device).

Post-test inspection results indicate all AVPPs were nominal. No motor pressure reached the AVPPs so no assessment of blowby or erosion can be made on the seals.

Training needs to be implemented to teach the correct use of the tool to prevent further problems with raised metal on the bottom plug. Presentation TWR-18838 documents a procedure on how to correctly use the AVPP installation tool.

7.4 RESULTS/DISCUSSION

The adjustable vent port plug installation fixture was successfully qualified. Each AVPP successfully passed leak check. All were below the 0.1 sccs allowable leak rate (Table 7.4-1).

Table 7.4-1. QM-8 Leak Rates, AVPP

Joint	Leak Rate (sccs)
Forward Field Joint	0.0015
Center Field Joint	0.0051
Aft Field Joint	-0.0055
Case-to-Nozzle Joint	-0.0015

8

LOADS AND ENVIRONMENTS

8.1 INTRODUCTION

This section is concerned with the strut loads experienced during the QM-8 test. The strut loads experienced during lift-off simulation and the High Q simulation are compared to the input load cases L02044 and ETMA352 respectively.

8.2 OBJECTIVES

The main test objective from Section 2 regarding Loads and Environments is:

BR Provide data for certification of the reliability of the RSRM design. (3.2.3)

8.3 CONCLUSIONS

The strut loads experienced during the QM-8 test followed the input load cases well with the exception of the diagonal member, P10, which deviated from the High Q input case slightly. The other members behaved correctly with any deviation in load being lower than the input load case. The lower strut, P8, had the best correlation for both the lift-off and High Q simulations.

8.4 RESULTS/DISCUSSION

The High Q condition, ETMA352, is considered the critical load case. Load case ETMA352 should produce the largest change in the gap sealing surface of the aft field joint during its load cycle.

During the test the struts are ramped up to an initial load before the load cycle starts (Figure 8.4.1). There was good correlation between the load case initial values and the initial values during the test. The largest difference occurred in the top member (Figure 8.4-2) during the High Q cycle. All of the other initial static values were less than 6 percent and the loads were generally less than the input case.

The dynamic loads for lift-off and High Q also compared well with the input load cases (Figures 8.4-3 through 8.4-8). The loads induced during the High Q cycle are the largest. The greatest deviation occurred in the diagonal member, with an increase of 6.8 percent over the input load case (Figure 8.4-6). The other strut members generally showed loads less than the input conditions; the bottom member, P8 (Figures 8.4-5 and 8.4-8), showed excellent correlation with both the lift-off and High Q load case.

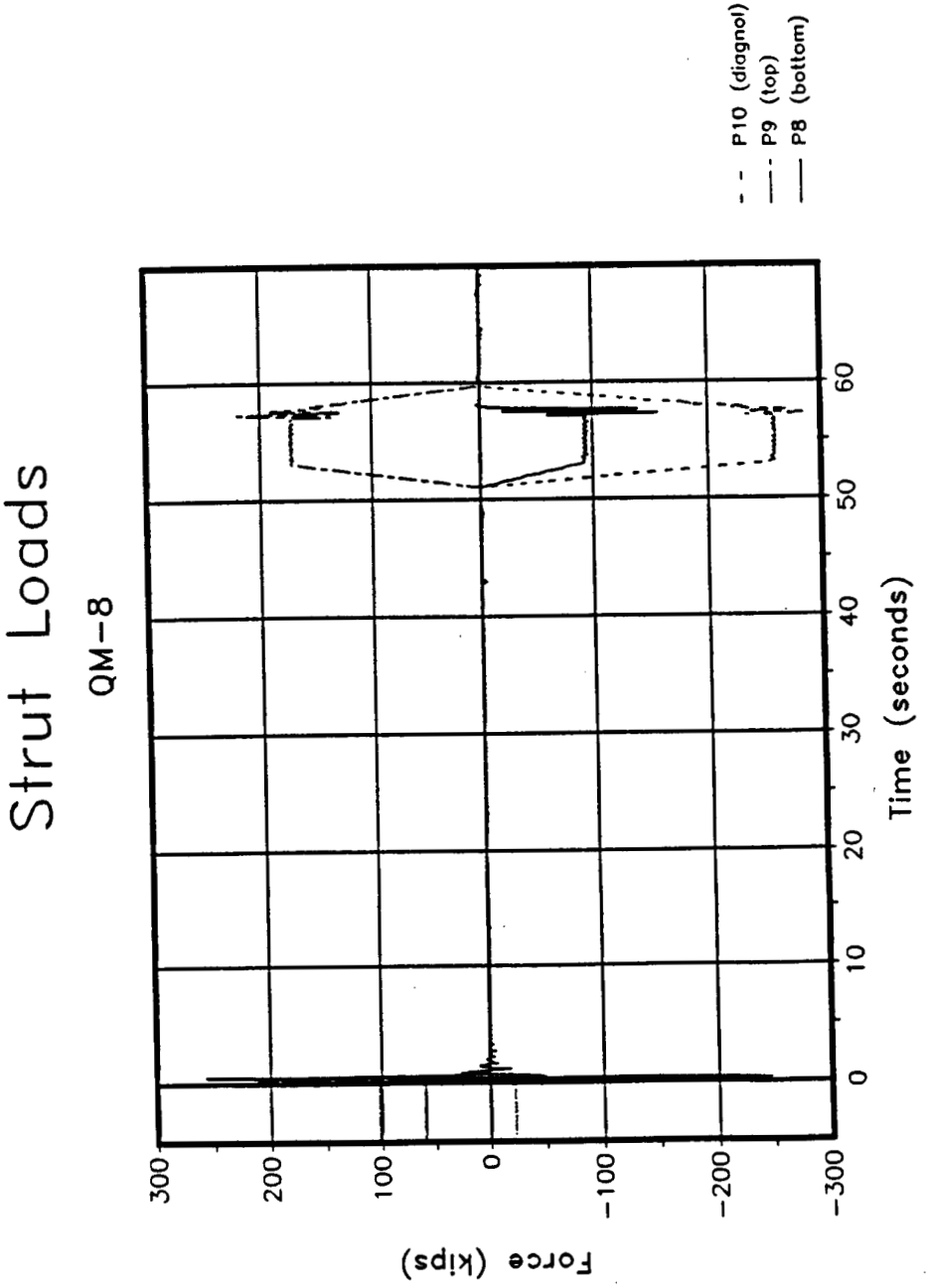

Figure 8.4-1. QM-8 Strut Loads

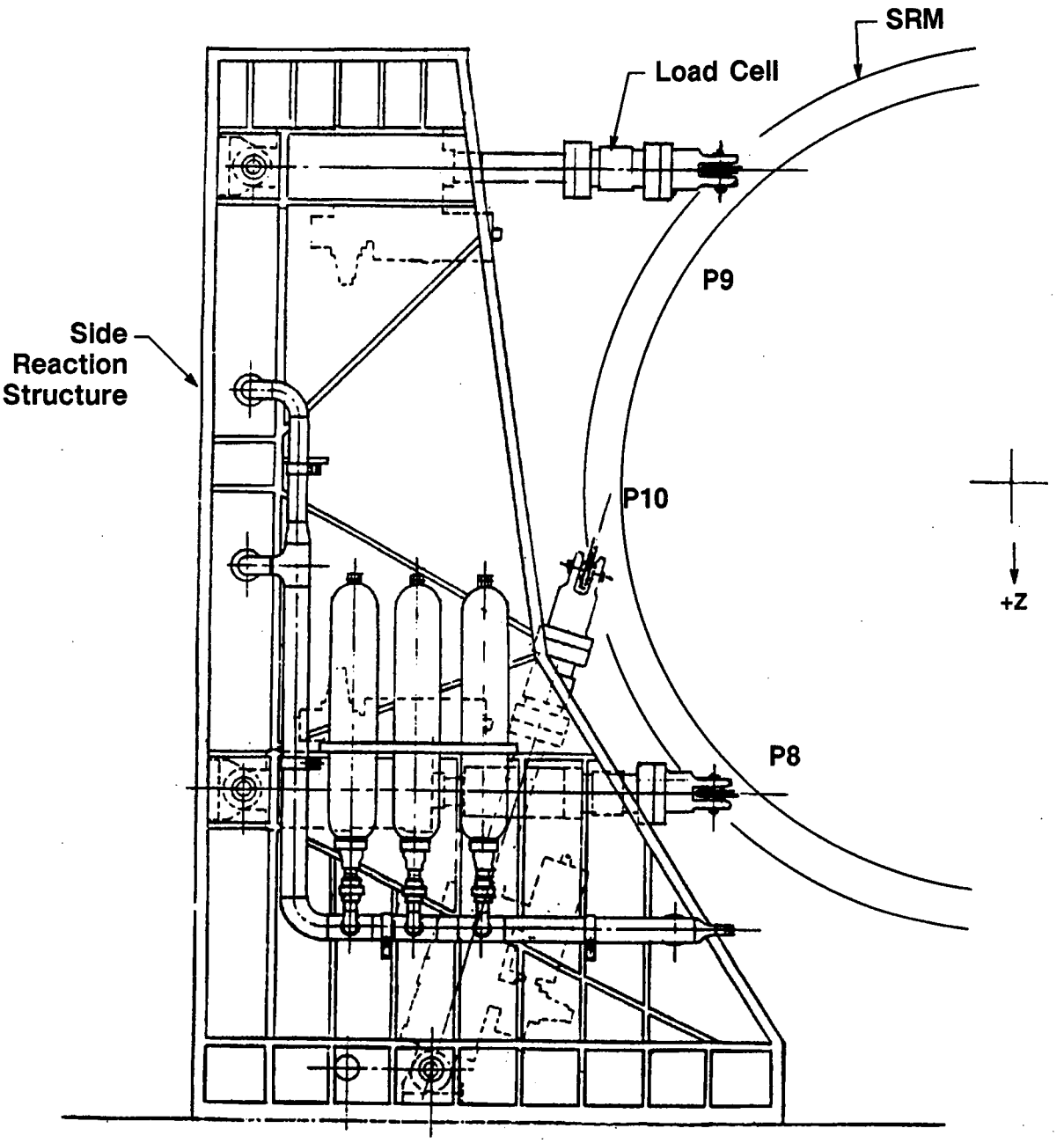

Figure 8.4-2. T-97 Test Facility

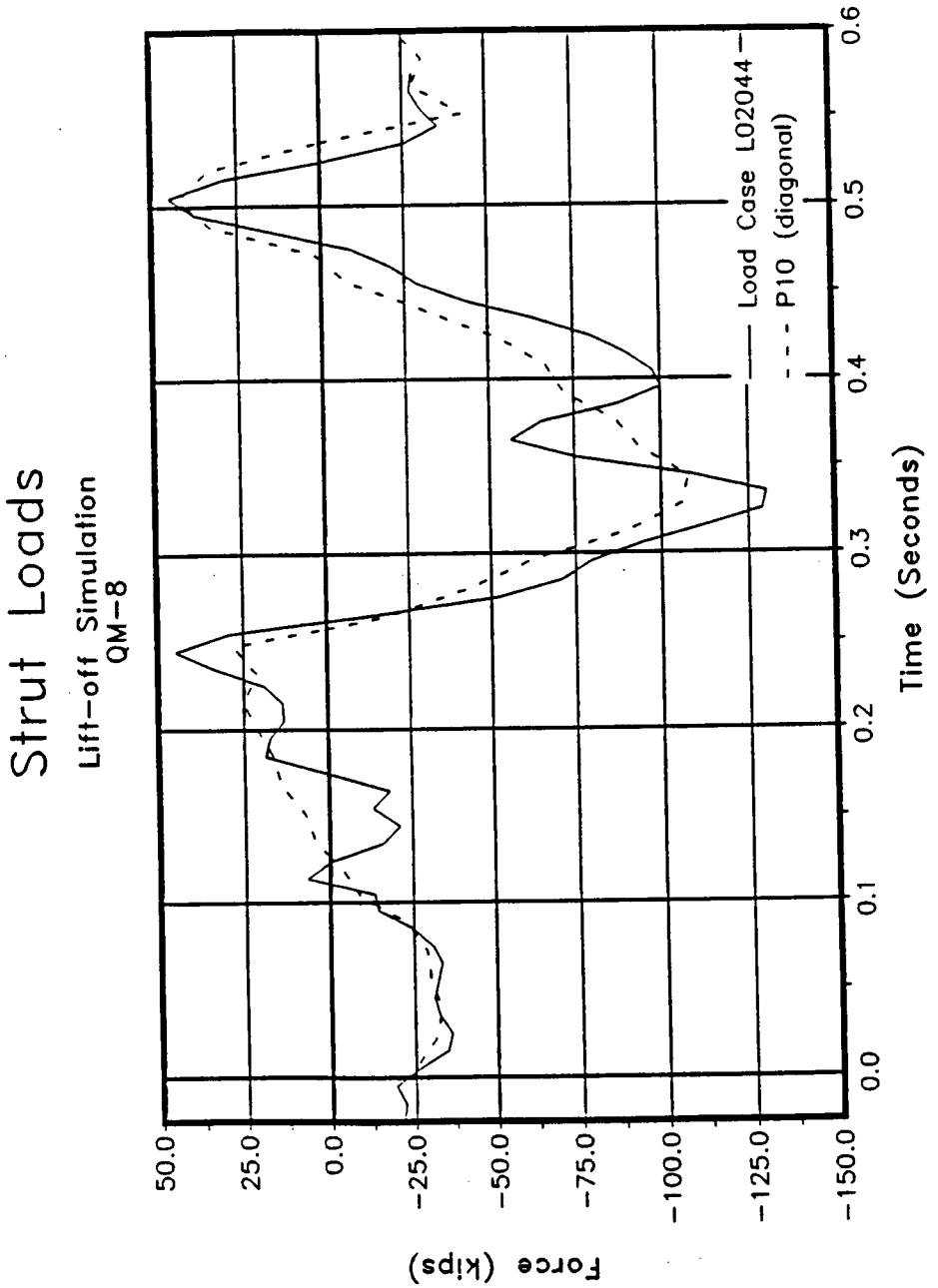

Figure 8.4-3. QM-8 Strut Loads Lift-off Simulation (P10)

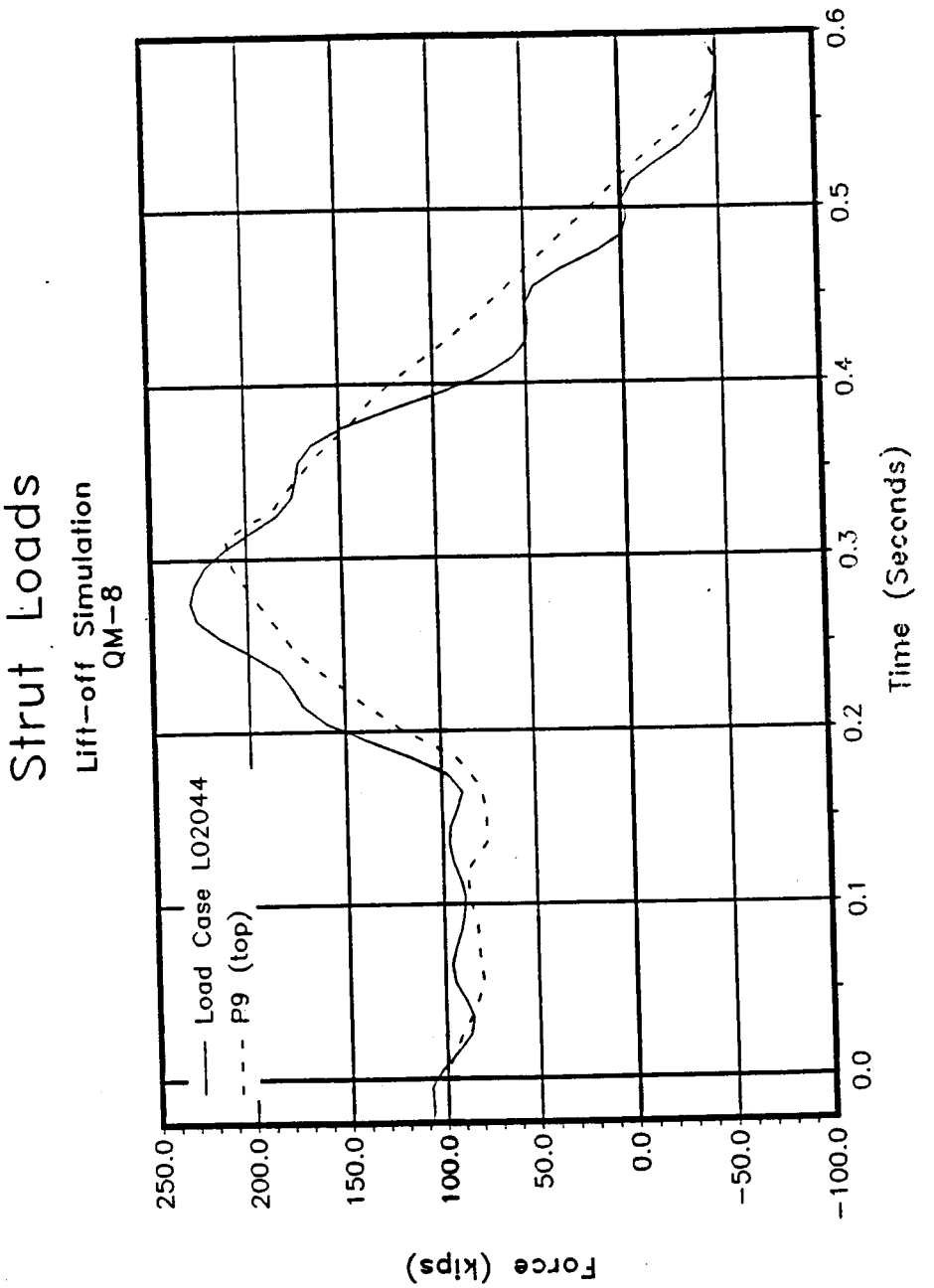

Figure 8.4-4. QM-8 Strut Loads Lift-off Simulation (P9)

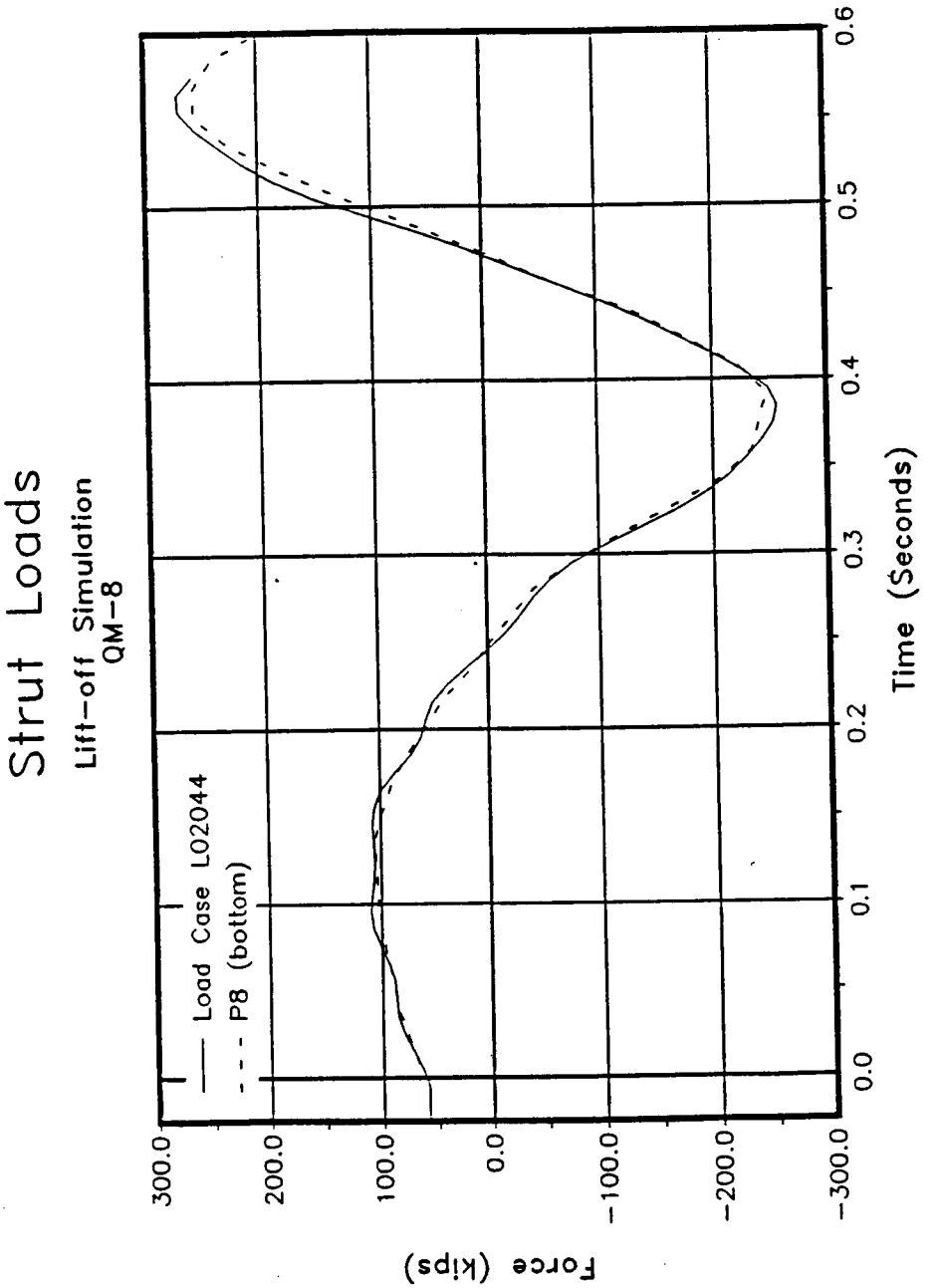

Figure 8.4-5. QM-8 Strut Loads Lift-off Simulation (P8)

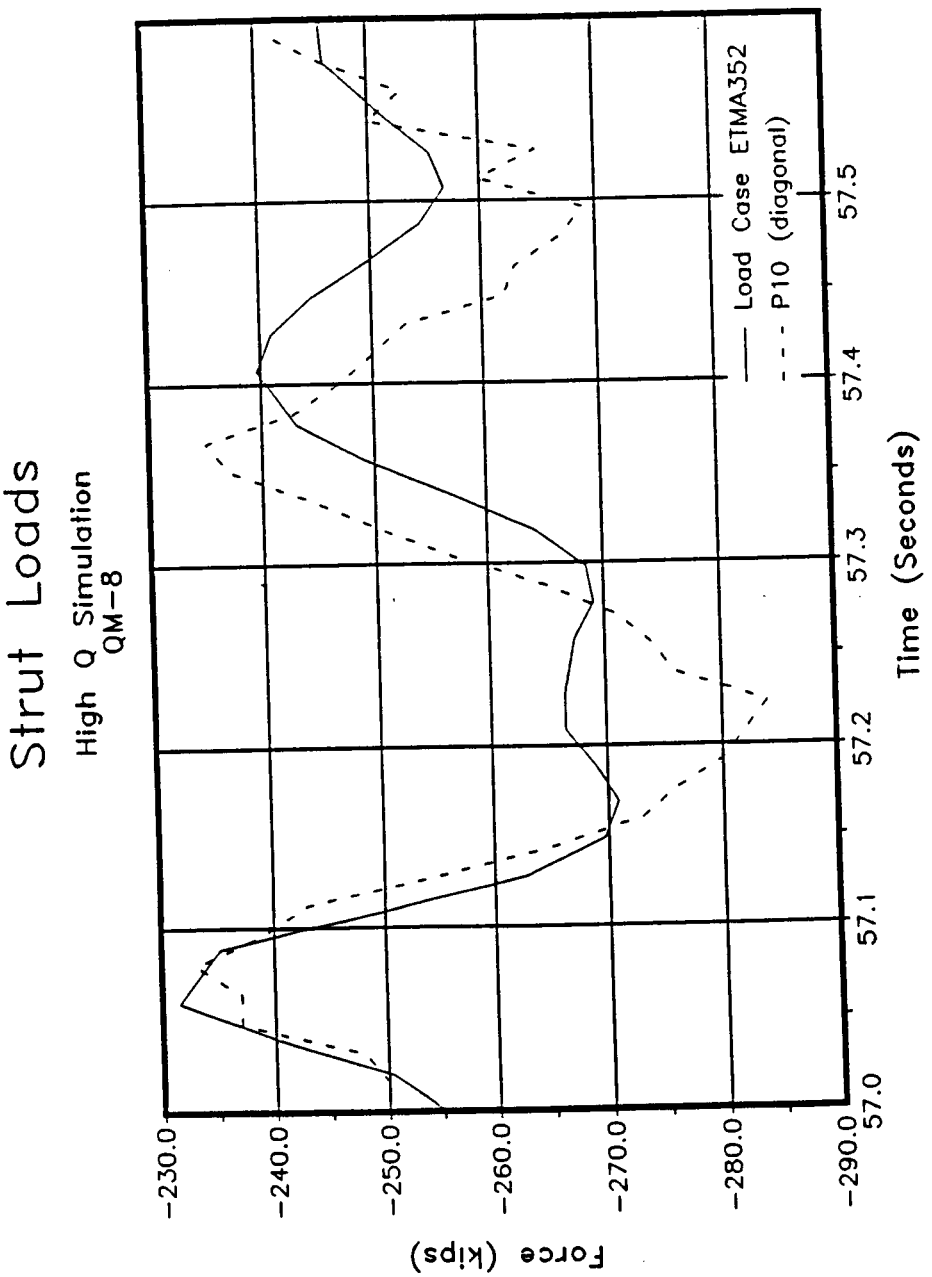

Figure 8.4-6. QM-8 Strut Loads High Q Simulation (P10)

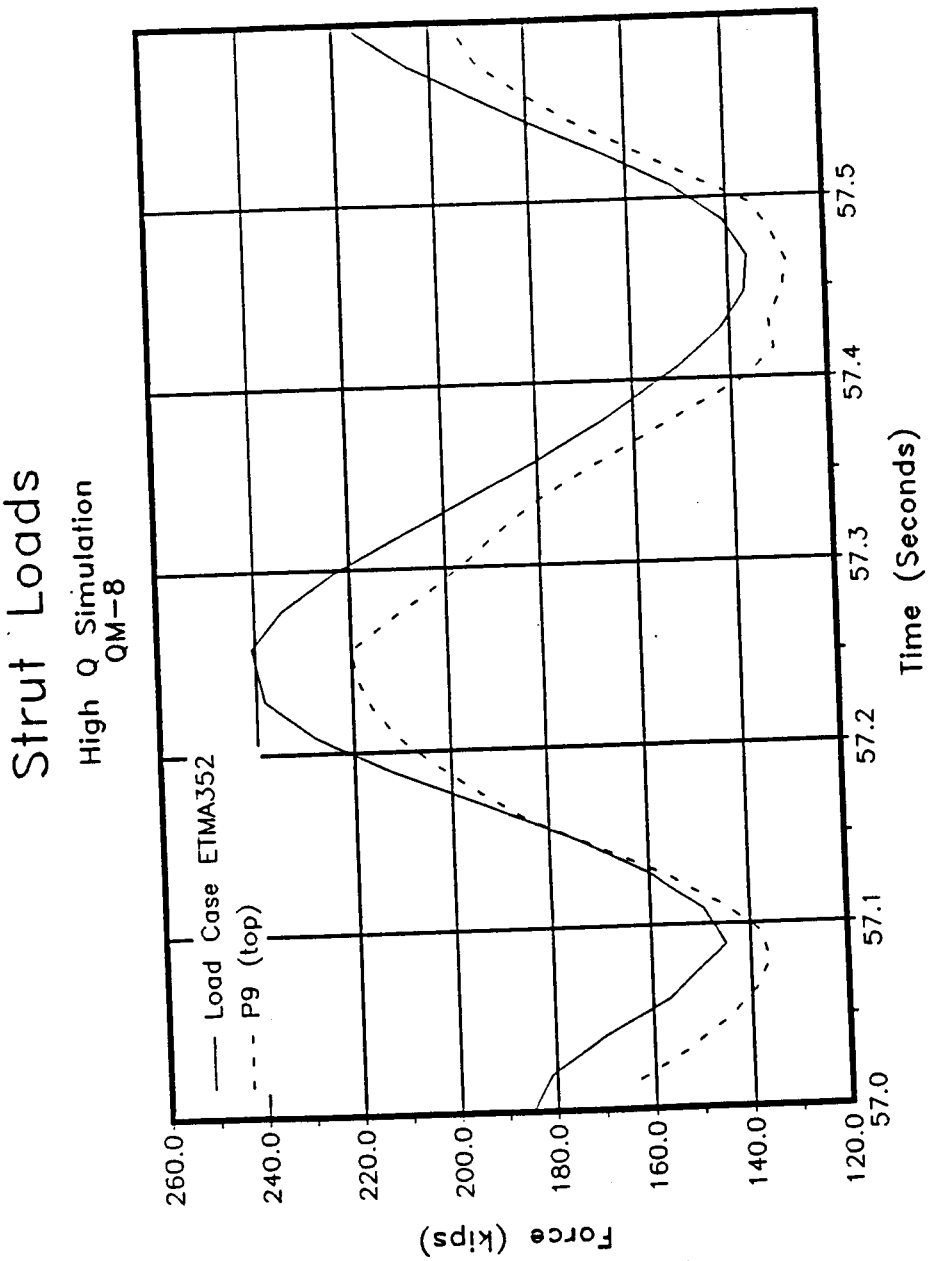

Figure 8.4-7. QM-8 Strut Loads High Q Simulation (P9)

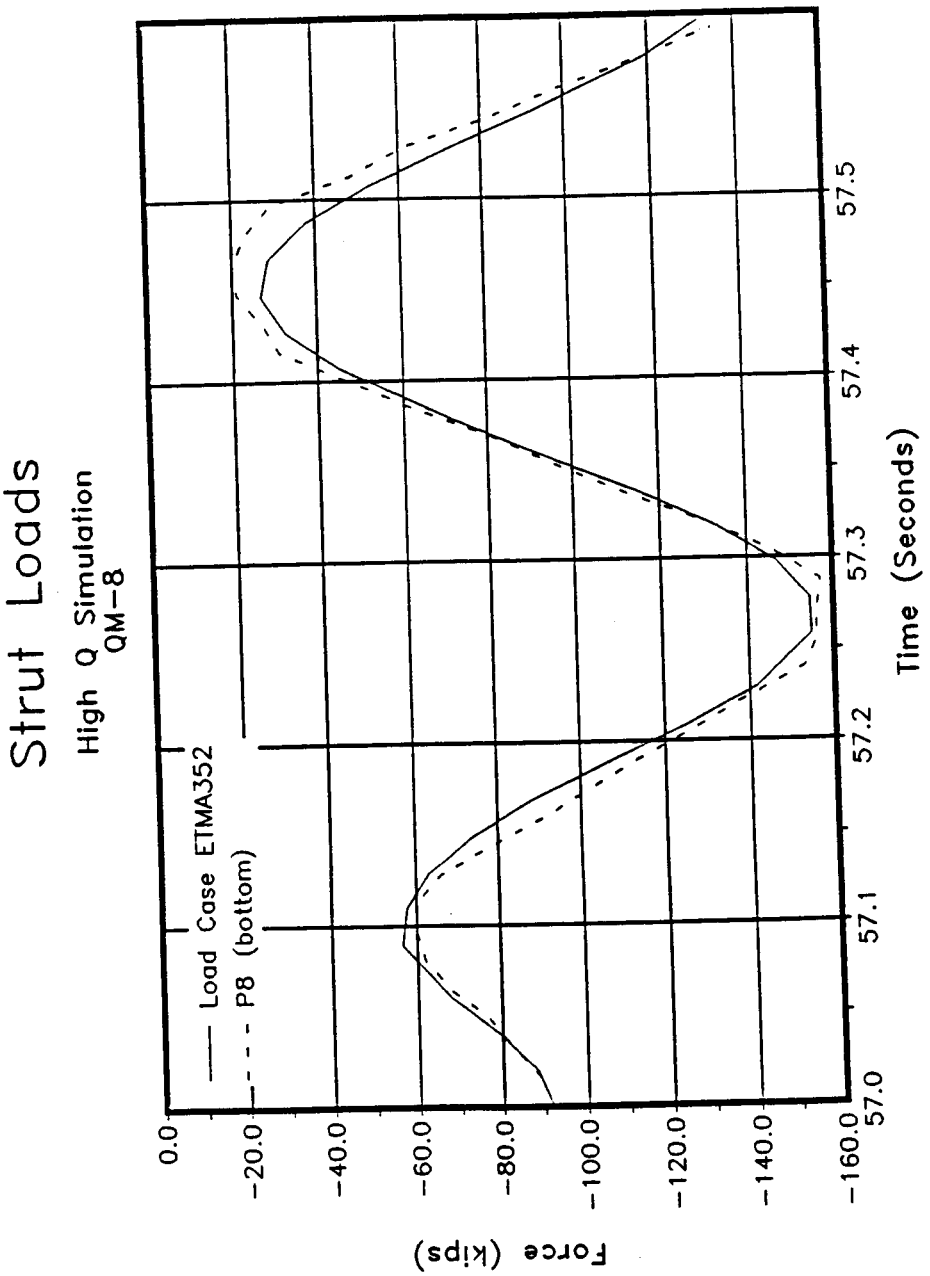

Figure 8.4-8. QM-8 Strut Loads High Q Simulation (P8)

9

AERO/THERMAL

9.1 INTRODUCTION

Aft end heating system

The aft end heating system proved to be very efficient for an average building temperature of 29°F. All critical components met their temperature criteria as shown in Table 3.1.11.3-1. The criteria for the flex bearing is that both the forward and aft parts of the flex bearing are at least 60°F. Since no sensor exists on the forward side of the flex bearing, the available temperature data are used to assure the minimum temperature is met. Both the forward inlet housing and the flexible boot temperatures show a minimum temperature of 59°F. They are further away from the heat source and closer to the cold side and, therefore, will be colder than the unmeasured forward side of the flex bearing. Thus, the forward side of the flex bearing is ensured of being higher than the 59°F recorded on the forward inlet housing.

RTDs

All but three RTDs functioned well, indicating that there was no leakage of the combustion gases through the igniter flange, the field joints, and the case-to-nozzle joint.

9.2 OBJECTIVES

The main test objective from Section 2 with regards to Aero/Thermal is:

BR Provide data for certification of the reliability of the RSRM design. (3.2.3)

9.3 CONCLUSIONS

Aft End Heating

Component temperatures remained fairly constant after the building was moved and up until time of firing, indicating that the 0.5-in. cork insulation on the aluminum aft skirt adequately reduced heat loss to the surroundings.

The heating unit was continuously operated to keep the flex bearing aft end ring sensor at 85°F, ensuring a minimum temperature of 60°F in the forward end ring. This condition was maintained until 18 January, when the heated inlet air temperature was reduced such that the nozzle-to-case joint sensor temperature was held at approximately 75°F. This meets the lower temperature limit cold test objective.

The heated components in the aft skirt reached their steady state temperatures in three days, and the flexible boot in five days. Nozzle throat and forward inlet housing temperatures also rose quickly with temperature differentials of about 10°F during heating. This indicates that heated air did enter and exit the cavity enclosed by the nozzle throat housing and flex bearing through 0.025 to 0.075 in. gaps between the snubber segments and aft end ring, or through an opening for instrumentation wires caused by removal of one snubber segment at the 90°F location.

Temperature data from the nozzle submerged region (nozzle throat, nozzle housing, and flexible boot cavity) indicate that there is a substantial cooling effect on the internal surfaces of the motor. This air was exchanging heat to the surroundings through the nozzle plug, nozzle exit cone, fixed housing, and the aft dome.

Aft end temperature data was monitored and studied to understand the air flow thermal distribution and thermal response of aft end region components. A correlation was performed using a two-dimensional (2-D) axisymmetric thermal model and different air flow environments at the 120 deg location to determine the average surface heat transfer coefficient. The results indicate that an average heat transfer coefficient for free air convection is 1.2 Btu/hr/ft^2/°F, it is 2.0 Btu/hr/ft^2/°F for the forced air on the motor case, and 1.5 Btu/hr/ft^2/°F for the heated forced air in the aft skirt compartment. The heat transfer coefficient used for the forced air in the aft skirt compartment is considerably lower, so a three-dimensional (3-D) flow thermal analysis is currently being conducted to better understand the test data.

Figure 9.3-1 shows the thermocouple locations with respect to the nozzle. Figure 9.3-2 shows the two inlets (at 16 and 270 deg) and one outlet (at 164 deg) of the recirculating air in the compartment. The temperature-time histories are shown in Figures 9.3-3 through 9.3-8. Figures 9.3-3 and 9.3-4 show the flex bearing forward sensors and nozzle-to-case joint sensors at 0, 120, and 240 deg, respectively. Figures 9.3-5 and 9.3-6 show the inlet, outlet, and free air temperatures adjacent to the nozzle-to-case joint sensors at 0, 120, and 240 deg, respectively. Figures 9.3-7 and 9.3-8 show the nozzle throat housing at 0,120, and 240 deg and the forward inlet housing at 0 and 180 deg, respectively. Figure 9.3-9 shows the flexible boot and its adjacent free air temperatures at 0 degrees. Most of the trends in the test data were expected, but some free air temperature data indicates that there were problems with Sensors T1013 for the entire period and T1017 from day 16 to day 20, and with a few other thermocouples at different time frames. As indicated in Figures 9.3-4 through 9.3-6, the steam heater control unit was set to the wrong outlet air temperature from day 16 to day 17. It was subsequently readjusted.

High temperatures are seen at the 240 deg region and low temperatures in the 120 deg region. A maximum temperature differential of each component is approximately 20°F. Maximum temperature difference between inlet and outlet air was about 40°F, indicating 3-D heat transfer effects in the solid components and in the air stream.

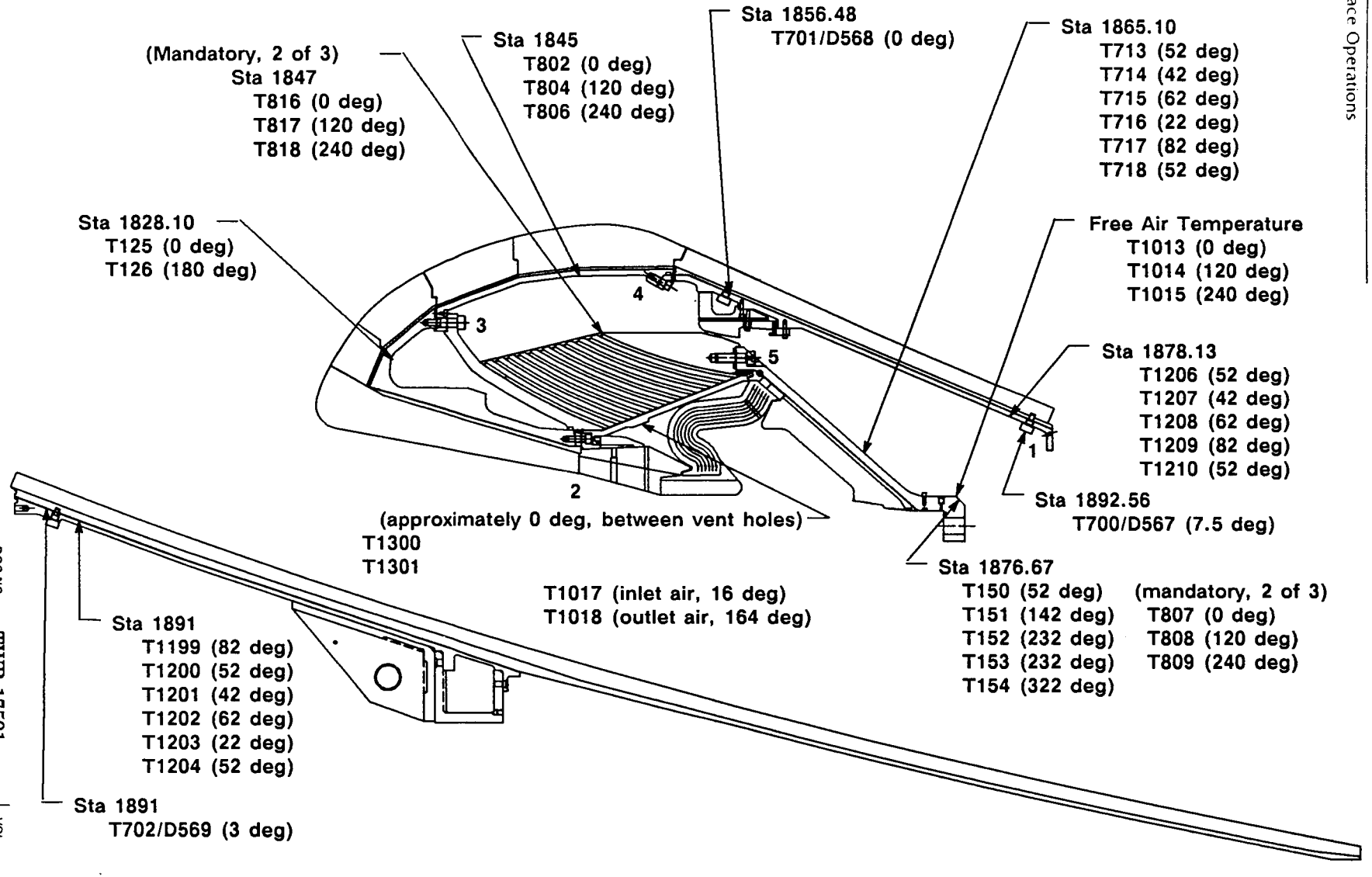

Figure 9.3-1. Monitored Instrumentation During Aft End Heating

A020819a

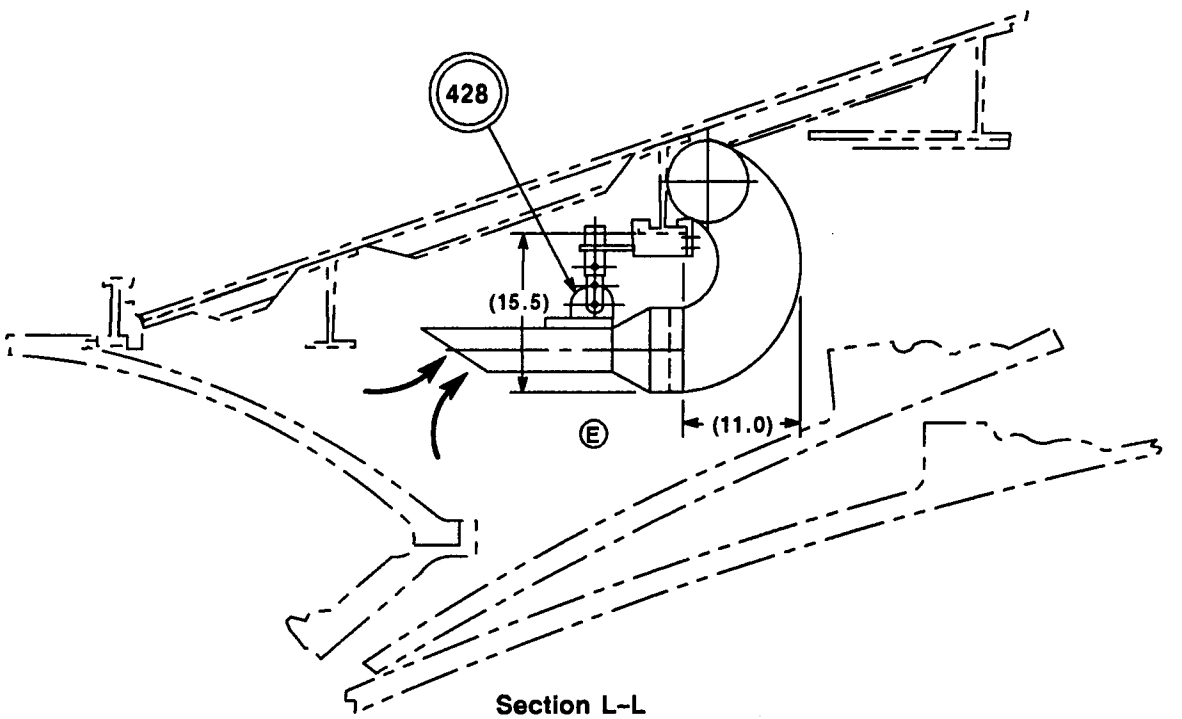

Section L-L
Rotated 16 deg CCW
1 Outlet (164 deg)

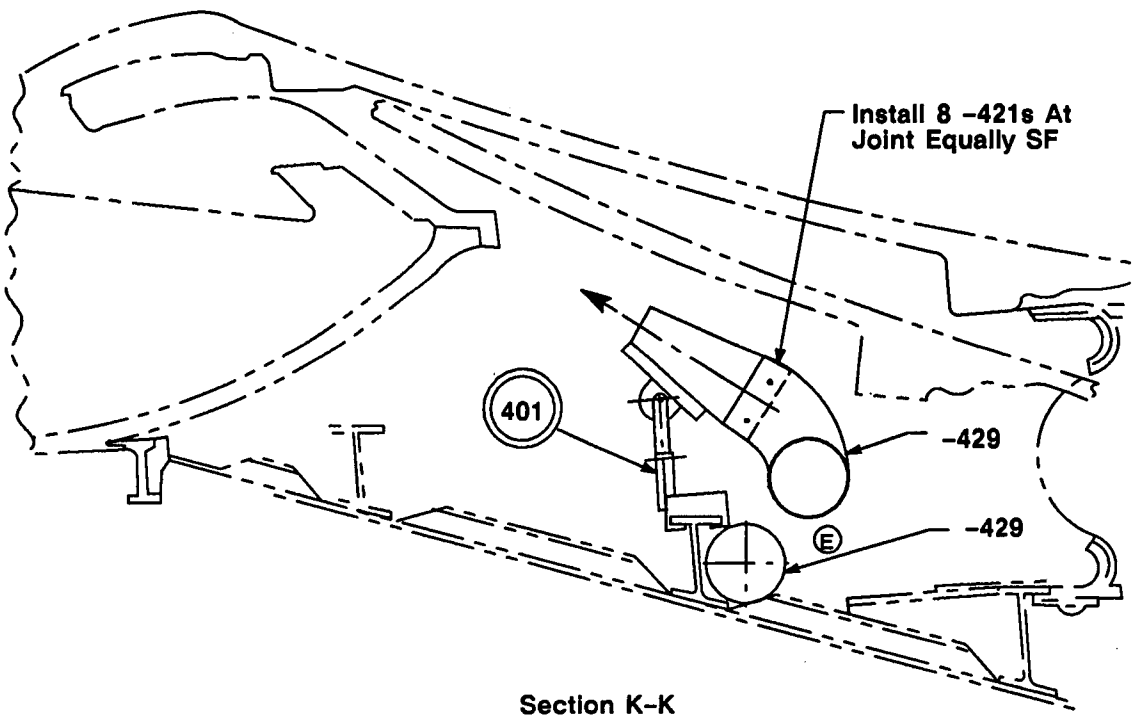

Section K-K
Rotated 90 deg CW
2 Inlets (16 deg and 270 deg)

Figure 9.3-2. Aft End Heating

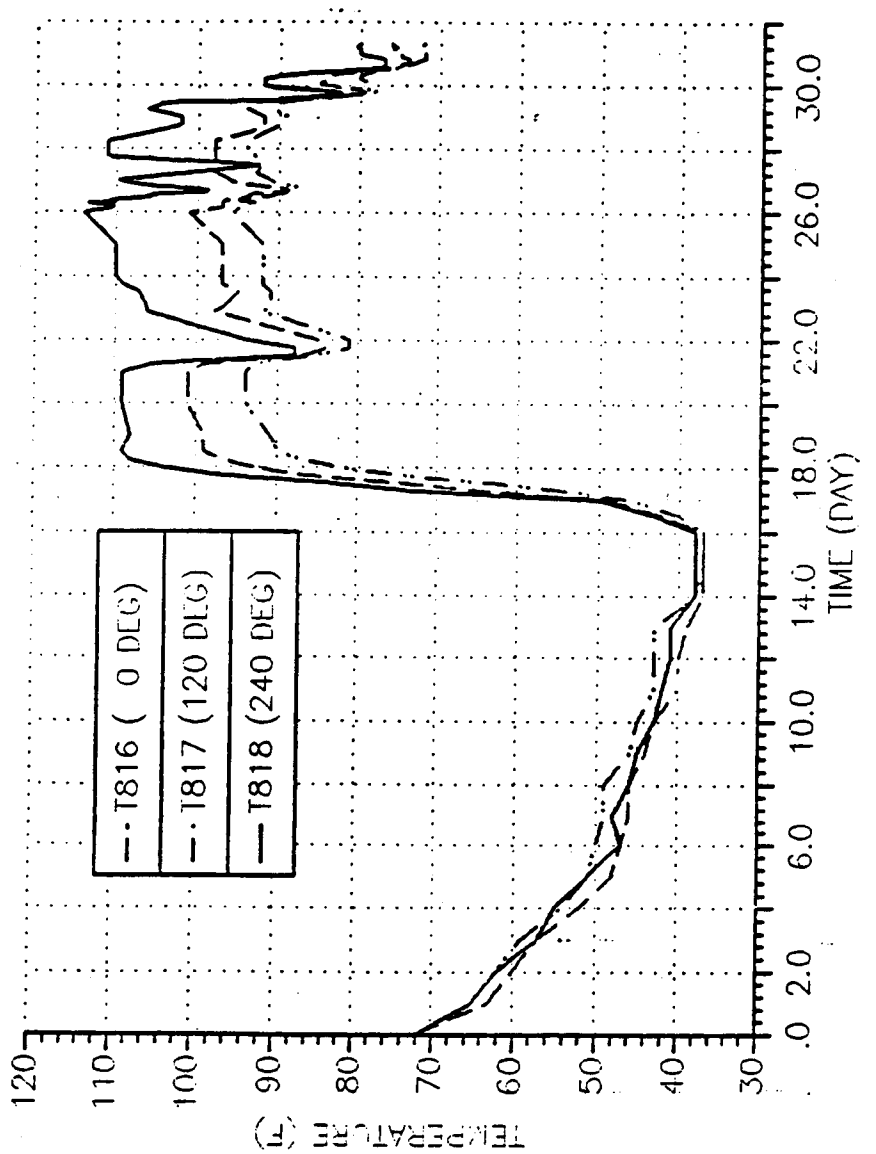

Figure 9.3-3. QM-8 Aft End Heating Flex Bearing Aft End Ring Sensor

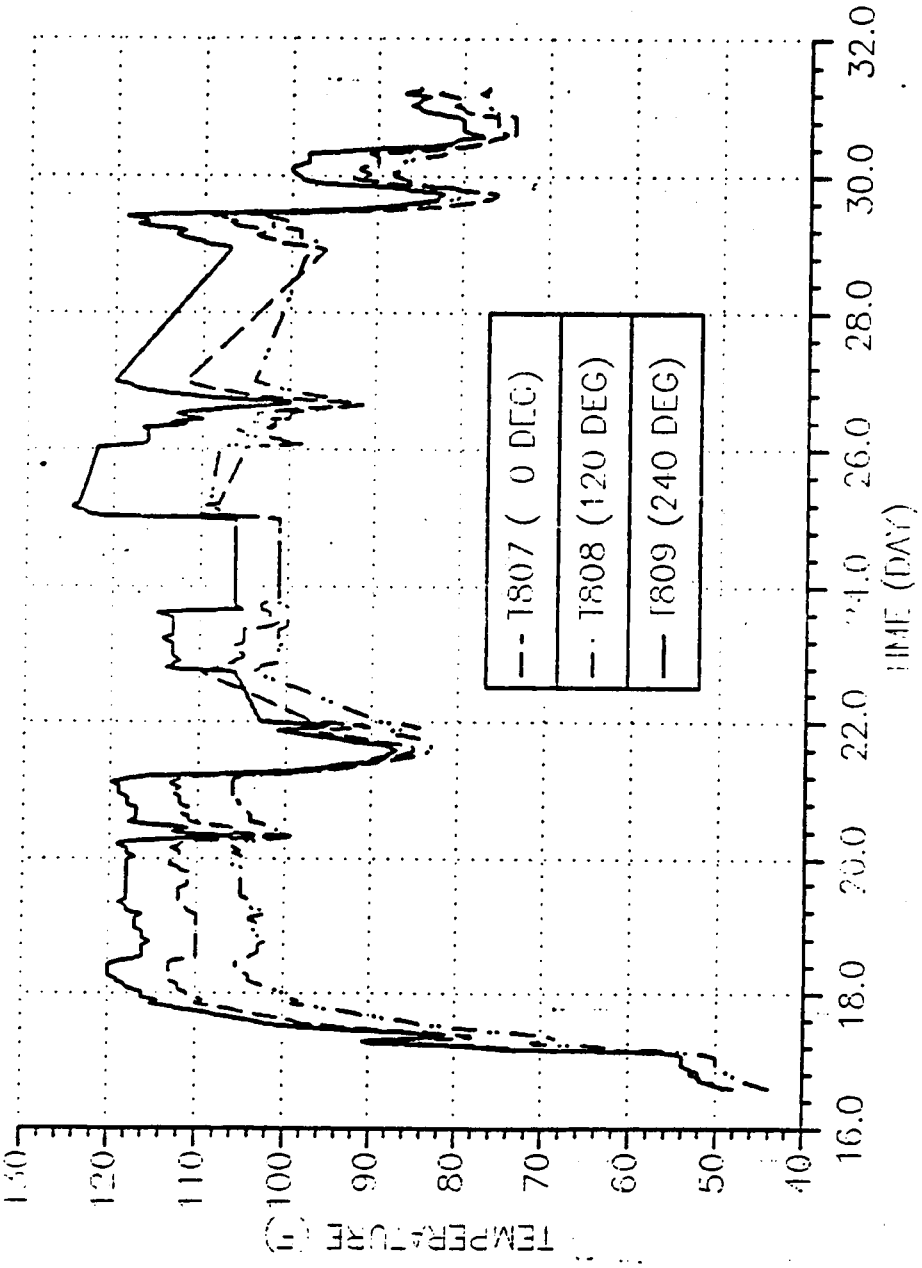

Figure 9.3-4. QM-8 Aft End Heating Case-to-Nozzle Joint Sensor

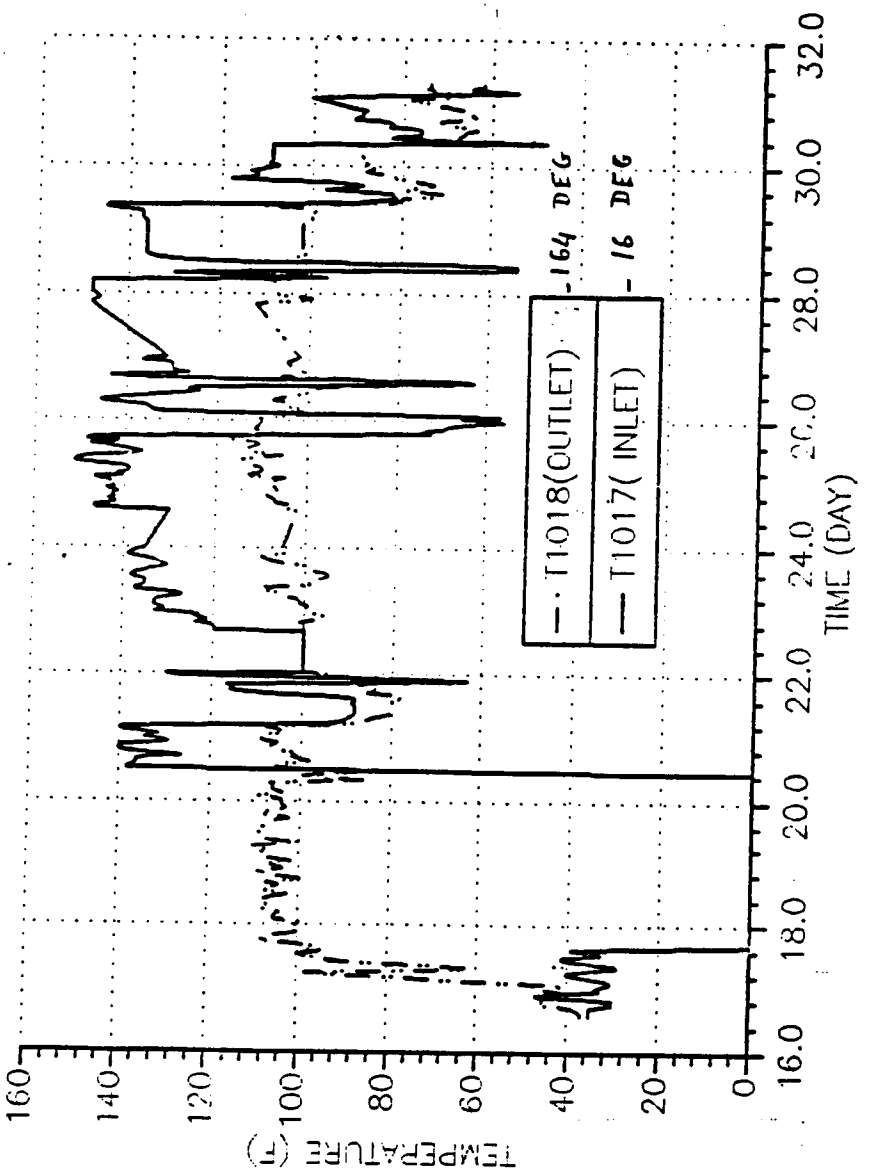

Figure 9.3-5. QM-8 Aft End Heating Aft Skirt Compartment Air Adjacent to Case-to-Nozzle Joint

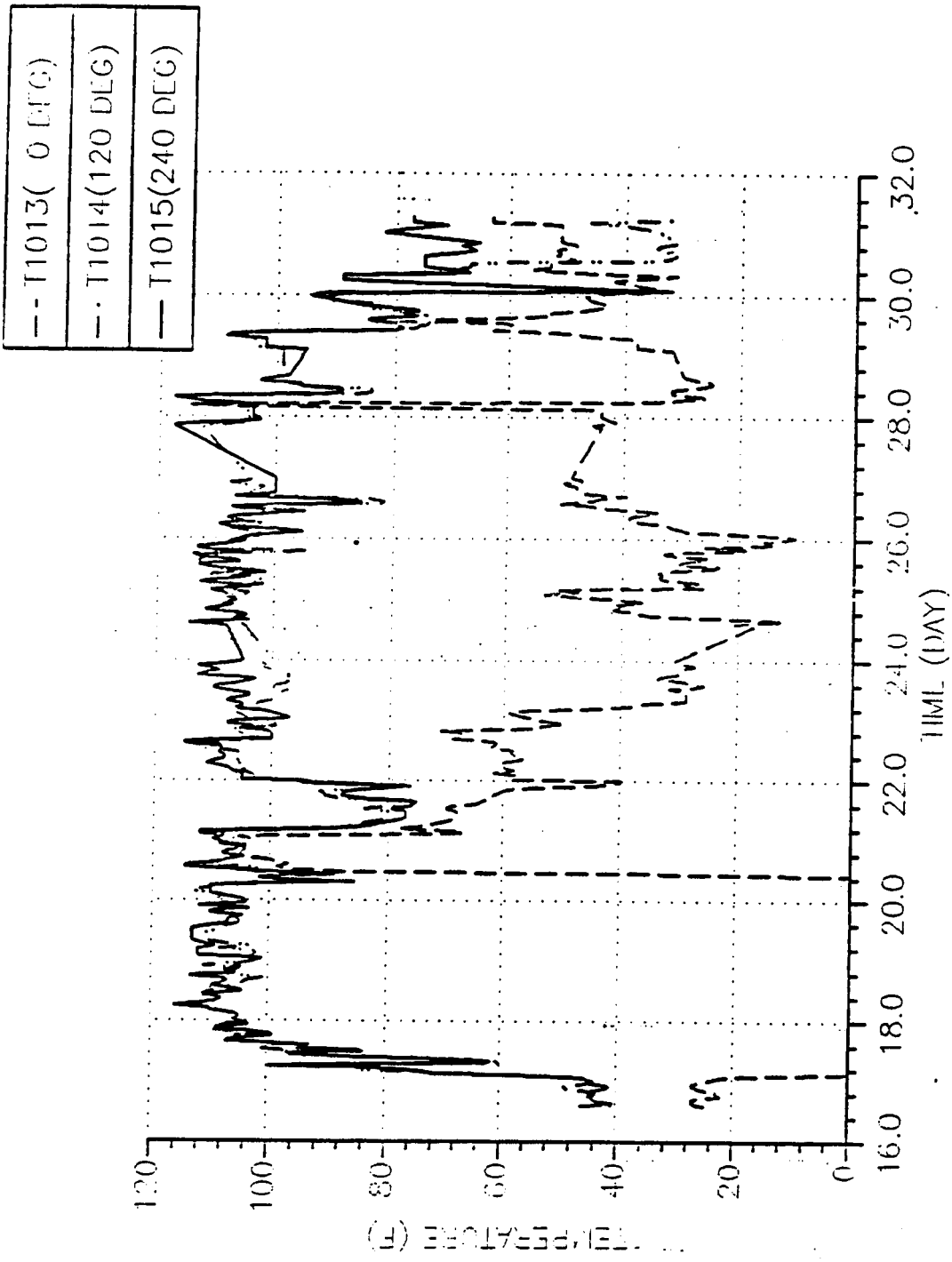

Figure 9.3-6. QM-8 Aft End Heating Aft Skirt Compartment Air Adjacent to Case-to-Nozzle Joint

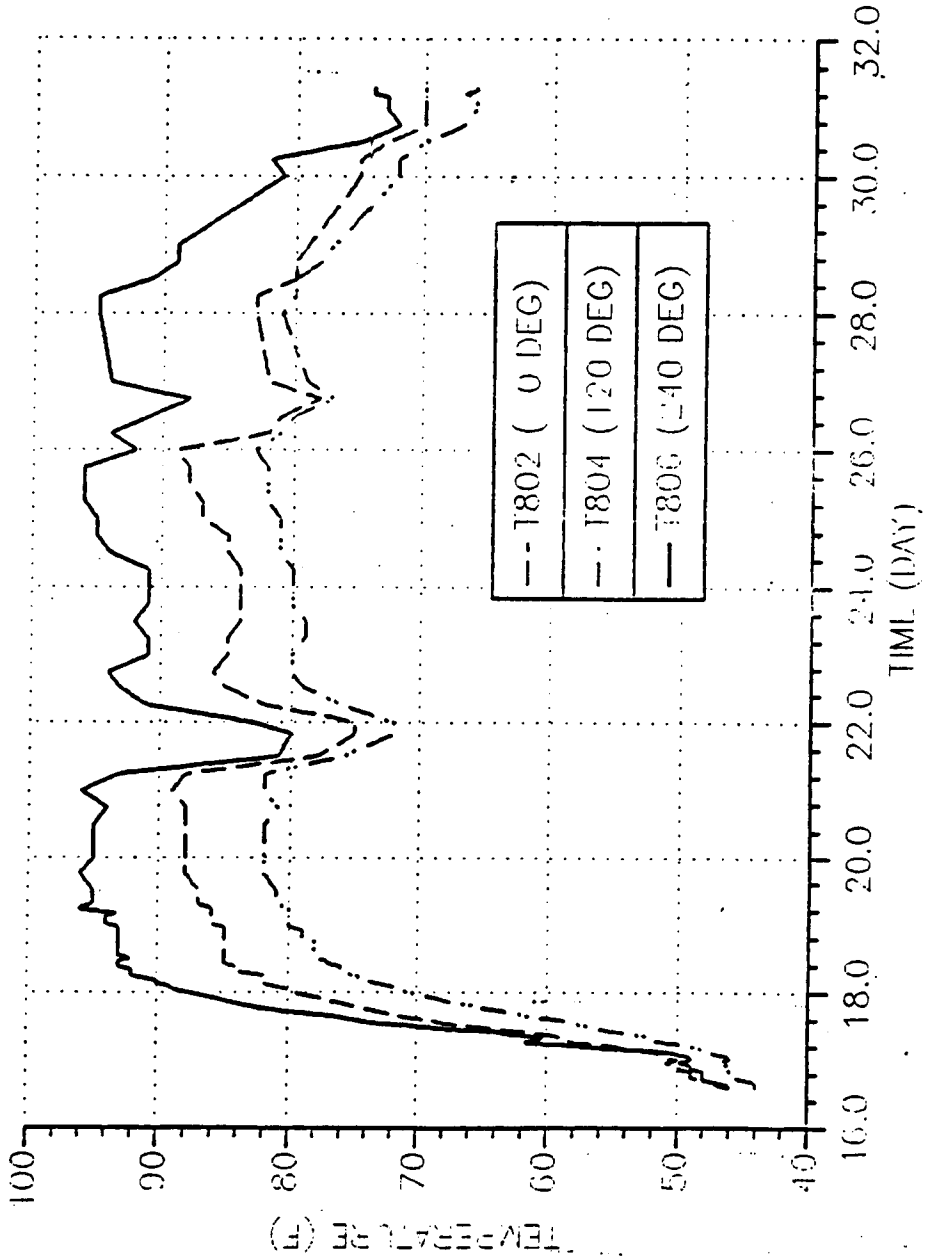

Figure 9.3-7. QM-8 Aft End Heating Nozzle Throat Housing

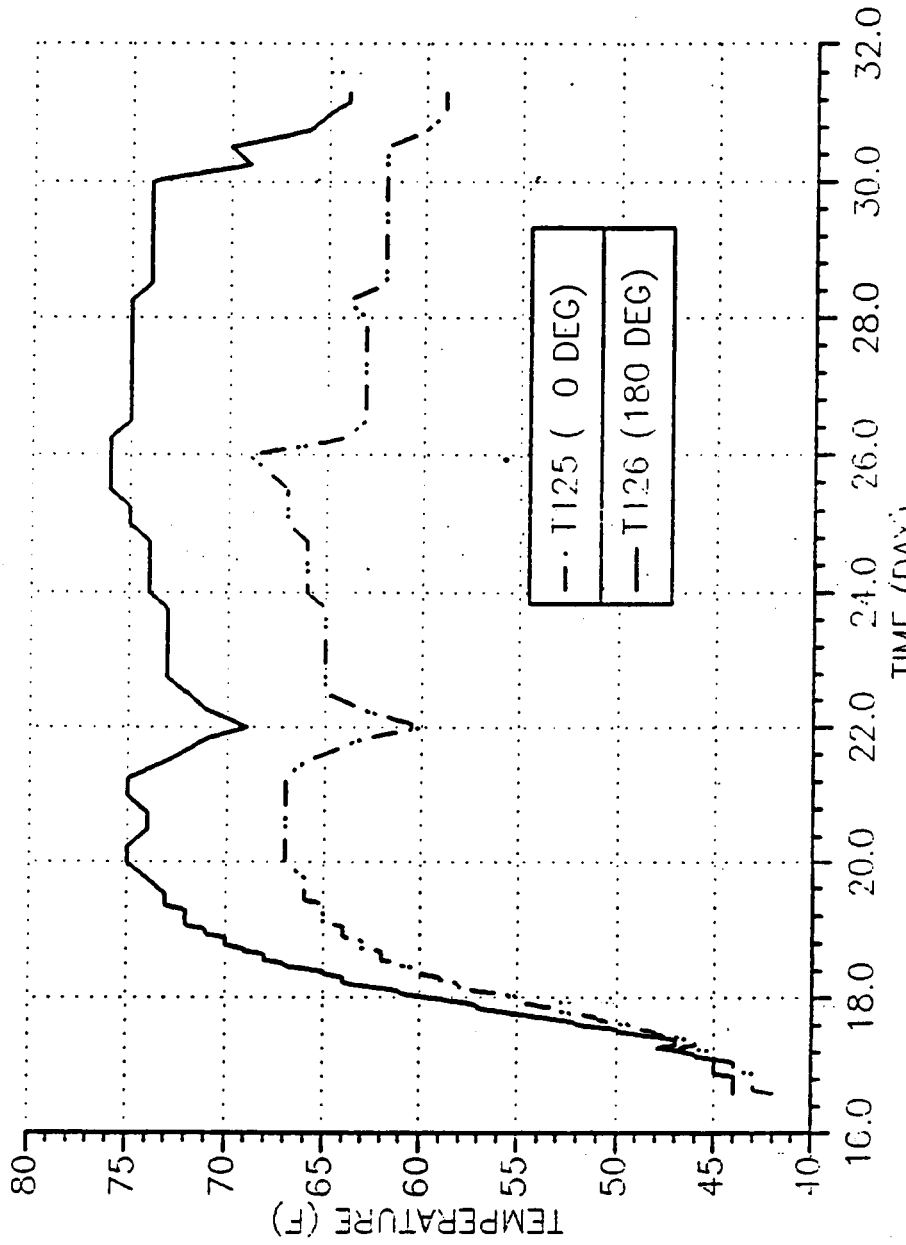

Figure 9.3-8. QM-8 Aft End Heating Nozzle Forward Inlet Housing

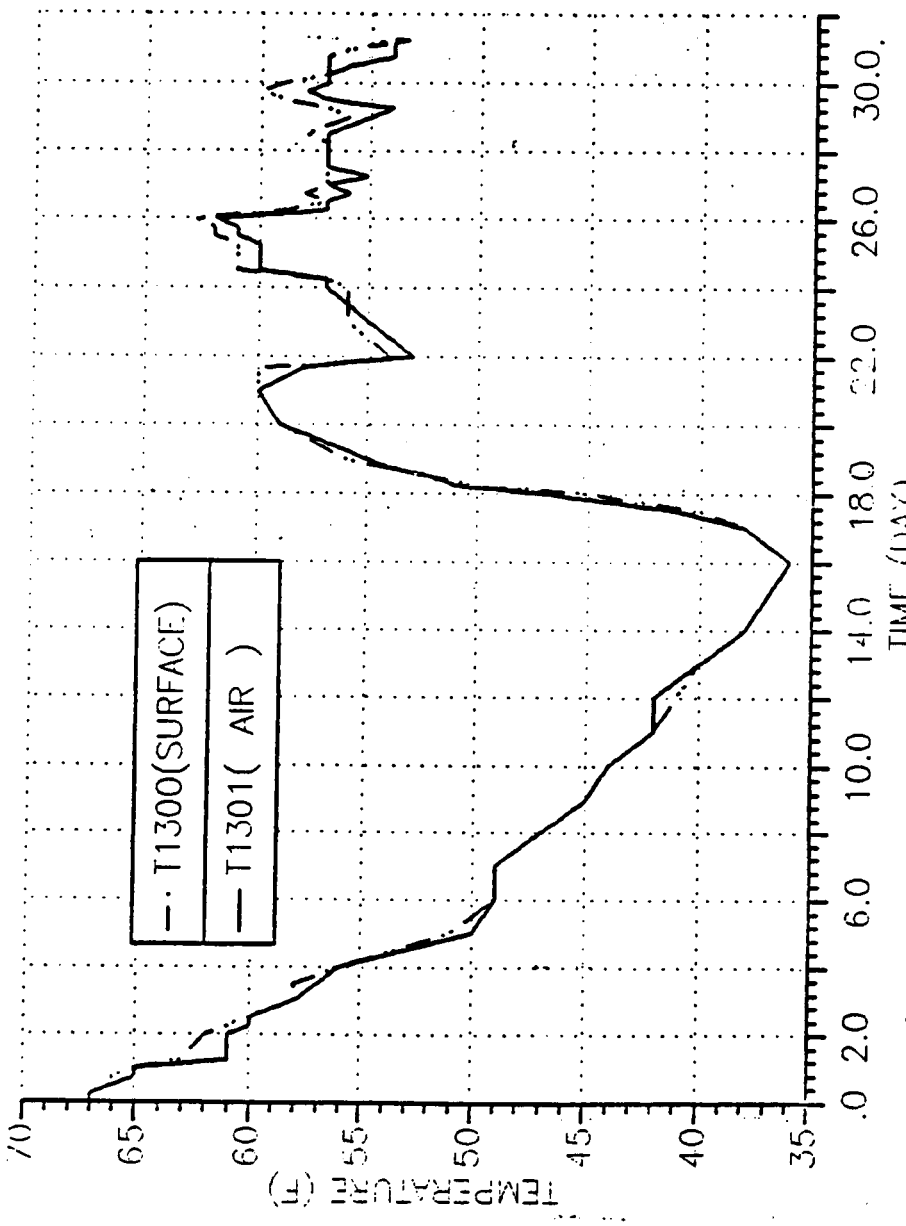

Figure 9.3-9. QM-8 Aft End Heating Flexible Boot at 0 deg

9.4 RESULTS/DISCUSSION

The sensor temperatures of the nozzle-to-case joint, flex bearing aft end ring, and other components in the aft skirt dropped much faster than predicted, in spite of 0.5-in. cork insulation over the aluminum aft skirt external wall and the plastic coverings over the six small square openings in the aft skirt. The following factors increased compartment cooling:

--Surrounding cold air was convected into the compartment through several openings of the thermal curtains.

--The compartment walls, such as the nozzle exit cone and aft skirt with its internal stiffeners, provided a substantial amount of heat transfer surface area. Also, the external aft end ducting system provided free air recirculation. For future conditioning, it is recommended that the thermal curtains be taped with aluminum foil to limit the amount of air entering or exiting the compartment. The inlet and outlet ducts should be inserted with valves at the thermal curtain entrance to reduce the internal air heat exchange with the environment.

Actual volumetric flow rates at the inlets and outlet have not been measured to ensure that there is no air leaking through the compartment walls, but a constant air flow rate was estimated to be between 1,900 to 2,100 cfm base on a 5-in. water gauge static air pressure, 70°F inlet air, 70°F temperature rise, 8-in. inlet and outlet diameters, and a 7.5 HP blower with a constant 3,059 RPM. Details are in Drawing 2U129410. The problem with the estimated volumetric flow rate is that the actual total flow resistance in the recirculating path is not known or accurately calculated. The air volumetric flow rate could be verified if the total and static pressures had been measured along with the static temperatures at the inlets and outlet.

RTDs

RTDs T000150, T000151, T000153, T000154 on Nozzle Fixed Housing

The initial temperature of these RTDs varied from 77° to 81°F, indicating that the heating system for the aft skirt base region was in operation. The temperature of these RTDs remained constant during and after the motor firing, indicating no leakage of the combustion gases through the nozzle-to-case joint.

RTDs T000125 and T000126 on Nozzle Nose Inlet Housing

The initial temperature of these RTDs varied from 60° to 65°F. They were partially heated by the aft skirt base region heating system because they were forward of the nozzle snubber segments, which provided a narrow opening to the hot air. Temperatures remained constant during and after motor firing, indicating no leakage of the combustion gases through the nozzle segments.

RTDs T0001300 and T0001301 on Nozzle Boot Cavity

The initial temperature recorded by RTD T0001300 was 58°F. The temperature of the boot cavity air rose sharply to about 870°F in 6 sec, indicating the flow of combustion gases into the cavity. After reaching that peak temperature, the boot cavity air temperature dropped to 450°F at 40 sec after ignition and to 275°F at the end of firing. Most probably, the vent holes close to RTD T0001300 were plugged after 6 sec, blocking the flow of the combustion gases. The drop in temperature after 6 sec was due to dissipation of the thermal energy to the flex bearing and boot materials.

The initial temperature recorded by RTD T0001301 was 55°F. The temperature of the boot cavity air rose sharply to about 900°F in 2.4 sec, and stayed constant at 900°F for an additional 9 sec. The boot cavity air temperature then dropped to 450°F at 31 sec after ignition and to 320°F at the end of firing. Most probably, the vent holes close to RTD T0001300 were plugged after 11.4 sec, blocking the flow of the combustion gases. The drop in temperature after 11.4 sec was due to dissipation of the thermal energy to the flex bearing and boot materials.

RTDs T000875 through T000878 on Igniter and S&A Joints

T000875 and T000878 were located on the igniter joint and T000876 and T000877 were located on the S&A joint. The igniter joint RTDs registered an initial temperature of 74° to 75°F at motor ignition and a temperature of 72° to 74°F at the end of motor operation, indicating that the igniter joint heater functioned well before the motor operation and that there was no leakage of the combustion gases through the joint during the motor operation. After motor operation, the temperatures began to drop continuously. The S&A joint initial temperatures were 59° to 62°F at motor ignition and reached 81° to 83°F at the end of motor operation. Because of the large mass to surface area ratio and the heat soak from the motor, these RTDs continued to register higher temperatures until they showed a peak temperature of about 110°F at about 425 sec. This behavior of the S&A flange is considered normal.

RTDs T001001 through T001004 on the Forward Field Joint

The initial temperatures of the four RTDs located circumferentially under the cork on the forward field joint were between 83° and 100°F, indicating that the heater functioned well in keeping the O-rings above 75°F before ignition. The temperatures registered remained more or less constant, between 83° and 99°F, indicating no leakage of combustion gases through the forward field joint.

RTDs T001005 through T001008 on the Center Field Joint

Four RTDs were located circumferentially under cork on the center field joint. The initial temperatures of the four RTDs were between 84° to 104°F, indicating that the joint heater functioned well and kept the joint O-ring above 75°F before the motor ignition. The temperature

registered by these RTDs remained constant, between 84° to 104°F, during the motor firing, indicating that there was no leakage of the combustion gages through the center field joint.

RTDs T001009 through T001012 on the Aft Field Joint

Four RTDs were located circumferentially under cork on the aft field joint. The initial temperatures of the four RTDs were between 85° to 105°F, indicating that the joint heater functioned well and kept the joint O-ring above 75°F before the motor ignition. The temperature registered by these RTDs remained more or less constant, between 91° to 105°F during the motor firing, indicating that there was no leakage of the combustion gases through the aft field joint.

RTDs T001009 and T001012 displaced oscillations during the motor firing. The oscillations, however, were around a mean temperature which was lower than the initial or the final temperatures of the two RTDs.

RTDs T000830 through T000846 on Motor Case Under Slag

These RTDs were installed to study the effect of the slag on the steel cases of the motor. RTD T000830 was installed on the forward segment, and RTDs T000831 and T000832 were installed on the aft center segment. The rest of the RTDs were on the aft segment. The initial temperatures of all the RTDs were between 33° to 42°F, reflecting the conditioning and the external environmental temperatures. As expected, the temperatures registered by all the RTDs showed a rise from 10° to 142°F. The maximum temperature rise occurred at Station 1598, indicating that the maximum accumulation of the slag within the case had no adverse heating effect. These case temperatures after the motor firing are normal, corroborating the normal functioning of the deluge system.

RTDs T000561 through T000568 on Nozzle Aft Exit Cone

These RTDs were installed between the cork and the glass-phenolic, 5 in. forward of the nozzle exit plane.

RTDs T000561 and T000568 both malfunctioned. They both started at 50°F and did not indicate any significant temperature rise during the motor firing. At the end of the motor firing they indicated wild oscillations in the temperatures.

RTDs T000562 through T000567 functioned well. The initial temperature of the RTDs varied from 50° to 76°F, and their final temperatures, after the heat soak, rose between 352° to 366°F (5 RTDs) in 425 sec from motor ignition. This final temperature of RTD T000562 rose to about 198°F in 425 sec.

RTDs T000301 Through T000304, T000306 Through T000308, T000310 Through T000312, T000221, and T000222 on Equipment in Base Region

These instruments were mounted on the gas generator beds, hydrazine tanks, hydraulic reservoirs, APU lubricating oil pipes, hydraulic lines, and return pipes. All were located in the base region. The base region was protected from the intense motor exhaust plume heat by a thermal curtain. The thermal analysis of this equipment is done by United States Boosters, Inc. (USBI), the NASA SRB integrator. All the RTDs in the base region registered initial temperatures from 88° to 110°F (220°F on the gas generator bed), indicating that the base region heating system functioned normally during the operation of the low temperature environment motor conditioning system.

RTD T000302H, located on the gas generator bed, malfunctioned. RTDs T000301L and T000302L, also located on the gas generator beds, recorded maximum temperatures between 1,070° to 1,100°F. These are considered normal. RTDs T000303 and T000304, located on the hydrazine fuel tanks, as expected did not show any temperature rise; their temperatures stayed constant at 89°F for T000303, and 95°F for T000304. RTDs T000306 and T000310 were located on two hydraulic reservoirs, and between them showed a temperature rise from 21° to 29°F. RTDs T000307 and T000308 were located on two APU lubricating oil lines (Tilt and Rock). The initial temperatures of these lines were 98° to 100°F and the maximum temperatures were between 182° to 205°F. These are considered normal. RTDs T000311 and T000312 were located on the two hydraulic return lines (Tilt and Rock). Their initial temperatures were between 88° to 100°F and their maximum temperatures were between 135° to 143°F. RTDs T000221 and T000222 were located on the hydraulic lines (Tilt and Rock). Their initial temperatures were between 100° to 101°F and their maximum temperatures were between 128° to 138°F.

All the RTDs in the base region that functioned well recorded normal temperatures.

10

QM-8 CONFIGURATION

10.1 TEST ITEM DESCRIPTION

The QM-8 static test article was configured to approximate the redesigned solid rocket motor (RSRM) flight motors. The RSRM static test consisted of a lined, insulated, segmented rocket motor case loaded with solid propellant; ignition system complete with electro-mechanical S&A device, initiators and loaded igniter; movable nozzle with flexible bearing and exit cone. A 360 deg ETA ring (primary structure only) and an SRB aft skirt were attached with TVC systems and actuators, electrical and instrumentation items, and a thermal curtain assembly. Side load actuators were attached to the ETA ring to introduce simulated flight loads. An overall view of the test article is shown in Figure 1.2-1. Table 10.1-1 summarizes the design/component differences in QM-7 and Flight-1 (360L001). Table 10.1-2 summarizes processing and assembly differences in QM-7 and Flight-1 (360L001). Table 10.1-3 summarizes QM-8 deviations from flight. The QM-8 drawing tree is included in Appendix A.

10.1.1 Propellant/Liner

The RSRM propellant, TP-H1148, is a composite-type solid propellant, formulated of polybutadiene acrylic acid acrylonitrile terpolymer binder (PBAN), epoxy curing agent, ammonium perchlorate (AP) oxidizer and aluminum powder fuel. A small amount of burning rate catalyst (iron oxide) is added to achieve the targeted propellant burn rate of 0.368 ips at 625 psia at 60°F.

The propellant grain design consists of a forward segment with an eleven-point star with a smooth bore-to-fin cavity transition region that tapers into a circular perforated (CP) configuration. The two center segments are double-tapered CP configurations and the aft segment is a triple-taper CP configuration with a cutout for the partially submerged nozzle (Figure 10.1.1-1). The aft segment nozzle cutback region is formed using net cast molding.

10.1.2 Insulation

The internal insulation system includes chamber insulation and propellant stress relief flaps. The insulation material for the chamber and stress relief flaps is an asbestos-silica filled acrylonitrile butadiene rubber (NBR). NBR is used as the basic case sidewall insulation. The aft dome insulation system is a composite carbon-fiber filled EPDM/asbestos silica NBR system. The carbon-fiber filled EPDM is installed to reduce the erosion of the insulator near the submerged nozzle and under the stress relief flaps in the center segments. The field joints had a J-joint

Table 10.1-1. Design/Component Differences

	QM-7	QM-8	Flight-1 (360L001)	Remarks
1.	Case			
	Same as Flight	Quarterweight configuration (standard ETA segment)	Lightweight configuration (lightweight ETA segment)	
2.	Systems Tunnel			
	Floor Plates Installed on All Segments	Floor plates installed on forward, center-forward, center-aft segments only	Full length	Tunnel installation on aft segment deleted (ref memo E130/SJH-FY89-102 dated 6 Oct 1988
	No Splice Plates	Same as QM-7	Splice plates installed	
	Installed on 180 deg Longitudinal Line	Same as QM-7	Installed on 90 deg longitudinal line	Relocated to accommodate static test configuration
	Same as Flight	Paint stripper used on center-aft segment only	Gritblast	RPRB approved 24 Aug 88 qualify paint stripper for future flight motors (possibly 14th flight)
3.	ETA Ring 360 deg			
	Same as Flight Except Not Insulated, Instrumented But Not Recorded	Same as QM-7	Flight configuration	Same ETA ring (LH) used on DM-9 (S/N 019). Required to apply side loads for static test

Table 10.1-1. Design/Component Differences (Cont)

	QM-7	QM-8	Flight-1 (360L001)	Remarks
4.	Stiffener Rings			
	Flight Configuration Except K5NA (cork-filled epoxy) Close-out	Same as QM-7	Flight configuration	K5NA close-out not required for static test and would damage hardware during post-test removal at test bay if applied. Handling interference with tooling if not removed
5.	Propellant/Liner			
	Same as Flight	Same as flight		
6.	Ignition System			
	RSRM Igniter Modified for CO_2 Quench Port	Same as QM-7	RSRM igniter	Quench port standard static test configuration to minimize post-test insulation burn and allow assessment of insulation erosion
	Same as Flight	1U52295-03 S&A device (O-ring squeeze requirement added)	1U52295-02 S&A device	PV-1 used 1U52295-02 S&A device Qualify 1U52295-03 S&A for 360L003 and subsequent
	Same as Flight	Putty not tamped	Putty tamped	Putty not tamped, 360L003 and subsequent
		Packing with retainer (Stat-O-Seal) lubricated with HD-2 grease		360Q004 and subsequent

Table 10.1-1. Design/Component Differences (Cont)

	QM-7	QM-8	Flight-1 (360L001)	Remarks
		Fabricated nozzle insert from new mold design (ETP-309)		360L002 and subsequent
		New external insulation layup procedure and ply thickness change (thinner)		No design change in insulation or thickness 360L002 and subsequent
	Temperature Control--Recirculating Hot Air	Temperature control configuration changes after incident (using G-03, same as Flight-3)--Joint strip heater	No temperature control--On-pad environment	Strip heater installed on 360L002 Joint strip heater installed on PV-1
7.	Case-to-Case Factory Joints			
	Same as Flight	Same as flight	Fluorocarbon O-rings (primary and secondary)	
	Same as Flight	Ply layup change, forward and center segments only		Ply layup change implemented in RSRM-4B aft, 360H005 and subsequent
		Aft segment ply layup--Same as 360L001		QM-8/4B aft segment swap
	Same as Flight	Same as flight	Vulcanized weatherseal	
	Same as Flight	Same as flight	RSRM case segments	
	Same as Flight	Same as flight	3-piece pin retainer band	
	Same as Flight	Same as flight	Custom shims	

Table 10.1-1. Design/Component Differences (Cont)

	QM-7	QM-8	Flight-1 (360L001)	Remarks
	Same as Flight	Same as flight	Leak test port plug	
8.	Case-to-Case Field Joints			
	Same as Flight	Same as flight	J-joint insulation	
	Same as Flight	Same as flight	Fluorocarbon O-rings (primary, secondary, CF)	
	Same as Flight	Same as flight	Fluorocarbon V_2 filler	
	Same as Flight Except Vent Valve Installed at 129 deg Only	Same as QM-7	JPS with vent valves at 45 and 129 deg	Vent valve at 45 deg cannot be installed because of instrumentation interference
	Same as Flight	Same as flight	Temperature Control--JPS	
	Same as Flight	Adjustable vent port plug (AVPP)	Customized vent port (135 deg) plug	AVPP installed on PV-1 Qualify AVPP for 360L003
	Leak Test Port Plug Replaced With Lockwired LVDT	Same as QM-7 (i.e., LVDT)	Leak test port (45 deg) plug	CEI spec requirement to verify gap opening and evaluate field joint performance. NRC action
	Same as Flight	Same as flight	Custom shims	
	Same as Flight	Same as flight	3-piece pin retainer band	
	Same as Flight	Same as flight	J-joint insulation	

Table 10.1-1. Design/Component Differences (Cont)

QM-7	QM-8	Flight-1 (360L001)	Remarks
	Flap bulb/ply layup change (tang end)		Flap bulb/ply layup change implemented in 360H005 and subsequent
	Tie ply layup change (clevis end)		
	Process change--Chemlok dimensions (clevis end)		Effective 360L003 and subsequent
9. Case-to-Nozzle Joint			
Same as Flight	Same as flight	RSRM aft dome/fixed housing	
Same as Flight	Same as flight	Fluorocarbon O-rings (wiper, primary, secondary)	
Temperature Control: Steam Heated, Recirculating Hot Air	Same as QM-7	Temperature control--Single orifice purge	Ground test heating system was used on DM-9, QM-6, and PV-1
Plug Not Used--Pressure Transducer Installed	AVPP installed	Customized vent port (43.2 deg) plug	Qualify AVPP for 360L003
Plug Not Used--Pressure Transducer Installed	Same as QM-7	Leak test port (90 deg) plug	Pressure transducer installed to assess joint performance
Same Bolts as Flight Except for Four Each Instrumented Radial Bolts	Same bolts as flight except for 16 each instrumented bolts (i.e., 8 each axial and 8 each radial)	Ultrasonicable case-to-nozzle bolts (100 each axial and 100 each radial)	Instrumented bolts not used in flight. Used to evaluate case-to-nozzle joint installation and during static test

Table 10.1-1. Design/Component Differences (Cont)

	QM-7	QM-8	Flight-1 (360L001)	Remarks
10.	Aft Skirt/TVC			
	Reconfigurated for Static Test	Same as QM-7	Flight configuration	Fuel lines are reconfigured for TVC operation at a horizontal position. Same aft skirt (S/N 002) was used on QM-7 and PV-1
	Insulated at the Aft End for Static Test	Improved external insulation	Flight insulated	Improved external insulation (0.5-in. cork) to minimize heat loss during aft end heating
	Added Instrumentation to Evaluate Effects of LSC and Side Load	Same as QM-7	Flight instrumented	
	Modified Thermal Curtain	Same as QM-7	Flight configuration thermal curtain	Eliminate outer panel of thermal curtain for static test. Not required. Minimized installation and removal time. Reduces replacement/refurbishment costs.
		Off-motor/refurb GN_2 spin-hot fire deleted		Ref memo E130/JM-FY89-071
11.	Insulation--TPS			

Table 10.1-1. Design/Component Differences (Cont)

	QM-7	QM-8	Flight-1 (360L001)	Remarks
	None	None	TPS installed	TPS not required for static test. Interferes with static test instrumentation. TPS system is unchanged and already qualified
12.	Instrumentation			
	Limited DFI and GEI Installed	Similar to QM-7	DFI and GEI installed	Different instrumentation requirements in lieu of motor orientation, test environment (e.g., motor sag, nozzle alignment, slag), and test bay requirements (e.g., side load, case water deluge)
	No Thrust Recorded	Same as QM-7		Representative gages are chosen from GEI/DFI and installed and recorded for correlation
				Installation of all types of DFI/GEI gages will be demon-strated on QMs (qualification of gages are being done by NTS)
	None	Low-pressure fairing and accelerometer blocks installed	None	Installed on 360L002. Data required from post-pull tests (i.e., PV-1 and QM-8)
13.	Nozzle Assembly			
	Same as Flight	Same as flight	RSRM forward exit cone assembly	

Table 10.1-1. Design/Component Differences (Cont)

QM-7	QM-8	Flight-1 (360L001)	Remarks
Same as Flight	Same as flight	RSRM fixed housing	
Same as Flight	Same as flight	RSRM nose inlet assembly	
Same as Flight	Same as flight	RSRM throat inlet assembly	
Same as Flight	Same as flight	RSRM cowl with structural support OBR	
Same as Flight	Same as flight	RSRM flex bearing	
Same as Flight	Same as flight	RSRM aft exit cone	
Same as Flight	Same as flight, and Joint 2	RTV backfill in three joints only (Joints 1, 3, 4)	Backfill in Joint 2 is a result of the nose cap-to-cowl process change, performed on PV-1. Currently not implemented on any flight motor
Same as Flight	Same as flight	Redundant and verifiable seals in all five joints	
Same as Flight	Same as flight	LSC is installed	
Same as Flight Except Ring at 90 deg Removed	Same as QM-7	Snubbers installed	90-deg section removed for test instrumentation cable access
Same as Flight	Altered	RSRM nozzle plug	QM-8 nozzle plug-altered to accommodate bore inspection after cold motor soak. RPRB 14 Sep 1988
Same as Flight	Same as flight	Exit cone shear pins, vented and positive-stop	

Table 10.1-1. Design/Component Differences (Cont)

QM-7	QM-8	Flight-1 (360L001)	Remarks
Same as Flight (Joint 5 screw was threaded to head)	Same as flight except in Joint 5	Locking fasteners used on all assemblies	QM-8 Joint 5 fastener has smooth shank under Stat-O-Seal (used in PV-1, 360L002 and subsequent)
Same as Flight	Same as flight	Lightning protection system	

Table 10.1-2. Processing and Assembly Differences

	QM-7	QM-8	Flight-1 (360L001)	Remarks
1.	JPS Cable Routing			
	Field Joint: Same as Flight Except at Aft End/ETA Interface	Same as QM-7		Interface to test bay is different
	NA	Igniter joint--Same as flight except no forward skirt interface		Forward skirt not installed in static test motors
2.	Igniter Strip Heater	Installation sequence/checkout change after 8 Dec 1988 incident		Water deluge in static test is used to cool case after firing
3.	Case Water Deluge			
	Manually Activated When Internal Motor Pressure Drops to 300 psig	Same as QM-7	Splashdown	Water deluge was redesigned after DM-8 post-test case hot spots--Performed successfully on DM-9, QM-6, QM-7, and PV-1
4.	Case-to-Nozzle Joint Insulation			
	No Repair Done	No repair done	Tear repaired on 360L001	Insulation baffle tear and repair exercise performed on QM-6
5.	Field Joint Leak Testing			
	Performed Prechock and Postchock	Prechock only	After segment stack	Discontinued postchock field joint leak testing starting PV-1

Table 10.1-2. Processing and Assembly Differences (Cont)

QM-7	QM-8	Flight-1 (360L001)	Remarks
6. Nozzle Assembly			
a. Nozzle Disassembly			
Not Disassembled	Disassembled due to QM-8/4B aft exchange	Nozzles were removed--Involute replaced by structural support OBR	Nozzle assemblies remained unchanged
b. Duty Cycle			
Similar to QM-6 Except Held at Null During Side Loading	Same as QM-7		Test unique
c. Case-to-Nozzle Joint Ultrasonic Preload			
Same as Flight	Higher preload (140 ±14 kips)	95.5 ±10 kips preload	Qualify higher U/T preload valve
d. Cowl-to-Nose Cap Assembly			
Same as Flight	Process change		Process change currently not implemented on flight motors Process change implemented on PV-1
e. Nozzle Plug Installation			
Same as Flight	Reinstall 3-ft-dia taper cut nozzle plug after bore inspection		Access to bore inspection (field joints and propellant grain) after motor cold soak

Table 10.1-2. Processing and Assembly Differences (Cont)

6. Nozzle Assembly (Cont)

	Component	DM-9	QM-6	QM-7	PV-1	QM-8	Flight-1A	Flight-1B
a.	Aft Inlet Ring	U.S. Poly	U.S. Poly	U.S. Poly	U.S. Poly	Fiberite*	U.S. Poly	U.S. Poly
b.	Forward Nose Ring	U.S. Poly	U.S. Poly	U.S. Poly	U.S. Poly	Fiberite*	U.S. Poly	U.S. Poly
c.	Nose Cap	U.S. Poly	U.S. Poly	U.S. Poly	U.S. Poly	Fiberite*	U.S. Poly	U.S. Poly
d.	Throat Ring	U.S. Poly	U.S. Poly	U.S. Poly	U.S. Poly	Fiberite*	U.S. Poly	U.S. Poly
e.	Throat Inlet Ring	Fiberite	Fiberite	Fiberite	Fiberite	Fiberite	U.S. Poly	Fiberite
f.	Fixed Housing Insulation	Fiberite	Fiberite	Fiberite	Fiberite	Fiberite	Fiberite	Fiberite
g.	Outer Boot Ring	U.S. Poly	Fiberite	Fiberite	Fiberite	Fiberite	Fiberite	Fiberite
h.	Cowl Liner	U.S. Poly	Fiberite	U.S. Poly	Fiberite	Fiberite	U.S. Poly	U.S. Poly
i.	Forward Exit Cone Liner	Fiberite	U.S. Poly	Fiberite	Fiberite	U.S. Poly	Fiberite	Fiberite
j.	Aft Exit Cone Liner	U.S. Poly	Fiberite	Fiberite	Fiberite	Fiberite	U.S. Poly	Fiberite

*Qualify use of Fiberite for flight motors

	QM-7	QM-8	Flight-1 (360L001)	Remarks
7.	Test Orientation and Assembly			
	Different From Flight Assembled and Tested Horizontally	Same as QM-7		Major differences are: Field joint assembled clevis-to-tang--Static test
	Utilizes Different Tooling/GSE			Nozzle alignment--Static test Motor sag--Static test

Table 10.1-2. Processing and Assembly Differences (Cont)

	QM-7	QM-8	Flight-1 (360L001)	Remarks
		S&A sequence and TVC-HPU start is moved earlier		Countdown checks and milestones are different--Static tests Arming sequence and TVC-HPU start was changed effective PV-1 (ref memo E130/FY89-032)
8.	Side Load			
	Load Cases L02044 and ETMA352 Used for Ignition Transient and Max Q Events, Respectively	Same as QM-7		Ref TWR-16674 Test Article Mechanical Loads
9.	Temperature Environments			
	a. Commit Criteria			
	1. Igniter Joints			
	83° to 113°F	75° to 123°F (78° ±1°F setpoint at the heater controller)	66° to 123°F (no heater)	QM-7 target was high side QM-8 target is low side Redline limits ensure igniter joint seals are within 64° to 130°F 360L002 heater setpoint is 95° ±5°F

Note: All values under item 9 connote at the sensors

Table 10.1-2. Processing and Assembly Differences (Cont)

	QM-7	QM-8	Flight-1 (360L001)	Remarks
2.	Field Joints			
	85° to 115°F	85° to 122°F (86° ±1°F setpoint at the heater controller)	85° to 122°F (98° ±1°F setpoint at the heater controller)	Controlled by the FJPS Redline limits ensure case field joint O-ring seals are within 75° to 130°F
9.	Temperature Environments			QM-8 target is low side
	a. Commit Criteria (Cont)			
	3. Case-to-Nozzle Joint/Nozzle Bondline			
	82° to 110°F	75° to 115°F	75° to 115°F	QM-7 target was high side QM-8 target will be low side Redline limits ensure case-to-nozzle O-ring seals are 75°F minimum, and nozzle bondlines are 115°F maximum

Note: All values under Item 9 connote at the sensors

Table 10.1-2. Processing and Assembly Differences (Cont)

QM-7	QM-8	Flight-1 (360L001)	Remarks
4. Flex Bearing Temperatures			
NA	80° to 115°F	60° to 115°F (OMRSD requirement)	QM-8 target will be low side but limited by the case-to-nozzle joint/nozzle bondline temperature limits (75° to 115°F) during aft end heating (for static test) Redline limits ensure flex bearing is 60°F minimum prior to duty cycle, both pretest hot fire and static test
5. Case Acreage Temperatures			
NA	20°F minimum	35°F minimum	Redline ensures adequate temperature to ensure proper safety factors on D6AC steel at time of firing Test currently ongoing at NASA-Langley and Morton Thiokol/Westinghouse Research Corp

Note: All values under Item 9 connote at the sensors

Table 10.1-2. Processing and Assembly Differences (Cont)

	QM-7	QM-8	Flight-1 (360L001)	Remarks
b.	Test Requirements			
	1. PMBT (calculated)			
	90°F	40°F	40° to 90°F	QM-7 and QM-8 require test bay conditioning
	2. System Tunnel Bondline			
	120°F	20°F minimum	NA	
		Eddy current inspection on all threaded holes, igniter chamber		360H005 and subsequent

Note: All values under Item 9 connote at the sensors

Table 10.1-3. QM-8 Deviations From Flight

Component Description	Difference From Flight Design	Certification Exclusions
Flex Bearing/Boot Assembly	Instrumentation installed	An exclusion is claimed if any test anomaly is instrumentation

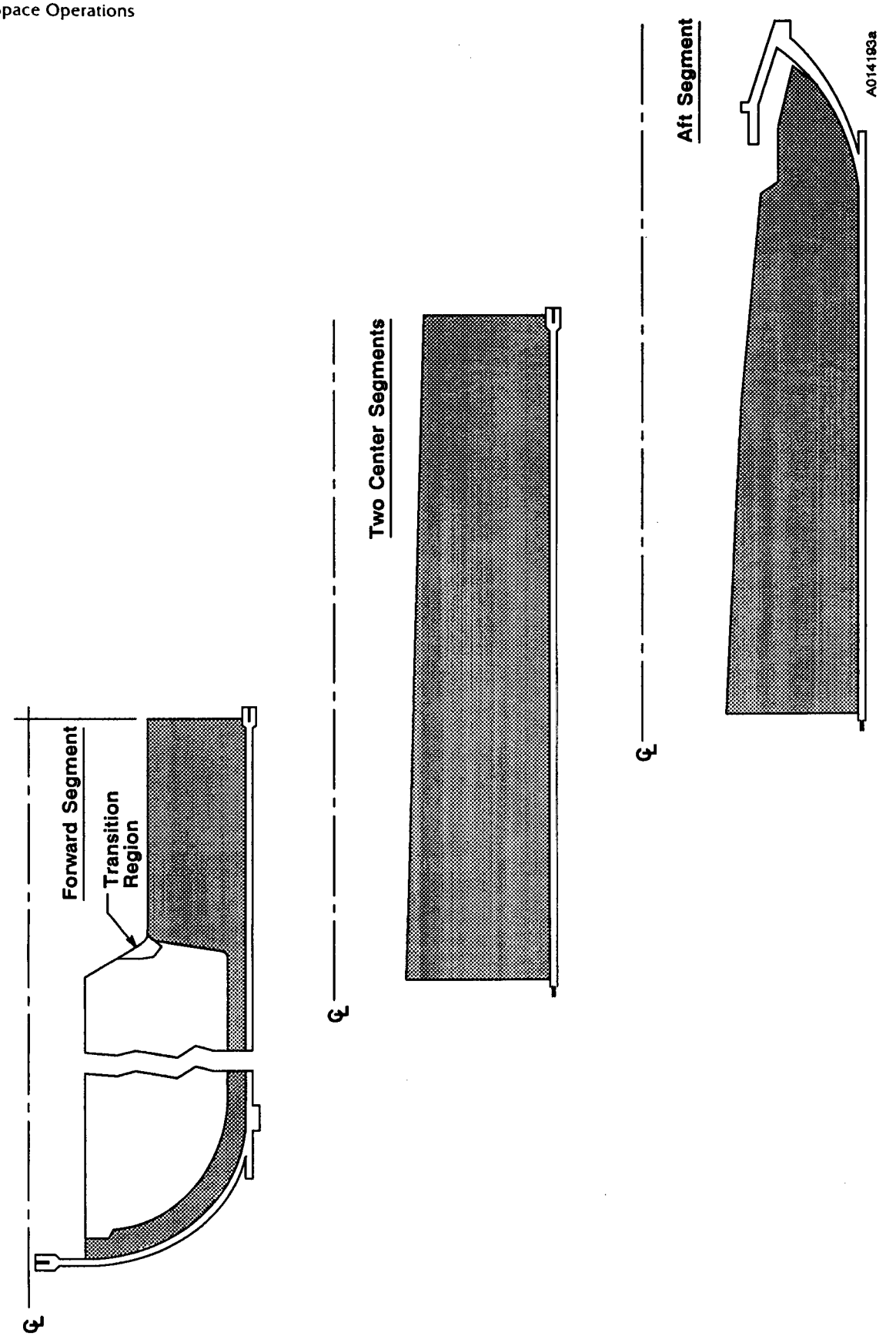

Figure 10.1.1-1. HPM Propellant Grain Design Configuration

insulation configuration as shown in Figure 10.1.2-1. The external insulation includes vulcanized silica-filled EPDM insulation over the factory joints.

10.1.3 Liner/Inhibitor

The inhibitor was the same as the HPM with castable inhibitors on aft end of the forward and center segments. The aft facing inhibitor material is a carboxyl-terminated polybutadiene (CTPB) polymer. NBR inhibitors are used on the forward face of the center and aft segments.

The liner material is an asbestos-filled CTPB polymer, which bonds the propellant to the case insulation in the SRM.

10.1.4 Nozzle/TVC

The nozzle assembly is a partially submerged convergent/divergent movable design with an aft pivot point flexible bearing.

A nozzle protective plug was installed to provide a hermetic seal, protect from environmental contamination, and provide thermal insulation during cold conditioning.

The nozzle plug was modified (Figure 10.1.4-1) by removal of a section from the center of the plug to allow access for a bore inspection toward the end of the cold conditioning. The removed section of the plug was bonded back in place after the bore inspection was completed. The nozzle consists of the following subassemblies (Figure 10.1.4-2).

A. Fixed housing assembly with radial bolts
    1. Insulation
    2. Fixed housing

B. Nose inlet assembly
    1. Nose cap
    2. Forward nose ring
    3. Aft inlet ring
    4. Nose inlet housing

C. Throat inlet assembly
    1. Throat inlet ring
    2. Throat ring
    3. Throat support housing

D. Forward exit cone assembly
    1. Forward exit cone liner
    2. Forward exit cone housing

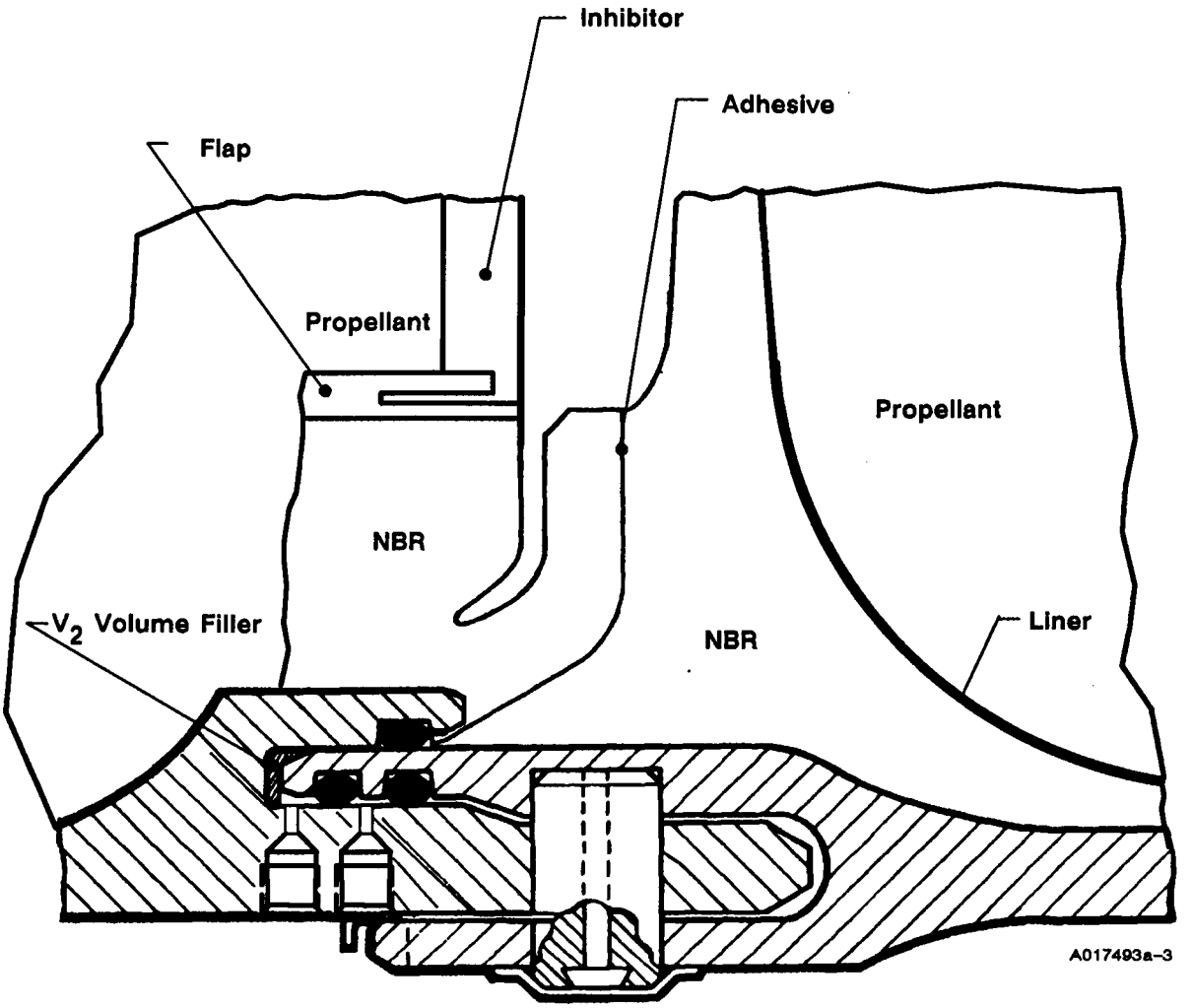

Figure 10.1.2-1. J-seal Case Field Joint Insulation

N108280-1

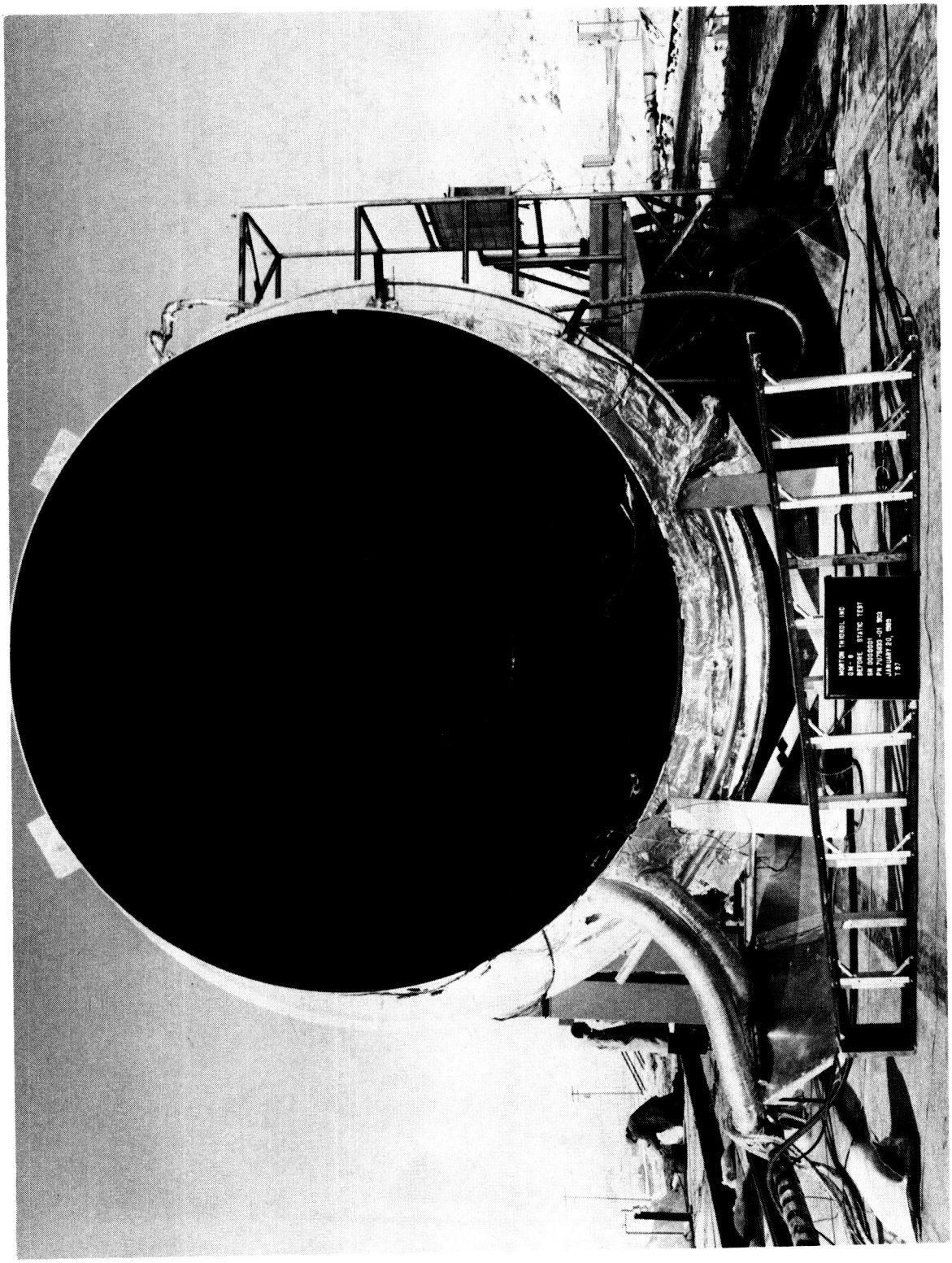

Figure 10.1.4-1. QM-8 Modified Nozzle Plug

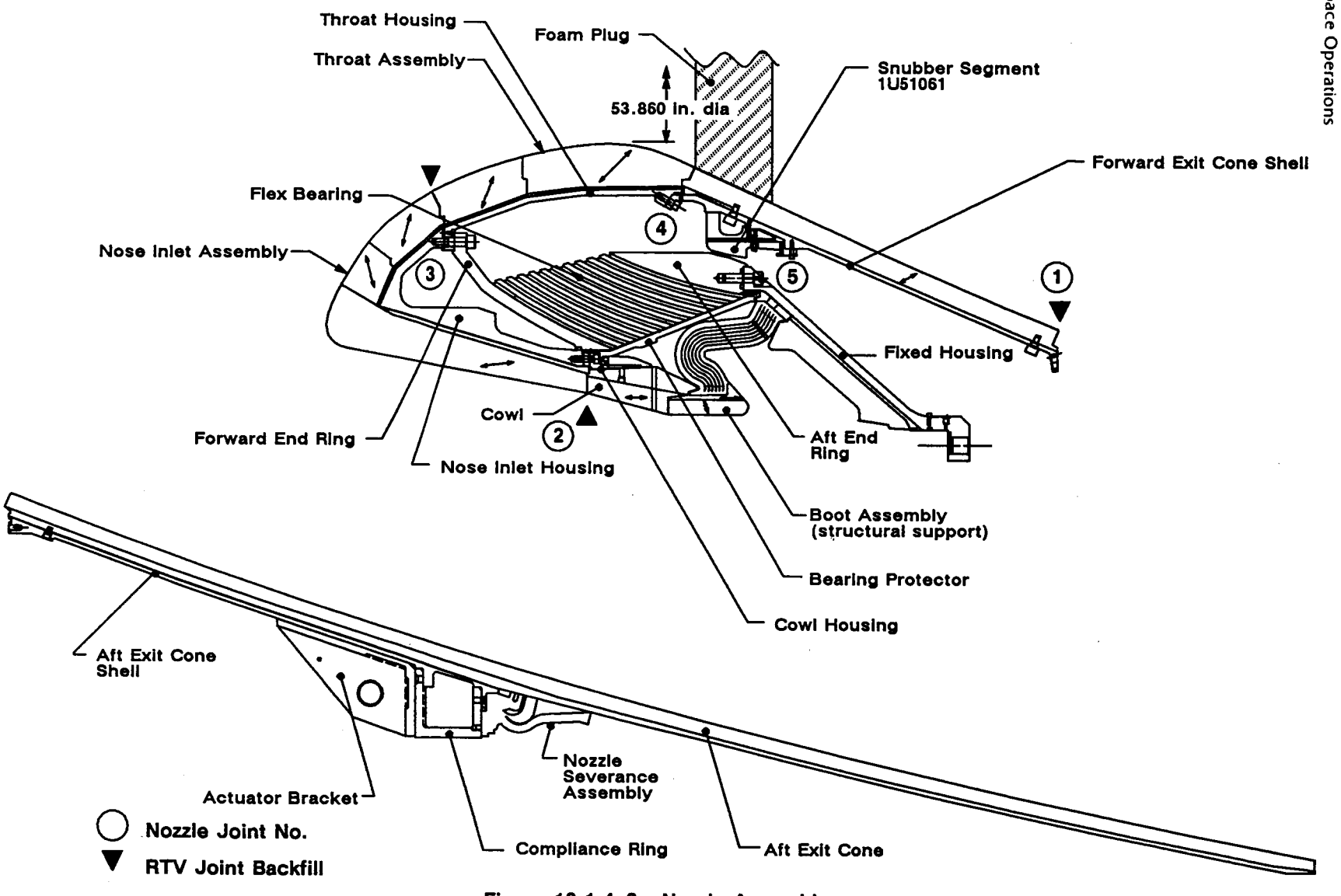

Figure 10.1.4-2. Nozzle Assembly

A020821a

E. Aft exit cone assembly
   1. Aft exit cone liner
   2. Aft exit cone shell

F. Flexible bearing
   1. Forward end ring
   2. Aft end ring

G. Cowl/outer boot assemblies
   1. Cowl liner
   2. OBR (structural support)

H. Snubber

I. Linear shaped charge (LSC)

The TVC subsystem is comprised of two SRB actuators and two hydraulic power units (HPU) located in the aft skirt.

The HPU ground test controller, HPU manual/automatic panel (MAP), and the ascent thrust vector control units (ATVC) serve as the control units for the TVC subsystem. A block diagram of the TVC subsystem and controllers is shown in Figure 10.1.4-3.

10.1.5 Case/Seals

The case consists of 11 individual weld-free segments: the forward dome, 6 cylinder segments, the ETA segment, 2 stiffener segments and the aft dome. The 11 segments are preassembled into 4 subassemblies before propellant casting. These 4 subassemblies are the forward segment assembly, the forward center segment assembly, the aft center segment assembly, and the aft segment assembly.

These individual casting segments are joined by means of capture feature (CF) tang and clevis field joints, which are held together by pins. The case-to-nozzle joint is formed by bolting the nozzle fixed housing into the aft dome with 100 axial and 100 radial bolts which are torqued ultrasonically. The assembled case is approximately 116 ft in length and 12 ft in diameter, as shown in Figure 1.2-1.

The assembly and joint configurations are as follows:

Field Joints

1. CF tang and clevis with long pins, custom shims, and pin retainer band.
2. J-joint insulation configuration is an unvented joint as shown in Figure 10.1.2-1. The field joint insulation layup and process are shown in Figure 10.1.5-1.
3. Clevis and CF O-rings are fluorocarbon (STW4-3339).

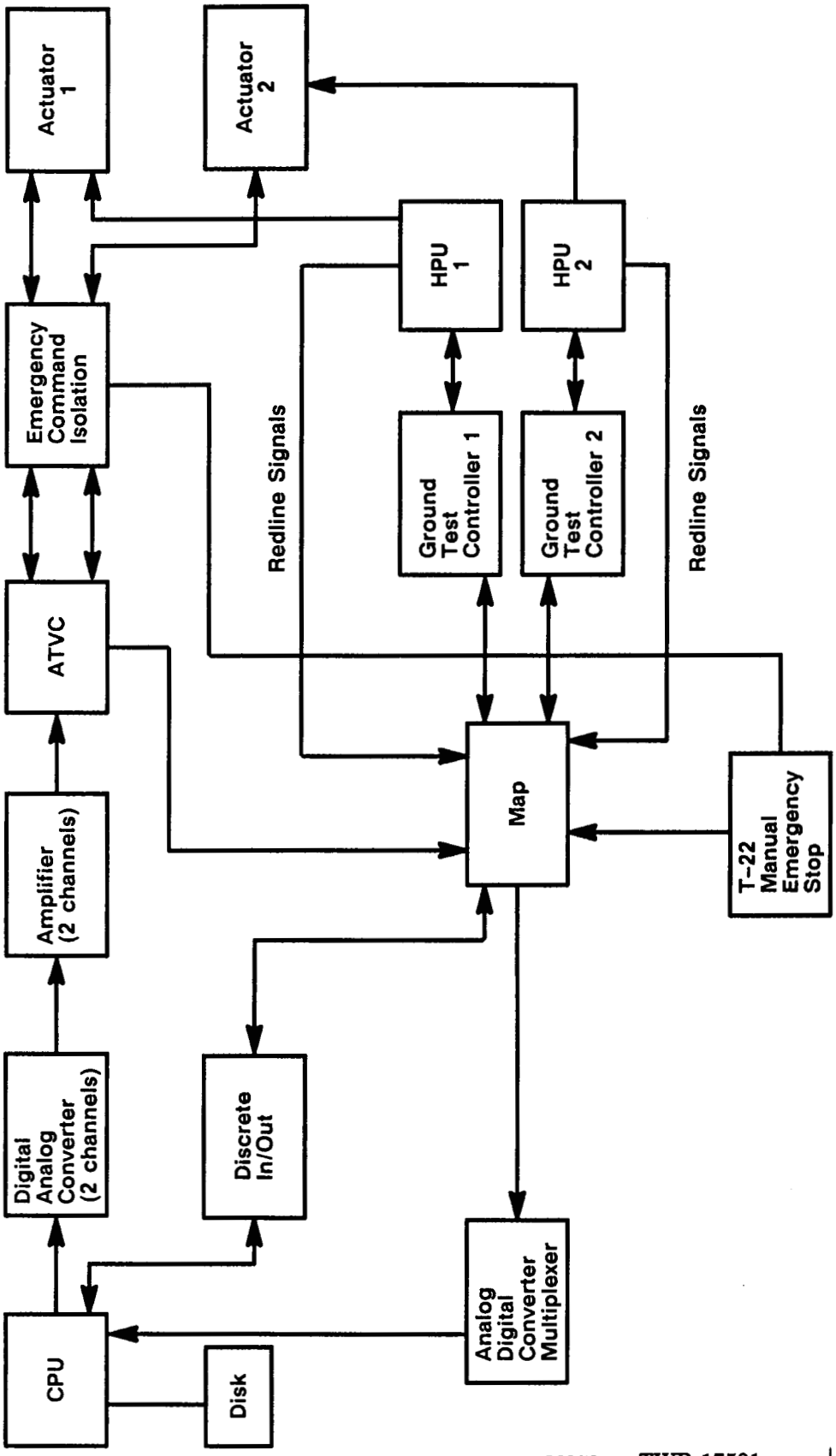

Figure 10.1.4-3. Thrust Vector Actuation (TVA) System

- Flap bulb dimensions changed to accommodate a gradual taper on the forward face
- Ply layup changed to reduce/eliminate the frequency and size of insulation-to-insulation voids and depressions on the insulation surface

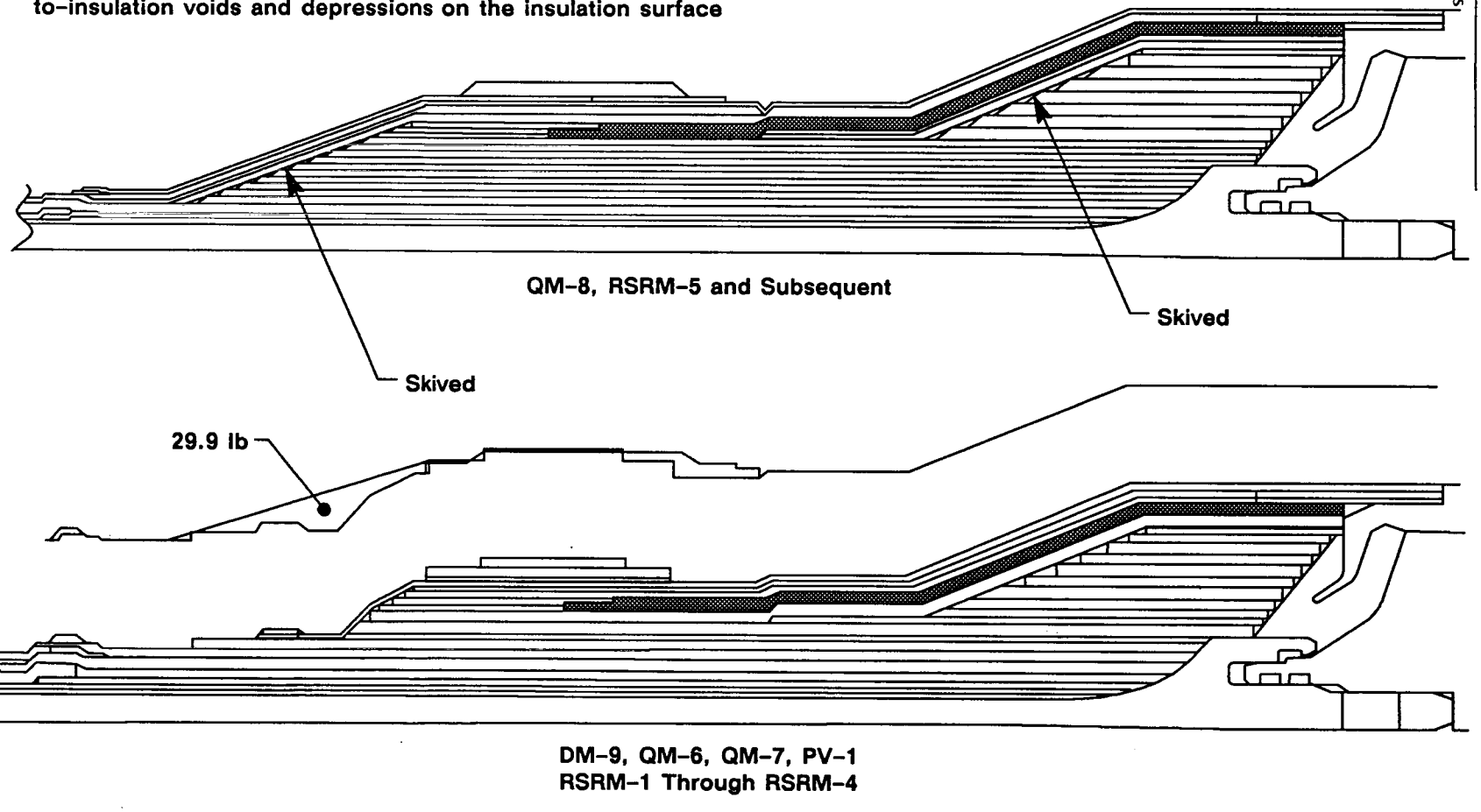

Figure 10.1.5-1a. Field Joint Insulation Layup

A020828a

- Tie ply under the NBR inhibitor extended forward under the clevis insulation extrusion

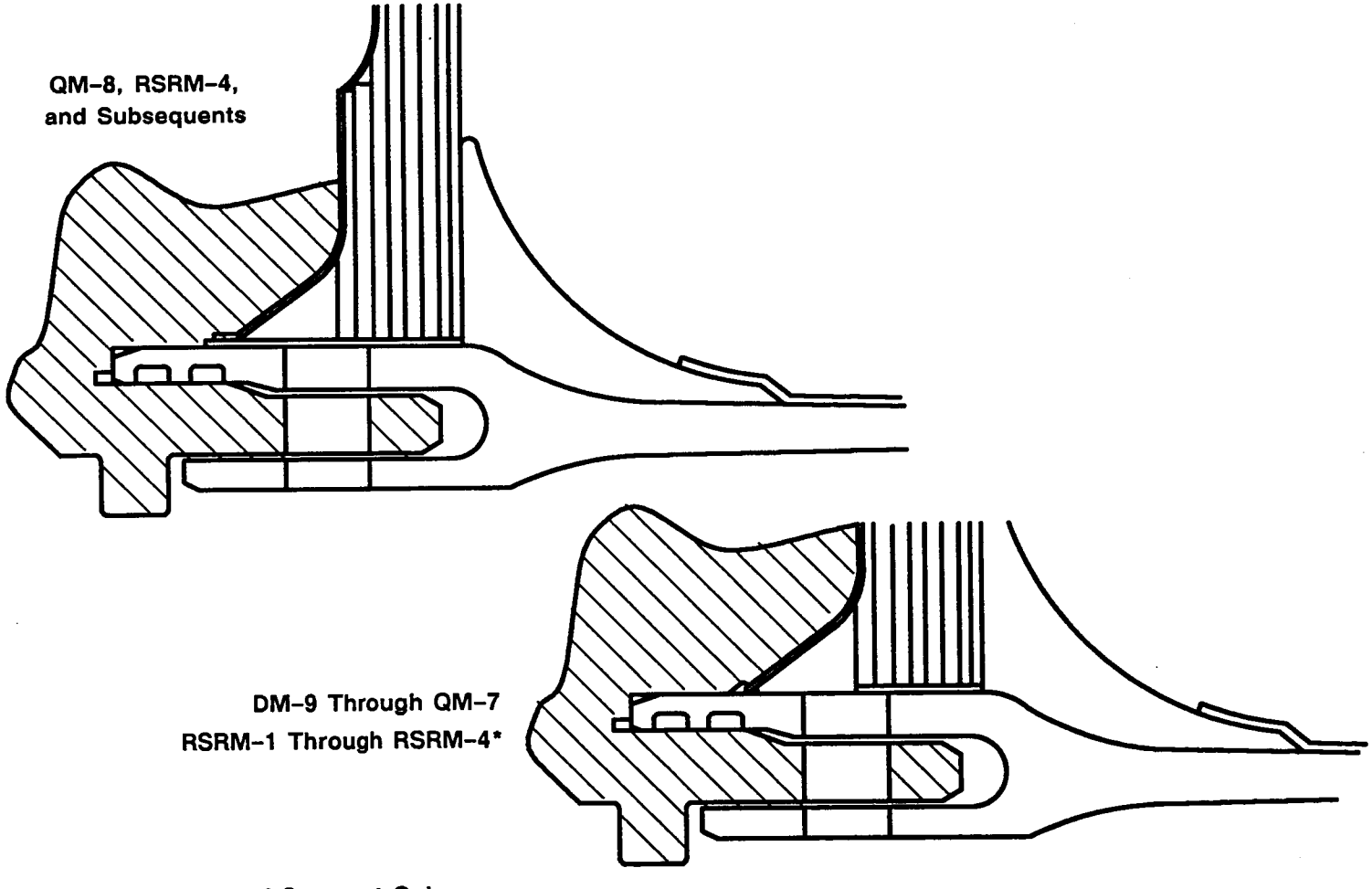

*RSRM-4B Center Forward Segment Only

Figure 10.1.5-1b. Field Joint Insulation Process

A020829a

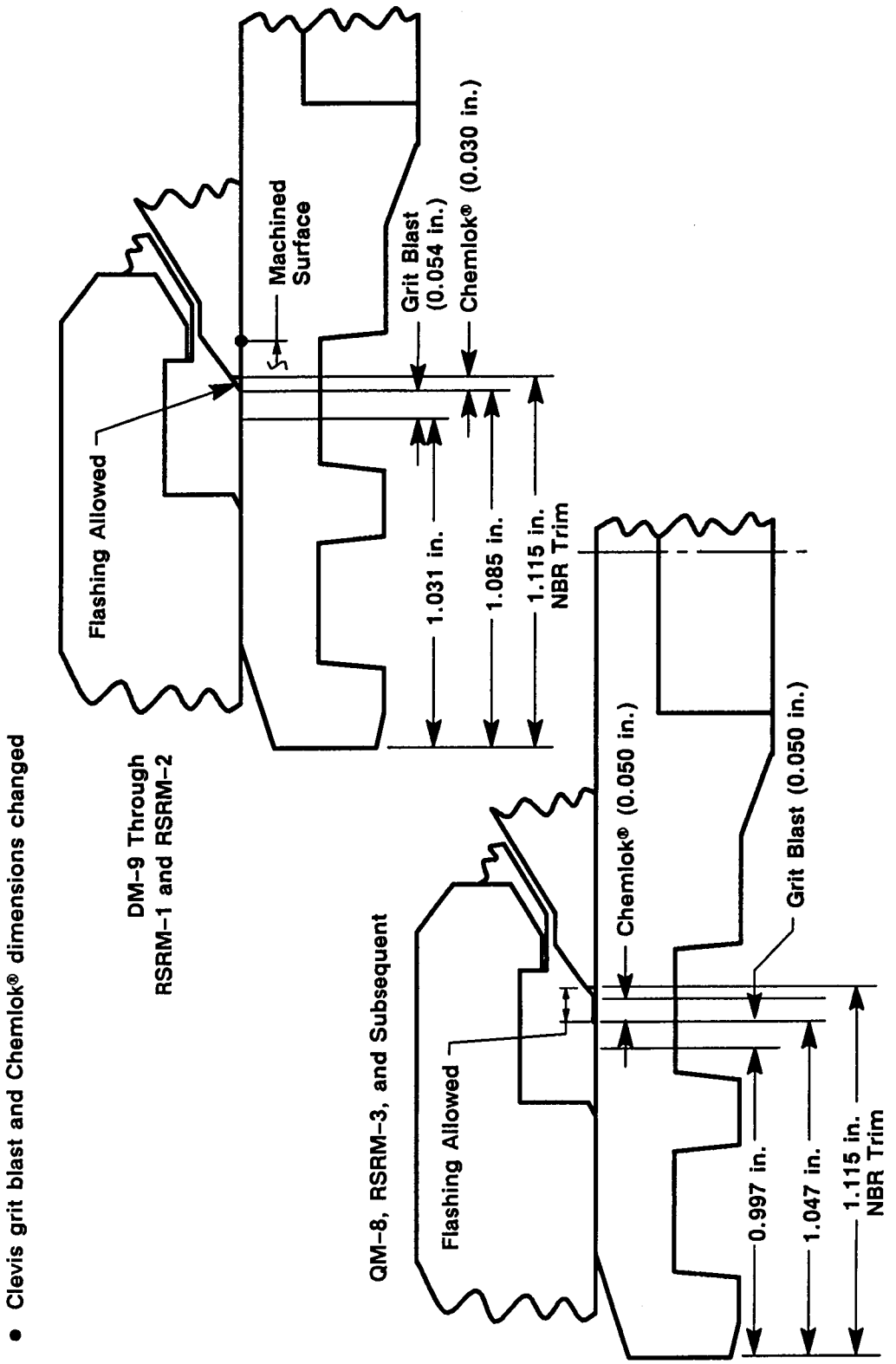

Figure 10.1.5-1c. Field Joint Insulation Process (Cont)

4. Fluorocarbon (STW3-3353) V_2 volume filler.
5. A joint protection system (JPS) with joint heater and weather seal as shown in Figure 10.1.5-2.
6. Adjustable vent port plugs (AVPP).

Case-to-nozzle Joint

1. Nozzle fixed housing with radial bolts.
2. Primary and secondary O-ring seals and the wiper O-ring were fluorocarbon (STW4-3339).
3. Radial bolts with Stat-O-Seals.
4. An unvented insulation configuration shown in Figure 10.1.5-3.
5. Adjustable vent port plugs (Figure 10.1.5-4).

Factory Joints

1. HPM tang and RSRM-modified clevis hardware design.
2. Insulation overlaid and cured over interior of the joint. Teflon tape has been added to all factory joints to prevent the NBR from bonding to the case, providing a stress relief. Figure 10.1.5-5 illustrates the factory joint ply layup.

Igniter-to-Forward Dome Joint

1. RSRM igniter modified for CO_2 quench port.
2. Putty was not tamped.
3. Igniter heater assembly installed as shown in Figure 10.1.5-6.

Corrosion protection consisted of full external paint and a film of grease (including O-rings, sealing surfaces, and pinholes).

10.1.6 Ignition System

The SRM ignition system is a modified HPM igniter (Figure 10.1.6-1). It contains a single nozzle, thickened steel chamber at the nozzle end, external insulation, and tapered internal insulation (Figure 10.1.6-2), new liner material, vacuum putty from a new manufacturer (Inmont Canada, Inc.) and solid propellant igniter containing a case-bonded 40-point star grain. The forward-mounted solid rocket-type igniter is modified with a CO_2 quench port.

The ignition system produced a short, predictable motor ignition which minimized thrust imbalance. An RSRM S&A device was installed on the igniter. Ultrasonically torqued bolts fastened the igniter adapter to the igniter chamber.

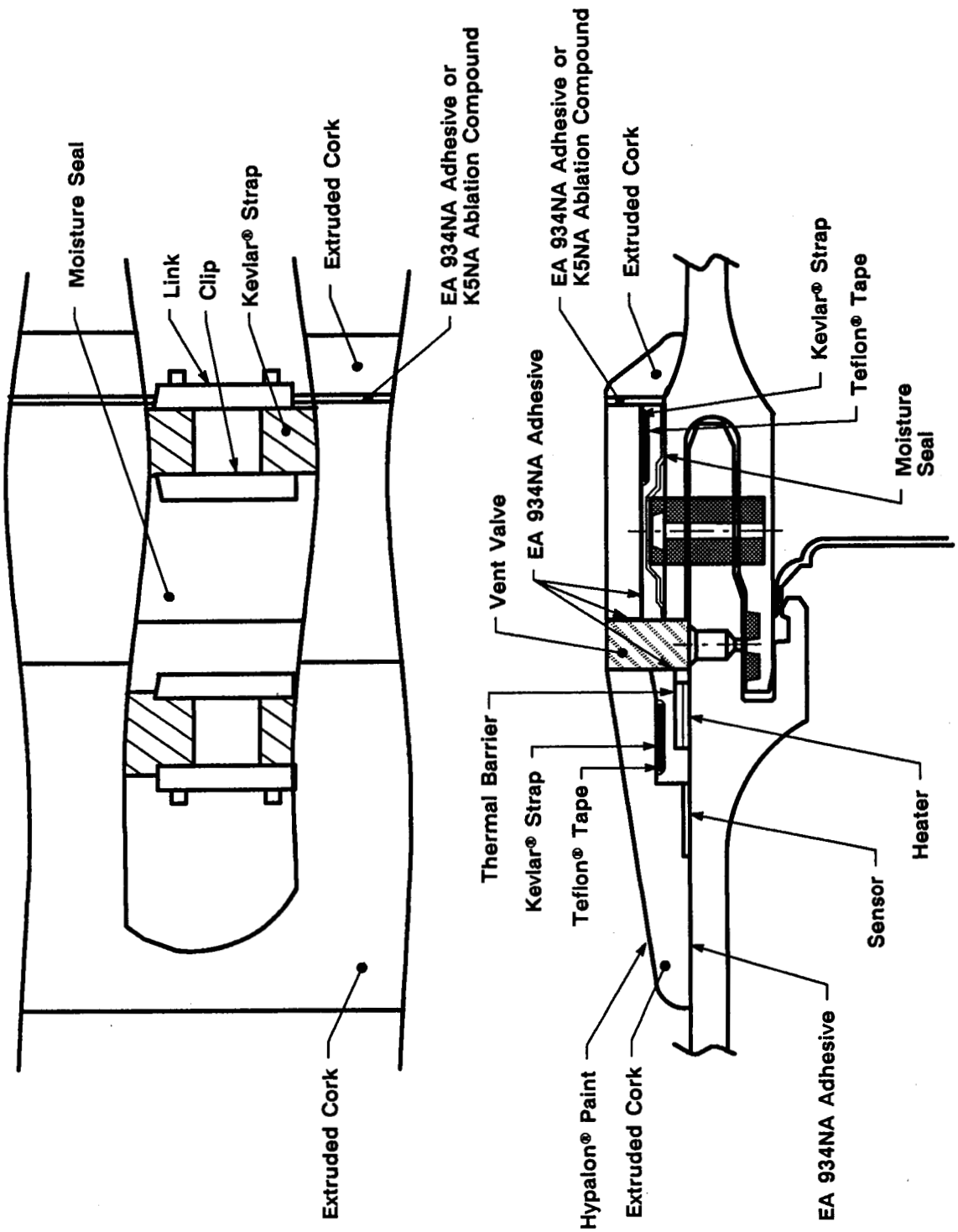

Figure 10.1.5-2. Field Joint Protection System

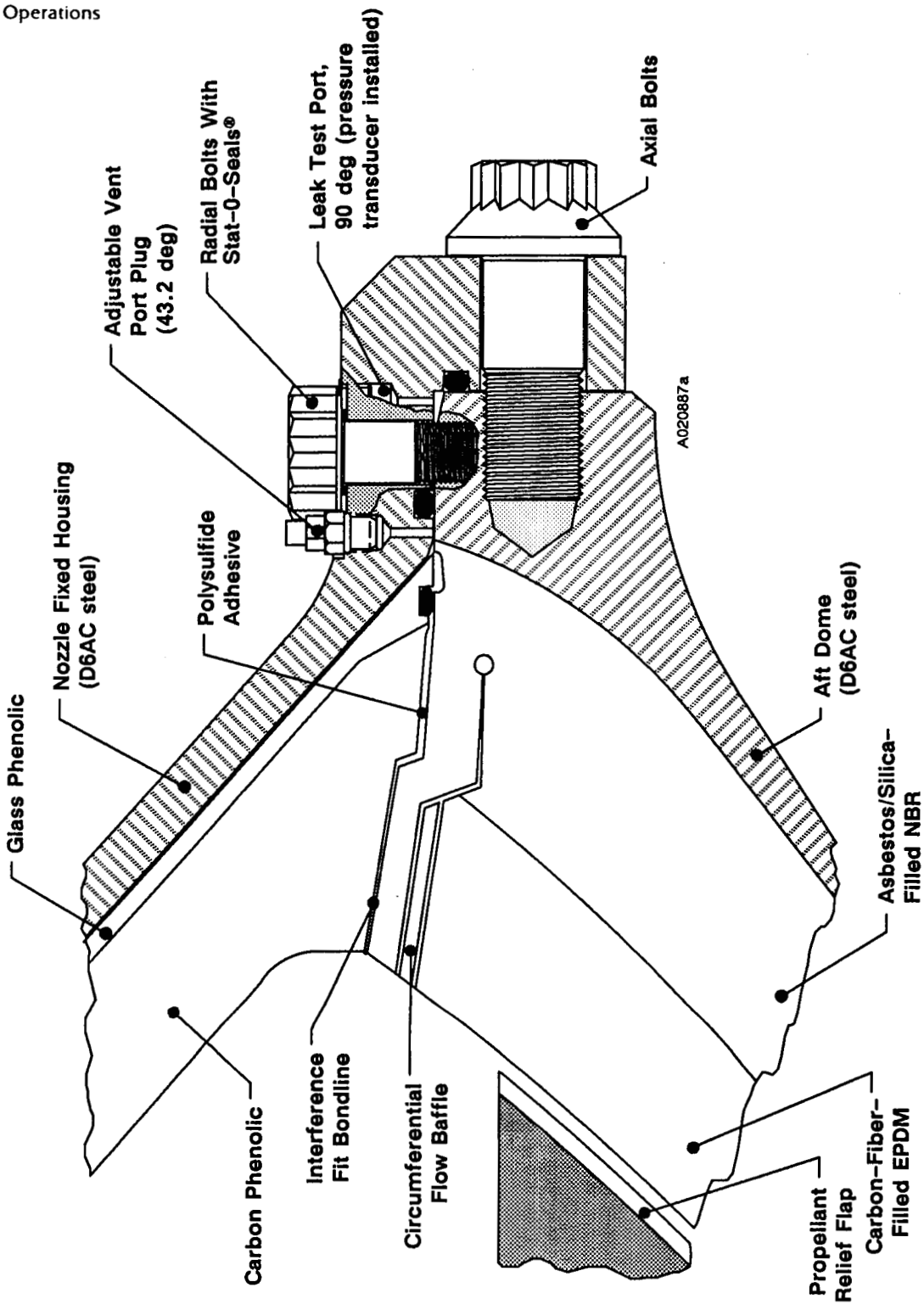

Figure 10.1.5-3. Case-to-Nozzle Joint

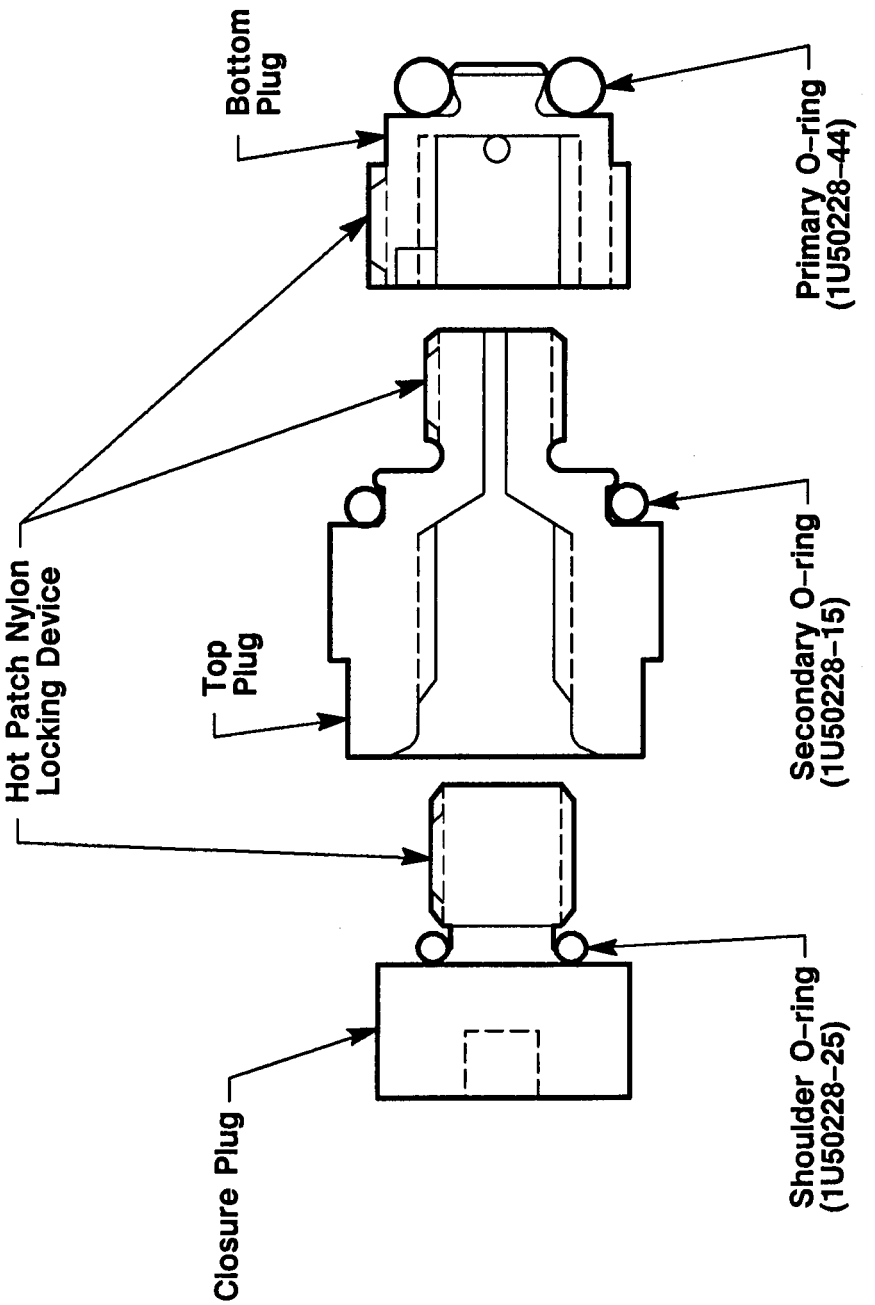

Figure 10.1.5-4. Adjustable Vent Port Plug

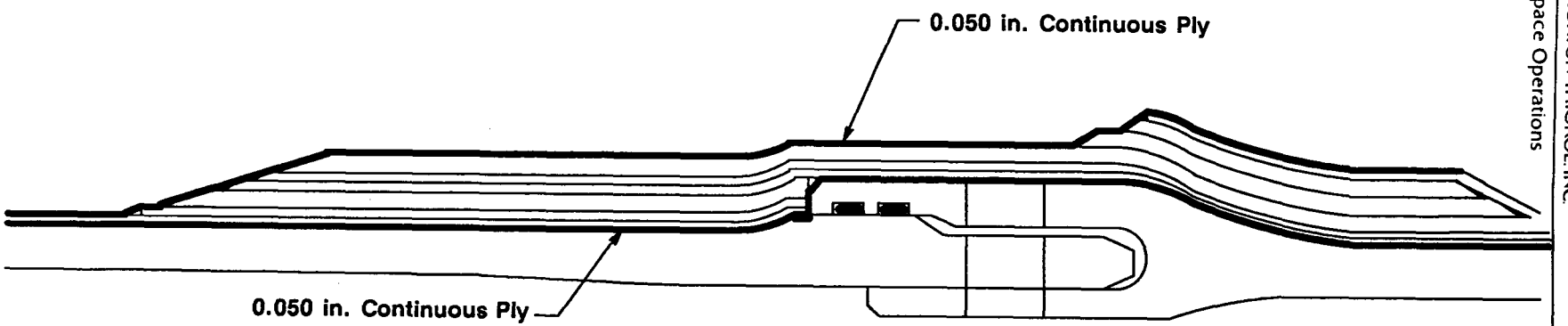

QM-8 Forward and Center Segments
RSRM-4B Aft Segment
RSRM-5 and Subsequent

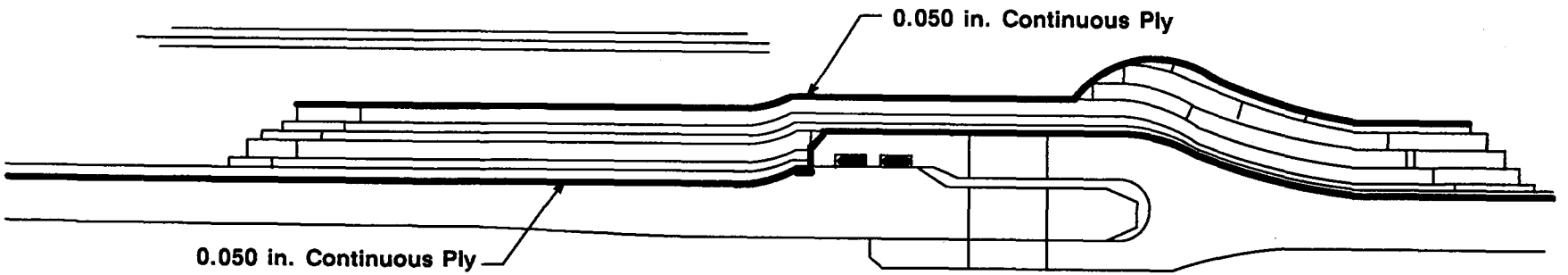

QM-8 Aft Segment
DM-9 Through QM-7
RSRM-1 Through RSRM-4*

*Except -4B aft segment

Figure 10.1.5-5. Factory Joint Ply Layup

A020827a

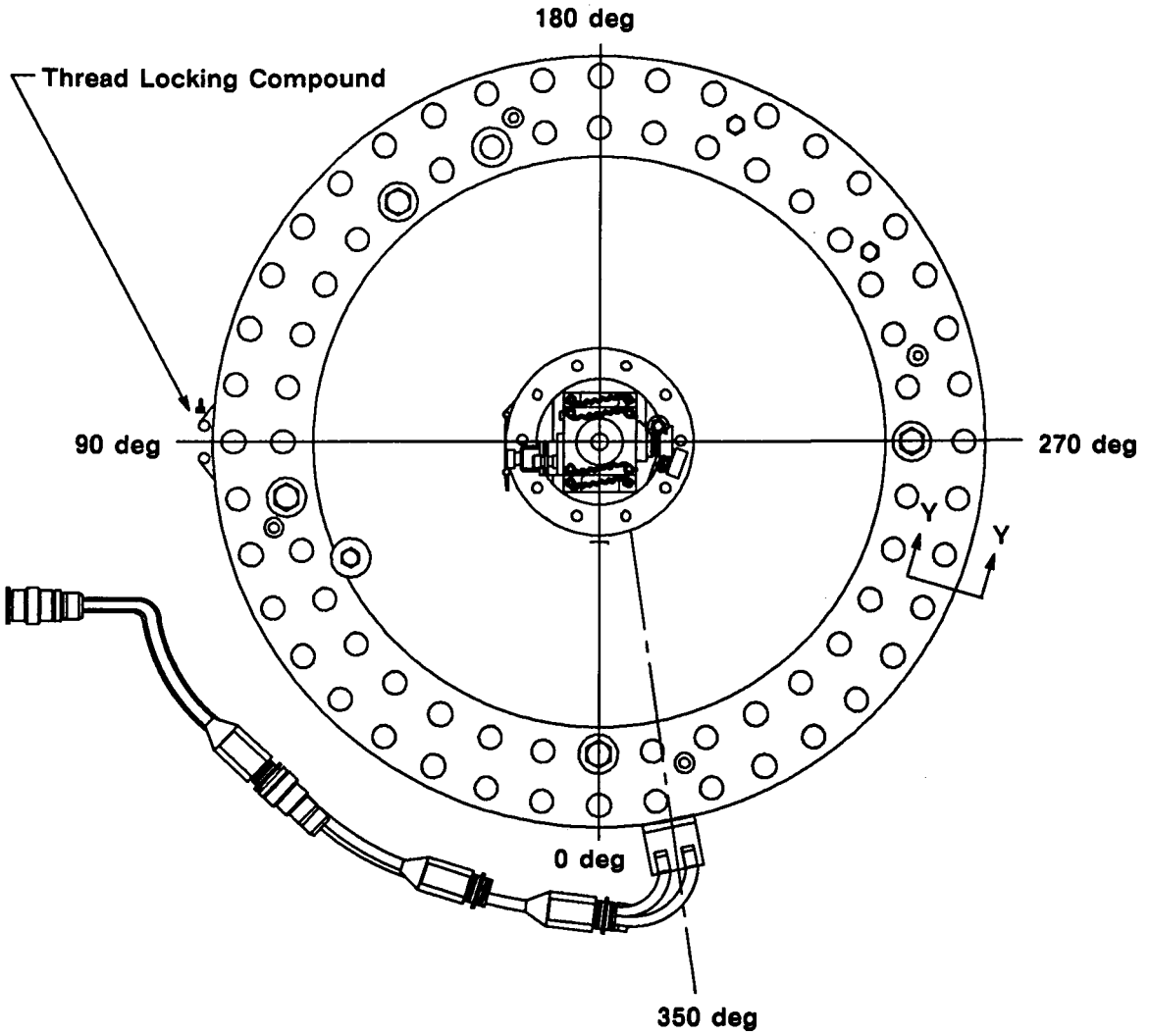

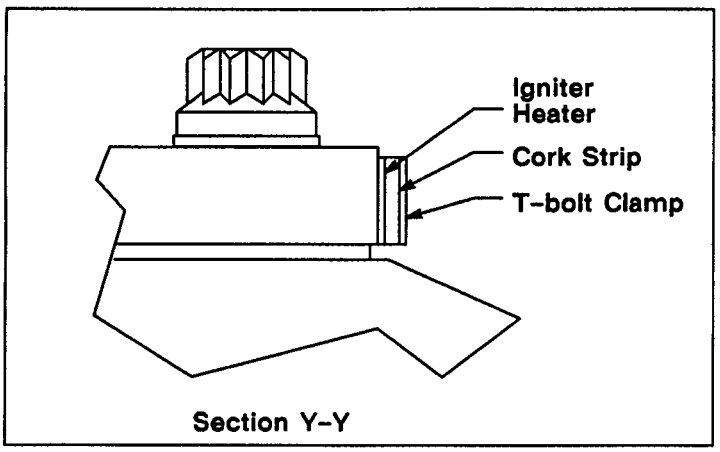

Figure 10.1.5-6. Igniter Joint Heater Components

A019175a

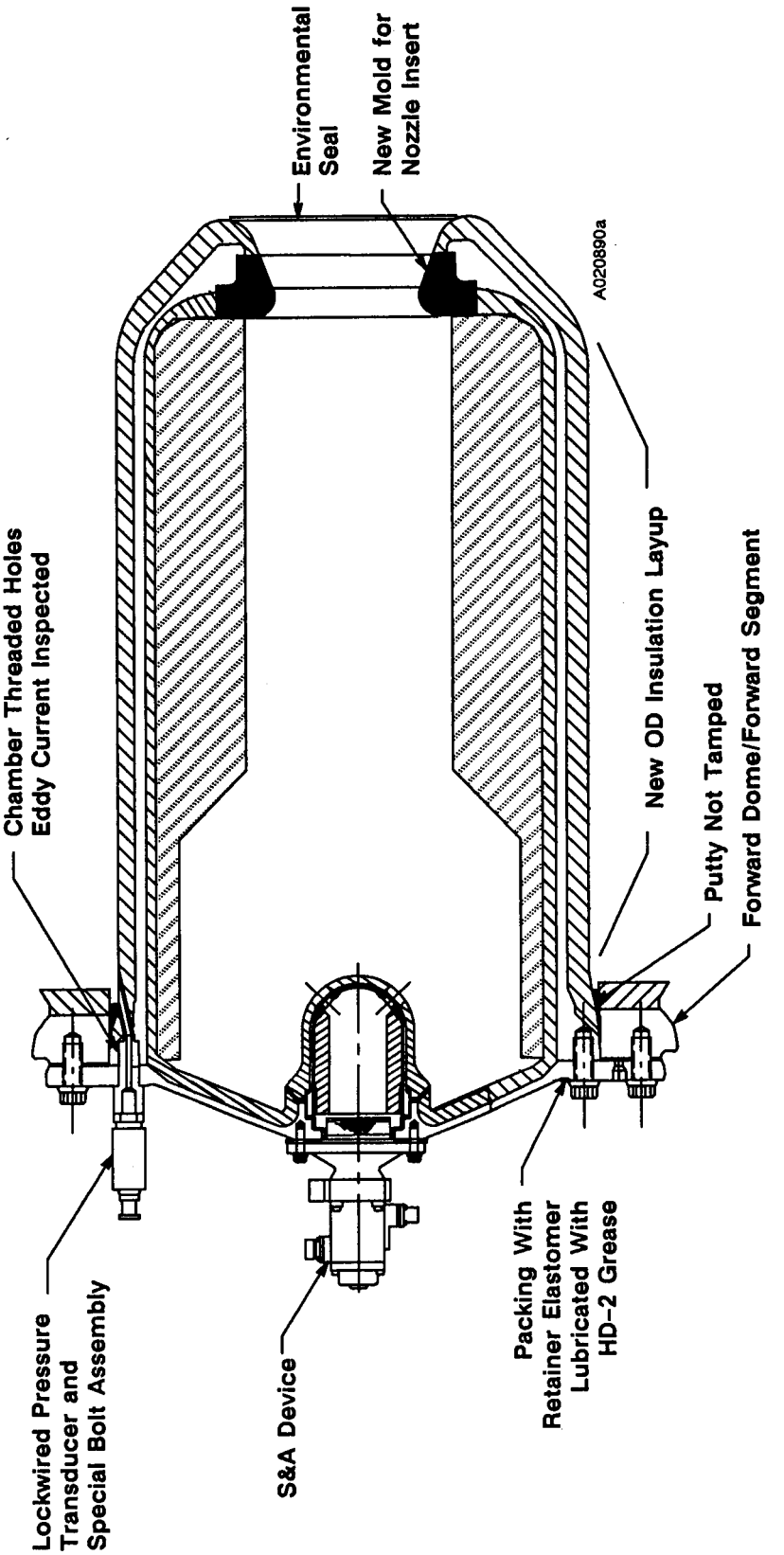

Figure 10.1.6-1. Ignition System

A020886a

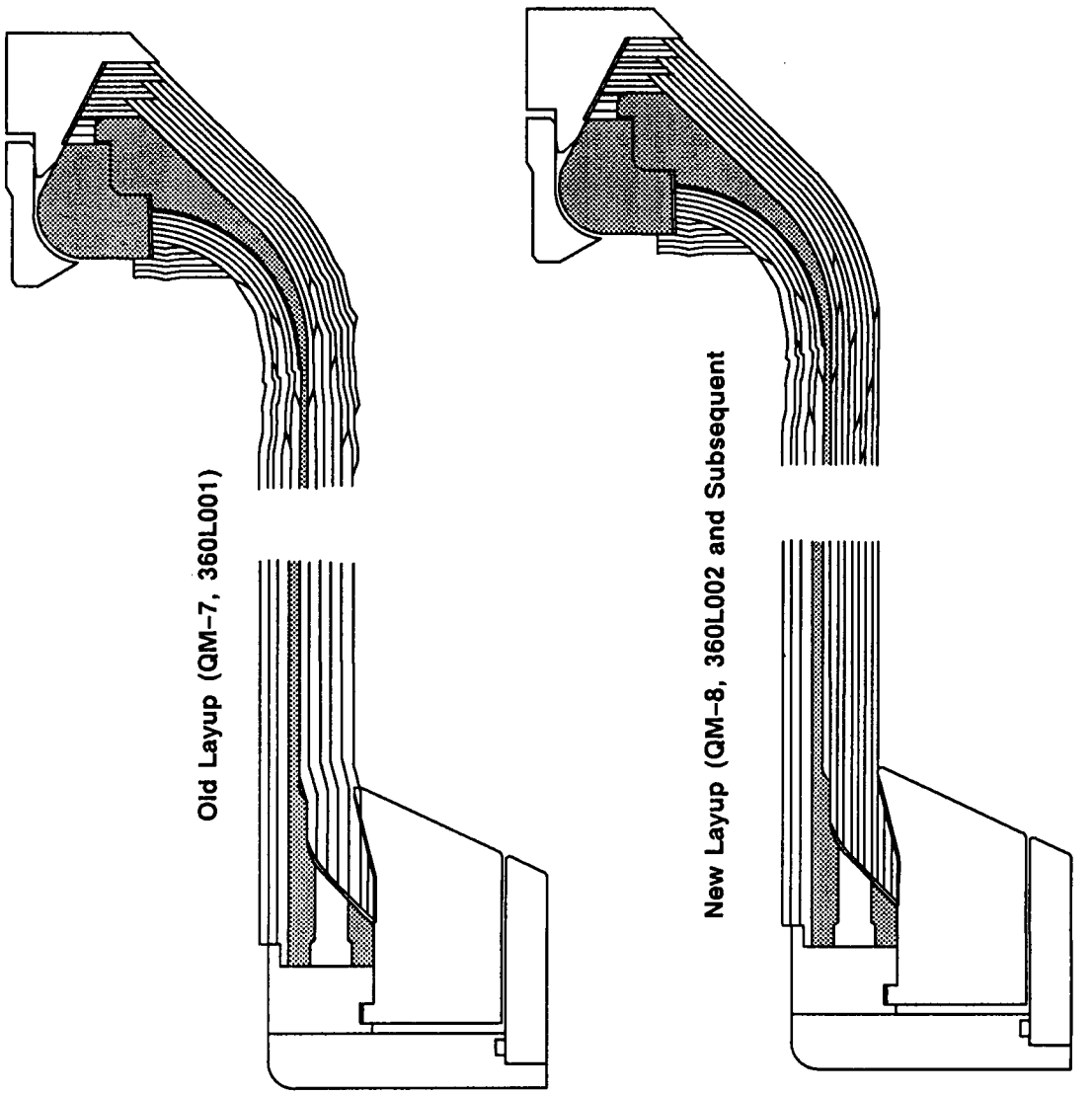

Figure 10.1.6-2. Igniter Insulation

10.1.7 JPS/Systems Tunnel

Field Joint Heaters

The QM-8 field joint heater assemblies were the 1U76698 flight configuration, containing one primary and one redundant 3,500 watt heater element. The heaters were powered with 208 Vac facility power.

The heater elements are laminated in Kapton and fluoroethylene polymer (FEP) Teflon with the redundant heater on top of the primary heater. The heating surface is 1.25 in. wide by 459.20 in. long. The heater assembly is approximately 0.062 in. thick. The underside of the Kapton surface is coated with a pressure-sensitive adhesive which serves as an installation aid.

The temperature sensor assembly consists of two 1-in. wide assemblies, each containing two resistive temperature device (RTD) temperature sensors. These temperature sensors are located at 15, 135, 195, and 285 deg. The sensor and associated conductors are laminated in Kapton and FEP Teflon. The underside Kapton surface is coated with a pressure-sensitive adhesive which serves as an installation aid. The sensor assemblies are secured in place by the cork insulation, which is bonded with EA 934NA over the FJPS components.

The temperature of the heater at each joint is controlled by an automatic controller. Control is from the coldest of the four joint sensors.

Field Joint Protection System (FJPS)

The field joint area and heaters are covered by EPDM extruded rubber moisture seal. The moisture seal is continuous around the circumference and is held in place by two Kevlar bands, one at each edge. A layer of cork completed the FJPS. The complete FJPS is shown in Figure 10.1.5-2.

Factory Joint Weather Seal

The factory joint moisture seal consisted of 0.70 in. thick extruded rubber vulcanized over the joint (Figure 10.1.7-1).

Systems Tunnel

Aluminum floor plate systems tunnel segments were installed on the forward three segments of QM-8. The forward and forward center segments were prepared by grit blasting. The aft center segment was prepared by use of a chemical paint stripper. The systems tunnel was not installed on the aft segment.

10.1.8 SRB Aft Skirt

The axillary test motor includes an SRB aft skirt assembly containing the TVC subsystem and the heat shield installation, including 0.5 in. thick cork external insulation (Figure 10.1.8-1). The

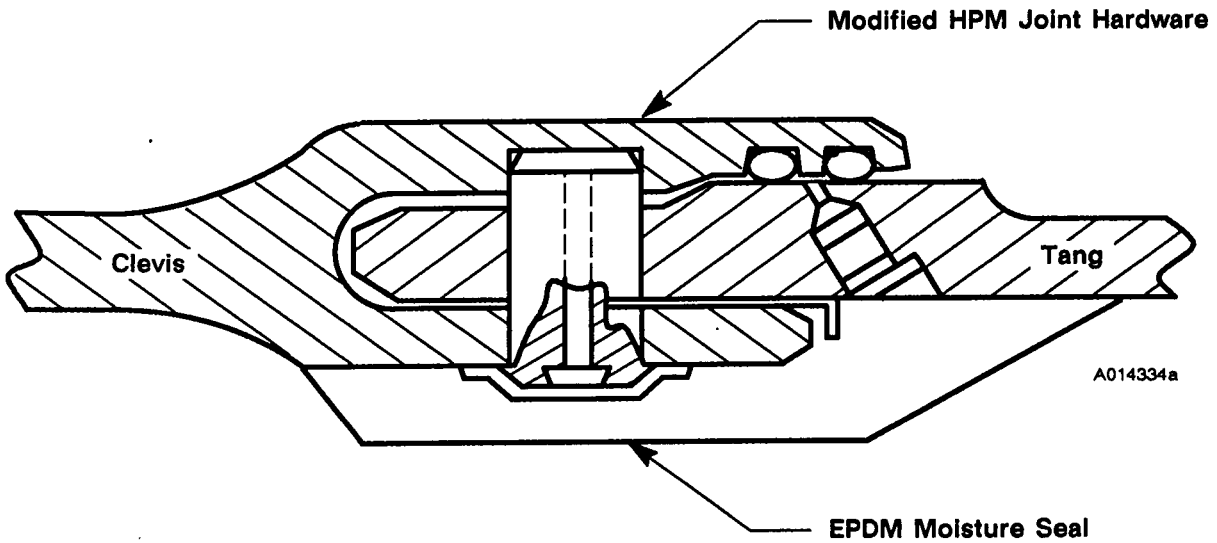

Figure 10.1.7-1. Factory Joint Moisture Seal

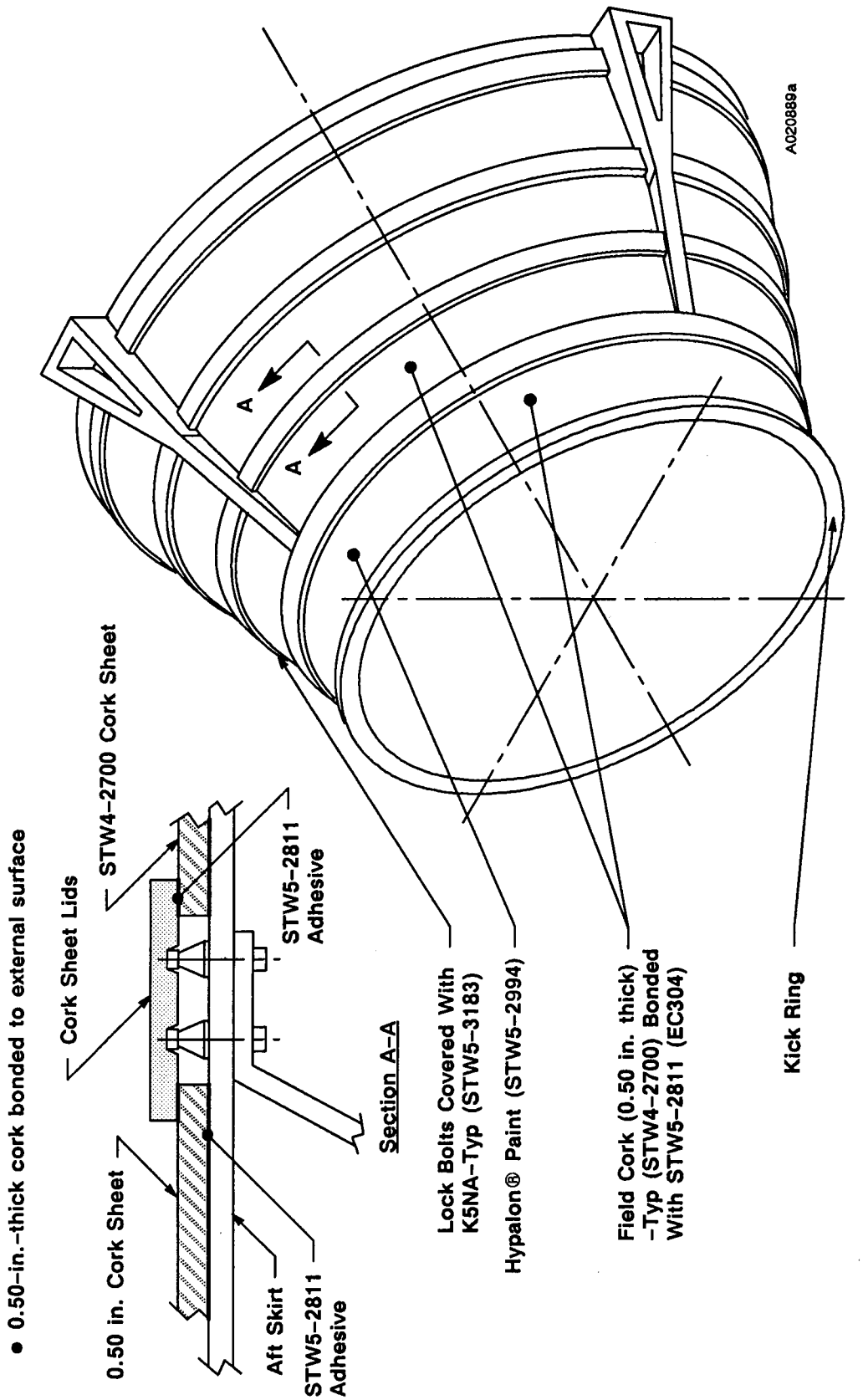

Figure 10.1.8-1. Insulated Aft Skirt

external cork insulation enhanced thermal performance during aft end heating while the bay was cold conditioned.

10.1.9 ETA Ring

A redesigned, 360 deg, left-hand configuration ETA ring was installed on the ETA segment.

11

APPLICABLE DOCUMENTS

The latest revisions of the following documents, unless otherwise specified, are applicable to this report.

Specification

CDW2-3679	Adjustable Vent Port Plug Installation Fixture
CPW1-3600, Addendum D	Prime Equipment Contract End Item Detail Specification (CEI)
CTP-0060, Rev D	Space Shuttle Qualification Motor No. 8 (QM-8) Static Fire Test Plan
TWR-15723, Rev C	Development and Verification of Nozzle Assembly
TWR-16340	Non-Destructive Radiographic Criteria for the Space Shuttle Solid Rocket Motor Nozzle Phenolics
TWR-16473, Vol I-IX	Motor Postfire Engineering Evaluation Limits
TWR-16674	TPTA and Pathfinder Mechanical Loads
TWR-17198	Postfire Engineering Evaluation Limits
TWR-18838	Procedure on how to correctly use the AVPP installation tool
TWR-17591, Vol II	Case Component Final Report
TWR-17591, Vol III	Case Internal Insulation Final Report
TWR-17591, Vol IV	Seals/Leak Check Component Final Report
TWR-17591, Vol V	Nozzle/Flex Bearing/Composite Structures/TVC Final Report
TWR-17591, Vol VI	Ignition System Component Final Report
TWR-17591, Vol VII	Joint Protection System/Factory Joint Weather Seal Component Final Report
TWR-17591, Vol VIII	Systems Tunnel Component Final Report
TWR-17591, Vol IX	Instrumentation Component Final Report
TWR-17591, Vol X	Performance and Mass Properties Final Report
TWR-17591, Vol XI	Dynamics/Reconstructed Loads
TWR-17331	Mass Properties History Log, Space Shuttle QM-8

DISTRIBUTION

Recipient	No. of Copies	Mail Stop
S. Harris	1	E12
D. M. Cox	1	L30
N. Black	1	L36
D. M. Garecht	3	L36
R. Jensen	1	L36
N. Watson	1	L35
D. M. Ketner	1	L21
T. A. Hoffman	1	L22
K. Albrectsen	1	L21
R. Lavery	1	L35
K. Parsons	1	L22
R. George	1	L23
M. Eastwood	1	L23
E. Hale	1	L23B
K. Sperry	1	L22
C. Change	1	L22
D. Bolieau	1	L22
T. Suatengco	1	L10
M. Williams	1	L36
D. Carner	1	L35
C. Johnson	1	l31
G. Paul	1	L33
D. Gurney	1	L22D
J. Curry	1	L22D
C. Greatwood	1	L23
L. Nelsen	1	L22D
T. Tran	1	L21
C. Prokop	1	L36
J. Donat	1	L23
P. McCluskey	1	L23
Guljani	1	L21
E. Mathias	1	L21
R. Buttars	1	L21
T. Daughtery	1	Z20
F. Call	45	E05
Print Crib	5	282
Data Management	5	L23E